

Universidad de Málaga
Escuela Técnica Superior de Ingeniería de Telecomunicación



TESIS DOCTORAL

Assessment and Performance Improvement of Multicarrier
Modulation for Underwater Acoustic Communications

Programa de Doctorado en
Ingeniería de Telecomunicación

Autor:

Mohsin Murad

Director:


Pablo Otero Roth

Málaga 2022



UNIVERSIDAD
DE MÁLAGA

AUTOR: Mohsin Murad

 <https://orcid.org/0000-0002-1924-1424>

EDITA: Publicaciones y Divulgación Científica. Universidad de Málaga



Esta obra está bajo una licencia de Creative Commons Reconocimiento-NoComercial-SinObraDerivada 4.0 Internacional:

<http://creativecommons.org/licenses/by-nc-nd/4.0/legalcode>

Cualquier parte de esta obra se puede reproducir sin autorización pero con el reconocimiento y atribución de los autores.

No se puede hacer uso comercial de la obra y no se puede alterar, transformar o hacer obras derivadas.

Esta Tesis Doctoral está depositada en el Repositorio Institucional de la Universidad de Málaga (RIUMA): riuma.uma.es

In loving memory of my aunt
Irshad Appa

This page intentionally left blank



UNIVERSIDAD
DE MÁLAGA



Escuela de Doctorado
Edificio Pabellón de Gobierno. Campus El Ejido
29071 Málaga
Tel.: 952 13 10 28 / 952 13 14 61 / 952 13 71 10
E-mail: doctorado@uma.es

DECLARACIÓN DE AUTORÍA Y ORIGINALIDAD DE LA TESIS PRESENTADA PARA OBTENER EL TÍTULO DE DOCTOR

Mohsin MURAD

Estudiante del programa de doctorado INGENIERÍA DE TELECOMUNICACIÓN de la Universidad de Málaga, autor/a de la tesis, presentada para la obtención del título de doctor por la Universidad de Málaga, titulada “Assessment and Performance Improvement of Multicarrier Modulation for Underwater Acoustic Communications”,

Realizada bajo la tutorización y dirección de Pablo OTERO ROTH,

DECLARO QUE:

La tesis presentada es una obra original que no infringe los derechos de propiedad intelectual ni los derechos de propiedad industrial u otros, conforme al ordenamiento jurídico vigente (Real Decreto Legislativo 1/1996, de 12 de abril, por el que se aprueba el texto refundido de la Ley de Propiedad Intelectual, regularizando, aclarando y armonizando las disposiciones legales vigentes sobre la materia), modificado por la Ley 2/2019, de 1 de marzo.

Igualmente asumo, ante a la Universidad de Málaga y ante cualquier otra instancia, la responsabilidad que pudiera derivarse en caso de plagio de contenidos en la tesis presentada, conforme al ordenamiento jurídico vigente.

En Málaga, a 24 de enero de 2022

Fdo.: Mohsin Murad

VºBº: Pablo Otero



EFQM AENOR



This page intentionally left blank



AUTORIZACIÓN DEL DIRECTOR DE TESIS DOCTORAL

El alumno del Programa de Doctorado en Ingeniería de Telecomunicación, Mohsin Murad, con pasaporte nº PAK BC0979712, es primer autor de los siguientes artículos publicados en revistas indexadas en los Journal Citation Reports (JCR) de la Web of Science (WoS):

- Mohsin Murad, Imran A. Tasadduq, Pablo Otero, and Javier Poncela. "Flexible OFDM Transceiver for Underwater Acoustic Channel: Modeling, Implementation and Parameter Tuning." *Wireless Personal Communications* (2020): 1423-1441. DOI: [10.1007/s11277-020-07850-w](https://doi.org/10.1007/s11277-020-07850-w).
- Mohsin Murad, Imran A. Tasadduq, and Pablo Otero. "Towards multicarrier waveforms beyond OFDM: Performance analysis of GFDM modulation for underwater acoustic channels." *IEEE Access* (2020). DOI: [10.1109/ACCESS.2020.3043718](https://doi.org/10.1109/ACCESS.2020.3043718).
- Mohsin Murad, Imran A. Tasadduq, and Pablo Otero. "Pilot-Assisted OFDM for Underwater Acoustic Communication." *Journal of Marine Science and Engineering* (2021). DOI: [10.3390/jmse9121382](https://doi.org/10.3390/jmse9121382).
- M. Murad, Imran A. Tasadduq, and Pablo Otero. "Ciphered BCH codes for PAPR reduction in the OFDM in underwater acoustic channels." *Journal of Marine Science and Engineering* (2022). DOI: [10.3390/jmse10010091](https://doi.org/10.3390/jmse10010091).

Además, el candidato es segundo autor del siguiente artículo:

- Imran A. Tasadduq, Mohsin Murad, and Pablo Otero. "CPM-OFDM Performance over Underwater Acoustic Channels." *Journal of Marine Science and Engineering* (2021). DOI: [10.3390/jmse9101104](https://doi.org/10.3390/jmse9101104).

Estos cinco artículos publicados avalan su tesis doctoral y ninguna otra tesis.

Por todo ello, su tutor y director, Pablo Otero, autoriza al Sr. Murad a depositar su tesis doctoral ante las Autoridades académicas de la Universidad de Málaga.

En Málaga, a 24 de enero de 2022.

Fdo: Pablo Otero Roth

This page intentionally left blank

Summary

Wireless underwater communication involves transmitting and receiving data below water without a wired interface. Acoustic waves have been reliably used for underwater communication for quite some time. In this type of communication, signals generated by the underwater transmitter are sent to the receiver in the form of sound waves—also called acoustic waves—using hydrophones. Acoustic waves have relatively lower loss and longer range in underwater environments when compared with electromagnetic waves which require larger antennas and high transmit power. Optical waves, on the other hand, have issues such as absorption and scattering due to turbidity of the medium. Both radio frequency (RF) and optical signals do not seem to be an appropriate choice of transmission for long range underwater communication. Acoustic waves propagate underwater through compression and rarefaction those are detected by the pressure sensitive hydrophone at the receiver. The frequency range commonly used for underwater acoustic communication is between 10 Hz to 1 MHz. Below 10 Hz, acoustic wave propagation is almost impossible whereas frequencies higher than 1 MHz are seldom used. In consequence, underwater acoustic (UWA) communication is currently an active area of research and finds its application in various systems e.g., underwater search and rescue operations, offshore installations, scientific data collection, protection of coastlines and submarine communications, to name a few. The application use cases, both military and commercial, continue to grow with rapid developments in acoustic communication domain together with the demand for enhanced performance and throughput requirements. There is a high need for real time communication with autonomous underwater vehicles and submarines, both in point to point as well as in a network of nodes. The underwater network of the future will consist of both mobile and stationary nodes allowing for underwater data exchange between its various elements and a surface station. A radio link will then enable communication between surface station and remote users. At present, efforts are underway to develop efficient coding and modulation schemes, multiple access techniques, signal processing algorithms and effective mobile communication methods.

Since acoustic waves travel at very low speeds—approximately 1500 m/s—this severely limits the rate at which data could be transferred in underwater environments. Another disadvantage with underwater acoustic communication is the limited channel bandwidth which is typically of the order of several kilohertz. Besides low propagation speeds, multipath propagation and frequency dependent path loss are major adversities in an underwater medium. System motion and changes in the medium induce time variation in propagation paths causing Doppler spreading and signal shifts. The system is characteristically wideband since effective acoustic propagation requires communication at low frequencies. Thus, large delay spreads usually affect UWA channels causing inter-symbol-interference (ISI) spanning a big sum of symbol intervals. Additionally, few propagation paths carry substantial energy making the impulse response of the channel sparse. Hence, a comprehensive modem and subsequent channel model should consider a channel with sparse impulse response, Doppler shifts, frequency dependent path loss and spreading. While recent advances have focused on improved performance and robustness in the presence of various anomalies intrinsic to underwater channel, accurate modelling of underwater channel is need of the hour. Various efforts have been carried out to successfully implement transceiver systems for deep water channels however the work done in the domain of shallow water communication is still limited.

To evaluate performance of an underwater communication system using simulations, several channel models have been proposed in literature. However, since most of them are approximations, none of the proposed models could be regarded as a complete model in all respects where a typical UWA system could be simulated using realistic variables encountered in a real underwater environment. Even though there is a lack of consensus on accurate modelling of an underwater channel, a good amount of published work is directed toward mathematical modeling of the UWA channel. This thesis is a small effort to bridge the existing gap and in doing so, enabling those working in other wireless mediums to have a better understanding of the UWA domain.

Prevailing UWA communication systems count on phase coherent single carrier modulation combined with decision feedback equalization to tackle the problem of time-varying and frequency selective underwater channels. Yet, as the symbol rate increases, the frequency selectivity of the channel grows substantially making equalizers more complex and it becomes difficult to achieve substantial rate improvements in single carrier modulation systems. Additionally, rapid spatial and temporal variations in UWA channel makes it hostile for communication systems based on single carrier modulation. Multicarrier modulation offers a good alternative as it simplifies the equalization procedure greatly by converting a frequency selective channel into a set of flat fading channels, boosting transmission rates. Multicarrier modulation techniques thus greatly improve bandwidth utilization and help deal with time dispersal effects. Recently, various studies have evaluated multicarrier schemes for enabling wireless transmission of data at higher rates in underwater acoustic channels.

Orthogonal frequency division multiplexing (OFDM) is a proven multicarrier communication scheme having capabilities to cope with frequency selectivity and delay spreads effectively. It started to get attention for being a simpler alternative to high complexity and high maintenance single carrier systems in UWA communication systems. It fights off ISI because of the long symbol duration and orthogonality of the subcarriers. However, the issues that arise from using OFDM in UWA are different than those experienced at radio frequencies. Since underwater channel is wideband in nature, the sensitivity of OFDM to frequency offset because of relative motion of the receiver and transmitter is a challenging problem. As mentioned earlier, even a small motion of the transmitter and receiver induces Doppler effects in an underwater environment because bandwidth in a UWA communication system is significant with respect to the center frequency while the velocity of acoustic signals is very low. This results in further problems such as inter-carrier-interference (ICI) and non-uniform shift over signal bandwidth. Despite its advantages, one of the foremost issues associated with OFDM is the high peak to average power ratio at the transmitter. A large peak to average power ratio (PAPR) value usually results from constructive overlapping of random symbol phases to create peaks in time domain. Moreover, since the UWA channel is both time and frequency variant, channel estimation becomes complex. In quest for higher data-rates and ease of equalization in the frequency domain, OFDM turns out to be an excellent choice for an underwater multi-carrier acoustic communication system. The mere availability of fast Fourier transform blocks simplifies the process of frequency domain equalization instead of complex equalization techniques in the time domain. With increasing data-rates in future UWA OFDM systems, the symbol duration will keep on decreasing and the amount of channel taps will drastically increase making the equalization process more complex.

Almost all OFDM receivers use channel estimation techniques to compute approximate values of the channel parameters. Several types of estimation techniques have been explored in the literature

to accurately estimate the channel for OFDM. These include blind, semi-blind, and pilot-based channel estimation techniques. Out of these techniques, the pilot-based technique is widely used mainly because of the ease in its implementation along with a better performance. The downside of this technique is the bandwidth overhead, resulting in poor spectral efficiency. For UWA channels, this type of technique is preferable because the underwater sensing nodes have limited power and limited processing capabilities. In a typical pilot-based channel estimation scheme, a few known symbols—also called training symbols—are inserted into the transmitted OFDM symbols at prespecified locations. These known symbols are then extracted by the receiver and are used for the synchronization and determination of the channel parameters.

Several estimation techniques have been used with OFDM receivers such as maximum likelihood (ML), minimum mean square error (MMSE) estimation, and least squares error (LSE) estimation. With the rise in data rates in future UWA systems, the symbol duration will keep on decreasing with the increasing data rates making the equalization process complex. As OFDM offers a higher data rate and one-tap equalization, it is an ideal candidate for UWA communication systems. Moreover, as the equalization is performed in the frequency domain, the fast Fourier transform (FFT) in the receiver of the OFDM further reduces the equalization complexity. Though, coping with Doppler shifts is a challenge as they affect the orthogonality of the subcarriers due to phase variations. Hence, the problem of equalization when using OFDM in UWA channels has been addressed and several solutions have been proposed in the literature. In radio-based systems, zero forcing equalizers have been used as they are simple to implement. However, they suffer from significant noise amplification near to the zeroes of the channel in an attempt to invert the channel completely. MMSE equalizers overcome the shortcomings of zero forcing (ZF) equalizers at the cost of complexity.

Affixing a cyclic prefix (CP) at the start of every symbol, as a guard interval to deal with ISI problem, makes an OFDM based communication system spectrally inefficient. Since a filter based on rectangular pulse shaping is used at the transmitter side, there are high out-of-band (OOB) leakages. OFDM also has a higher PAPR due to random addition of in-phase subcarriers. To deal with an OFDM system limitation, and with rapid advancements in the field of wireless communication, many potential multicarrier waveforms have emerged as contenders for next generation networks – also called 5G. Among them, the most prominent ones are generalized frequency division multiplexing (GFDM), filtered OFDM (F-OFDM), universally filtered multicarrier (UFMC) and filter bank multicarrier (FBMC). While the research and implementation of these promising techniques in the radio frequency (RF) domain have gained momentum, very limited literature is available evaluating the efficacy of these techniques for an underwater channel.

Compared to OFDM, in a GFDM system, the data transmitted is in two dimensional blocks (frequency and time) divided into sub-symbols and subcarriers, with the subcarriers filtered by a pulse shaping prototype. The time and frequency responses of the prototype filter are altered according to the requirements. This leads to reduced OOB emissions compared to a cyclic prefix OFDM (CP-OFDM) system. The ability to utilize fragmented spectrum and varying spectral efficiency through various pulse shapes and their roll-off factors makes GFDM an ideal choice for spectrum limited UWA networks. FBMC is another promising technique that performs well in doubly dispersive acoustic channels, and it has a higher bandwidth efficiency given the absence of a cyclic prefix. There are two flavors of FBMC, vis-à-vis filtered multi tone filter bank multicarrier (FMT- FBMC) and offset QAM filter bank

multicarrier (QAM). Former is based upon quadrature amplitude modulation (QAM) and the latter is based upon offset-QAM. OQAM-FBMC achieves spectral efficiency in the real domain while orthogonality is achieved in FMT-FBMC by reducing the frequency domain overlapping of subcarriers. Filtered OFDM is one of the 5G candidate waveforms and a promising alternative to OFDM due to its reduced OOB emissions. While the rest of design is like OFDM, in F-OFDM, a filtering operation is performed after the IFFT (Inverse FFT) stage of the receiver. At the transmitter end, the received signal is filtered and then passed on to the FFT stage after analog to digital conversion. UFMC is a more generalized realization of filtered OFDM and FBMC where group of subcarriers are filtered in frequency domain. The total number of subcarriers are split into multiple sub-bands and each one is filtered through a filter of specific length. This filtering operation results in lowest OOB emissions compared to the other waveforms. The number of sub-bands used for transmission can be controlled and only limited number can be used for transmission. While the gains offered by UFMC systems are promising, its higher complexity makes it less suitable for scenarios where system power is limited.

Continuous phase modulation (CPM) employing correlated phase states and continuous phase frequency shift keying (CPFSK) have been used in communication systems for more than four decades. However, very limited work has been done incorporating CPM in the mapper of an OFDM system particularly in the domain of underwater acoustic channels. Key advantages of employing these schemes in OFDM are that the signal is power and spectrum efficient, has a constant envelope, has less out of band radiation, and possesses phase continuity. Traditional OFDM systems use memoryless modulation schemes such as PSK and QAM in the mapper. The introduction of correlation among neighboring symbols through proper selection of mapping parameters is a key advantage of CPM based OFDM systems. This allows for multi-symbol detection techniques as memory can be introduced through appropriate selection of a single parameter h while allowing exceptional flexibility for the communication system designer to control memory introduced at the transmitter. One of the concerns, in CPM-OFDM systems, is the complexity of receivers. Consequently, detection of CPM signals is a complex process. Nevertheless, it becomes less complex and economical if a maximum likelihood Viterbi decoder is employed. Restricting the modulation index h to be rational, the number of states in CPM trellis can be kept to a manageable number that also facilitates the use of Viterbi algorithm (VA). The distance between received signal and all the trellis paths entering each state at an instant i is calculated by VA. This is followed by the removal of those paths that are probably not the candidates for maximum likelihood. For two paths entering the same state, the one having the best metric is selected and it is named the “surviving path”. For all the states, similar surviving paths are selected. By continuing in a similar manner, VA advances deeper into the trellis and the decisions are made by removing the paths that are least likely. Although such decisions are not maximum likelihood in the true sense, but if decision depth is long enough, these decisions can be almost as good as in the case of true maximum likelihood. Literature suggests that Viterbi decoders—though suboptimum—when used to detect CPM signals, offers performance that is comparable to optimum CPM receivers at a much-reduced complexity.

Despite its advantages, one of the foremost issues associated with OFDM is high peak to average power ratio at the transmitter. It is a widely studied topic in the field of radio OFDM systems, however computational and bandwidth limitation renders it a unique problem in the acoustic domain. A large PAPR value usually results from constructive overlapping of random symbol phases to create

peaks in time domain. The presence of non-linear power amplifiers at the transmitter side makes it mandatory to reduce the average power of the system which triggers a loss in performance. In-band distortions and spectral spreading are observed when such a signal passes through non-linear devices such as high-power amplifiers (HPA). Thus, a high peak to average power ratio causes in-band distortions in an OFDM system and further increases the complexity of implementation of other blocks such as analog-to-digital (A/D) and digital-to-analog (D/A) convertors. Various techniques have been suggested to reduce PAPR of OFDM systems including: (1) signal distortion techniques e.g. clipping and filtering, windowing, companding and peak cancellation; (2) probabilistic techniques including partial transmit sequences (PTS), selective mapping (SL), tone injection and tone reservation; (3) schemes based upon coding such as linear block coding (LBC), Golay sequences and turbo coding.

Bose Chaudhuri Hocquenghem (BCH) codes have been used in communication systems for error correction and reducing bit error rates. BCH codes are cyclic codes operating on a group of data bits or blocks rather than individual bits. Due to their ability to fix multiple errors and simplicity in coding and decoding implementations, they find their uses in various applications. The decoding energy consumption of BCH codes is observed to be a linear function of the number of corrected errors t and the length of code words. Vernam cipher was first used by Gilbert Vernam in 1917 for encrypting telegraph messaging. Also called XOR cipher, its biggest advantage is that the encryption and decryption are both achieved using the same operation. At the transmitter, the input data is converted into binary and divided into blocks. An XOR operation is performed for the input message data with a predefined key of the same block length. The obtained ciphertext is then transmitted whereby the receiver performs an XOR operation for the received data with the same key to get the original message.

In this thesis, multiple techniques have been proposed to improve the viability of an OFDM transceiver for underwater acoustic transmission. First, an underwater acoustic testbed based on cyclic prefix (CP) OFDM transceiver is developed and evaluated using MATLAB. The OFDM system is assumed to have guard intervals larger than the delay spread and a zero-forcing equalizer is used considering ideal channel estimation. Moreover, the proposed system can tune multiple parameters of the transceiver and perform bit error rate (BER) comparisons for multiple scenarios. In addition, a channel characterization is proposed based on Rician shadowed fading model as it perfectly characterizes the way in which a shallow UWA channel behaves. The underwater acoustic multipath channel model is based on Rician distribution with adjustable constraints of noise and UWA absorption. System performance is evaluated for various signal to noise ratios (SNR) over multiple distances, number of subcarriers, length of cyclic prefix and delay spreads. The proposed design allows implementation of and evaluation of a variety of OFDM modulation schemes through varying different parameters and to perform Monte Carlo simulations for bit error rate comparisons together with the ability to tune multiple UWA channel parameters. The model has been used to simulate M-ary phase shift keying (MPSK)-OFDM although it can be used for other mapping schemes as well such as QAM and differential phase-shift keying (DPSK), etc. The testbed allows for evaluating the transceiver for different UWA environments by simply modifying the channel parameters such as ambient noise and multipath fading along with bathymetry and geometrical profiles.

Second, we use the proposed OFDM UWA testbed for the investigation of a pilot aided channel estimation algorithm based upon a least squares error estimation. It employs a least-squares error (LSE) based channel estimator using pilot subcarriers for UWA OFDM with linear frequency domain

equalization. The estimation algorithm is applied to a typical OFDM system, in which pilot signals are used for a UWA channel. In this algorithm, the pilot signals are inserted at predefined subcarriers and the receiver estimates the channel using LSE algorithm. Based upon channel delay spread, we tune the position and number of pilots as well as vary the length of the cyclic prefix to improve performance. In addition, we explore two equalizers for improving the error performance of an OFDM-based UWA system. One equalizer is a least squares (LS) equalizer, and the other is ZF equalizer. Using testbed simulations, it is observed that, for an acceptable error performance, the number of pilots should be one-fourth the number of subcarriers. Any further increase in the number of pilots does not improve error performance. Moreover, if the energy of the pilots is increased without changing the overall symbol energy, the error performance degrades. It is also noted that both the LS and ZF equalizers give an acceptable error performance with the ZF performing marginally better than the LS. Furthermore, the error performance of the proposed system is evaluated as a function of the transmitter-receiver distance and an acceptable error performance is observed even at 1250 m. We provide several bit error rate (BER) plots to show the performances of the equalizers as a function of the various parameters. These simulations are performed over a UWA channel model that uses a Rician fading distribution and incorporates absorption loss and ambient noise.

Since in OFDM systems, a filter based on rectangular pulse shaping is used at the transmitter side, there are high out-of-band (OOB) leakages. Third contribution of this work assesses the performance of a GFDM transceiver for underwater acoustic high data-rate transmission. Error performance analysis of proposed GFDM system is evaluated over varying acoustic channel conditions and transmitter-receiver (TX-RX) distances and its comparison with CP-OFDM. A comprehensive overview of the work done in the field of next generation multicarrier techniques beyond OFDM for underwater acoustic channels has been presented. In doing so, a thorough survey of latest developments in next generation candidate waveforms is performed for underwater acoustic communication, findings, and some recommendations have been detailed. The overview touches upon all the work, till date, related to advanced multicarrier transmission techniques in UWA medium which will potentially supersede OFDM. Since very little work has been done in determining the feasibility of acoustic GFDM, the performance of proposed GFDM transceiver in terms of spectral efficiency, peak to average power ratio, error rates and computational complexity using simulations and its comparison with CP-OFDM. A GFDM based modem for UWA communication is developed and evaluated using the proposed testbed. Two types of receivers have been considered - matched filter and zero forcing and their performances for several system configurations were evaluated. Results presented show that the zero-forcing receiver outperforms the matched filter receiver at high SNR values for almost all the configurations; exceptions being the cases where 1st and 4th Xia pulse shapes are employed with higher values of the roll off factor. The performance comparison of proposed GFDM transceiver with that of OFDM shows that GFDM outperforms OFDM by almost 4 dB for a symbol error rate of 10^{-2} . For several values of the roll off factor, the performance of the zero forcing receiver is better than that of the matched filter receiver when the pulse shape employed is raised cosine (RC) or root raised cosine (RRC). On the other hand, the performance of the matched filter receiver is better than that of the zero forcing receiver when the pulse shape employed is 1st or 4th Xia. In conclusion, if SER performance is the sole design criterion, a pulse shape of 1st Xia with a roll off factor of 0.1 seems to be the most appropriate choice. It is concluded that while GFDM is computationally more demanding than OFDM,

it is still an appealing technique for future UWA communications due to its higher spectral efficiency, flexibility, and better error performance. It was noted that the PAPR performance of GFDM signals was comparable to OFDM with several cases marginally worse than OFDM. It is further noted that pulse shaping filters significantly impact the PAPR of GFDM and the best PAPR performance is exhibited when the pulse shape is 4th Xia. Moreover, for all the pulse shapes, the higher the value of the roll off factor, the worse is the PAPR.

As fourth contribution, we propose and evaluate the performance of a continuous phase modulation based OFDM transceiver for underwater acoustic communication. In our proposed technique, the mapper is replaced by CPM while a realistic model of underwater channel proposed earlier is employed. It is pertinent to mention that we evaluated the performance of binary CPM-OFDM without any PAPR reduction techniques employed. Bit error rate performance of the proposed scheme was evaluated using Monte Carlo simulations. The error performance observed clearly establishes the superiority of CPM-OFDM over traditional OFDM schemes. The best error performance is achieved when the CPM modulation index h is chosen as either $7/16$ or $9/16$. Furthermore, the error performance of the proposed scheme is within acceptable values up to a transmitter–receiver distance of 1.5 km. The PAPR performance of CPM-OFDM was also evaluated and shown to be almost similar to those offered by other traditional OFDM schemes. Additionally, PAPR performance of the proposed scheme suggests that like other OFDM schemes, a PAPR reduction scheme is mandatory for acceptable PAPR performance of CPM-OFDM for underwater acoustic channels. Through computer simulations, it has been shown that CPM-OFDM is an attractive candidate for underwater acoustic communication. The proposed technique offers an excellent error performance without employing any equalization technique. The performance of M-ary CPM-OFDM with PAPR reduction technique remains to be studied. Besides, another advantage CPM-OFDM signals can bring along is the reduction in PAPR when multi-amplitude CPM is utilized in conjunction with partial transmit sequences.

The presence of non-linear power amplifiers at the transmitter side makes it mandatory to reduce the average power of the system which causes a loss in performance. In-band distortions and spectral spreading are observed when such a signal passes through non-linear devices such as HPA. Thus, a high peak to average power ratio causes in-band distortions in an OFDM system and further increases the complexity of implementation of other blocks such as analog-to-digital (A/D) and digital-to-analog (D/A) convertors. In underwater acoustic OFDM systems, PAPR reduction is a challenging task due to low bandwidth availability along with computational and power limitations. As a final contribution of this thesis, we propose an effective, low complexity and multifaceted scheme for peak to average power ratio reduction of an orthogonal frequency division multiplexing based communication system. The proposed coded-BCH scheme takes advantage of XOR-ciphering and generates ciphered BCH codes that have low PAPR. Since keys for XOR-ciphering of BCH codes are computed offline, this technique is ideal for UWA systems as it does not require additional computational power at the transceiver during transmission. The only overhead is an XOR operation, but this operation also adds a level of encryption to the system. The advantage of proposed scheme is threefold. First, it reduces the PAPR, second, since it uses BCH codes, the BER of the system improves, and third, a level of encryption is introduced via XOR-ciphering, enabling secure communication. Simulations are performed in a realistic UWA channel to evaluate the proposed technique showing

PAPR as well as BER reduction. The results demonstrated that the proposed scheme indeed achieves all the three objectives with minimum computational power.

Resumen

La telecomunicación submarina inalámbrica mediante ondas electromagnéticas es prácticamente imposible, debido a la intensa atenuación que las ondas de esa naturaleza sufren al propagarse en el agua. En este tipo de comunicación, las señales generadas por el transmisor submarino se envían al receptor en forma de ondas sonoras, también llamadas ondas acústicas, mediante unos transductores electroacústicos llamados hidrófonos. Las ondas acústicas se han utilizado de manera confiable para la comunicación submarina durante bastante tiempo, ya que la absorción que presenta el medio de transmisión es relativamente menor y, por consiguiente, se consigue mayores alcances en entornos submarinos, en comparación con las ondas electromagnéticas, que requieren antenas más grandes y mayor potencia de transmisión. Las comunicaciones ópticas, como alternativa, tienen problemas como la absorción y la dispersión debido a la turbidez del medio. Tanto las señales de radiofrecuencia (RF) como las ópticas no parecen ser una opción de transmisión adecuada para la comunicación submarina de medio y largo alcance.

Las ondas sonoras se propagan bajo el agua a través de la compresión y la rarefacción que son detectadas por el hidrófono sensible a la presión en el receptor. El rango de frecuencia utilizado para la comunicación acústica subacuática es de 10 Hz a 1 MHz. Por debajo de 10 Hz, la propagación de la onda acústica es casi imposible, mientras que las frecuencias superiores a 1 MHz rara vez se utilizan.

En consecuencia, la comunicación acústica subacuática (UWA) es actualmente un área activa de investigación y encuentra su aplicación en varios sistemas, por ejemplo, operaciones de búsqueda y rescate submarino, instalaciones en alta mar, recopilación de datos científicos, protección de costas y comunicaciones submarinas, por nombrar algunos. Los casos de uso de aplicaciones, tanto militares como civiles, continúan creciendo con los rápidos desarrollos en el dominio de las comunicaciones acústicas, junto con la demanda de requisitos y rendimiento mejorados. Existe una gran necesidad de comunicación en tiempo real con vehículos submarinos, tripulados o autónomos, tanto punto a punto como en una red de nodos. La red submarina del futuro consistirá en nodos fijos y móviles que permitirán el intercambio submarino de datos entre sus diversos terminales y una o más estaciones de superficie que actúen como interfaces con el mundo no submarino. Un enlace, probablemente de radio, permitirá las comunicaciones entre las estaciones de superficie y los usuarios remotos. En la actualidad, se están realizando esfuerzos para desarrollar esquemas de codificación y modulación eficientes, técnicas de acceso múltiple, algoritmos de procesamiento de señales y métodos efectivos de comunicaciones móviles submarinas.

Dado que las ondas acústicas se propagan a velocidades muy bajas (aproximadamente 1500 m/s), esto limita gravemente la velocidad a la que pueden transferirse los datos en entornos submarinos. Otra desventaja de la comunicación acústica subacuática es que el canal es de banda estrecha, con valores típicos que a lo sumo son del orden de varios kilohercios. Las velocidades de propagación bajas, la propagación por trayectos múltiples y la pérdida de transmisión variable con la frecuencia dentro del canal (*frequency selective channel*) son las principales adversidades en un medio submarino. El movimiento de los terminales y los cambios en el medio inducen una variación temporal en las rutas de propagación, lo que provoca dispersión Doppler y la distorsión de la señal. El sistema es característicamente de banda ancha, ya que la propagación acústica eficaz requiere comunicación a bajas frecuencias. Por tanto, los grandes márgenes de retardo suelen afectar a los canales UWA

provocando interferencias entre símbolos (ISI) que abarcan un gran número de tiempos de símbolo. Además, la propagación multicamino provoca que la respuesta al impulso del canal se ensanche. Por lo tanto, un módem completo y un modelo de canal subsiguiente deberían considerar un canal con respuesta al impulso ensanchada, cambios Doppler y pérdida de transmisión dependiente de la frecuencia. Si bien los avances recientes se han centrado en mejorar el rendimiento y la robustez en presencia de diversas anomalías intrínsecas al canal submarino, el modelado preciso del canal submarino sigue siendo una necesidad. Se han realizado varios esfuerzos para implementar con éxito módems de comunicaciones para canales de aguas profundas; sin embargo, el trabajo realizado en el ámbito de la comunicación en aguas poco profundas es todavía limitado.

Se han propuesto varios modelos de simulación en la literatura científico-técnica para evaluar el comportamiento o prestaciones de un sistema subacuático de comunicaciones. Sin embargo, dado que la mayoría de ellos son aproximaciones, ninguno de los modelos propuestos podría considerarse un modelo completo en todos los aspectos en el que un sistema UWA típico podría simularse utilizando variables realistas encontradas en un entorno submarino real. Si bien existe una falta de consenso general sobre el modelado preciso de un canal submarino, una buena cantidad de los trabajos publicados se dirigen hacia el modelado matemático del canal UWA. Uno de los objetivos de este trabajo es un esfuerzo por cerrar la brecha existente y, al hacerlo, permitir que aquellos que trabajan en otros medios inalámbricos tengan una mejor comprensión del ámbito UWA.

Los sistemas de comunicación UWA predominantes cuentan con modulación coherente de fase de portadora única, combinada con igualación (*decision feedback equalization*) para enfrentar el problema de los canales submarinos de selectivos en frecuencia y variantes en el tiempo. A medida que aumenta la tasa de símbolos, la selectividad de frecuencia del canal aumenta sustancialmente, lo que hace que los igualadores sean más complejos y se vuelve difícil lograr mejoras sustanciales de régimen binario en sistemas de modulación de portadora única. Además, las rápidas variaciones espaciales y temporales en el canal UWA lo hacen muy hostil para los sistemas de comunicación basados en modulación de portadora única. La modulación multiportadora ofrece una buena alternativa ya que simplifica enormemente el procedimiento de igualación al convertir un canal de frecuencia selectiva en un conjunto de canales de desvanecimiento plano, aumentando las tasas de transmisión. Las técnicas de modulación multiportadora mejoran enormemente la utilización de la anchura de banda y ayudan a lidiar con los efectos de dispersión temporal. Recientemente, varios estudios han evaluado esquemas de múltiples portadoras para permitir la transmisión inalámbrica de datos a velocidades más altas en canales acústicos submarinos.

La multiplexión por división de frecuencias ortogonales (OFDM) es un esquema de comunicación multiportadora probado que tiene capacidades para hacer frente a la selectividad de frecuencia y al retardo de propagación de manera eficaz. Comenzó a llamar la atención por ser una alternativa más simple a los sistemas de portadora única de alta complejidad y alto mantenimiento en los sistemas de comunicación UWA. Lucha contra la interferencia entre símbolos que aparece debida al largo tiempo de símbolo y la ortogonalidad de las subportadoras. Sin embargo, los problemas que surgen del uso de OFDM en UWA son diferentes a los experimentados en los sistemas radioeléctricos comúnmente usados. Dado que el canal submarino es de banda ancha por naturaleza, la sensibilidad de OFDM al desplazamiento de frecuencia debido al movimiento relativo del receptor y el transmisor es un problema grave. Como se mencionó anteriormente, incluso un pequeño movimiento del transmisor

o del receptor induce efectos Doppler en un entorno submarino porque la anchura de banda relativa en un sistema de comunicación UWA es muy grande, dado lo pequeña que es la frecuencia central, mientras que la velocidad de las señales acústicas es muy baja. Esto da lugar a problemas adicionales, como la interferencia entre portadoras (ICI) y el desplazamiento no uniforme sobre el ancho de banda de la señal. A pesar de sus ventajas, uno de los problemas más importantes asociados con OFDM es la alta relación de potencia de pico a potencia media en el transmisor (PAPR). Un gran valor de PAPR generalmente resulta de la superposición constructiva de fases de símbolos aleatorios para crear picos en el dominio del tiempo. Además, dado que el canal UWA es una variante tanto en el tiempo como en la frecuencia, la estimación del canal se vuelve compleja. Con el objetivo de alcanzar mayores regímenes binarios y facilitar la igualación en el dominio de la frecuencia, OFDM resulta ser una excelente opción para un sistema UWA de múltiples portadoras. La mera disponibilidad de rutinas numéricas de cálculo de la transformada rápida de Fourier simplifica el proceso de igualación en el dominio de la frecuencia, en lugar de las complejas técnicas de igualación en el dominio del tiempo. Con el aumento de las velocidades de datos en los futuros sistemas UWA-OFDM, el tiempo de símbolo seguirá disminuyendo, lo que hará que el proceso de igualación sea más complejo.

Casi todos los receptores OFDM utilizan técnicas de estimación de canal para calcular valores aproximados de los parámetros del canal. En la literatura se han explorado varios tipos de técnicas de estimación para estimar con precisión el canal para OFDM. Estos incluyen técnicas de estimación de canal ciegas, semi ciegas y basadas en piloto. Fuera de estas técnicas, la técnica basada en piloto se usa ampliamente, sobre todo debido a la facilidad en su implementación junto con un mejor rendimiento. La desventaja de esta técnica es la sobrecarga del ancho de banda, lo que resulta en una eficiencia espectral reducida. Para los canales UWA, este tipo de técnica es preferible porque los terminales sumergidos suelen tener una potencia y unas capacidades de procesamiento limitadas. En un esquema típico de estimación de canal basado en piloto, algunos símbolos conocidos, también llamados símbolos de entrenamiento, se insertan en los símbolos OFDM transmitidos en ubicaciones pre-especificadas. A continuación, el receptor extrae estos símbolos conocidos y los utiliza para la sincronización y determinación de los parámetros del canal.

Se han utilizado varias técnicas de estimación con los receptores OFDM, como la estimación de máxima verosimilitud (ML), la estimación del error cuadrático medio mínimo (MMSE) y la estimación del error de mínimos cuadrados (LSE). Con el aumento de las tasas de datos en los futuros sistemas UWA, la duración del símbolo seguirá disminuyendo con el aumento de las tasas de datos, lo que hace que el proceso de igualación sea complejo. Como OFDM ofrece una velocidad de datos más alta y una igualación de un toque, es un candidato ideal para los sistemas de comunicación UWA. Además, como la igualación se realiza en el dominio de la frecuencia, la transformada rápida de Fourier (FFT) en el receptor del OFDM reduce aún más la complejidad de la igualación. Sin embargo, hacer frente a la deriva Doppler es un desafío, ya que afectan a la ortogonalidad de las subportadoras debido a las variaciones de fase. Por lo tanto, se ha abordado el problema de la igualación cuando se usa OFDM en canales UWA y se han propuesto varias soluciones en la literatura. En los sistemas basados en radio, se han utilizado igualadores “zero forcing” (ZF), ya que son fáciles de implementar. Sin embargo, estos igualadores sufren de una amplificación de ruido significativa cerca de los ceros del canal en el proceso de invertir el canal por completo. Los igualadores MMSE superan las deficiencias de los igualadores ZF a costa de aumentar la complejidad.

La colocación de un prefijo cíclico (CP) al comienzo de cada símbolo, como intervalo de protección para tratar el problema de ISI, hace que un sistema de comunicación basado en OFDM sea espectralmente ineficaz. Dado que en el transmisor se utiliza un filtro basado en la conformación de pulsos rectangulares, se produce una alta emisión fuera de banda (OOB). La OFDM también tiene una PAPR más alta debido a la adición aleatoria de subportadoras en fase. Para superar las limitaciones de la OFDM y con los rápidos avances en el campo de la comunicación inalámbrica, muchas formas de onda de múltiples portadoras potenciales han surgido como alternativas para las redes de comunicaciones inalámbricas de próxima generación, también llamadas 5G, de las que ya existen algunas instalaciones operativas. Entre ellos, los más destacados son la multiplexión por división de frecuencia generalizada (GFDM), OFDM filtrado (F-OFDM), multiportadora universalmente filtrada (UFMC) y multiportadora de banco de filtros (FBMC). Si bien la investigación y la implementación de estas técnicas prometedoras en el dominio de la radiofrecuencia (RF) han cobrado impulso, se dispone de literatura muy limitada que evalúe la eficacia de estas técnicas cuando se utilicen en un canal submarino.

En un sistema GFDM, los datos a transmitir se colocan en bloques bidimensionales (frecuencia y tiempo) divididos en subsímbolos y subportadoras, con las subportadoras filtradas por un prototipo de modelado de pulsos. Las respuestas de tiempo y frecuencia del filtro prototipo se modifican según los requisitos. Esto conduce a emisiones OOB reducidas en comparación con un sistema OFDM de prefijo cíclico (CP-OFDM). La capacidad de utilizar un espectro fragmentado y una eficiencia espectral variable a través de varias formas de pulso y sus factores de atenuación hace que GFDM sea una opción ideal para las redes UWA de espectro limitado. FBMC es otra técnica prometedora que funciona bien en canales acústicos doblemente dispersivos y tiene una mayor eficiencia de ancho de banda dada la ausencia de un prefijo cíclico. Hay dos tipos de FBMC, en comparación con el sistema de multiportadora de banco de filtros multitono filtrado (FMT-FBMC) y la multiportadora de banco de filtros con modulación de amplitud en cuadratura (QAM) compensado (QQAM). El primero se basa en QAM y el último se basa en offset-QAM. OQAM-FBMC logra la eficiencia espectral en el dominio real mientras que la ortogonalidad se logra en FMT-FBMC al reducir la superposición de las subportadoras en el dominio de frecuencia. El OFDM filtrado es una de las formas de onda candidatas para ser usadas en 5G y una alternativa prometedora a OFDM debido a sus emisiones OOB reducidas. Mientras que el resto del diseño es como en OFDM, en F-OFDM se realiza una operación de filtrado a continuación de la etapa IFFT (FFT inversa) del receptor. En el extremo del transmisor, la señal recibida se filtra y luego pasa a la etapa FFT después de la conversión analógica a digital. UFMC es una realización más generalizada de OFDM y FBMC filtrados donde un grupo de subportadoras se filtra en el dominio de frecuencia. El número total de subportadoras se divide en múltiples subbandas y cada una se filtra a través de un filtro de longitud específica. Esta operación de filtrado da como resultado las emisiones OOB más bajas en comparación con las otras formas de onda. El número de subbandas utilizadas para la transmisión se puede controlar y solo se puede utilizar un número limitado para la transmisión. Si bien las ganancias que ofrecen los sistemas UFMC son prometedoras, su mayor complejidad lo hace menos adecuado para escenarios donde la energía disponible del sistema es limitada, como es el caso de sistemas submarinos autónomos.

La modulación de fase continua (CPM) que emplea estados de fase correlacionados y modulación por desplazamiento de frecuencia de fase continua (CPFSK) se ha utilizado en sistemas de

comunicaciones durante más de cuatro décadas. Sin embargo, se ha llevado a cabo un trabajo muy limitado para incorporar CPM en la codificación de línea de un sistema OFDM especialmente en el dominio de los canales acústicos submarinos. Las ventajas clave de emplear estos esquemas en OFDM son que la señal es eficiente en cuanto a potencia y espectro, tiene una envolvente constante, tiene menos radiación fuera de banda y posee continuidad de fase. Los sistemas OFDM tradicionales utilizan esquemas de modulación sin memoria como PSK y QAM en el codificador de línea. La introducción de correlación entre símbolos vecinos mediante la selección adecuada de los parámetros de codificación es una ventaja clave de los sistemas OFDM basados en CPM. Esto permite técnicas de detección de múltiples símbolos y la memoria puede introducirse mediante la selección adecuada de un único parámetro h , al tiempo que permite una flexibilidad excepcional para que el diseñador del sistema de comunicaciones controle la memoria introducida en el transmisor. Una de las preocupaciones, en los sistemas CPM-OFDM, es la complejidad de los receptores. La detección de señales CPM es un proceso complejo. Sin embargo, se vuelve menos complejo y económico si se emplea un decodificador Viterbi de máxima probabilidad. Restringiendo el índice de modulación h para que sea un número racional, el número de estados en el codificador trellis CPM puede mantenerse en un número manejable que también facilita el uso del algoritmo de Viterbi (VA). La distancia entre la señal recibida y todas las trayectorias enrejadas que entran en cada estado en un instante i es calculada mediante el algoritmo VA. A esto le sigue la eliminación de aquellos caminos que probablemente no sean los más indicados para obtener la máxima probabilidad. Para dos rutas que entran en el mismo estado, se selecciona la que tiene la mejor métrica y se denomina "ruta de supervivencia". Para todos los estados, se seleccionan rutas de supervivencia similares. Al continuar de manera similar, VA avanza más profundamente en el enrejado y las decisiones se toman eliminando los caminos que son menos probables. Aunque tales decisiones no son de máxima probabilidad en el sentido verdadero, si la profundidad de la decisión es lo suficientemente larga, estas decisiones pueden ser casi tan buenas como en el caso de la máxima probabilidad verdadera. La literatura sugiere que los decodificadores Viterbi, aunque subóptimos, cuando se utilizan para detectar señales CPM, ofrecen un rendimiento comparable al de los receptores CPM óptimos, con una complejidad mucho menor. Además, otra ventaja que pueden aportar las señales CPM-OFDM es la reducción de PAPR cuando se utiliza CPM de amplitud múltiple junto con secuencias de transmisión parciales.

A pesar de sus ventajas, uno de los problemas más importantes asociados a OFDM es la alta PAPR en el transmisor. Es un tema ampliamente estudiado en el campo de la OFDM en radifrecuencia, mientras que la limitación computacional y del ancho de banda lo convierte en un problema único en el ámbito acústico. Un valor de PAPR grande suele ser el resultado de la superposición constructiva de fases de símbolo aleatorias que crean picos en el dominio del tiempo. La presencia de amplificadores de potencia no lineales en el transmisor hace que sea obligatorio reducir la potencia media del sistema, lo que provoca una pérdida de rendimiento. Se observan distorsiones dentro de banda y dispersión espectral cuando dicha señal pasa a través de dispositivos no lineales como amplificadores de alta potencia (HPA). Por lo tanto, una alta relación de potencia pico a promedio causa distorsiones dentro de banda en un sistema OFDM y aumenta aún más la complejidad de implementación de otros bloques como analógico a digital (A/D) y digital a analógico (D/A) convertidores. Se han sugerido varias técnicas para reducir la PAPR de los sistemas OFDM, que incluyen: (1) técnicas de distorsión de la señal como, por ejemplo, recorte y filtrado, creación de ventanas, compresión y cancelación de picos;

(2) técnicas probabilísticas que incluyen secuencias de transmisión parcial (PTS), mapeo selectivo (SL), inyección de tono y esquemas de reserva de tono; (3) esquemas basados en codificación, como codificación de bloques lineales (LBC), Secuencias golay y codificación turbo.

Los códigos BCH se han utilizado en sistemas de comunicaciones para la corrección de errores a fin de reducir las tasas de error de bits. Los códigos BCH son códigos cíclicos que operan en un grupo de bits o bloques de datos en lugar de bits individuales. Debido a su capacidad para corregir múltiples errores y la simplicidad en las implementaciones de codificación y descodificación, encuentran su uso en varias aplicaciones. Se observa que el consumo de energía de descodificación de los códigos BCH es una función lineal del número de errores corregidos y la longitud de las palabras de código. El cifrado Vernam fue utilizado por primera vez por Gilbert Vernam en 1917 para cifrar los mensajes telegráficos. También llamado cifrado XOR, su mayor ventaja es que el cifrado y el descifrado se logran utilizando la misma operación. En el transmisor, los datos de entrada se convierten en binarios y se dividen en bloques. Se realiza una operación XOR para los datos del mensaje de entrada con una clave predefinida de la misma longitud de bloque. El texto cifrado obtenido se transmite entonces por lo que el receptor realiza una operación XOR para los datos recibidos con la misma clave para obtener el mensaje original.

En esta tesis doctoral se han propuesto múltiples técnicas para mejorar la viabilidad de un transceptor OFDM para transmisión acústica submarina. En primer lugar, se desarrolla y evalúa un banco de pruebas acústico subacuático basado en el transceptor OFDM de prefijo cíclico (CP) utilizando Matlab. Se supone que el sistema OFDM tiene intervalos de guarda mayores que la dispersión de retardo y se utiliza un igualador ZF, considerando la estimación del canal ideal. Además, el sistema propuesto permite ajustar múltiples parámetros del transceptor y realizar comparaciones de tasa de error de bit (BER) para múltiples escenarios. Además, se ha propuesto una caracterización de canal basada en el modelo de desvanecimiento sombreado de Rician, ya que caracteriza perfectamente la forma en que se comporta un canal UWA de aguas someras. El modelo de canal acústico multitrayecto subacuático se basa en la distribución Rician con restricciones ajustables de ruido y atenuación. El rendimiento del sistema se evalúa para varias relaciones señal/ruido (SNR) en múltiples distancias, número de subportadoras, longitud del prefijo cíclico y dispersiones de retardo. El diseño propuesto permite la implementación y evaluación de una variedad de esquemas de modulación OFDM mediante la variación de diferentes parámetros y realizar simulaciones Monte Carlo para comparaciones de tasas de error de bits junto con la capacidad de sintonizar múltiples parámetros de canal UWA. El modelo se ha utilizado para simular MPSK-OFDM pero también se puede utilizar para otros esquemas de modulación como QAM y DPSK, etc. El banco de pruebas permite evaluar el transceptor para diferentes entornos UWA simplemente modificando los parámetros del canal, como son el ruido ambiental y el desvanecimiento multitrayecto junto con la batimetría y los perfiles geométricos.

En segundo lugar, utilizamos el banco de pruebas OFDM UWA propuesto para la investigación de un algoritmo de estimación de canal asistido por piloto basado en una estimación de error de mínimos cuadrados (LSE). El banco de pruebas emplea un estimador de canal LSE que utiliza subportadoras piloto para UWA OFDM e igualación lineal en el dominio de la frecuencia. El algoritmo de estimación se aplica a un sistema OFDM típico, en el que se utilizan señales piloto para un canal UWA. En este algoritmo, las señales piloto se insertan en subportadoras predefinidas y el receptor estima el canal utilizando el algoritmo LSE. Basándose en el ensanchamiento del retardo del canal, se ajustan la

posición y el número de pilotos, así como también se varían la longitud del prefijo cíclico para mejorar el rendimiento. Además, se han considerado dos igualadores para mejorar el rendimiento de errores de un sistema UWA basado en OFDM. Ambos igualadores emplean subportadoras piloto para estimar el canal UWA. Uno es un igualador de mínimos cuadrados (LS) y el otro es un igualador ZF. Usando simulaciones de banco de pruebas, se observa que, para un comportamiento de error aceptable, el número de pilotos debe ser un cuarto del número de subportadoras. Cualquier aumento adicional en el número de pilotos no mejora el rendimiento del error. Además, si la energía de los pilotos aumenta sin cambiar la energía global del símbolo, el comportamiento de error se degrada. También se observa que los igualadores LS y ZF consiguen un rendimiento aceptable en términos de BER, con el ZF funcionando marginalmente mejor que el LS. La VER del sistema propuesto se evalúa en función de la distancia transmisor-receptor y se observa un comportamiento de error aceptable incluso a 1250 m. Se han proporcionado varios gráficos de tasa de error de bit para mostrar el rendimiento de los igualadores en función de los diversos parámetros. Estas simulaciones se realizan sobre un modelo de canal UWA que utiliza una distribución de desvanecimiento de Rician e incorpora pérdida de absorción y ruido ambiental.

Dado que en los transmisores de los sistemas OFDM se utiliza un filtro basado en la conformación de pulsos rectangulares, el nivel de energía fuera de banda (OOB) es muy alto. La tercera contribución de este trabajo evalúa el rendimiento de un transceptor GFDM para la transmisión acústica subacuática de alta velocidad de transmisión. El análisis de la característica de error del sistema GFDM propuesto se evalúa en diferentes condiciones de canal acústico y distancias transmisor-receptor (TX-RX) y su comparación con CP-OFDM. Se ha presentado una descripción general completa del trabajo realizado en el campo de las técnicas multiportadora de próxima generación más allá de OFDM para canales acústicos submarinos. Se ha llevado a cabo un estudio exhaustivo de las últimas investigaciones en formas de onda candidatas de próxima generación para la comunicación acústica subacuática, se han detallado los resultados encontrados y se han proporcionado algunas recomendaciones. La descripción general abarca todo el trabajo, hasta la fecha, relacionado con las técnicas avanzadas de transmisión multiportadora en un medio UWA que potencialmente reemplazará a OFDM. Dado que se ha realizado muy poco trabajo para determinar la viabilidad del GFDM acústico, se ha analizado el rendimiento del transceptor GFDM propuesto en términos de eficiencia espectral, PAPR, BER y complejidad computacional usando simulaciones y los resultados obtenidos se han comparado con los correspondientes de CP-OFDM. Se ha desarrollado y evaluado un módem basado en GFDM para comunicación UWA utilizando el banco de pruebas propuesto. Se han considerado dos tipos de receptores: filtro adaptado y ZF, y se han evaluado sus prestaciones para varias configuraciones del sistema. Los resultados presentados muestran que el receptor SF supera al receptor de filtro adaptado a valores altos de SNR para casi todas las configuraciones; las excepciones son los casos en los que se emplean formas de pulso de 1ª y 4ª Xia con valores más altos del factor de redondeo, o factor de “roll-off”. La comparación de rendimiento del transceptor GFDM propuesto con el de OFDM muestra que GFDM supera a OFDM en casi 4 dB para una tasa de error de símbolo de 10^{-2} . Para varios valores del factor de caída, el rendimiento del receptor de fuerza cero es mejor que el del receptor de filtro adaptado cuando la forma de pulso empleada es coseno alzado (RC) o raíz de coseno alzado (RRC). Por otro lado, el rendimiento del receptor de filtro adaptado es mejor que el del receptor de fuerza cero cuando la forma de pulso empleada es la 1ª o la 4ª Xia. En conclusión, si el rendimiento de SER es el único

criterio de diseño, una forma de pulso de 1ª Xia con un factor de redondeo de 0,1 parece ser la opción más adecuada. Se concluye que, si bien GFDM es computacionalmente más exigente que OFDM, sigue siendo una técnica atractiva para futuras comunicaciones UWA debido a su mayor eficiencia espectral, flexibilidad y mejor rendimiento de errores. Se ha observado también que el rendimiento PAPR de las señales GFDM era comparable al OFDM con varios casos ligeramente peor que el OFDM. Se observa además que los filtros de conformación de pulsos impactan significativamente en el PAPR de GFDM y el mejor rendimiento de PAPR se exhibe cuando la forma del pulso es 4ª Xia. Además, para todas las formas de pulso, cuanto mayor sea el valor del factor de redondeo, peor será el PAPR.

Como cuarta contribución, se ha propuesto - y evaluado su rendimiento - un transceptor OFDM basado en modulación de fase continua para comunicación acústica subacuática. En nuestra técnica propuesta, el codificador en OFDM tradicional es reemplazado por CPM mientras que se ha empleado el modelo realista del canal acústico submarino propuesto anteriormente. Es pertinente mencionar que se han evaluado las prestaciones de CPM-OFDM binario sin ninguna técnica de reducción de PAPR empleada. La BER del esquema propuesto se ha evaluado utilizando simulaciones Monte Carlo. El comportamiento observado del error establece claramente la superioridad de CPM-OFDM sobre los esquemas OFDM tradicionales. La mejor característica de error se logra cuando el índice de modulación CPM h se elige como $7/16$ o $9/16$. Además, la característica de error del esquema propuesto está dentro de valores aceptables hasta una distancia de transmisor-receptor de 1,5 km. También se evaluó el rendimiento PAPR de CPM-OFDM y se demostró que es casi similar a los ofrecidos por otros esquemas OFDM tradicionales. Además, el rendimiento PAPR del esquema propuesto sugiere que, al igual que otros esquemas OFDM, un esquema de reducción de PAPR es obligatorio para un rendimiento PAPR aceptable de CPM-OFDM para el tipo de canales considerados. Mediante simulaciones por ordenador, se ha demostrado que CPM-OFDM es una alternativa atractiva para las comunicaciones acústicas subacuáticas. La técnica propuesta ofrece un rendimiento de error excelente sin emplear ninguna técnica de igualación. Queda por estudiar el rendimiento de M-ario CPM-OFDM con la técnica de reducción de PAPR.

La presencia de amplificadores de potencia no lineales en el transmisor hace que sea obligatorio reducir la potencia media del sistema, lo que provoca una pérdida de rendimiento. Se observan distorsiones dentro de banda y dispersión espectral cuando dicha señal pasa a través de dispositivos no lineales como amplificadores de alta potencia (HPA). Por lo tanto, una alta PAPR causa distorsiones dentro de banda en un sistema OFDM y aumenta aún más la complejidad de implementación de otros bloques como los conversores analógico-digital (A/D) y digital-analógico (D/A). En los sistemas OFDM acústicos subacuáticos, la reducción de PAPR es todo un desafío, debido a la baja disponibilidad de ancho de banda junto con las limitaciones computacionales y de potencia. La cuarta contribución de esta tesis propone un esquema eficaz, de baja complejidad y multifacético para la reducción de la relación de potencia pico a promedio de un sistema de comunicación basado en OFDM. El esquema de BCH codificado propuesto aprovecha el cifrado XOR y genera códigos Bose Chaudhuri Hocquenghem (BCH) cifrados que tienen un PAPR bajo. Dado que las claves para el cifrado XOR de los códigos BCH se calculan fuera de línea, esta técnica es ideal para sistemas UWA ya que no requiere potencia de cálculo adicional en el transceptor durante la transmisión. La ventaja del esquema propuesto es triple. Primero, reduce el PAPR, segundo, dado que usa códigos BCH, mejora la BER del sistema, y tercero, se introduce un nivel de cifrado a través de cifrado XOR, lo que permite una comunicación segura. Las

simulaciones se realizan en un canal UWA realista para evaluar la técnica propuesta que muestra la reducción de PAPR y BER. Los resultados demostraron que el esquema propuesto efectivamente logra los tres objetivos con un poder computacional mínimo.

This page intentionally left blank

Acknowledgements

This dissertation was made possible through resolute guidance, repeated assurance and meandering through the difficult patches of five years journey by several individuals both in personal and professional capacity of their own.

My parents lent me warranted support from back home, my little ones ensured I stay up late till night to be able to use the laptop only after they slept, my better half helped me with keeping my spirits alive through her well-cooked meals and motivation throughout.

My supervisor Prof. Pablo Otero, who treated me as his protégé to follow his footsteps in years to come and light the candle of wisdom through the same vein in future generations. Apart from his caliber and grip over the subject, his element of providing comfort and guiding along with empathy made it possible, for often the absence of which makes learning a burden and arrests productivity.

Prof. Imran A. Tasadduq, without his guidance and directions I would not have accomplished all this. He provided me with the right tools to successfully complete this research.

I must not forget two individuals whom I lost during the course of this degree, yet they stand tall by my shoulder today and tomorrow- my co-supervisor Prof. Javier Poncela, for his mentorship, direction and keen interest throughout and my friend Usman Khan whose great sense of humor still tickles me in my memories and ears.

I appreciate the excellent facilities and support provided by the Institute of Oceanic Research, Telecom Engineering School, University of Malaga, and the Spanish Government towards my doctoral research.

This page intentionally left blank

Table of Contents

Summary	ix
Resumen.....	xvii
Acknowledgements.....	xxvii
Table of Contents.....	xxix
List of Tables	xxxii
List of Figures	xxxiii
Chapter 1: Introduction.....	1
1.1. Underwater acoustic communication.....	2
1.2. Orthogonal Frequency Division Multiplexing	2
1.2.1. Channel Encoder.....	4
1.2.2. Serial to Parallel Converter	4
1.2.3. Signal Mapper.....	4
1.2.4. Inverse Fast Fourier Transform (IFFT).....	5
1.2.5. Parallel to Serial Converter	5
1.2.6. Cyclic Prefix and Guard Interval	5
1.2.7. Digital to Analog (D/A) Converter	5
1.2.8. IQ (In-phase and Quadrature-phase) Modulation	6
1.2.9. OFDM Receiver.....	6
1.3. Motivation.....	7
1.4. Research Objectives.....	8
1.5. Thesis Contributions	8
1.6. Thesis Organization	11
1.7. Related Publications.....	12
1.7.1. Journals	12
1.7.2. Conference Papers.....	12
Chapter 2: Underwater Acoustic OFDM	13
2.1. Introduction.....	14
2.2. Related Work	15
2.3. Proposed Transceiver.....	16
2.3.1. Modem Architecture	16
2.3.2. Underwater Acoustic Channel	18

2.4.	Simulation Setup.....	21
2.5.	Results.....	23
2.6.	Conclusion	24
Chapter 3: Pilot Aided Channel Estimation and Linear Equalization.....		25
3.1.	Introduction.....	26
3.2.	Related Work	26
3.3.	System Architecture.....	28
3.3.1.	OFDM Transceiver Model.....	28
3.3.2.	Least Squares Channel Estimation.....	29
3.3.3.	Linear Equalization Techniques.....	30
3.3.4.	Channel Model.....	31
3.4.	Simulation Setup.....	33
3.5.	Results.....	34
3.6.	Conclusion	38
Chapter 4: Generalized Frequency Division Multiplexing		39
4.1.	Introduction.....	40
4.2.	Related Work	41
4.2.1.	Generalized Frequency Division Multiplexing.....	42
4.2.2.	Filter Bank Multicarrier	45
4.2.3.	Filtered Orthogonal Frequency Division Multiplexing.....	48
4.2.4.	Concluding Remarks.....	49
4.3.	System Architecture of the Proposed GFDM Transceiver.....	49
4.3.1.	Transmitter Architecture	50
4.3.2.	Pulse Shaping Filters.....	51
4.3.3.	Receiver Architecture	51
4.4.	Shallow Underwater Acoustic Channel	52
4.4.1.	Deterministic channel response	53
4.4.2.	Random channel.....	54
4.4.3.	Noise power	55
4.5.	Simulation Setup.....	56
4.6.	Results.....	57
4.6.1	Power Spectral Density	57

4.6.2.	Peak to Average Power Ratio	59
4.6.3.	Symbol Error Rate	61
4.7.	Conclusion	66
Chapter 5:	PAPR Reduction using Ciphered-BCH Codes.....	67
5.1.	Introduction.....	68
5.2.	Related Work	69
5.3.	System Architecture.....	70
5.3.1.	OFDM Transceiver	71
5.3.2.	XOR Encryption	71
5.3.3.	Shallow Underwater Channel Model	72
5.3.4.	Peak to Average Power Ratio	73
5.4.	Proposed Technique.....	74
5.5.	Simulation Setup and Results	77
5.5.1.	PAPR Performance	77
5.5.2.	BER Performance	82
5.6.	Conclusion	84
Chapter 6:	Continuous Phase Modulation OFDM.....	85
6.1.	Introduction.....	86
6.2.	Related Work	87
6.3.	System Architecture.....	88
6.3.1.	CPM-OFDM Transmitter.....	88
6.3.2.	Continuous Phase Modulation (CPM)	89
6.3.3.	CPM-OFDM Receiver	90
6.3.4.	Shallow Underwater Channel Model	91
6.4.	Simulation Setup and Results	94
6.5.	Conclusion	99
Chapter 7:	Conclusions and Future Work.....	101
7.1.	Conclusions.....	102
7.2.	Future work.....	103
Bibliography	104
Appendix A	114
Curriculum Vitae	114

List of Tables

Table 2.1: Proposed UWA-OFDM system parameters.....	22
Table 2.2: Proposed channel parameters.....	22
Table 2.3: Reference modem comparison.....	24
Table 3.1: Simulation Parameters	33
Table 3.2. BER performance for 64, 128, 256, and 512 subcarriers at a fixed distance of 500 m.	38
Table 4.1: Comparison of Next Generation Multicarrier Waveforms against OFDM	42
Table 4.2: Summary of Work Done in GFDM for UWA Channels	42
Table 4.3: Summary of Work Done in FBMC for UWA Channels.....	45
Table 4.4: Summary of Work Done in F-OFDM for UWA Channels.....	48
Table 4.5: Pulse Shaping Filters [138].....	51
Table 4.6: Simulation Parameters	56
Table 4.7: Channel Parameters	56
Table 5.1: BCH Coding Parameters.....	68
Table 5.2: Selected Keys and Gains Achieved	76
Table 5.3: Transceiver Parameters.....	77
Table 5.4: Channel Parameters	77
Table 6.2. BER values for various modulation indices and SNRs (sorted on values of p and q).	97
Table 6.3. BER values for various modulation indices and SNRs (sorted on values of BER at SNR = 20 dB).	98

List of Figures

Figure 1.1. Typical OFDM transmitter and receiver.....	4
Figure 1.2. Typical signal mapper with (a) BPSK and (b) QPSK scheme.	5
Figure 2.1. Block diagram of OFDM transceiver over the proposed UWA channel.....	18
Figure 2.2. Illustration of the underwater acoustic channel model.	19
Figure 2.3. Pathloss transfer function for various distances.	20
Figure 2.4. Spectrum plots for baseband and up-converted signals.....	22
Figure 2.5. Simulation results for various stages of the proposed channel.....	23
Figure 2.7. BER plots for multiple cyclic prefix lengths with equalization.....	24
Figure 3.1. A typical CP-OFDM transceiver with a channel estimation using pilots.....	28
Figure 3.2. CP-OFDM equalization using pilots.	31
Figure 3.3. Illustration of the underwater channel.....	31
Figure 3.4. Channel impulse response for a shallow underwater acoustic channel.	33
Figure 3.5. BER as a function of the number of pilots for CP-OFDM with a transmitter-receiver distance of 50 m: (a) 64 subcarriers; (b) 128 subcarriers; (c) 256 subcarriers; (d) 512 subcarriers.	34
Figure 3.6. BER as a function of the pilot energies for CP-OFDM with 64 subcarriers, a transmitter-receiver distance of 50 m, and the number of pilots as 16.....	35
Figure 3.7. BER as a function of the equalizer used for QPSK CP-OFDM with 128 subcarriers, a transmitter-receiver distance of 800 m, and the number of pilots as 32.	35
Figure 3.8. BER of CP-OFDM when using the LS and ZF equalizers as a function of the transmitter-receiver distance with 64 subcarriers and 16 pilots.	36
Figure 3.9. BER of CP-OFDM when using the LS and ZF equalizers as a function of the transmitter-receiver distance with 128 subcarriers and 32 pilots.	37
Figure 3.10. BER of CP-OFDM when using the LS and ZF equalizers as a function of the number of subcarriers with a transmitter-receiver distance of 500 m and the number of pilots one-fourth the number of subcarriers.....	37
Figure 4.1. GFDM transceiver architecture.....	50
Figure 4.2. Pulse shapes for the five pulses used in this work.....	51
Figure 4.3. Proposed UWA channel model.	53
Figure 4.4. Frequency dependent absorption.....	54
Figure 4.5. Channel impulse response.	55
Figure 4.6. PSD comparing OFDM with $K = 512$ and GFDM with $K= 512$, $M = 25$, RRC pulse with roll-off of 0.25 and various M_{ON} (actual time slots utilized) values.	57
Figure 4.7. PSD of the transmitted and received signals.	58
Figure 4.8. PSD OOB emissions comparison for various roll-off factors of RRC pulse.....	58
Figure 4.9. PSD OOB emissions comparison for RC pulse with varying values of α	58
Figure 4.10. PSD OOB emissions comparison for various roll-off factor values of 1st Xia.....	59
Figure 4.11. PSD OOB emissions comparison for multiple values of roll-off factor of 4th Xia.....	59
Figure 4.12. PAPR performance for various roll-off factors of RC pulse.	60
Figure 4.13. PAPR performance for RRC pulse with varying values of α	60
Figure 4.14. PAPR performance for various values of roll-off factor of 1st Xia.....	60

Figure 4.15. PAPR performance for various values of roll-off factor of 4th Xia.	61
Figure 4.16. SER performance for both MF and ZF equalizers at various TX-RX distances with $K = 128$, $M = 7$, RC pulse with roll-off value of 0.6, 10 kHz bandwidth and $\mu = 2$	62
Figure 4.17. SER performance for both MF and ZF equalizers at various bandwidths with $K = 128$, $M = 3$, RC pulse with roll-off value of 0.6 and $\mu = 2$	62
Figure 4.18. SER performance for both MF and ZF equalizers for various M_{ON} values with $K = 128$, $M = 25$, RRC pulse with roll-off value of 0.6 and $\mu = 2$	62
Figure 4.19. SER comparison of GFDM and OFDM for $d = 1$ km, $K = 128$, $\mu = 2$ and a similar bandwidth of 5 kHz.....	63
Figure 4.20. SER performance for different roll-off factors for RC pulse shape.	63
Figure 4.21. SER performance for RRC pulse with varying values of α	64
Figure 4.22. SER performance for various values of roll-off factor α with Xia 1 st pulse shape.....	65
Figure 4.23. SER performance for various roll-off factor α values of Xia 4 th pulse shape.	65
Figure 4.24. GFDM and OFDM comparison (higher is better).	65
Figure 5.1. Proposed Ciphered-BCH OFDM Architecture.....	70
Figure 5.2. XOR encryption [168].	72
Figure 5.3. UWA Channel Model [170, 171]	72
Figure 5.4. Channel impulse response	73
Figure 5.5. An example of generation of ciphered BCH(n,k) codes for an 8-subcarrier OFDM system with $k = 4$, $n = 7$	74
Figure 5.6. Possible PAPR gain from a set of multiple random keys.	78
Figure 5.7. Gain in maximum PAPR as a function of various ciphered BCH codes.....	78
Figure 5.8. PAPR performance of the proposed technique for Ciphered-BCH(31, k).....	79
Figure 5.9. PAPR performance of the proposed technique for Ciphered-BCH(63, k).....	81
Figure 5.10. PAPR performance of the proposed technique for Ciphered-BCH(127, k).	82
Figure 5.11. BER performance of C-BCH(31, k), C-BCH(63, k) and C-BCH(127, k).	83
Figure 6.1. Proposed CPM-OFDM transceiver for underwater acoustic channel.	88
Figure 6.2. Trellis diagram for $h = 1/2$	90
Figure 6.3. Constellation diagram for (a) $h = 2/5$ (b) $h = 1/4$	90
Figure 6.4. All the possible paths through the trellis for $h = 1/2$. Solid lines indicate bit 1, broken lines indicate bit 0, and bold lines indicate a typical bit sequence of 1011. The complex numbers beside the figure are the possible CPM mapper output.....	91
Figure 6.5. Shallow underwater acoustic channel model.....	92
Figure 6.6. Shallow acoustic channel characteristics: (a) frequency dependent absorption; (b) channel impulse response.....	93
Figure 6.7. Error performance of CPM-OFDM for 23 rational values of modulation index h with $N = 512$ and transmitter-receiver distance 500 meters.....	95
Figure 6.8. BER performance of CPM-OFDM as a function of transmitter-receiver distances with $N = 512$, $h = 7/16$	96
Figure 6.9. BER performance of CPM-OFDM as a function of channel bandwidth with $N = 512$, $h = 7/16$	97

Figure 6.10. PAPR performance of CPM-OFDM as a function of 23 values of h with $N = 512$ and transmitter-receiver distance 500 m. 99

This page intentionally left blank

Chapter 1: Introduction

This chapter introduces acoustic communication in shallow underwater acoustic channels and a typical OFDM transceiver system. Next, the motivation and research objectives of this dissertation have been indicated. These are followed by our contributions and organization of the dissertation. The list of publications is provided at the end of chapter.

1.1. Underwater acoustic communication

Acoustic communication is rapidly becoming the scheme of choice when it comes to high data-rate wireless underwater communication. Because of their relatively long range underwater, acoustic signals instead of radio waves are sent via hydrophones from transmitter to the receiver. The velocity of sound is less as compared to electromagnetic waves causing the underwater acoustic (UWA) channel to have a larger delay spread. The channel's larger delay spread introduces inter-symbol interference (ISI) that spans over a significant number of symbols. Multipath propagation and a pathloss that is frequency dependent further complicates the issue [1]. Furthermore, Doppler shifts are not uniform across the entire bandwidth since the channel is ultrawideband in nature as the system bandwidth is significant compared to the center frequency. The UWA channel is doubly selective due to multipath fading and a Doppler shift [2].

When compared with radio waves, acoustic waves have lower speeds and the bandwidth is higher when compared with the carrier [1]. The channel is a time variant as Doppler shifts are induced due to the relative motion of the transmitter and receiver [3]. Furthermore, the underwater acoustic channel is wideband and, as fewer path components carry most of the energy, the channel is sparse. It is considered one of the most complex channels [4], having a fairly long delay spread that causes frequency selectivity due to multiple paths and time selectivity due to Doppler effect. Thus, single carrier and multicarrier acoustic communication systems experience ISI and inter-carrier interference (ICI), respectively. Further, acoustic transmission generally utilizes lower frequencies and the bandwidth is extremely limited [5]. This makes the channel wideband in nature as the bandwidth is not negligible compared to the center frequency. Traditionally, single carrier techniques have been used for underwater data transmission but the increasing complexity of the equalization schemes limits their ability to achieve higher data rates [6].

While acoustic signals enable short, medium and long range data transmission in the underwater channel [1], multi-path fading, variation in speed of sound and absorption based pathloss severely limit the communication bandwidth and make the channel complex. Moreover, the UWA channel is wideband in nature since the bandwidth is of the order of carrier frequency [7]. This results in a larger delay spread of the channel and causes ISI. Since the propagation speed of sound is quite low compared to radio frequency (RF) signals, even small motion of the transmitter and receiver in the channel causes Doppler spreading and signal shifts. This complexity of the underwater channel severely limits the transmission data-rates. Consequently, for a better utilization of the limited bandwidth and to increase the data-rate of the system, several multicarrier communication schemes have been suggested in the past two decades [8-14].

1.2. Orthogonal Frequency Division Multiplexing

Unlike traditional frequency division multiplexing (FDM) systems where multiple subcarriers are spaced so that reception is being done using conventional demodulators and filters, "orthogonality" is maintained via a particular mathematical relationship among multiple subcarriers. This eliminates the need for using guard bands, as the subcarriers are spaced such that their sidebands overlap, improving spectrum efficiency. Because of its long symbol duration, OFDM is an effective multicarrier modulation technique against ISI. However, it is prone to frequency offsets due to the motion of receiving and transmitting nodes, in an underwater environment [15]. An OFDM based multicarrier

system splits a channel, that is frequency selective, into several flat fading channels. Delay spread of the channel is used to calculate the length of the cyclic prefix (CP). CP larger than the delay spread, is added to the start of every OFDM symbol to prevent ISI [16]. Since underwater acoustic channel is doubly selective in nature; both time as well as frequency selectivity must be considered. Similarly, since the bandwidth is significantly small in UWA OFDM systems, the subcarrier spacing is reduced introducing ICI [17, 18].

Among the multicarrier modulation schemes, OFDM has been shown to be effective against inter-symbol interference (ISI) because of its longer symbol duration. Due to the motion of transmitting and receiving nodes in a UWA channel, OFDM is prone to frequency offsets [15]. OFDM works by splitting the frequency selective channel into several flat fading channels. Moreover, an OFDM symbol contains a CP whose length is kept equal to or greater than the delay spread of the channel to combat ISI [16]. When using OFDM in a UWA channel, the subcarrier spacing must be reduced as the bandwidth of the UWA channel is significantly small. However, this introduces ICI [17, 18].

OFDM has reliably been used in multicarrier underwater acoustic communication (UAC) systems where high data rate transmission over longer distances is required [19]. It can effectively counter ISI by dividing the bandwidth into smaller overlapping subcarriers that are orthogonal to each other, producing a longer symbol duration [20]. This also simplifies the equalization scheme to a greater degree. Since there is a demand for higher data rates in future underwater acoustic systems, it will cause the symbol duration to become shorter and shorter. This will increase the complexity of equalization [21]. OFDM not only offers higher data rates, it also reduces the complexity of the equalizer to just one tap.

Furthermore, the equalization is carried out in the frequency domain and the fast Fourier transform (FFT) in the receiver reduces the equalizer complexity even further [22]. However, the orthogonality of the subcarriers of an OFDM system is severely affected by Doppler shifts due to variations in phase.

For enabling multicarrier high data-rate acoustic communication, OFDM has recently gained a lot of attention in the UWA domain, and several research works have evaluated the performance of OFDM systems for underwater acoustic channels [7, 21, 23, 24]. It is a reliable and well-studied multicarrier technique with the ability to deal with frequency selectivity of the channel and longer delay spreads [25, 26]. Because of the longer duration of the OFDM symbols, it can counter ISI caused by severe multipath in the UWA channels. OFDM involves parallel transmission of information symbols using many subcarriers.

The block diagram of a typical OFDM transceiver system is given in Figure 1.1. The serial input data stream is a combination of binary digits $\{b_0, b_1, b_2, b_3, \dots\}$ where

$$b_i = 1 \text{ or } 0; i = 0, 1, 2, \dots \quad (1.1)$$

having equal occurrence probability. The data rate is R_b in bits per second (bps) while as the bit duration T_B in seconds will be equal to $1/R_b$.

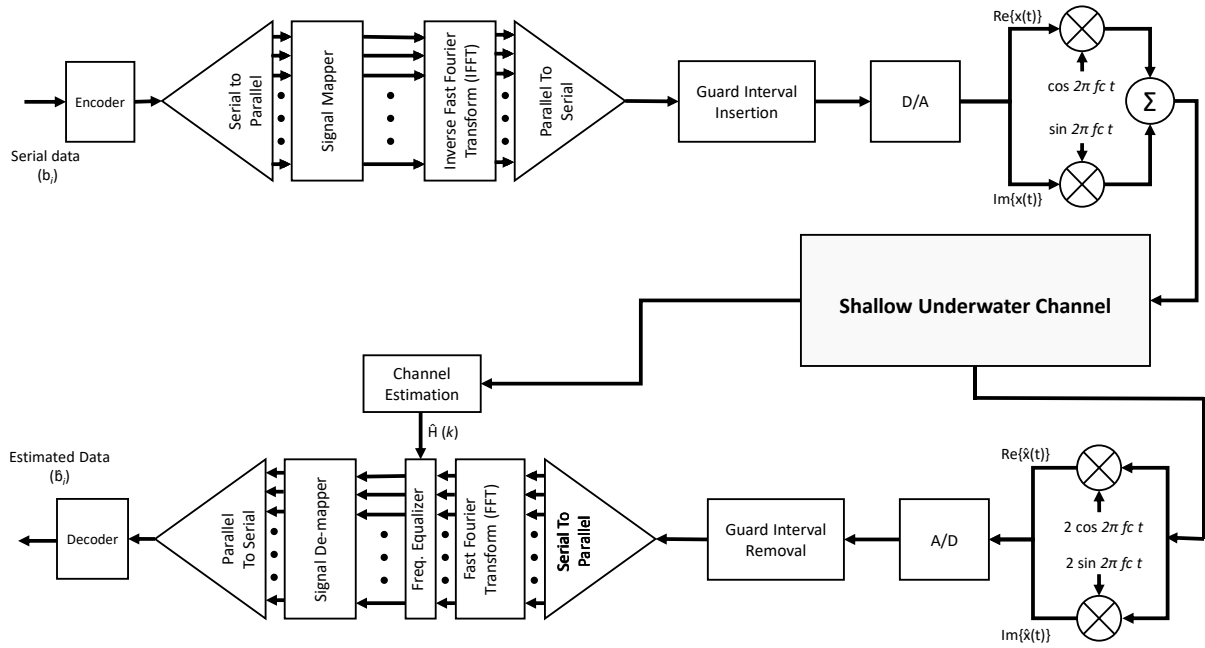


Figure 1.1. Typical OFDM transmitter and receiver.

1.2.1. Channel Encoder

The channel encoder is used to introduce a level of redundancy in the serial input data stream that can be used to counter the effects of various channel impairments like noise and multipath encountered during transmission. The redundant data improves the reliability of the received data and signal fidelity. Several encoding techniques exist such as block codes, turbo codes and convolutional codes etc. Selection of a particular scheme depends on the available bandwidth, complexity of the system and reliability required. Block based channel encoders used in this work takes a block of k bits and maps it to another block of n bits where $n > k$. The level of redundancy is measured using the ration n/k . The inverse k/n is thus called the code rate of the system. The bit duration after channel encoding in seconds will be $T_c = \left(\frac{k}{n}\right) T_b$.

1.2.2. Serial to Parallel Converter

The output binary sequency from the channel encoder block then enters the serial-to-parallel converter where it is divided into N parallel symbols. The serial-to-parallel block acts as a demultiplexer for separating the incoming stream into N sequences. Size of each N outputs is defined by the constellation scheme used at the signal mapper block. For an M point signal mapper, the number of bits in one of the N output sequences will carry symbols carrying information of $\log_2 M$ bits. Therefore, duration of each symbol in parallel stream in seconds will be $T = N * T_s$ where $T_s = T_c * \log_2 M$.

1.2.3. Signal Mapper

The parallel streams of data from serial-to-parallel block are fed into the signal mapper block. The mapping block converts the incoming symbols into points on the complex plane. Thus, the output is a discrete time and amplitude signal. Signal mappers are of two types i.e. discrete memory and memoryless mappers. M-ary phase shift keying and quadrature amplitude modulation are type of memoryless mappers as their output depends only on the input symbols in a particular interval and not on symbols from previous intervals. Such mappers and their receivers are simple to implement. In case

of memory mappers, the output for a given interval depends on the input as well as symbols from the past intervals with differential phase shift keying and differential amplitude phase shift keying being two examples. Unlike memoryless mappers, memory-based mappers are complicated and difficult to implement. For a phase shift keying mapper, the constellation for BPSK and QPSK are shown in Figure 1.2. For BPSK based mapper, the output sequence will carry one bit of information while two bits of information will be carried when QPSK is used.

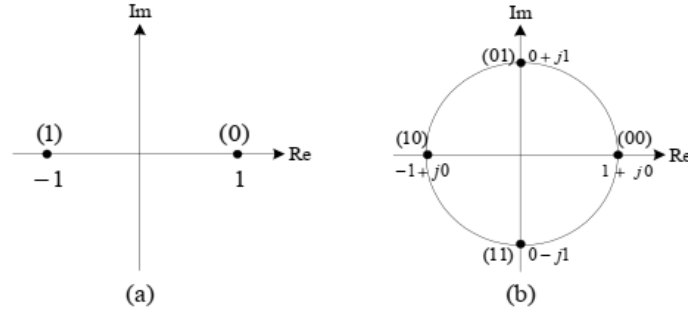


Figure 1.2. Typical signal mapper with (a) BPSK and (b) QPSK scheme.

1.2.4. Inverse Fast Fourier Transform (IFFT)

Signal decomposition into sinusoidal components take place in Fourier transform representations. Using the decomposition property, a signal can be transformed into frequency domain when Fourier transform is employed and vice versa if inverse Fourier transform is utilized. The signal mapper outputs a complex discrete-time signal, whose vector for any k th OFDM symbol duration is given by

$$C_k = [c_{k,0}, c_{k,1}, c_{k,2}, \dots, c_{k,N-1}]^T \quad (1.2)$$

An N-point IFFT block is supplied with the above discrete-time signal which converts it into a transformed discrete time domain signal represented by

$$X_k = [x_{k,0}, x_{k,1}, \dots, x_{k,N-1}]^T \quad (1.3)$$

1.2.5. Parallel to Serial Converter

The parallel to serial module converts an input vector into a discrete-time signal having period N and a sample spacing T_s seconds. The discrete-time signal is given by

$$x[iT_s] = \begin{cases} x_{k,i}; & i = 0, 1, \dots, N - 1 \\ 0; & \text{elsewhere} \end{cases} \quad (1.4)$$

1.2.6. Cyclic Prefix and Guard Interval

In the next step, a cyclic prefix is added to the signal to help with symbol synchronization and to counter the effects of multipath fading. The length of CP or cyclically extended guard interval in OFDM system is kept larger than the longest channel response or the maximum delay spread to maintain orthogonality of the carriers. The total symbol duration becomes $T + T_g$ where T_g is the duration of CP. The extra data transmitted will result in loss of bandwidth but the gains in mitigating interference are much significant.

1.2.7. Digital to Analog (D/A) Converter

This is followed by digital-to-analog (D/A) converter block that converts discrete time signal to continuous time signal. The baseband equivalent time domain signal can be expressed as

$$x_k(t) = 1/\sqrt{T} \sum_{p=0}^{N-1} c_{k,p} e^{j2\pi f_p t} \quad (1.5)$$

The above signal represents a set of modulated subcarriers which are transmitted in parallel. It is fully represented by its samples $x(qT_s)$, $q = 0, 1, 2, \dots, N + G - 1$, over interval $0 \leq t \leq T + T_g$ where G is the number of guard samples.

1.2.8. IQ (In-phase and Quadrature-phase) Modulation

The signal $x(t)$ is fed to the IQ mixer block which modulates the incoming signal to a carrier frequency f_c . The up-converted time-domain signal to be transmitted is

$$s(t) = \sum_{k=0}^{\infty} m_I(t - kT) \cos 2\pi f_c t - m_Q(t - kT) \sin 2\pi f_c t; \quad 0 \leq t < \infty \quad (1.6)$$

where $m_I(t)$ and $m_Q(t)$ are the real and imaginary components of $x(t)$ respectively.

1.2.9. OFDM Receiver

At the receiver side, the recovered signal can be mathematically represented as

$$r(t) = s(t) * h(t) + n(t); \quad 0 \leq t \leq \infty \quad (1.7)$$

where $h(t)$ denotes the impulse response of the channel and $n(t)$ is the added noise. At first, the received signal is down converted using an IQ detector. The resulting baseband signal $\hat{x}(t)$ is corrupted and attenuated version of the original time-domain signal $x(t)$. An A/D converter is used to convert $\hat{x}(t)$ into complex discrete-time signal. Later, the CP is removed from the samples received at the output of A/D converter. The discrete sequence fed to the fast Fourier transform (FFT) block is given by

$$\hat{X}_k = [\hat{x}_{k,0}, \hat{x}_{k,1}, \dots, \hat{x}_{k,N-1}]^T \quad (1.8)$$

The FFT block transforms the sequence \hat{X}_k into a frequency domain vector \hat{C}_k that is given by

$$\hat{C}_k = [\hat{c}_{k,0}, \hat{c}_{k,1}, \hat{c}_{k,2}, \dots, \hat{c}_{k,N-1}]^T \quad (1.9)$$

One benefit of using an OFDM system is the ability to perform frequency domain equalization. The received attenuated and distorted frequency domain discrete sequence can be written as

$$\hat{C}_k = H_k C_k + n_k \quad (1.10)$$

where H_k is the fading channel factor for the k th OFDM symbol. C_k is signal of the k th OFDM symbol and n_k is the additive noise. The estimated sequence \tilde{C}_k after frequency domain equalization is given by

$$\tilde{C}_k = \frac{H_k^*}{|H_k|^2} \hat{C}_k = C_k + \frac{H_k^*}{|H_k|^2} n_k \quad (1.11)$$

The estimated sequence \tilde{C}_k then passes through the signal de-mapping block followed by parallel to serial converter. The received bit stream \hat{b}_l provides estimate of the serial data that was transmitted.

1.3. Motivation

Underwater acoustic communication is currently an active area of research and development and finds its application in various commercial and defense systems e.g., underwater search and rescue operations, offshore installations, scientific data collection, protection of coastlines and submarine communication to name a few. Wireless underwater communication involves transmitting and receiving data below water without a wired interface. Acoustic waves have been reliably used for underwater communication for quite some time since radio waves attenuates inside water while as optical communication is affected by scattering and require extra precision.

While recent advances have focused on improved performance and robustness in deep water channels, research efforts in the domain of shallow underwater acoustic channel modeling have started to take off due to unique nature and the presence of various anomalies intrinsic to shallow under water channels. Low propagation speeds of around 1500m/s, multipath propagation and frequency dependent path loss are the major challenges in an underwater medium. This research aims to better understand underwater acoustic propagation with focus on developing a more robust multicarrier communication schemes to improve performance. In doing so, we also aim to develop a flexible transceiver architecture for a soft modem and a mathematical realization of a shallow underwater channel, that can be exploited for testing various algorithms and physical layer simulation testing.

Prevailing UWA communication systems count on phase coherent single carrier modulation combined with decision feedback equalization to tackle the problem of time-varying and frequency selective underwater channels. Yet, as the symbol rate increases, the frequency selectivity of the channel grows substantially making equalizers more complex and it becomes difficult to achieve substantial rate improvements in single carrier modulation systems. Additionally, rapid spatial and temporal variations in UWA channel makes it hostile for communication systems based on single carrier modulation. Multicarrier modulation offers a good alternative as it simplifies the equalization procedure greatly by converting a frequency selective channel into a set of flat fading channels, boosting transmission rates. Multicarrier modulation techniques thus greatly improve bandwidth utilization and help deal with time dispersal effects. Recently, various studies have evaluated multicarrier schemes for enabling wireless transmission of data at higher rates in underwater acoustic channels.

In prevalent communication systems, OFDM is a proven multicarrier scheme having capabilities to cope with frequency selectivity and delay spreads effectively. It started to get attention for being a simpler alternative to high complexity and high maintenance single carrier systems in underwater communication systems. It fights off ISI because of the long symbol duration and orthogonality of the subcarriers. In quest for higher data-rates and ease of equalization in the frequency domain, OFDM turns out to be an excellent choice for an underwater multi-carrier acoustic communication system. The mere availability of fast Fourier transform blocks simplifies the process of frequency domain equalization instead of complex equalization techniques in the time domain.

However, the issues that arise from using OFDM in UWA are different than those experienced at radio frequencies. Since underwater channel is wideband in nature, the sensitivity of OFDM to frequency offset because of relative motion of the receiver and transmitter is a challenging problem. As mentioned earlier, even a small motion of the transmitter and receiver induces Doppler effects in an underwater environment because bandwidth in a UWA communication system is significant with respect to the center frequency while the velocity of acoustic signals is very low. This results in further

problems such as ICI and non-uniform shift over signal bandwidth. Despite its advantages, one of the foremost issues associated with OFDM is the high peak to average power ratio at the transmitter. A large PAPR value usually results from constructive overlapping of random symbol phases to create peaks in time domain. Since in OFDM systems, a filter based on rectangular pulse shaping is used at the transmitter side, there are high out-of-band leakages. Moreover, since the UWA channel is both time and frequency variant, channel estimation becomes complex. Similarly, with increasing data-rates in future UWA OFDM systems, the symbol duration will keep on decreasing and the amount of channel taps will drastically increase making the equalization process more complex.

1.4. Research Objectives

With aim to build better understanding of multicarrier communication in shallow underwater acoustic channels, core objectives of this work are:

- To develop an OFDM testbed that utilizes a shallow underwater acoustic channel model for assessment of our proposed techniques via simulations.
- To develop an improved channel estimation and equalization scheme for OFDM systems in acoustic channels and assess its performance.
- To explore 5G contender waveforms and their viability for multicarrier underwater acoustic communication and to assess performance of a spectrally efficient multicarrier waveform.
- To exploit channel coding techniques for PAPR reduction of OFDM along with BER improvements and assess their performance for UWA channels.
- To study the mapping of OFDM symbols using the idea of correlated phase states of a CPM signal.

1.5. Thesis Contributions

In this thesis, multiple techniques have been proposed to assess and improve the viability of a multicarrier transceiver for underwater acoustic transmission.

- OFDM transceiver for underwater acoustic channels.* First, an underwater acoustic testbed based on a CP OFDM transceiver is developed. The OFDM system is assumed to have guard intervals larger than the delay spread and a zero-forcing equalizer is used considering ideal channel estimation. Moreover, the proposed system can tune multiple parameters of the transceiver and perform bit error rate (BER) comparisons for multiple scenarios. In addition, a channel characterization is proposed based on Rician shadowed fading model as it perfectly characterizes the way in which a shallow UWA channel behaves. The underwater acoustic multipath channel model is based on Rician distribution with adjustable constraints of noise, UWA absorption and delay spread. System performance is evaluated for various signal to noise ratios (SNR) over multiple distances, number of subcarriers, length of cyclic prefix and delay spreads. The model has been used to simulate M-ary phase shift keying (MPSK)-OFDM although it can be used for other mapping schemes as well such as QAM and differential phase-shift keying (DPSK), etc. The testbed is developed in MATLAB, and it allows for evaluating transceivers for different UWA environments by simply modifying the channel parameters such as ambient noise and multipath fading along with bathymetry and geometrical profiles.

- b) *Pilot aided channel estimation and linear equalization.*** Second, we use the proposed OFDM UWA testbed for the investigation of a pilot-aided channel estimation algorithm. It employs a least-squares error (LSE) based channel estimator using pilot subcarriers for UWA OFDM with linear frequency domain equalization. In this algorithm, the pilot signals are inserted at predefined subcarriers wherein the receiver estimates the channel using LSE algorithm. Based upon channel delay spread, we tune the position and number of pilots as well as vary the length of the cyclic prefix to improve performance. In addition, we explore two equalizers for improving the error performance of an OFDM-based UWA system; a least squares (LS) equalizer, and a ZF equalizer. Using testbed simulations, it is observed that, for an acceptable error performance, the number of pilots should be one-fourth the number of subcarriers. Any further increase in the number of pilots does not improve error performance. Moreover, if the energy of the pilots is increased without changing the overall symbol energy, the error performance degrades. Furthermore, the error performance of the proposed system is evaluated as a function of the transmitter-receiver distance and an acceptable error performance is observed even at 1250 m. We provide several bit error rate plots to show the performances of the equalizers as a function of the various parameters. These simulations are performed over a shallow UWA channel model.
- c) *GFDM transceiver for underwater acoustic channels.*** Since in OFDM systems, a filter based on rectangular pulse shaping is used at the transmitter side, there are high out-of-band leakages. Third contribution of this work assesses the performance of a GFDM transceiver for underwater acoustic high data-rate transmission. Error performance analysis of proposed GFDM system is evaluated over varying acoustic channel conditions and transmitter-receiver distances and its comparison with CP-OFDM. A comprehensive overview of the work done in the field of next generation multicarrier techniques beyond OFDM for underwater acoustic channels has been presented. In doing so, a thorough survey of latest developments in next generation candidate waveforms is performed for underwater acoustic communication, findings, and some recommendations have been detailed. A GFDM based modem for UWA communication is developed and evaluated using the proposed testbed. Two types of receivers have been considered - matched filter and zero forcing and their performances for several system configurations were evaluated. The performance comparison of proposed GFDM transceiver with that of OFDM shows that GFDM outperforms OFDM by almost 4 dB for a symbol error rate of 10^{-2} . For several values of the roll off factor, the performance of the zero-forcing receiver is better than that of the matched filter receiver when the pulse shape employed is raised cosine (RC) or root raised cosine (RRC). In conclusion, if SER performance is the sole design criterion, a pulse shape of 1st Xia with a roll off factor of 0.1 seems to be the most appropriate choice. It is concluded that while GFDM is computationally more demanding than OFDM, it is still an appealing technique for future UWA communications due to its higher spectral efficiency, flexibility, and better error performance. Through our assessments, it was noted that the PAPR performance of GFDM signals was comparable to OFDM with several cases marginally worse than OFDM. It is further noted that pulse shaping filters significantly impact the PAPR of GFDM and the best PAPR performance is exhibited when the pulse shape is 4th Xia. Moreover, for all the pulse shapes, the higher the value of the roll off factor, the worse is

the PAPR. So, a roll-off factor trade-off must be made to achieve low BER, low OOB or low PAPR.

- d) ***CPM-OFDM modulation for underwater acoustic channels.*** As fourth contribution, we propose and evaluate the performance of a continuous phase modulation based orthogonal frequency division multiplexing transceiver for underwater acoustic communication. In our proposed technique, the mapper in traditional OFDM is replaced by CPM while a realistic model of underwater channel proposed earlier is employed. Bit error rate performance of the proposed scheme was evaluated using Monte Carlo simulations. The error performance observed clearly establishes the superiority of CPM-OFDM over traditional OFDM schemes. The best error performance is achieved when the CPM modulation index h is chosen as either 7/16 or 9/16. Furthermore, the error performance of the proposed scheme is within acceptable values up to a transmitter–receiver distance of 1.5 km. The PAPR performance of CPM-OFDM was also evaluated and shown to be almost like those offered by other traditional OFDM schemes. Additionally, PAPR performance of the proposed scheme suggests that like other OFDM schemes, a PAPR reduction scheme is mandatory for acceptable PAPR performance of CPM-OFDM for underwater acoustic channels. Through computer simulations, it has been shown that CPM-OFDM is an attractive candidate for underwater acoustic communication. The proposed technique offers an excellent error performance without employing any equalization technique. The performance of M-ary CPM-OFDM with PAPR reduction technique remains to be studied.
- e) ***PAPR reduction using ciphered-BCH codes.*** The presence of non-linear power amplifiers at the transmitter side makes it mandatory to reduce the average power of the system which causes a loss in performance. As a final contribution of this thesis, we propose an effective, low complexity and multifaceted scheme for peak to average power ratio reduction of an orthogonal frequency division multiplexing based communication system. The proposed coded-BCH scheme takes advantage of XOR-ciphering and generates ciphered BCH codes that have low PAPR. Since keys for XOR-ciphering of BCH codes are computed offline, this technique is ideal for UWA systems as it does not require additional computational power at the transceiver during transmission. The advantage of proposed scheme is threefold. First, it reduces the PAPR, second, since it uses BCH codes, the BER of the system improves, and third, a level of encryption is introduced via XOR-ciphering, enabling secure communication. Simulations are performed in a realistic UWA channel to assess the proposed technique showing PAPR as well as BER reduction. The results demonstrated that the proposed scheme indeed achieves all the three objectives with minimum computational power.

1.6. Thesis Organization

The dissertation consists of seven chapters and has been organized as follows:

Chapter 1 introduces acoustic communication in shallow underwater acoustic channels and a typical OFDM transceiver system. Next, the motivation and research objectives of this dissertation have been indicated. These are followed by our contributions and organization of the dissertation. The list of publications is provided at the end of chapter.

Chapter 2 gives an overview of the proposed underwater acoustic OFDM testbed. Section 2.2 details state of art in underwater acoustic OFDM communication. Section 2.3 demonstrates the proposed transceiver system along with the underwater acoustic channel used. The simulation setup and parameters used are detailed in section 2.4. Section 2.5 discusses the obtained results whereas section 2.6 concludes the chapter.

Chapter 3 introduces pilot aided channel estimation techniques and linear equalization. Section 3.2 of the chapter details the background and literature review. Section 3.3 explains the proposed OFDM system architecture along with the channel estimator and equalizer. It also details the channel model used for simulations. Section 3.4 presents the simulation setup used along with transceiver and channel parameter and section 3.5 has a discussion on the reported results. The chapter is concluded in section 3.6 along with future enhancements.

Chapter 4 is arranged as follows: Section 4.1 discusses the limitation of an OFDM system in terms of spectral efficiency. In section 4.2, we present a survey of all the related work associated with GFDM, OQAM-FBMC, FMT-FBMC and F-OFDM for UWA transmission. In doing so, we also discuss the effects of UWA channel on various multicarrier communication schemes. In section 4.3, we present the proposed GFDM modem for UWA channels. Our proposed underwater channel model that is based on Rician shadowed fading is discussed in section 4.4. Section 4.5 contains simulation setup and section 4.6 discusses the results. Finally, section 4.7 concludes the chapter.

Chapter 5 introduces OFDM limitation with respect to PAPR. Section 5.2 details the recent advances in the domain of PAPR reduction for underwater acoustic channels, coding techniques proposed for UWA OFDM and using coding for PAPR reduction in OFDM systems. Section 5.3 briefly describes the OFDM transceiver architecture, the UWA channel model and the coding technique utilized. Section 5.4 gives a detailed overview of the proposed PAPR reduction technique followed by section 5.5 which is devoted to results and discussions. In the end, a short conclusion is provided in section 5.6.

Chapter 6 details CPM based OFDM systems. Section 6.2 contains a survey of the work done in the domain of CPM-OFDM and related technologies. Section 6.3 presents the details of a typical CPM-OFDM transceiver that includes CPM modulator and demodulator. In sub section 6.3.4, we give a detailed description of the underwater acoustic channel that was used for the simulations. Simulation setup and results are presented in section 6.4 along with discussions on the outcome of our simulation studies. Finally, the chapter is concluded in section 6.5.

Chapter 7 summarizes the dissertation and provides conclusions with the future directions.

1.7. Related Publications

1.7.1. Journals

- Mohsin Murad, Imran A. Tasadduq, Pablo Otero, and Javier Poncela. "Flexible OFDM Transceiver for Underwater Acoustic Channel: Modeling, Implementation and Parameter Tuning." *Wireless Personal Communications* (2020): 1423-1441. DOI: [10.1007/s11277-020-07850-w](https://doi.org/10.1007/s11277-020-07850-w).
- Mohsin Murad, Imran A. Tasadduq, and Pablo Otero. "Towards multicarrier waveforms beyond OFDM: Performance analysis of GFDM modulation for underwater acoustic channels." *IEEE Access* (2020). DOI: [10.1109/ACCESS.2020.3043718](https://doi.org/10.1109/ACCESS.2020.3043718).
- Mohsin Murad, Imran A. Tasadduq, and Pablo Otero. "Pilot-Assisted OFDM for Underwater Acoustic Communication." *Journal of Marine Science and Engineering* (2021). DOI: [10.3390/jmse9121382](https://doi.org/10.3390/jmse9121382).
- Imran A. Tasadduq, Mohsin Murad, and Pablo Otero. "CPM-OFDM Performance over Underwater Acoustic Channels." *Journal of Marine Science and Engineering* (2021). DOI: [10.3390/jmse9101104](https://doi.org/10.3390/jmse9101104).
- Mohsin Murad, Imran A. Tasadduq, and Pablo Otero. "Ciphred BCH codes for PAPR reduction in the OFDM in underwater acoustic channels." *Journal of Marine Science and Engineering* (2022). DOI: [10.3390/jmse10010091](https://doi.org/10.3390/jmse10010091).

1.7.2. Conference Papers

- Mohsin Murad, Pablo Otero and Javier Poncela. "An OFDM Transceiver Model for Experimental Investigations in Underwater Acoustic Channel." 3rd Global Conference on Wireless and Optical Communications (GCWOC'18) (2018), Malaga, Spain.
- Mohsin Murad, Imran A. Tasadduq, and Pablo Otero. "Pilots based LSE Channel Estimation for Underwater Acoustic OFDM Communication." *Global Conference on Wireless and Optical Technologies (GCWOT)* (2020), Malaga, Spain.
- Mohsin Murad, Imran A. Tasadduq, and Pablo Otero. "Linear Equalization Techniques for Underwater Acoustic OFDM Communication." *Global Conference on Wireless and Optical Technologies (GCWOT)* (2020), Malaga, Spain.

Chapter 2: Underwater Acoustic OFDM

Chapter 1 described the motivating factors behind this dissertation along with a basic OFDM modem architecture and the complexities of a shallow underwater acoustic channel. This chapter proposed a reconfigurable testbed that has been divided into two different parts; an OFDM modem architecture and our proposed shallow underwater channel model. A CP-OFDM modem has been proposed that can be reconfigured according to the simulation parameters. The receiver utilizes a frequency domain zero-forcing equalizer considering that the channel parameters are known. In order to simulate a UWA channel, a Rician fading based UWA model is being proposed together with realistic absorption loss and colored Gaussian noise.

The rest of chapter is structured in the following order. Section 2.2 touch upon the background and state of art. Section 2.3 details the proposed OFDM architecture and the channel model with absorption, multipath fading and noise. Section 2.4 introduces the simulation setup used for experimentation and its parameters. Section 2.5 contains the simulation results for different parameter settings. Eventually, section 2.6 has the concluding remarks.

2.1. Introduction

Wireless underwater communication involves transmitting and receiving data below water without a wired interface. In this type of communication, signals generated by the underwater transmitter are sent to the receiver in the form of sound waves – also called acoustic waves – using hydrophones [1]. Acoustic waves have been reliably used for underwater communication for quite some time as they have relatively lower loss and longer range in underwater environments when compared with electromagnetic waves which require larger antennas and high transmit power [27, 28]. Optical waves, on the other hand, have issues such as absorption and scattering due to turbidity. They do not seem to be an appropriate choice of transmission for long range underwater communication [1, 29]. For these reasons, UWA communication is currently an active area of research and finds its application in various systems e.g., underwater search and rescue operations, off-shore installations, scientific data collection, protection of coastlines and submarine communication to name a few [1, 30].

While recent advances have focused on improved performance and robustness in the presence of various anomalies intrinsic to under water channel, accurate modelling of underwater channel is need of the hour. Low propagation speeds of around 1500m/s, multipath propagation and frequency dependent path loss are the major adversities in an underwater medium [1]. System motion and changes in the medium induce time variation in propagation paths causing Doppler spreading and signal shifts. The system is characteristically wideband since effective acoustic propagation requires communication at low frequencies. The fact that the system is wideband, large delay spreads usually affect UWA channels causing ISI spanning a big sum of symbol intervals [31]. Additionally, few propagation paths carry substantial energy making the impulse response of the channel sparse [1]. Hence, a comprehensive modem and subsequent channel model should consider a channel with sparse impulse response, Doppler shifts, frequency dependent path loss and spreading.

OFDM is a proven multicarrier communication scheme having capabilities to cope with frequency selectivity and delay spreads effectively [25, 26]. It fights off ISI because of the long symbol duration. However, the issues that arise from using OFDM in UWA are different than those experienced at radio frequencies. Since underwater channel is wideband in nature, the sensitivity of OFDM to frequency offset because of relative motion of the receiver and transmitter is a challenging problem [31]. As mentioned earlier, even a small motion of the transmitter and receiver induces Doppler effects in an underwater environment because bandwidth in a UWA communication system is significant with respect to the center frequency while the velocity of acoustic signals is very low. This results in further problems such as ICI and non-uniform shift over signal bandwidth [32, 33].

To evaluate the performance of an underwater communication system, several simulation models have been proposed in the literature [34-37]. However, since most of them are approximations, none of the proposed models could be regarded as a complete model in all respects where a typical UWA system could be simulated using realistic variables encountered in a real underwater environment. While there is lack of a general consensus on accurate modelling of an underwater channel, a good amount of published work is directed toward mathematical modeling of the UWA channel [5, 15, 38-40]. This work is an effort to bridge this gap and in doing so, enabling those working in other wireless mediums to have a better understanding of the UWA domain.

In this chapter, a MATLAB based cyclic prefix-OFDM (CP-OFDM) transceiver model for a shallow UWA channel is discussed. Proposed system has the ability to tune multiple parameters of the

transceiver and perform BER comparisons for multiple scenarios. Moreover, we have developed an underwater acoustic multipath channel model based on Rician distribution with adjustable constraints of noise and UWA absorption. A zero-forcing equalizer is used considering ideal channel estimation. System performance is evaluated for various Signal to Noise Ratios (SNR) over multiple distances, number of carriers, and length of cyclic prefix and delay spreads.

2.2. Related Work

Single carrier modulation schemes have been quite common for underwater acoustic communication due to their ease of implementation despite low data-rates [41]. With growing interest in high data-rate underwater acoustic communication, several multicarrier modulation schemes have been explored in the recent past [42]. OFDM has been the scheme of choice in most of the latest empirical works [43]. Several investigations have taken place in coastal waters, where the team has effectively demonstrated high data-rate communication utilizing OFDM and other multicarrier modulation techniques [44]. Yan, H [45, 46] has proposed an OFDM modem utilizing both fixed-point and floating-point DSP hardware and has evaluated the performance of SISO and MIMO OFDM transceivers using a data-set collected earlier from open sea trials. Another modem in [47] has been developed using VHDL and implemented on an FPGA for underwater communication in shallow water. The proposed modem employs a forward error correction technique for user data estimation. A coherent OFDM based communication technique in MATLAB has been proposed in [21] and tested both in air and in an underwater tank with the modems 2 meter apart from each other. Graphical user interfaces are used for both the transmitter and receiver to adjust various basic parameters on each side. A long range OFDM modem architecture for UWA communication in the polar oceans [48], having ice and subzero temperatures, is believed to achieve communication range of nearly 200 kms. The transceiver is tested using two different OFDM techniques; binary phase shift keying (BPSK)-OFDM and Trellis Coded Modulation based OFDM. Authors in [48] also explain the use of an underwater acoustic channel simulator design; based on arctic-BELLTEX ray tracing software using BELLHOP [49] core.

The use of adaptive coding techniques [50] is believed to enhance OFDM based communication system's efficiency by varying a number of parameters according to the prevalent underwater channel conditions. Several different OFDM modems have been designed for being used in autonomous underwater vehicles (AUVs). The transmitter of an AUV modem in [51] utilizes adaptive power adjustments based on receiver feedback loop so the transmit power is always kept at a minimum. The receiver side signal is equalized through a least-squares (LS) algorithm using pilot subcarriers and a power amplifier is used to increase the signal's SNR. The domain of multicarrier UWA transmission is still in its infancy and there is a strong need for an open and easy-to-configure platform that could be utilized for testing and simulations along with parameter tuning and channel manipulations. Recently, several acoustic modem architectures have been proposed based on OFDM for UWA communication in order to achieve higher data rates over longer distances. The proposed modems utilize different OFDM techniques depending upon the applications and the underwater channel conditions that they are designed for.

Authors in [11] have proposed an OFDM modem design for multicarrier UWA communications and have compared two different estimation techniques for Doppler shifts, both based on modeling of the wideband Doppler effect. The Doppler shift that a signal undergoes can be modelled as a non-linear time warp [32], and can be corrected by estimating time warp parameters from observed

signal and using them to reverse the effects of time warp. Doppler estimation technique using a single training sequence (Doppler-sensitive) has been proposed in [33]. It can be used both for Doppler estimation besides channel estimation as the sequence is not dedicated considering only a flat fading channel.

Tran M. in [52] has proposed a continual pilot based Doppler shift estimation and correction in a vertical link OFDM underwater communication. It is assumed that the Doppler rate is the same for all paths. In [53] authors propose a method based on symbol rebuilding in order to compensate for Doppler distortions in underwater channels. However, symbol rebuilding introduces incorrect bits and is computationally expensive. High peak to average power ratio (PAPR) is a known problem in OFDM systems. One way of combatting the issue of high PAPR is by using non-linear transformations. Authors in [54] have proposed companding transformation to improve BER performance while reducing PAPR significantly. The improvements are insignificant at low SNR scenarios.

A discrete cosine based OFDM has been proposed with better BER performance and has been combined with low density parity check (LDPC) codes to decrease PAPR significantly [55]. A discrete Fourier transform spread based OFDM system is proposed for an underwater channel with improved BER performance and low signal PAPR [56]. Andreja et al. [57] propose an adaptive modulation technique employing OFDM in UWA channel where limited bandwidth and fading multipath channel significantly reduces system throughput. Since adaptive modulation techniques have widely been employed in radio-frequency channels, their application in UWA channels is scarce and only preliminary results are available.

Xiaolin et al. [58] have proposed an OFDM transceiver that is capable of long range communications enabled by optimal frequency estimation and selection. They have adopted a 7-ray channel model and used frequency domain equalizer to counter multipath and noise effect. Xin Wang [37] has proposed an OFDM system that employs time reversal technique to avoid the use of CP in order to increase spectral efficiency and has tested the system through a Rayleigh channel model as well as in real underwater channel in a lake. Hardware implementation of a reconfigurable OFDM modem has been proposed in [59] for enhanced adaptability in UWA channel. A number of channel estimation techniques have been utilized based on pilot subcarriers. Erdal et al. [60] have suggested a new channel estimation technique that implements orthogonal matching pursuit algorithm together with maximum a posteriori probability technique. They have used Rician channel for evaluating their proposed model.

2.3. Proposed Transceiver

This section has been divided into two different parts; the OFDM modem architecture and the underwater channel model. A CP-OFDM modem has been proposed that can be reconfigured according to the simulation parameters. The receiver utilizes a frequency domain zero-forcing (ZF) equalizer considering that the channel parameters are known. In order to simulate a UWA channel, a Rician fading based underwater channel is being proposed together with absorption loss model and colored Gaussian noise.

2.3.1. Modem Architecture

An OFDM system for acoustic communication is shown in Fig. 2.1. The random binary data $\{b_0, b_1, b_2, \dots\}$ is generated serially where

$$b_i = 1 \text{ or } 0; i = 0, 1, 2, \dots \quad (2.1)$$

At first, the input bitstream b_i is converted to N parallel outputs. The number of bits assigned to each of the output is defined by the constellation used in the signal mapper. Generally, in an M point signal mapper, the number of bits in each of the N parallel outputs will be $\log_2 M$. The signal mapper modulates these N parallel symbols using the M -ary phase-shift keying (MPSK) technique. Hence, when using BPSK, one bit of information is carried by an output sequence. While as, two bits of information is carried by each output sequence in case of QPSK mapper. An n -th subcarrier will have a baseband frequency of

$$f_n = n * \Delta f; \quad n = 0, 1, \dots, N - 1 \quad (2.2)$$

where Δf is the frequency separation between two adjacent subcarriers. If the entire system bandwidth is B ; $\Delta f = \frac{B}{N}$ and thus the total time duration of each OFDM symbol will be

$$T = \frac{N}{B} \quad (2.3)$$

The signal mapper outputs a complex discrete-time signal, whose vector for any k th OFDM symbol duration is given by

$$C_k = [c_{k,0}, c_{k,1}, c_{k,2}, \dots, c_{k,N-1}]^T \quad (2.4)$$

An N -point Inverse Fast Fourier Transform (IFFT) block is supplied with the above discrete-time signal which converts it into a transformed discrete time domain signal represented by

$$X_k = [x_{k,0}, x_{k,1}, \dots, x_{k,N-1}]^T \quad (2.5)$$

The parallel to serial module converts an input vector into a discrete-time signal having period N and a sample spacing T_s seconds. The discrete-time signal is given by

$$x[iT_s] = \begin{cases} x_{k,i}; & i = 0, 1, \dots, N - 1 \\ 0; & elsewhere \end{cases} \quad (2.6)$$

In the next step, a cyclic prefix (CP) is added to the signal to help with symbol synchronization and to counter the effects of multipath fading. The length of CP or cyclically extended guard interval in OFDM system is kept larger than the longest channel response or the maximum delay spread to maintain orthogonality of the carriers. The total symbol duration becomes $T + T_g$ where T_g is the duration of CP. This is followed by digital-to-analog (D/A) converter block that converts discrete time signal to continuous time signal. The baseband equivalent time domain signal can be expressed as

$$x_k(t) = 1/\sqrt{T} \sum_{p=0}^{N-1} c_{k,p} e^{j2\pi f_p t} \quad (2.7)$$

The signal $x(t)$ is fed to the IQ mixer block which modulates the incoming signal to a carrier frequency f_c . The up-converted time-domain signal to be transmitted is

$$s(t) = \sum_{k=0}^{\infty} m_I(t - kT) \cos 2\pi f_c t - m_Q(t - kT) \sin 2\pi f_c t; \quad 0 \leq t < \infty \quad (2.8)$$

where $m_I(t)$ and $m_Q(t)$ are the real and imaginary components of $x(t)$ respectively. The transmitted signal $s(t)$ then passes through the underwater channel explained in section 2.3.2. At the receiver the same operations are performed in reverse order.

At first, the received signal is down converted using an IQ detector. The resulting baseband signal $\hat{x}(t)$ is corrupted and attenuated version of the original time-domain signal $x(t)$. An analog-to-digital (A/D) converter is used to convert $\hat{x}(t)$ into complex discrete-time signal. Later, the CP is removed from the samples received at the output of A/D converter. The discrete sequence fed to the fast Fourier transform (FFT) block is given by

$$\hat{X}_k = [\hat{x}_{k,0}, \hat{x}_{k,1}, \dots, \hat{x}_{k,N-1}]^T \quad (2.9)$$

The FFT block transforms the sequence \hat{X}_k into a frequency domain vector \hat{C}_k that is given by

$$\hat{C}_k = [\hat{c}_{k,0}, \hat{c}_{k,1}, \hat{c}_{k,2}, \dots, \hat{c}_{k,N-1}]^T \quad (2.10)$$

One benefit of using an OFDM system is the ability to perform frequency domain equalization. The received attenuated and distorted frequency domain discrete sequence can be written as

$$\hat{C}_k = H_k C_k + n_k \quad (2.11)$$

where H_k is the fading channel factor for the k th OFDM symbol. C_k is signal of the k th OFDM symbol and n_k is the additive noise. The estimated sequence \tilde{C}_k after frequency domain equalization is given by

$$\tilde{C}_k = \frac{H_k^*}{|H_k|^2} \hat{C}_k = C_k + \frac{H_k^*}{|H_k|^2} n_k \quad (2.12)$$

The estimated sequence \tilde{C}_k then passes through the signal de-mapping block followed by parallel to serial converter. The received bit stream provides estimate of the serial data that was transmitted.

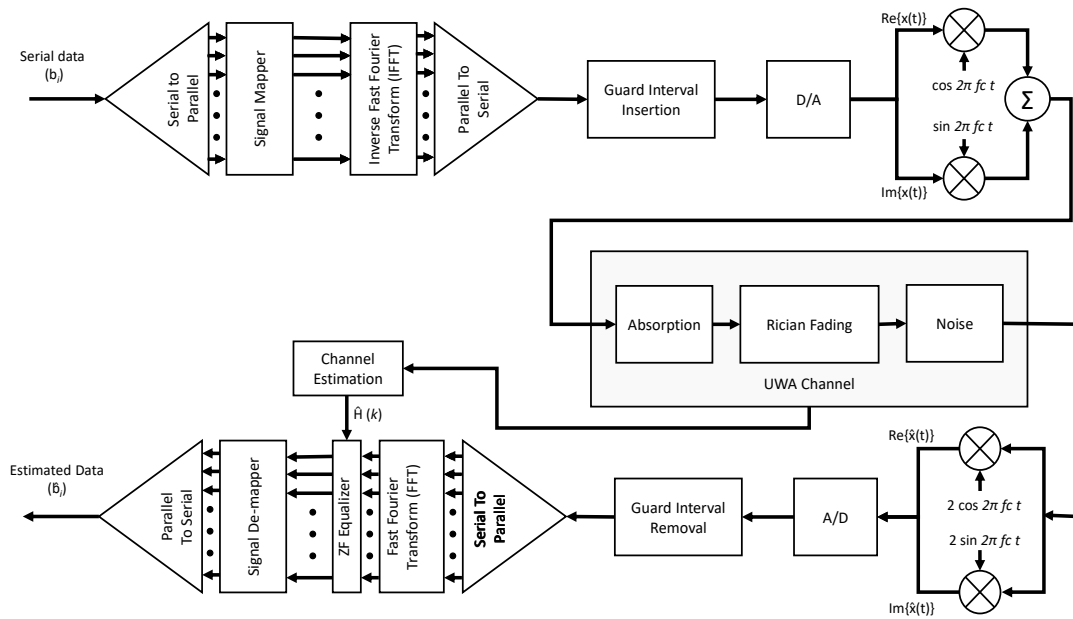


Figure 2.1. Block diagram of OFDM transceiver over the proposed UWA channel.

2.3.2. Underwater Acoustic Channel

As described in section 2.1, OFDM system sends data over several orthogonal carriers. With adequate number of subcarriers and suitable CP length, the orthogonality is maintained even in the presence of frequency-selective fading. Previously, in some implementations, OFDM was simulated for channels where time selectivity was ignored. But due to the doubly selective nature of the UWA channel, both time and frequency selectivity must be considered [18]. For OFDM systems in RF domain, there is a continuous push for higher capacities which is achieved by bringing the subcarriers close together. Correspondingly, since the bandwidth is very low, subcarrier spacing in UWA OFDM systems is also small [17]. This introduces ICI and makes the system susceptible to distortion even with small Doppler shifts. In an underwater channel there are fast variations in the multipath delays due to low velocity of sound. In other words, because the sound velocity is very low compared to radio signals, acoustic signals get severely distorted due to motion [15]. Doppler effect causes different multipath components get dilated and compressed differently causing signal distortion. A time varying UWA channel with discrete multipath components is modeled in [2] as

$$H(t, \tau) = \sum_{p=1}^L A_p(t) \delta(\tau - \tau_p(t)) \quad (2.13)$$

where $\tau_p(t)$ and $A_p(t)$ are the time varying delay and amplitude of p th multipath component respectively, and $\delta(t)$ is the Dirac delta function. The channel envelope response can be split in two factors:

- The deterministic channel response.
- The random fading.

The upconverted signal $s(t)$ in equation 2.8 passes through an underwater channel model that considers the absorption and angular pathloss, multipath fading as well as noise in an underwater channel (Fig. 2.2). The model gives us the ability to control signal to noise ratio, introduce multipath fading using Rician shadowing model as well as the absorption in underwater channel as per Thorp's formula [61]. The parameter settings include selecting ocean depth profile, channel geometry, delay spread, doppler frequency, average multipath gains, parameters affecting the speed of sound underwater, distance between transmitter and receiver and their depth. For a typical UWA channel, the delay spread is approximately 10ms to 20ms and can be as large as 100ms.

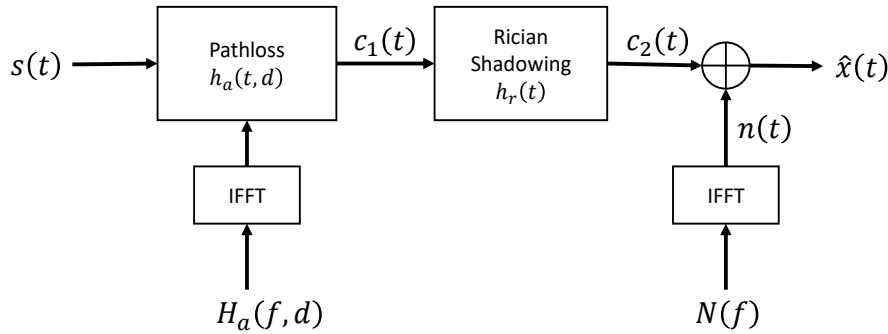


Figure 2.2. Illustration of the underwater acoustic channel model.

Deterministic Channel Response:

The energy of a signal gets attenuated as a function of both frequency and distance. Fundamentally, the path loss of a signal in an underwater medium is a mix of both absorption and geometric spreading. In the frequency domain, the mathematical transmission loss expression of a scalar wave propagating in the positive d direction, when time variation is $e^{j\omega t}$, the deterministic channel transfer function $H_a(f, d)$ [62, 63] follows the equation:

$$H_a(f, d) = A_d e^{-\gamma(f)d} \quad (2.14)$$

where A_d is a scaling constant, d is channel's physical length in meters and γ is the complex propagation constant in m^{-1} which is given by:

$$\gamma(f) = \alpha(f) + j\beta(f) \quad (2.15)$$

where $\alpha(f)$ is the absorption coefficient and $\beta(f)$ is the phase constant. In a UWA channel, the absorption is dependent on frequency of the system because significant energy is lost to heat, decreasing the acoustic pressure. The absorption coefficient $\alpha_{dB}(f)$ is calculated in dB/km using the Thorp formula [61]:

$$\alpha_{dB}(f) = 1.094 \left(0.003 + \frac{0.1f^2}{1+f^2} + \frac{40f^2}{4100+f^2} + 0.000275f^2 \right) \quad (2.16)$$

and converted to Np/m using formula:

$$\alpha(f) = \frac{\alpha_{dB}(f)}{8686} \quad (2.17)$$

The phase constant $\beta(f)$ in $\frac{rad}{m}$ is computed as:

$$\beta(f) = \frac{2\pi f}{c_s} \quad (2.18)$$

where c_s is the sound speed [64] in ms^{-1} , computed as:

$$c_s = 1449.2 + 4.6T - 0.055T^2 + 0.00029T^3 + ((1.34 - 0.01)T)(S - 35) + 0.016 Z_M \quad (2.19)$$

where T is temperature (in degrees Celsius), S is the value of salinity (in parts per thousand), Z_M is depth in *meters*. This equation is also called Medwin's equation [64] and it considers realistic values; temperature in the range of 0° to $35^\circ C$, salinity between 0 to $45 PPT$ and depth of up to $1000 m$. The signal $c_1(t)$ (Fig. 2.2) is then computed as:

$$c_1(t) = h_a(t, d) \otimes s(t) \quad (2.19)$$

$h_a(t, d)$ is obtained by taking IFFT of channel transfer function $H_a(f, d)$ and the symbol \otimes stands for time convolution.

Random Channel:

While there is a consensus on fading models for the RF channel, there lacks an agreement over the fading models used in UWA communication. However, experimental observations suggest that the fading in UW channel is closer to Rician Fading. In this work, the random fading is statistically modeled using a Rician shadowed distribution [65, 66]. The Rician shadowed distribution parameters used in this work are: $k = 2.0$; $m = 0.4$ [65]. The spreading factor $k = 1.5$ can also be considered [67].

$$c_2(t) = h_r(t) \otimes c_1(t) + n(t) \quad (2.20)$$

where $n(t)$ is the additive noise and $h_r(t)$ – the impulse response of the Rician channel [68] – is the IFFT of $H_r(f)$ – the Rician channel transfer function, and is modeled using the Matlab's Rician channel object.

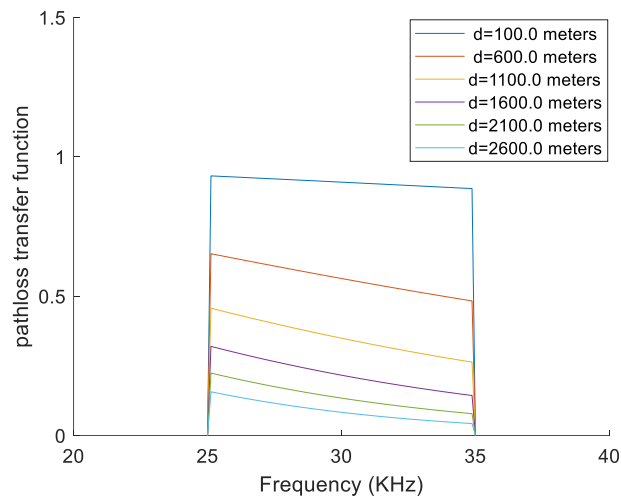


Figure 2.3. Pathloss transfer function for various distances.

Noise Power:

In a realistic UWA channel, the noise is not white and depends upon various acoustic frequencies. We propose using additive white Gaussian noise, since it is the worst-case additive noise. Therefore, signal to noise (SNR) ratio in decibels (dB) for a given transmitted signal is given by

$$SNR = 10 * \log_{10} \frac{c_2(t)^2}{n(t)^2} \quad (2.21)$$

Thus, the noise power $\overline{n^2(t)}$ added to the signal is

$$\overline{n^2(t)} = \overline{c_2(t)^2} \times 10^{-SNR/10} \quad (2.22)$$

where $c_2(t)$ is the signal at the output of the multipath fading block. For a more realistic realization of the ambient noise in an underwater channel, the recommended approach is to model frequency dependent noise from four sources; thermal, shipping, turbulence and wave noise [69]. The noise is modelled as colored Gaussian noise and the power spectral densities (PSD) in dB *re* $\mu Pa/Hz$ are given as:

$$10 \log N_{shipping}(f) = 40 + 20(s - 0.5) + 26 \log f - 60 \log(f + 0.03) \quad (2.23)$$

$$10 \log N_{turbulence}(f) = 17 - 30 \log f \quad (2.24)$$

$$10 \log N_{wave}(f) = 50 + 7.5\sqrt{w} + 20 \log f - 40 \log(f + 0.4) \quad (2.25)$$

$$10 \log N_{thermal}(f) = -15 + 20 \log f \quad (2.26)$$

where s is the shipping activity factor having a value 0 for light shipping, 0.5 for moderate and 1 for high shipping. w is the wind speed in ms^{-1} and f is frequency in KHz . The total noise PSD comes out to be

$$N(f) = 10 \log \left(10^{\frac{N_{shipping}(f)}{10}} + 10^{\frac{N_{turbulence}(f)}{10}} + 10^{\frac{N_{wave}(f)}{10}} + 10^{\frac{N_{thermal}(f)}{10}} \right) \quad (2.27)$$

Fig. 2.2 illustrates the complete UWA channel model, where $s(t)$ is the transmitted signal and $\hat{x}(t)$ is the received signal. The proposed channel has been divided into three unique components; initially the transmitted signal is convolved with the IDFT version of the deterministic channel response and the resulting signal $c_1(t)$ undergoes shadowing based on Rician distribution. Finally, AWGN or frequency dependent ambient noise is added to the signal $c_2(t)$.

2.4. Simulation Setup

The proposed system is simulated in MATLAB and we have performed our tests using BPSK-OFDM with CP. A separate script file is used for declaring and setting system parameters including number of carriers N , total number of symbols to be transmitted N_{sym} , number of pilots (if any) N_p , bandwidth of the system Bw , carrier frequency for the IQ modulator F_c , subcarrier spacing $delF$, duration of guard interval T_g , CP length based on guard interval N_{cp} , the total duration of an OFDM symbol T_{total} and the number of bits in that symbol N_{bits} .

It is followed by initializing channel parameters including the SNR vector snr , doppler frequency F_d , the path delays τ and path gain vectors P_g , sampling frequency F_s , the Rician K-factor K and the variables for temperature T , depth Z , salinity S and distance D . Minimum and maximum frequency limits F_{min} and F_{max} are computed using bandwidth Bw to create a frequency vector for calculating absorption and phase constants and ambient noise PSD. To generate the binary data for CP-OFDM, Matlab's pseudorandom number generator `randi()` function is used to create a binary vector of uniformly distributed random data for one OFDM symbol. The data is then placed in a frequency vector and zeroes are added if null carriers are required.

Table 2.1: Proposed UWA-OFDM system parameters

Parameter	Variable	Value
Modulation type	M	2 (BPSK), 4 (QPSK), ...
Number of symbols	Nsym	1000
Cyclic prefix length	Ncp	Multiple
Bandwidth	Bw	2.5KHz – 10KHz
Carrier frequency	Fc	30KHz
Number of carriers	N	64, 128, 256, ...

Serial to parallel operation is performed via transpose operation. Using the `ifft()` function, these vectors are converted to their complex time domain forms and normalized. Cyclic prefix is added next and the whole process is repeated in a loop N_{sym} times till we have all the baseband complex symbols to be transmitted.

Table 2.2: Proposed channel parameters

Parameter	Variable	Value
Channel taps	ntaps	2, 3, 4, ...
Tx-Rx distance	d	100-1500KM
Rician K-factor	k	1.5, 2
Tx depth	tx	20m
Rx depth	rx	20m
Maximum Doppler frequency	fd	3Hz, 6Hz, 10Hz, ...

The plot for all the baseband symbols is given in Fig. 2.4a. A time vector of length T_{sym} is generated for IQ modulation and symbol by symbol up-conversion is performed using carrier frequency F_c . The resultant signal (Fig. 2.4b) is then passed through the channel after passing through a bandpass filter.

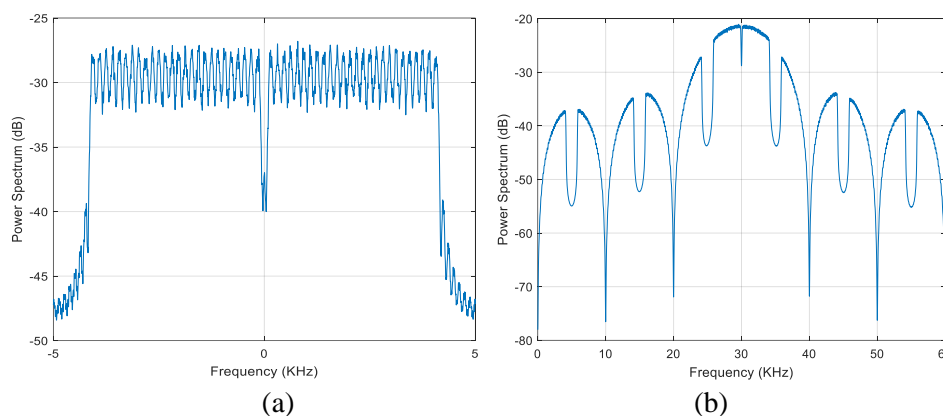


Figure 2.4. Spectrum plots for baseband and up-converted signals.

Transfer function for the propagation loss of the channel is computed and its inverse Fourier transform is taken using `ifft()` function. The up-converted signal is then convolved using the `conv()` function and the resultant signal is passed on to the Rician channel object. For this work, we have used Matlab's RicianChannel system object that filters a signal through a channel with multipath Rician fading. We then use the `awgn()` function which measures the signal power and then adds uniform white Gaussian noise to the faded signal based on the snr value in decibels. The same methods are used at the receiver side in reverse order with the exception of the equalizer. Since we are using a ZF equalizer considering perfect channel estimation, the known channel estimates are passed on to the equalizer for frequency domain equalization and the estimated symbols are then used for BER calculations.

2.5. Results

Figure 2.5 shows a plot of BER vs SNR at various stages, when no channel correction techniques have been employed. For this simulation, the transmitter-receiver distance is kept at 1 km. The multipath channel is assumed to have three paths having delays of 0, 2.5 and 3 ms respectively. BER is the best when only AWGN is present. BER degrades when the effect of water absorption is added. BER degrades even further when the effect of multipath fading is also included in addition to AWGN and absorption. This is to be expected since no equalization has been performed on the received signal.

Figure 2.6 shows a plot of BER Vs SNR with zero-forcing equalization when the transmitter-receiver distance is varied from 100 meters to 2,100 meters. The multipath channel is assumed to have two paths with path delays of 0 and 1.5 ms respectively. It can be seen that due to equalization, BER has improved considerably. Moreover, the BER degrades as the transmitter-receiver distance increases. This degradation is expected as more the distance between the transmitter and receiver, more is the pathloss as has been shown in Fig. 2.3.

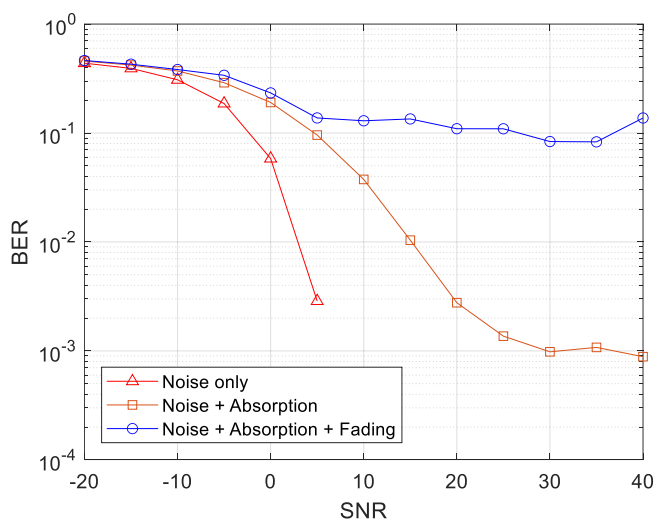


Figure 2.5. Simulation results for various stages of the proposed channel

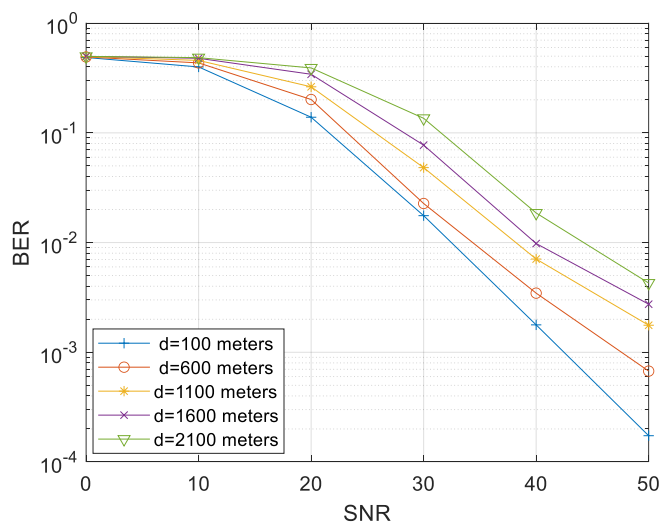


Figure 2.6. BER plots for multiple distances for a multipath channel with equalization.

Results in Fig. 2.7 demonstrate the benefits of cyclic prefix to counter ISI. For a 3-tap channel with highest delay equal to period of four symbols, it can be observed that there is a significant

improvement when using CP length greater than the maximum delay spread i.e. CP length greater than 4. But there will not be any further improvements for any longer length cyclic prefixes as evident from the BER results above.

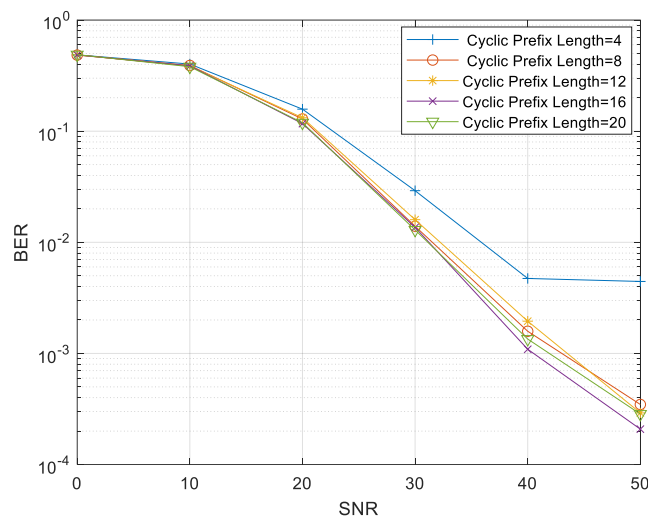


Figure 2.7. BER plots for multiple cyclic prefix lengths with equalization.

Simulation results of proposed model were compared against a reference model of Chitre et al [70] using the same channel parameters and delay profile as has been mentioned in Tables I and II of Reference [70]. Table 2.3 details the BER comparison of the two models for identical range, cyclic prefix length and number of carriers. It can be seen that the BER results of proposed model are comparable with those of [70] for an uncoded OFDM system validating the model and the results presented in this thesis.

Table 2.3: Reference modem comparison

Number of Carriers	Range	CP Length	Simulated BER [Proposed model]	Simulated BER [32]
128	800 m	32	1.9×10^{-2}	8.1×10^{-2}
512	800 m	128	4.7×10^{-2}	1.2×10^{-1}
128	1000 m	32	3.6×10^{-2}	0.8×10^{-1}
512	1000 m	128	5.1×10^{-2}	1.1×10^{-1}

2.6. Conclusion

A reconfigurable OFDM soft modem architecture for underwater communication has been presented along with a capability to modify and tune various parameters. An underwater channel model that incorporates ambient noise and AWGN, acoustic absorption in water and multipath has been developed in MATLAB. Rician shadowing model has been assumed for the multipath channel. Simulations have been carried out using Monte-Carlo simulations and BER plots have been presented. Results have been shown with and without equalization. Zero-forcing equalization has been used assuming perfect channel information. The model has been used to simulate MPSK-OFDM but it can be used for other mapping schemes as well such as QAM and DPSK, etc. The ability to add different channel estimation techniques further allows us to try and test various methods used to reduce bit errors. The channel model allows for evaluating the transceiver for different UWA environments by simply modifying the channel parameters such as ambient noise and multipath fading along with bathymetry and geometrical profiles.

Chapter 3: Pilot Aided Channel Estimation and Linear Equalization

Chapter 2 described various motivating factors behind this dissertation including the development of a testbed based on a soft reconfigurable OFDM modem architecture and a shallow underwater channel model for assessment. This chapter proposes a pilot-based channel estimation technique, utilizing the same testbed, while comparing two equalizers to improve the error performance of an OFDM-based UWA system [71]. Both equalizers employ pilot subcarriers to estimate the UWA channel. One equalizer is a LS equalizer and the other is a ZF equalizer. Using computer simulations, it is observed that, for an acceptable error performance, the number of pilots should be one-fourth the number of subcarriers. Moreover, if the energy of the pilots is increased without changing the overall symbol energy, the error performance degrades. It is also noted that both the LS and ZF equalizers give an acceptable error performance with the ZF performing marginally better than the LS. Furthermore, the error performance of the proposed system is evaluated as a function of the transmitter-receiver distance and an acceptable error performance is observed even at 1250 m.

The chapter is organized as follows. Section 3.2 details the background and state of the art research. Section 3.3 explains the OFDM system architecture along with the channel estimator and equalizer. The channel model is detailed in section 3.4. Section 3.5 presents the results from the simulations and provides a discussion on the reported results. The chapter is concluded in section 3.6 along with future enhancements.

3.1. Introduction

Almost all OFDM receivers use a channel estimation technique to compute approximate values of the channel parameters. Several types of estimation techniques have been explored in the literature to accurately estimate the channel for OFDM. These include blind, semi-blind, and pilot-based channel estimation techniques. Out of these techniques, the pilot-based technique is widely used mainly because of the ease in its implementation along with a better performance. The downside of this technique is the bandwidth overhead, resulting in poor spectral efficiency [72-74]. For UWA channels, this type of technique is preferable because the underwater nodes have limited power and limited processing capabilities. In a typical pilot-based channel estimation scheme, a few known symbols—also called training symbols—are inserted into the transmitted OFDM symbols at prespecified locations. These known symbols are then extracted by the receiver and are used for the synchronization and determination of the channel parameters [75]. Several estimation techniques have been used with OFDM receivers such as maximum likelihood (ML), minimum mean square error (MMSE) estimation, and least squares error (LSE) estimation.

With the rise in data rates in future UWA systems, the symbol duration will keep on decreasing with the increasing data rates making the equalization process complex [21]. As OFDM offers a higher data rate and one-tap equalization, it is an ideal candidate for UWA communication systems. Moreover, as the equalization is performed in the frequency domain, the fast Fourier transform in the receiver of the OFDM further reduces the equalization complexity [31]. However, coping with Doppler shifts is a challenge as they affect the orthogonality of the subcarriers due to phase variations. Hence, the problem of equalization when using OFDM in UWA channels has been addressed and several solutions have been proposed in the literature. In radio-based systems, zero forcing equalizers have been used as they are simple to implement. However, they suffer from significant noise amplification near to the zeroes of the channel in an attempt to invert the channel completely. MMSE equalizers overcome the shortcomings of ZF equalizers at the cost of complexity.

The work proposed in this chapter adds to the body of research in two ways. First, investigation of a channel estimation algorithm based upon a least squares error technique is carried out. This algorithm is applied to a typical OFDM system, in which pilot signals are used for a UWA channel. In this algorithm, the pilot signals are inserted at predefined subcarriers and the receiver estimates the channel using the LSE algorithm. Second, we compare LSE estimator against ZF equalizer with known channel state information. Based upon the channel delay spread, we tune the position and number of pilots as well as vary the length of the cyclic prefix to improve performance. Using a Monte Carlo simulation, we provide several bit error rate plots to show the performances of the equalizers as a function of the various parameters. These simulations are performed over a UWA channel that uses a Rician fading distribution and incorporates absorption loss and ambient noise.

3.2. Related Work

In the wireless domain, pilot-based estimation has long been used with multicarrier systems such as OFDM. In the UWA channels, several estimation algorithms have also been suggested when using OFDM systems. In the following, we present an overview of the work recently undertaken in this domain, mainly for UWA channels.

An adaptive channel estimation technique was proposed in [76] for a MIMO-OFDM system. In this work, a least squares estimation algorithm was used along with a block-adaptive method. This had the additional advantage of avoiding the computational complexity of a matrix inversion. The accuracy of the proposed algorithm depended upon its ability to determine the channel parameters from the pilot estimates of the previous block. An algorithm that inserted multiple pilots in an OFDM system to estimate the UWA channel was investigated in [24]. The authors employed three types of pilots, namely, comb, block, and scatter. It was shown that the scatter type of pilots gave the best performance in terms of robustness against the time selectivity and frequency selectivity of the channel. In [77], a deep neural network (DNN) was trained on estimated pilot symbols. The trained network was then used to estimate the impulse response of the underwater channel. A simulation testbed that used OFDM for a UWA communication system was presented by Wang et al. [23]. The results were reported for two channel estimation techniques, namely, LSE and MMSE. A channel estimation scheme designed for radio frequency CP-OFDM that used LSE was presented in [78]. The authors also compared the estimated channel with a real channel. Using pilots for an adaptive estimation of the UWA channel, a recursive least squares algorithm was proposed in [79] to estimate the channel for a MIMO-OFDM system. Moreover, a maximum likelihood decoder was employed to estimate the transmitted data. In another publication [80], the authors used multiple channel sensing and estimation techniques to capture the time-varying behavior of a UWA channel.

One of the advantages of OFDM is that it simplifies the equalization in the frequency domain. The literature is full of equalization techniques for OFDM with a few of them covered in this section. In [7], the authors proposed a zero-padded OFDM that used a mean square error combining technique to estimate the transmitted data after obtaining the channel estimates. A high data rate acoustic modem for coherent OFDM was proposed by Sean et al. [21]. In this work, the received signal was equalized using a scalar inversion of the channel estimates. Using a decision feedback equalizer along with time reversal was employed for an OFDM system over a UWA channel by Gomes et al. [81]. When comparing the computational complexity of the proposed equalizer, it was of the same order as that of a single carrier system. In [82], it was argued that as zero forcing equalizers have a tendency to enhance noise, they should not be used for a UWA OFDM system. They also argued that a minimum mean square error equalizer is not only complex, but it also needs an estimate of the SNR. Consequently, the authors proposed a low complexity zero forcing equalizer that addressed these concerns. In another work [83], a combination of matching pursuit and maximum a posteriori algorithms was used to estimate a UWA channel. The authors also employed a linear minimum mean square equalizer at the receiver. An iterative least squares equalizer was proposed in [84] and its performance was compared with a conventional frequency domain equalizer. In [85], a channel was divided into several sub-bands. Each sub-band was treated as a narrowband channel. A minimum mean square error equalizer was employed with soft information. The complexity was reduced by exploiting the narrowband sub-bands. An equalizer that had a single tap and used a least mean square algorithm was reported in [86]. The proposed equalizer was also compared with a mean square error equalizer implemented in an OFDM system over a UWA channel. In [87], turbo equalization was used in field experiments performed in shallow water. The trials were conducted for three months with a negligible Doppler but a variable multipath channel. It was shown that turbo equalization with a 4-PSK modulation outperformed a decision feedback equalizer.

3.3. System Architecture

This section presents the architecture of OFDM transceiver, and the equalization schemes proposed. A typical OFDM transceiver in a UWA channel is presented in the first subsection. A detailed description of the least squares channel estimator is given in the second subsection. Lastly, linear equalization techniques are discussed followed by the shallow underwater acoustic channel model.

3.3.1. OFDM Transceiver Model

A typical pilots-based CP-OFDM transceiver model working in a UWA channel is shown in Figure 3.1. Let B represent the vector of a serial binary bit stream where each element of B is either a binary 0 or 1. This binary stream is fed into the OFDM transmitter. A serial to parallel converter, represented by S/P in the figure, converts the serial stream into a parallel stream that has N symbols where N is the number of subcarriers.

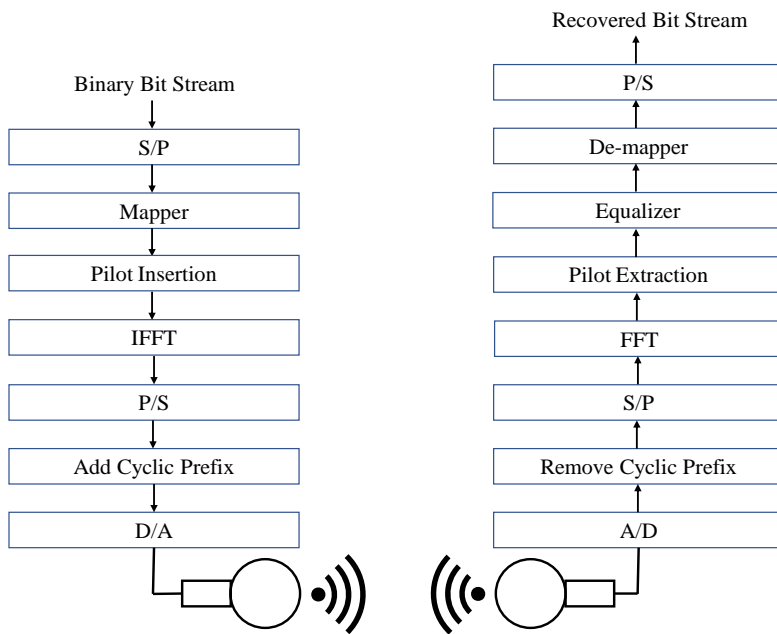


Figure 3.1. A typical CP-OFDM transceiver with a channel estimation using pilots.

Each parallel stream of N samples makes one OFDM symbol where each element of N consists of $\log_2 M$ bits. M is the modulation order to be used in the next block, i.e., the mapper. For example, if the mapper is BPSK, each symbol at the output of the S/P block will have only one bit. On the other hand, if the mapper is QPSK, each symbol will consist of two bits. The parallel stream of N symbols then passes through the mapper and is converted into complex numbers based upon the type of mapper used. Let these complex numbers be represented by a vector C_k where k is the k th OFDM symbol and each element of the vector C_k is a complex number. Mathematically, this can be shown as:

$$C_k = [c_{k,0}, c_{k,1}, c_{k,2}, \dots, c_{k,N-1}]^T. \quad (3.1)$$

In the proposed OFDM system, pilots are inserted at predetermined intervals into each OFDM symbol. This is achieved by using certain subcarriers as pilots. Further details of these pilots will be described later in the chapter. The parallel stream of complex numbers then passes through the inverse fast Fourier transform that transforms the complex numbers into another set of complex numbers that are orthogonal to each other. Let this new stream of complex numbers be represented by X_k , which can be shown mathematically as:

$$X_k = [x_{k,0}, x_{k,1}, \dots, x_{k,N-1}]^T. \quad (3.2)$$

The P/S block then converts the parallel stream of complex numbers into a serial stream. To combat the effects of a multipath, a cyclic prefix—denoted by CP—is appended to each OFDM symbol before it is converted into an analog signal for the final transmission. If T represents the duration of the OFDM symbol and f_p the frequency of the p th subcarrier, then the transmitted signal can mathematically be expressed as:

$$x_k(t) = 1/\sqrt{T} \sum_{p=0}^{N-1} c_{k,p} e^{j2\pi f_p t}. \quad (3.3)$$

In the above equation, \sqrt{T} is a scaling factor. After passing through the UWA channel, the signal is processed by the receiver in reverse order, as shown in Figure 3.1. Let $\hat{x}(t)$ be the received signal that is a noisy and distorted version of the transmitted signal. This signal is converted into a digital signal by the A/D block. In the next step, the cyclic prefix is removed. The S/P block converts the serial stream into parallel streams of N symbols and the fast Fourier transform (FFT) is applied to each parallel stream. As the signal has been distorted by the UWA channel and noise has been added to it, the complex numbers at the output of the FFT can mathematically be represented as:

$$\hat{C}_k = H_k C_k + n_k. \quad (3.4)$$

In the above equation, \hat{C}_k is a vector that represents the noisy and distorted version of the transmitted vector C_k . H_k is the channel transfer function affecting the k th OFDM symbol and n_k is the additive white Gaussian noise affecting the k th OFDM symbol. The pilots are extracted next and used by the equalizer to neutralize the effects of the UWA channel and estimate the transmitted complex numbers. The de-mapper block converts the estimated OFDM symbol of complex numbers into digital data and the P/S block converts the parallel stream of digital data into a serial stream.

3.3.2. Least Squares Channel Estimation

In this work, we used the pilot-based channel estimation approach proposed by Cai et al. [88]. Originally, the approach was used for a single input multiple output (SIMO) OFDM system. We applied the same approach for a single input single output (SISO) OFDM for a shallow UWA channel-based model on a Rician distribution, explained in sub section 3.3.4. In this approach, the channel estimates were obtained via pilots and then maximum ratio combining (MRC) was used to estimate the transmitted data. Consider the OFDM system of Figure 3.2. Let:

- I_p be the set of those subcarriers that carry the pilots;
- $y[n]$ be the signal on n th subcarrier after the extraction of pilots;
- s_n be the pilot symbol with $n \in I_p$;
- $H_{k,n}$ be the channel transfer function for n th subcarrier of the k th OFDM symbol;
- ω_n be the AWGN on the n th subcarrier;
- \mathcal{E}_p be the transmit power of the pilot symbol.

The signal $y[n]$ is then given by:

$$y[n] = \sqrt{\mathcal{E}_p} H_{k,n} s_n + \omega_n, n \in I_p. \quad (3.5)$$

Let $h = [h_0, \dots, h_{L-1}]^T$ represent a vector of the impulse response of a Rician channel where each element of the vector is a complex Gaussian variable with a zero mean and L represents the number of taps. Consider a matrix F having $L \times N$ dimensions where N represents the number of subcarriers in the OFDM system. Each element of matrix F is defined as:

$$[F]_{l,n} := e^{\left(\frac{j2\pi(l-1)(n-1)}{N}\right)}. \quad (3.6)$$

Let $F_p := [f_{n_1}, \dots, f_{n_p}]$ where f_{n_i} is the n th column of F . Define G as:

$$G := (\mathcal{E}_p F_p \mathcal{D}^{\mathcal{H}}(s_p) \mathcal{D}(s_p) F_p^{\mathcal{H}})^{-1} (\sqrt{\mathcal{E}_p} \mathcal{D}(s_p) F_p^{\mathcal{H}})^{\mathcal{H}}. \quad (3.7)$$

In this equation, $\mathcal{D}(s_p)$ is a diagonal matrix, s_p are the pilots in a diagonal, and \mathcal{H} represents the Hermitian. If the estimated channel impulse response is \hat{h} , obtained by using LSE, then:

$$\hat{h} = Gy = h + \eta \quad (3.8)$$

with $\eta = G\omega$ [89]. Finally, the estimate of the channel transfer function for the k th OFDM symbol and the n th subcarrier—denoted by $\hat{H}_{k,n}$ —is given by:

$$\hat{H}_{k,n} = f_n^{\mathcal{H}} \hat{h}. \quad (3.9)$$

3.3.3. Linear Equalization Techniques

The fact that equalization can be done in the frequency domain makes OFDM an attractive choice for radio as well as UWA channels. In this work, two linear equalizers that operated in the frequency domain were evaluated. The performance of both equalizers was compared in terms of the BERs that they offered over a shallow UWA channel. For one equalizer, the channel was estimated using pilots and an LS estimator. For the other, it was assumed that perfect channel estimates were available and the ZF equalizer was used to estimate the transmitted sequence.

Least Squares (LS):

The proposed LSE-based estimator uses one-fourth of the number of subcarriers in the OFDM system. If \hat{C}_k represents the vector of the estimated sequence and H_k represents the estimated channel transfer function in the frequency domain, then the equalized sequence \tilde{C}_k is given by:

$$\tilde{C}_k = \frac{\hat{C}_k}{|H_k|} \quad (3.10)$$

Zero Forcing (ZF):

Assuming a perfect knowledge of the channel in terms of H_k , i.e., the channel transfer function for the k th OFDM symbol, the equalized sequence \tilde{C}_k is given by:

$$\tilde{C}_k = \frac{H_k^*}{|H_k|^2} \hat{C}_k = C_k + \frac{H_k^*}{|H_k|^2} n_k \quad (3.11)$$

where H_k in above equation is the estimated channel in frequency domain when the estimation is assumed to be perfect. In this equation, n_k represents the AWGN added to the k th OFDM symbol and $*$ represents the conjugate.

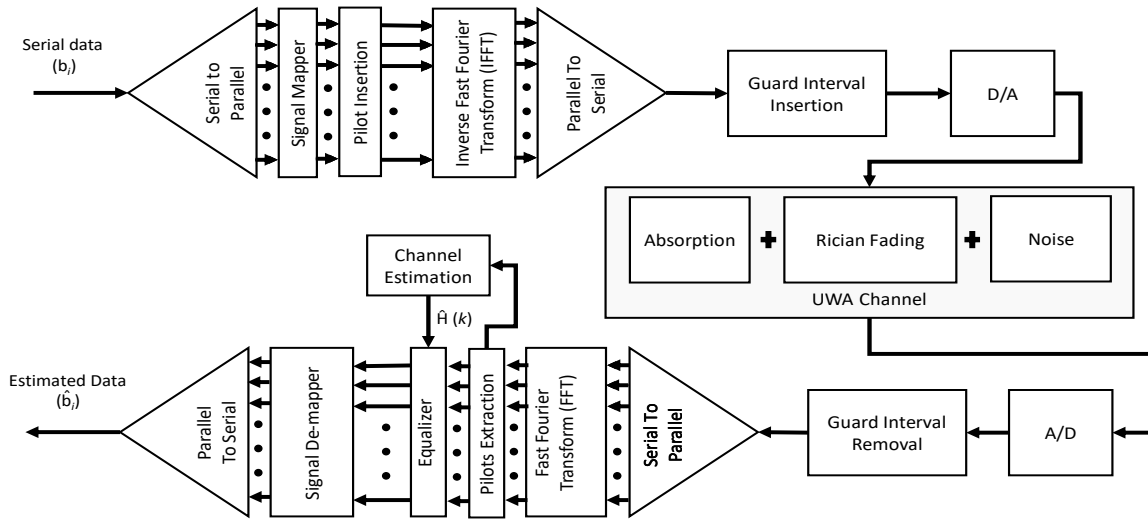


Figure 3.2. CP-OFDM equalization using pilots.

3.3.4. Channel Model

An underwater channel is doubly selective in nature as the signals undergo both frequency and time selectivity [2, 90]. Over longer distances, the bandwidth is limited (a few kilohertz), restricting intercarrier spacing and thus making the system sensitive to even smaller Doppler shifts [17, 91]. Motion induced attenuation is significant because the speed of sound is much less compared with RF waves [15]. For time shifted L multipath components [2], the response can mathematically be represented as:

$$H(t, \tau) = \sum_{p=1}^L A_p(t) \delta(\tau - \tau_p(t)) \quad (3.12)$$

where A_p represents the amplitude of the p th multipath component, τ_p denotes the delay coefficient, and δ indicates the Dirac delta function. The effect of Doppler frequency shifts differ for different subcarriers because the bandwidth and center frequency are comparable. The envelop channel response consists of random multipath fading and deterministic responses.

Figure 3.3 features the modulated time domain signal $s(t)$ from Equation (3.3) passing through several channel blocks. The elaborated system enabled the tuning of various parameters including the channel taps, absorption-related path loss from Thorp’s formula [61], and the SNR. For a shallow underwater acoustic channel, the delay spread is usually between 10 to 20 ms and can be up to 100 ms [92].

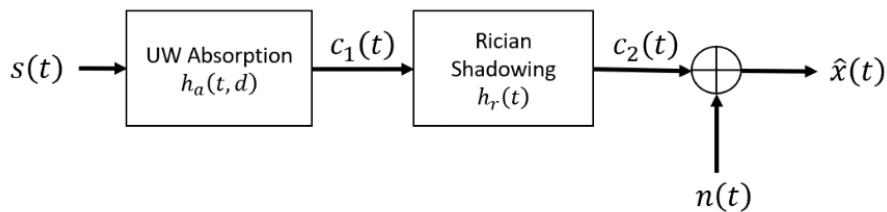


Figure 3.3. Illustration of the underwater channel

3.3.4.1. Deterministic Response

The energy of an acoustic signal attenuates both with respect to distance as well as a function of the frequency. The path loss thus combines both geometric spreading and absorption. If the time variation is represented as $e^{j\omega t}$, the expression for the frequency domain transmission loss in a positive z direction is mathematically expressed as:

$$E(z) = E_0 e^{-\gamma z} = E_0 e^{-\alpha z} e^{-j\beta z} \quad (3.13)$$

where E_0 denotes the scaling constant. The deterministic transfer function $H_a(f, d)$ [62, 63] becomes:

$$H_a(f, d) = A_d e^{-\gamma(f)d} \quad (3.14)$$

where A_d is the scaling constant, d is the distance between the transmitter and receiver, and γ represents the propagation constant in m^{-1} :

$$\gamma(f) = \alpha(f) + j\beta(f) \quad (3.16)$$

where

$\alpha(f)$ and $\beta(f)$ are the absorption and phase constants, respectively. The Thorp formula [61] expresses the absorption coefficient in dB/km as:

$$\alpha_{dB}(f) = 1.094 \left(0.003 + \frac{0.1f^2}{1+f^2} + \frac{40f^2}{4100+f^2} + 0.000275f^2 \right). \quad (3.17)$$

The phase constant in rad/m is expressed as:

$$\beta(f) = \frac{2\pi f}{c_s} \quad (3.18)$$

where c_s represents the sound velocity in ms^{-1} and is computed using Medwin's equation [64]. The signal $c_1(t)$ in Figure 3.3 was computed through convolution as:

$$c_1(t) = h_a(t, d) \otimes s(t) \quad (3.19)$$

where $h_a(t, d)$ is the IFFT of the channel transfer function.

3.3.4.2. Random Channel

Various experimental studies suggest that fading in a shallow UWA channel is more accurately represented using a Rician fading model [93]. Researchers in [66, 94] studied sea trial data from several experiments where the Rician shadowed distribution was found to have the closest fit. In this work, the parameters used were $m = 0.4$ and $k = 2.0$ [94]. The signal $c_2(t)$ was computed as:

$$c_2(t) = h_r(t) \otimes c_1(t) + n(t) \quad (3.20)$$

where $n(t)$ and $h_r(t)$ are the ambient noise and the Rician fading impulse response [68, 95] modelled together with the Doppler shift using the Rician object in MathWorks MATLAB R2019. Figure 3.4 represents the sample delay profile and path gains.

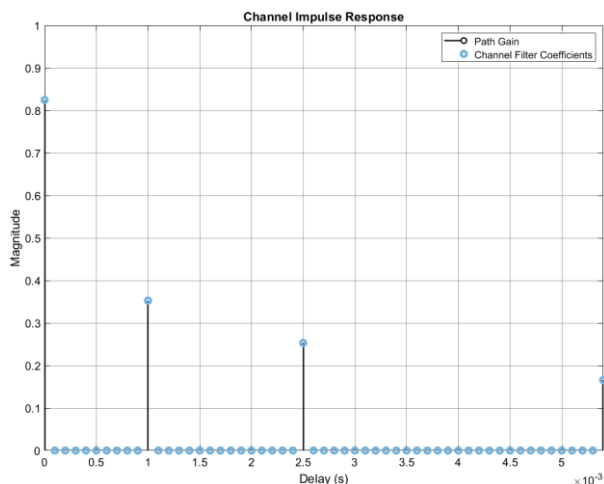


Figure 3.4. Channel impulse response for a shallow underwater acoustic channel.

3.3.4.3. Ambient Noise

The noise in a shallow underwater acoustic channel is location specific, frequency dependent, and cannot be modelled as white noise. For the simulations, an ambient noise model combining thermal, shipping, wave, and turbulence noise [69] was incorporated. The power spectral density was computed as:

$$N(f) = 10 \log \left(10^{\frac{N_{shipping}(f)}{10}} + 10^{\frac{N_{turbulence}(f)}{10}} + 10^{\frac{N_{wave}(f)}{10}} + 10^{\frac{N_{thermal}(f)}{10}} \right) \quad (3.21)$$

It could be modelled as colored noise and had a high amplitude around the lower and higher end of the acoustic communication spectrum and was the lowest at around 60 kHz [96].

3.4. Simulation Setup

In this section, we present the simulation results for both the pilot-based channel estimation and the linear equalization. To evaluate the performance of the proposed system, a CP-OFDM transceiver communicating over a UWA channel was assumed. The parameters used for the OFDM transceiver are shown in Table 3.1. In our simulations, we used 10,000 iteration runs for each E_b/N_0 point. Every iteration had one OFDM symbol with N subcarriers.

Table 3.1: Simulation Parameters

Type	Parameters	Values
Transceiver	Number of Subcarriers	64, 128, 256, 512
	Number of Pilots	8 to 128 (typically one-fourth of the number of subcarriers)
	Modulation Scheme	BPSK, QPSK
	CP Length	One-fourth of the number of subcarriers
	Data Rates	8 kbps for BPSK and 16 kbps for QPSK
Channel	Bandwidth	10 kHz
	Carrier Frequency	30 kHz
	Number of Taps	3
	Distance	50 to 1250 m
	Transmitter Depth	20 m
	Receiver Depth	20 m
	Doppler Frequency	10 Hz
	Path Gains	(0; -8.3; -4.4; -6.2)
	Delay	(0; 1.5×10^{-3} ; 4×10^{-3} ; 7×10^{-3}) s

3.5. Results

Figure 3.5 is a BER plot for BPSK CP-OFDM as a function of the number of pilots used when the number of subcarriers were 64, 128, 256, and 512. The transmitter-receiver distance was kept at 50 m. As shown in Figure 3.5a, 16 pilots offered the best BER performance for 64 subcarriers; using 4 or 8 pilots gave an unacceptably poor performance. This was because 4 or 8 pilots were insufficient to capture the channel behavior. It was also noted that increasing the number of pilots from 16 to 32 marginally deteriorated the BER. For 128 subcarriers, 16 pilots also gave the best BER, as evident from Figure 3.5b. The case of 256 subcarriers is shown in Figure 3.5c. It was noted that the best BER was given by 32 and 64 pilots as it was hard to distinguish between the two cases. Figure 3.5d shows the BER performance when the number of subcarriers was 512. In this case, the best BER was observed when the number of pilots was either 32 or 64. By comparing the four figures, it can be seen that for 64 subcarriers, the optimum number of pilots was one-fourth the number of subcarriers; for 128, it was one-eighth the number of subcarriers; for 256, it was also one-eighth; and, finally, for 512 subcarriers, it was one-sixteenth the number of subcarriers.

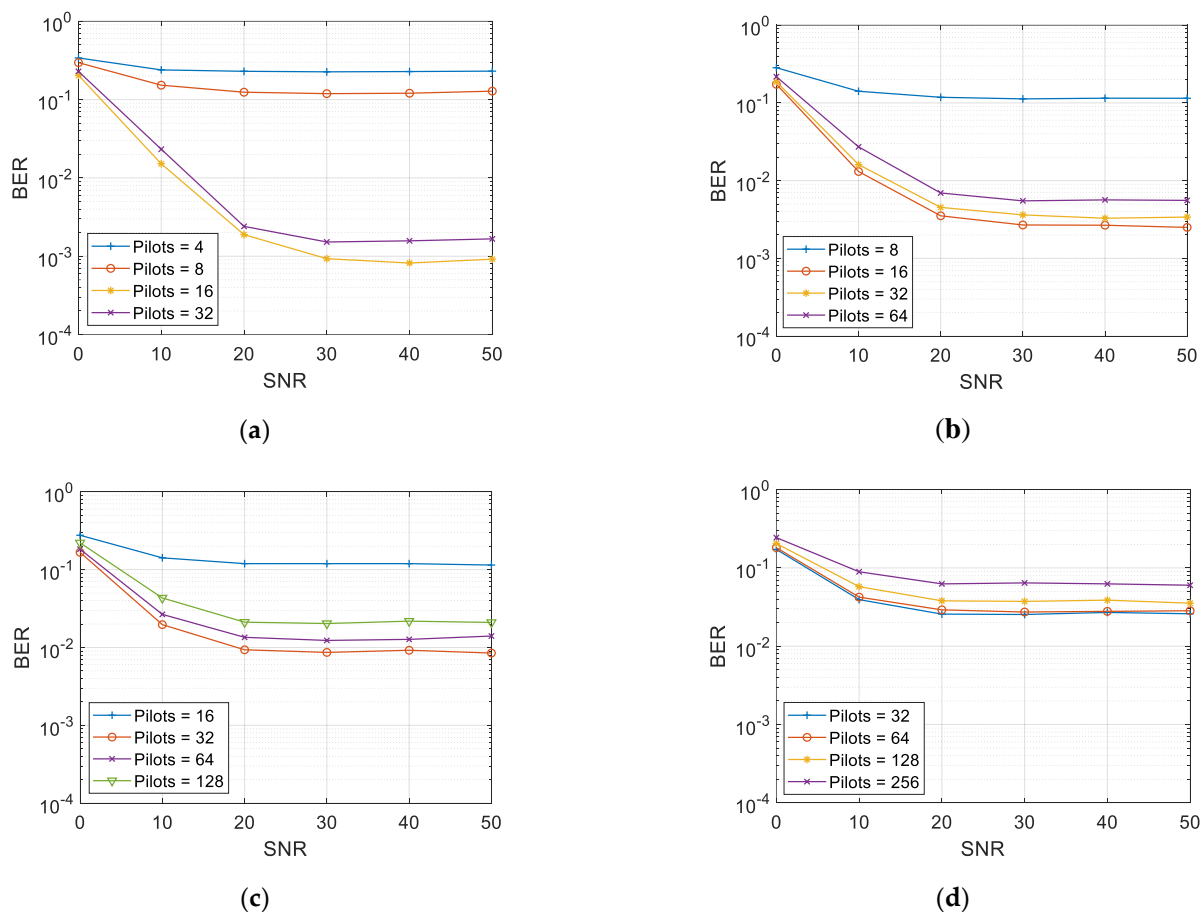


Figure 3.5. BER as a function of the number of pilots for CP-OFDM with a transmitter-receiver distance of 50 m: (a) 64 subcarriers; (b) 128 subcarriers; (c) 256 subcarriers; (d) 512 subcarriers.

The BER performance of the proposed system as a function of the pilot energies is shown in Figure 3.6. In this figure, the number of pilots was 16, the number of subcarriers was 64, and the transmitter-receiver distance was 50 m. It was noted that as we increased the energy of the pilots, the BER degraded. The reason for this behavior was that as the overall energy of the symbol was kept

constant, increasing the pilot energy decreased the energy of the data symbols, which resulted in BER degradation.

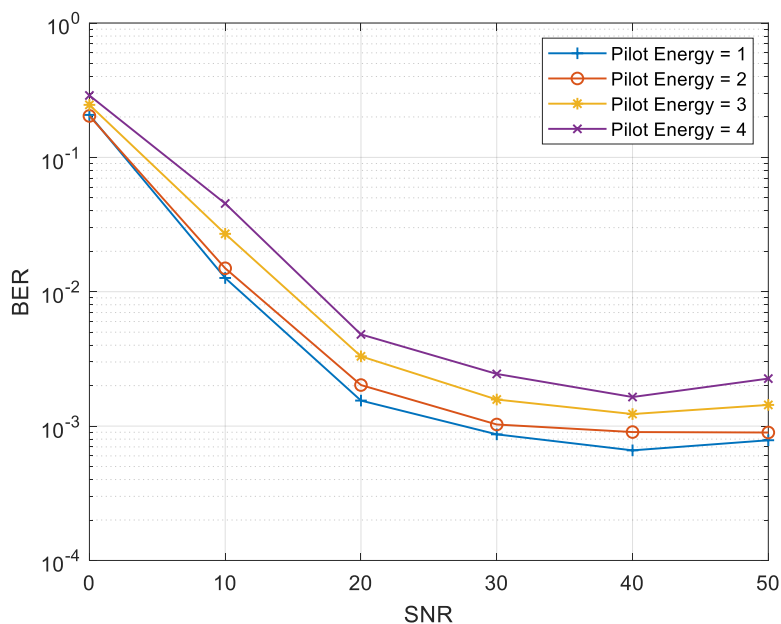


Figure 3.6. BER as a function of the pilot energies for CP-OFDM with 64 subcarriers, a transmitter-receiver distance of 50 m, and the number of pilots as 16.

Figure 3.7 shows the BER performance of QPSK CP-OFDM as a function of the equalizers used. In this plot, the number of subcarriers was 128, the number of pilots was 32, and the transmitter-receiver distance was 800 m. As expected, the performance was poor when no equalizer was used. It was also observed that the BER given by both the LS and ZF equalizers was almost the same for a low SNR. At a high SNR, the ZF outperformed the LS equalizer.

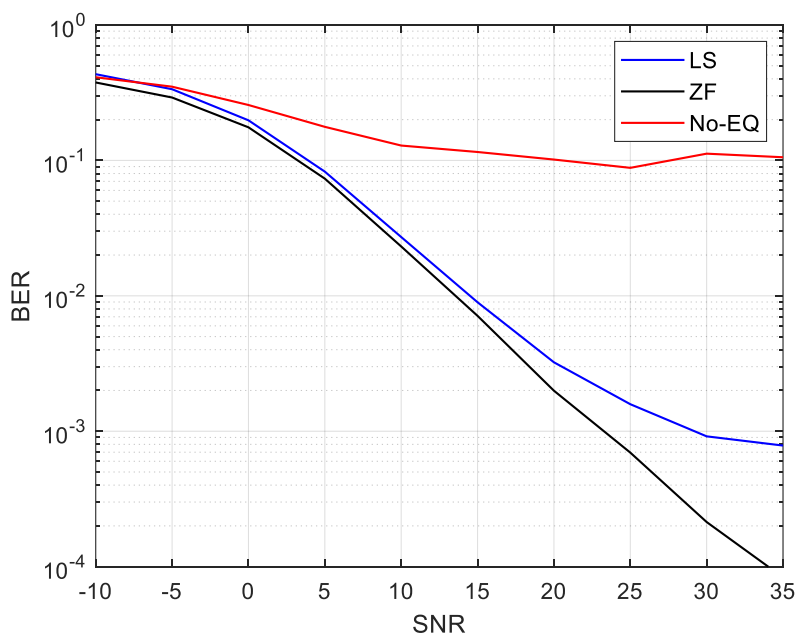


Figure 3.7. BER as a function of the equalizer used for QPSK CP-OFDM with 128 subcarriers, a transmitter-receiver distance of 800 m, and the number of pilots as 32.

Figure 3.8 shows the BER plots when using the LS and ZF equalizers with multiple transmitter-receiver separations that ranged from 50 to 1250 m. The number of subcarriers was 64 with 16 pilots and BPSK was used in the mapper. As expected, increasing the transmitter-receiver distance deteriorated the BER performance. However, even at 1250 m, the performance was acceptable and a good error correcting code would bring down the BER curve even further.

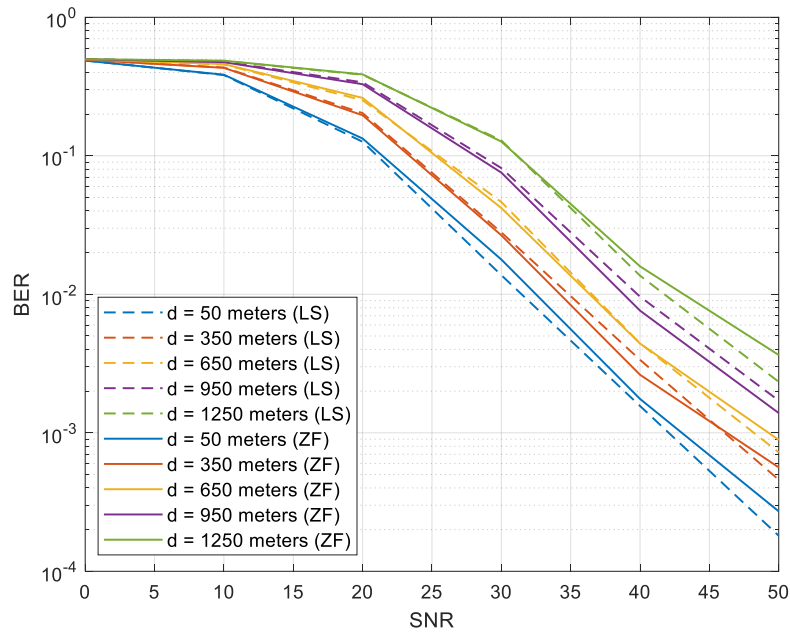


Figure 3.8. BER of CP-OFDM when using the LS and ZF equalizers as a function of the transmitter-receiver distance with 64 subcarriers and 16 pilots.

Figure 3.9 shows the BER performance for the LS and ZF equalizers when the transmitter-receiver distance was varied from 50 m to 1250 m. The number of subcarriers used was 128 with 32 pilots and BPSK was used in the mapper. The behavior that was observed in Figures 3.6 and 3.7 was also noted in these figures. However, the BER was marginally inferior in this case owing to a higher number of subcarriers.

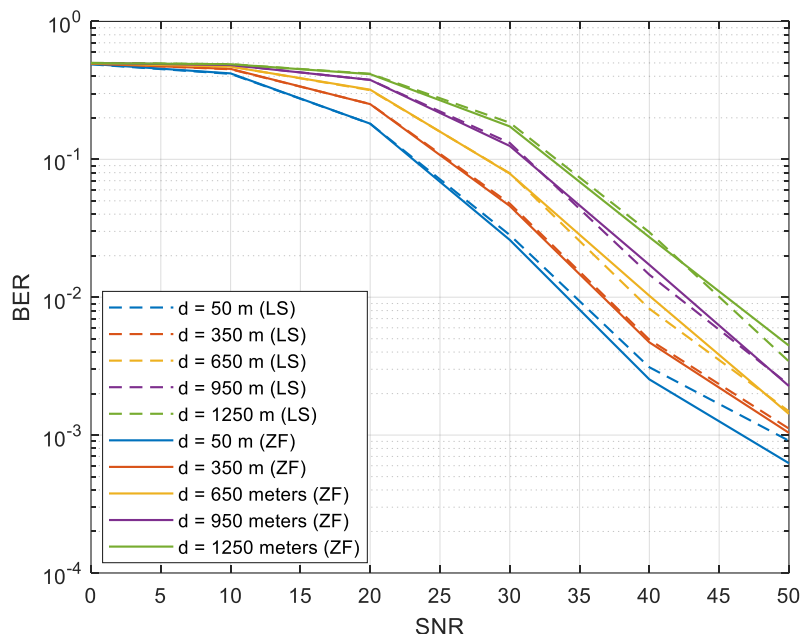


Figure 3.9. BER of CP-OFDM when using the LS and ZF equalizers as a function of the transmitter-receiver distance with 128 subcarriers and 32 pilots.

Figure 3.10 shows the BER performance for the LS and ZF equalizers when the number of subcarriers was varied from 64 to 512 and QPSK was used in the mapper. The number of pilots in both cases was one-fourth the number of subcarriers and the transmitter-receiver distance was kept constant at 500 m. It was observed that the performance with the ZF equalizer was marginally better than that of the LS equalizer. Moreover, as the number of subcarriers increased, the BER degraded owing to an increased ICI. We also provide a summary of our findings in Table 3.2 for a fixed SNR of 40 dB. It was evident that the BER deteriorated with the number of subcarriers.

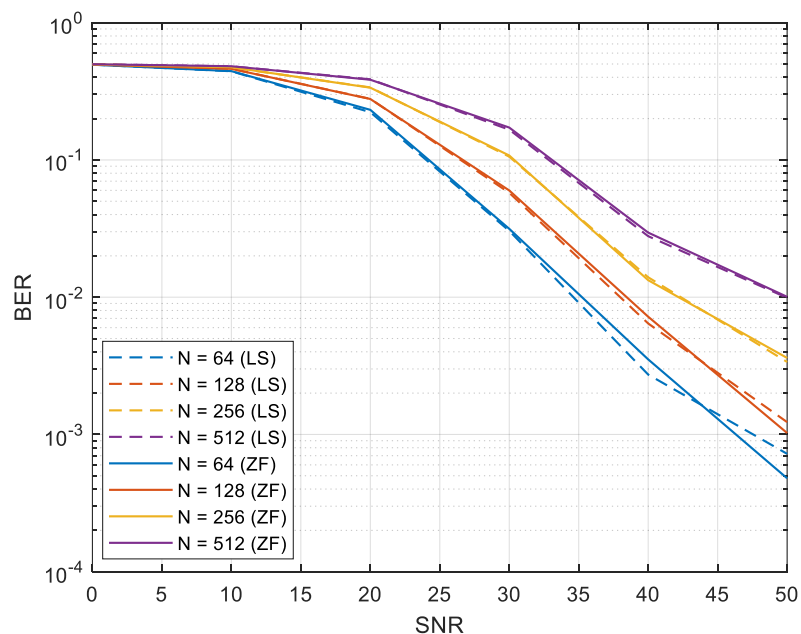


Figure 3.10. BER of CP-OFDM when using the LS and ZF equalizers as a function of the number of subcarriers with a transmitter-receiver distance of 500 m and the number of pilots one-fourth the number of subcarriers.

Table 3.2. BER performance for 64, 128, 256, and 512 subcarriers at a fixed distance of 500 m.

Equalizer	N = 64	N = 128	N = 256	N = 512
LS	0.002729	0.006434	0.0133	0.02782
ZF	0.003521	0.007205	0.01396	0.02955

3.6. Conclusion

We investigated the BER performance of CP-OFDM in underwater acoustic channels for the proposed pilot-based channel estimation and two equalizers, namely, least squares and zero forcing equalizers. The underwater channel model used in this work was based on Rician shadowing. Through this model, we evaluated the performance of a system in UWA channels more realistically. This model also enabled us to adjust the various channel parameters such as fading, Doppler shift, and ambient noise. The main conclusions obtained after extensively simulating the proposed system by varying several system parameters were: (1) the best BER performance was achieved if the number of pilots was kept as one-fourth the number of subcarriers; (2) the BER performance degraded if the energy of the pilots increased whilst keeping the overall symbol energy constant; (3) an acceptable BER performance was observed when using the LS or ZF equalizer; (4) the performance of the ZF equalizer was marginally better than that of the LS equalizer; (5) increasing the number of subcarriers deteriorated the BER performance because of an increased ICI; and (6) an acceptable error performance was observed even at a transmitter-receiver distance of 1250 m with both equalizers. This work could be extended by employing MMSE with soft channel estimates and a decision feedback equalizer in a UWA environment. The proposed technique needs to be further evaluated using a Bellhop core model and/or a Water Mark simulator [97, 98].

Chapter 4: Generalized Frequency Division Multiplexing

Chapter 3 focused on our proposed channel estimation and equalization techniques for an OFDM system and their assessment. This chapter focuses on a spectrally efficient GFDM transceiver and presents a thorough survey of latest developments in next generation candidate waveforms for underwater acoustic communication, findings, and recommendations. The overview touches upon all the work, till date, related to advanced multicarrier transmission techniques in UWA medium which will potentially supersede OFDM. A GFDM based modem for UWA communication is developed in MATLAB that uses our realistic underwater channel model. Error performance analysis of proposed GFDM system over varying acoustic channel conditions and transmitter-receiver distances and its comparison with CP-OFDM. Performance analysis of proposed GFDM system in respect to spectrum utilization, computational complexity and peak-to-average-power ratio, and its comparison with CP-OFDM.

The chapter is arranged as follows: In Section 4.2, we present a survey of all the related work associated with GFDM, OQAM-FBMC, FMT-FBMC and F-OFDM for UWA transmission. In doing so, we also discuss the effects of UWA channel on various multicarrier communication schemes. In section 4.3, we present the proposed GFDM modem for UWA channels. Our proposed underwater channel model that is based on Rician shadowed fading is discussed in section 4.4. Section 4.5 contains simulation setup and section 4.6 discusses the results. Finally, section 4.7 concludes the chapter.

4.1. Introduction

Underwater acoustic communication has always been the preferred choice for data transmission in one of the most complex channels [5]. Recently, several multicarrier (MC) techniques have found their grounds in a domain where single carrier communication was dominant [99]. OFDM, the prominent one, is being extensively studied for its ability to fight off inter symbol interference (ISI) while also handling frequency selectivity in the underwater channel. However, with advancements in next generation communication technologies and their ability to further enhance bandwidth utilization, several emerging multicarrier waveforms have been evaluated for the UWA domain [100].

The underwater channel is doubly selective wherein there is frequency selectivity as well as Doppler shift [17]. Low speed of acoustic signals, pathloss dependent on signal frequency, a large delay spread of 20 ms that at times may go up to 100 ms and bandwidth in the order of a few kilohertz severely limits transmission rates. The channel is wideband in nature since data is transmitted at bandwidths nearly the order of carrier frequencies [3]. Also, most of the energy is carried by a few path components making the channel sparse. Relative motion of the transmitter and receiver in an underwater medium induce Doppler shifts making the channel time variant.

OFDM is a well-researched multicarrier technique having the ability to efficiently handle multipath fading of the UWA channel and its larger delay spread [7]. The fact that its symbols are long, it can overcome ISI. However, like any other scheme, OFDM has its disadvantages. It is prone to frequency offsets caused by the time variations due to comparative motion of the receiver and transmitter in the underwater channel. Affixing a cyclic prefix (CP) at the start of every symbol, as a guard interval to deal with ISI problem, makes an OFDM based communication system spectrally inefficient [101]. Since a filter based on rectangular pulse shaping is used at the transmitter side, there are high out-of-band (OOB) leakages. OFDM also has a higher PAPR due to random addition of in-phase subcarriers [55].

To deal with an OFDM system limitation, and with rapid advancements in the field of wireless communication, many potential multicarrier waveforms have emerged as contenders for next generation networks – also called 5G. Among them, the most prominent ones are GFDM, filtered OFDM (F-OFDM), universally filtered multicarrier (UFMC) and filter bank multicarrier (FBMC). In a GFDM system, the data transmitted is in two dimensional blocks (frequency and time) divided into sub-symbols and subcarriers, with the subcarriers filtered by a pulse shaping prototype [102]. The time and frequency responses of the prototype filter are altered according to the requirements. This leads to reduced OOB emissions compared to a cyclic prefix OFDM (CP-OFDM) system.

FBMC is another promising technique that performs well in doubly dispersive acoustic channels and it has a higher bandwidth efficiency given the absence of a cyclic prefix [8, 13]. There are two flavors of FBMC, vis-à-vis filtered multi tone filter bank multicarrier (FMT- FBMC) and offset QAM filter bank multicarrier (OQAM). Former is based upon QAM and the latter is based upon offset QAM. OQAM-FBMC achieves spectral efficiency in the real domain while orthogonality is achieved in FMT-FBMC by reducing the frequency domain overlapping of subcarriers [103].

Filtered OFDM is one of the 5G candidate waveforms and a promising alternative to OFDM due to its reduced OOB emissions [104]. While the rest of design is like OFDM, in F-OFDM, a filtering operation is performed after the IFFT stage of the receiver. At the transmitter end, the received signal is filtered and then passed on to the FFT stage after analog to digital conversion.

UFMC is a more generalized realization of filtered OFDM and FBMC where group of subcarriers are filtered in frequency domain [103]. The total number of subcarriers are split into multiple sub-bands and each one is filtered through a filter of specific length. This filtering operation results in lowest OOB emissions compared to the other waveforms. The number of sub-bands used for transmission can be controlled and only limited number can be used for transmission. While the gains offered by UFMC systems are promising, its higher complexity makes it less suitable for scenarios where system power is limited.

While the research and implementation of these promising techniques in the radio frequency (RF) domain have gained momentum [103, 105, 106], very limited literature is available evaluating the efficacy of these techniques for an underwater channel. In this work, we provide a detailed overview of all the work done thus far in the domain of multicarrier waveforms beyond OFDM for UWA medium. We share our findings and observations and suggest recommendations for future UWA communications. Major contributions of this work include:

- A thorough survey of latest developments in next generation candidate waveforms for underwater acoustic communication, findings, and recommendations. The overview touches upon all the work, till date, related to advanced multicarrier transmission techniques in UWA medium which will potentially supersede OFDM.
- A GFDM based modem for UWA communication developed in MATLAB that uses a realistic underwater channel. Besides using the well-known underwater absorption model, the underwater channel also includes a Rician shadowing model for shallow waters.
- Error performance analysis of proposed GFDM system over varying acoustic channel conditions and transmitter-receiver (TX-RX) distances and its comparison with CP-OFDM.
- Performance analysis of proposed GFDM system in respect to spectrum utilization, computational complexity and peak-to-average-power ratio, and its comparison with CP-OFDM.

4.2. Related Work

This section provides a comprehensive overview of post-OFDM multicarrier techniques for a UWA channel. FBMC and GFDM research for UWA medium has gained momentum in the past few years owing to their ability to better utilize the limited bandwidth that is available. We did not find any comprehensive work evaluating UFMC for acoustic multicarrier transmission. It is probably because of the fact that UFMC complexity is quite high compared to a CP-OFDM system and other 5G candidate waveforms [107]. However, with recent developments in low complexity implementations [108], UFMC could be a prominent technique in future UWA communications. Consequently, we restrict ourselves to FBMC and GFDM only and compare them with OFDM.

Table 4.1 compares GFDM, FBMC and F-OFDM against a CP-OFDM system for a UWA channel based on various aspects of these techniques. While an OFDM system has only K subcarriers distributed in frequency domain, FBMC and GFDM systems both further divide the spectrum into time blocks based on the number of sub-symbols. To maintain orthogonality in a multipath fading channel, OFDM adds a CP to each block, whose length must be larger compared to the channel delay spread, increasing the overhead. The flexibility of CP-OFDM, F-OFDM and GFDM are high in terms of frequency localization, MIMO integration and scalability.

Table 4.1: Comparison of Next Generation Multicarrier Waveforms against OFDM

	OFDM	GFDM	FBMC-FMT	FBMC-OQAM	F-OFDM
sub-carriers	K	K	K	K	K
sub-symbols	1	M	M	M	1
cyclic prefix	yes	yes	no	no	yes
orthogonal	yes	no	yes	yes	yes
spectral efficiency	low	medium	high	high	medium
comp. complexity [18, 19]	low	medium	high	high	high
peak to avg. power [12]	high	high	high	high	high
out of band	high	medium	low	low	low
flexibility	high	high	low	low	high
benefits	orthogonality	flexible, CP once every M sub-symbols	low OOB, no CP	low OOB, no CP	compatibility with legacy OFDM systems

In a GFDM system, CP is affixed once every M sub-symbol lowering the CP overhead, while no CP is required in an FBMC system. Both GFDM and FBMC offer high spectral efficiency due to their low OOB emissions due to filtering operations at the transmitter. A CP-OFDM is computationally least expensive of the three, while FBMC is most complex of all. GFDM is more flexible and suited to the UWA domain where power and bandwidth are limited and the signals face both time and frequency selectivity. The next three subsections are devoted to a survey of GFDM, FBMC and F-OFDM respectively, for UWA channels.

We describe the proposed underwater communication testing system architecture in the following Section 4.3.

4.2.1. Generalized Frequency Division Multiplexing

GFDM was first introduced in 2009 [102]. It is a versatile MC scheme and despite its slightly higher complexity compared to a traditional CP-OFDM, its greatest strength is that it can treat single-carrier frequency domain equalization and CP-OFDM as its special cases. When the number of subcarriers $K = 1$ and the pulse shape used is Dirichlet, SC-FDE is realized. OFDM like system is obtained [109] when the number of sub-symbols $M = 1$ and the pulse shape is rectangular. Making it possible to utilize multiple waveforms optimally, in a single implementation, according to the channel conditions. In a doubly selective underwater channel, GFDM can significantly reduce ISI and ICI as well as efficiently utilizing the limited UW spectrum.

Table 4.2 summarizes the work done so far in GFDM for UWA channels. Detailed survey of these works is presented in the upcoming subsections.

Table 4.2: Summary of Work Done in GFDM for UWA Channels

Performance Metric	Contribution	Related Work	UWA Channel Modeling
SER	Performance evaluation through simulations	[96, 110]	5-tap, 10-tap Rayleigh multipath fading
SER	Spread-spectrum based GFDM transceiver	[111]	Actual water pool
PAPR	Performance evaluation as a function of pulse shapes and roll off factors	[109, 112]	Not required
OOB Emissions	Closed-form expressions to compute OOB at the TX as well as RX	[113]	Time-variant multipath propagation channel

4.2.1.1. GFDM scheme for UWA communication

Hebbar and Poddar (H&P) in [96] and [110] have analyzed a GFDM transceiver using statistical underwater acoustic channel model based on Rayleigh multipath fading. GFDM's low OOB leakages compared to CP-OFDM and the latter's ICI issue arising due to time variation/doppler spread, motivated H&P to explore GFDM for a doubly selective UWA channel. Both BPSK and QPSK modulations have been evaluated while employing root raised cosine (RRC) filter as pulse shape.

A matrix-based approach is used for signal generation and matching filter (MF) is utilized at the receiver side to preserve computational simplicity instead of zero forcing (ZF) or minimum mean square error (MMSE) equalizer. However, it is not mentioned as to which equalizer/receiver has been used to generate the reported results. The channel model utilized has three major components: noise, attenuation and multipath. For modelling noise, H&P have generated a zero mean gaussian noise and passed it through a low pass filter to produce colored gaussian noise. Thus, additive white gaussian noise (AWGN) and additive colored gaussian noise (ACGN) have been added together to generate UWA ambient noise [110].

It is observed that the signal to noise ratio (SNR) is slightly worse, in ambient channel noise, than in the presence of only AWGN. An existing model has been employed, for attenuation in the UWA channel, depending upon distance between the transmitter and receiver as well as carrier frequency. H&P have implemented multipath using a single-tap Rayleigh fading based model with doppler shift of 0, 10 and 100 Hz. At the receiver end, a 1-tap equalizer is employed and a known channel state information (CSI) is presumed. The system is simulated in MATLAB and SER plots for multiple scenarios have been presented including time variant, time invariant, only ambient noise, ambient noise with attenuation and with 5 and 10 tap Rayleigh multipath fading channels. No reasons for selecting Rayleigh multipath channel for simulating a UWA channel have been provided. The results have been reported only for one instance of distance, i.e., 1 km.

The results are compared against FBMC and OFDM implementations [114, 115] for UWA channel but the performance of similar FBMC and OFDM systems is not shown in the results, rather, the reader is referred to the work of [114, 115] to compare the results by themselves. The paper also lacks the performance evaluation as a function of pulse shapes and the roll off factors.

4.2.1.2. Chaotic Sequence Spread Spectrum (CSSS) For GFDM

Since channel estimation in GFDM systems operating in underwater acoustic channel remains an unsolved challenge, Jinqiu-Gang-Pengbin (JGP) [111] have proposed a spread spectrum technique based GFDM transceiver. At the receiver side, through despreading, the strongest signal is detected preventing the need for a channel estimation block. By using cyclic prefix once for M sub-symbols, GFDM is spectrally more efficient. Spread spectrum technique can be applied both in time and frequency domain, a time domain version is adopted by JGP since frequency domain spreading will distort subcarriers. In a CSSS system [116], chaotic sequence is combined with spread spectrum technique that traditionally utilize pseudo-noise (PN) codes. They tend to improve performance of a spread spectrum system due to their aperiodic nature compared to PN sequences. In their proposed GFDM-CSSS system, the encoded data is spread using a chaotic sequence before the modulator block. On the receiver side, a de-spreading operation is performed using a locally generated sequence. Two types of filter banks were employed including RC and RRC with a rolling factor of 0.1 and 0.9. However, it is observed that, the roll-off factor has not much effect on the SER of GFDM-CSSS system.

To evaluate the effects of variation in the number of subcarriers and sub-symbols while keep the transmitted bits same, two type of matrix structures were used: $M = 2 \times K = 29$ and $M = 29 \times K = 2$. Due to improved performance of system with $K = 2$, JGP have deduced that the SER performance with small number of subcarriers will be better due to lower chances of ICI. Physical experimentation is carried out in a pool with 11.5 m transmitter-receiver distance and 3 m depth. The resulting SER of CSSS-GDFM is superior to that of a standard GFDM system.

4.2.1.3. PAPR performance of a UWA GFDM system

Wu-Ma-Qi-Babar-Zheng (WMQBZ) have studied the impact of various pulse shaping filters on the PAPR of a UWA-GFDM transmission system [109]. As discussed earlier, the use of prototype filters for pulse shaping reduces the OOB emissions of the GFDM system resulting in a reduced PAPR. The modulation scheme is BPSK and the sampling frequency is kept being 48 kHz and bandwidth of 6 kHz centered at 9 kHz is used in experiments. Since the channel delay spread is understood to be between 10 to 20 ms, the CP duration is 20.8 ms. CP is kept the same for GFDM and CP-OFDM system used for comparison. WMQBZ have presented the results using complementary cumulative distribution function (CCDF) curves to observe the overall distribution of the system's PAPR. Eq. 4.1 expresses the PAPR of a GFDM system:

$$\text{PAPR (dB)} = 10 \log_{10} \max_{0 \leq n \leq N-1} \frac{|x_n|^2}{E[|x_n|^2]} \quad (4.1)$$

where x_n is the time domain version of the discrete GFDM signal [109]. Four different pulse shaping filters have been evaluated including 1st Xia, 4th Xia, RC and RRC with roll-off factors varied from 0.1 to 0.9. The PAPR of the system increases for increasing K values, but always turns out to be lower than that of a CP-OFDM transmitting same number of bits. However, this is the only work that reports PAPR performance of GFDM to be better than OFDM. Otherwise, all the literature that we reviewed, and our own simulation results do not support this notion. Rather, the PAPR of GFDM is comparable to that of OFDM system.

When the number of subcarriers is kept the same, 1st Xia and 4th Xia have near identical PAPR performance and the lowest among the 4. RC has the higher PAPR compared to the previous two and RRC filter results in the highest PAPR of all. For roll-off factors, an RC filter is used with varying values from 0.1 to 0.9. It was observed that for every 1 step increase, the PAPR is observed to rise 0.1 dB.

Authors in [112] have briefly analyzed PAPR of GFDM system for the underwater acoustic channel. CCDF plots, only for the transmitted signal, have been presented for different number of subcarriers. The results show that GFDM outperforms OFDM in terms of PAPR.

4.2.1.4. Spectral analysis calculations for UWA GFDM

To reduce the computational overhead of simulating a GFDM system for the underwater channel, Hilario-Tacuri [113] came up with a set of closed-form mathematical equations. The expressions are then used to evaluate spectral efficiency in terms of OOB emissions for a GFDM system. The underwater channel is modelled as a time variant channel with multipath propagation and is expressed as:

$$\tilde{h}(t, v) = \sum_{p=0}^{P-1} a_p \mu_p(t) \delta(v - v_p) \quad (4.2)$$

where p is the number of propagation paths, μ_p is a zero mean gaussian complex number, a_p is the attenuation coefficient while as v_p is the delay coefficient and $\delta(\cdot)$ represents impulse response. Several

equations have been derived to calculate PSD of the GFDM signal as well as OOB emissions of the received signal. QPSK modulation scheme has been used with an RC shaping pulse. The Doppler shift in channel is assumed to be 15 Hz. It is observed that the OOB emissions, while lower for large values of number of subcarriers (N) or sub-symbols (M), are largely dependent on the values of N . The results are compared against a GFDM with $M = 1$ which is equivalent to an OFDM system and has the worst OOB emission performance. Results are obtained for the received signal after passing it through the proposed UWA channel and points to the fact that with reduced mobility, the spectral efficiency of the system increases.

4.2.2. Filter Bank Multicarrier

The concept of FBMC has been around for a long time as FBMC modulation schemes were proposed decades ago [117]. Nevertheless, these techniques did not get much attention owing to their higher computational complexity costs. The two most prominent flavors of FBMC are: filtered multi-tone (FMT-FBMC), and offset quadrature amplitude modulation-based FBMC (OQAM-FBMC) [118]. Due to the absence of a CP and having reduced OOB emissions, an FBMC system can achieve higher efficiency against OFDM in a UWA channel with multipath and Doppler shifts. In this section we look at developments in the domain of FBMC for underwater acoustic transmission. Table 4.3 gives a summary of the work done so far in the domain of FBMC for UWA channels. Detailed overview is presented in the upcoming subsections.

Table 4.3: Summary of Work Done in FBMC for UWA Channels

Performance Metric	Contribution	Related Work	UWA Channel Modeling
SER	Performance evaluation via closed-form expressions and validation via real data	[13]	Doubly dispersive channel
MSE	A new decision feedback equalization technique combined with channel estimation	[8]	Real environment
SER	A new MMSE based equalization technique combined with channel estimation	[119]	Indoor pool
Transmit Power Savings	Proposed and evaluated a transceiver for image and video communication	[120]	Real channel used in [121, 122]
Transmit Power Savings	Proposed and evaluated Direct-mapping based MIMO FBMC for UWA channels	[123]	Real channel used in [121, 122]
SER	Compared OQAM-FBMC and FMT-FBMC with OFDM	[114]	Rayleigh multipath channel model
SER	Compared OFDM with OQAM-FBMC	[124]	Channel details not given
SER	Proposed and evaluated a transceiver for video transmission in a MIMO OQAM-FBMC and compared with OFDM	[91]	An underwater acoustic channel

4.2.2.1. Novel FMT-FBMC based communication technique for UWA channel

Amini-Chen-Farhang-Boroujeny (ACFB) have proposed a new cost function optimization technique [13] for FBMC system operating in a doubly dispersive underwater channel. ACFB argue that OFDM systems dedicate some portion of the symbol length to CP and since it must be equal to the length of channel impulse response, in UWA communication the symbol length drastically increases due to a long delay spread. A long symbol will result in increased ICI based degradation, since UWA channels introduce frequency dispersion. FBMC based systems were conceived long before OFDM and have widely been studied for their ability to deal with both time and frequency spreading in doubly dispersive channels. ACFB have focused on an FMT-FBMC based technique due to its simplicity and its ability to scale in multiple-input multiple-out (MIMO) systems. Compared to a traditional FMT, where a square root Nyquist filter is employed to have subcarriers in non-overlapping bands, a simpler single-tap equalizer is incorporated by increasing the number of subcarriers significantly, overlapping subcarrier bands and following the Nyquist criterion in both frequency and time while designing the prototype filters.

While SFB and AFB increase the complexity of the system, it is a relatively small cost to be borne for increased system performance. They have compared their proposed technique against a traditional FMT system and OFDM. The carrier frequency used was 20 kHz, modulation schemes used were QPSK, 8-PSK, and 16-QAM.

It is observed that square root Nyquist filter design performs well in channels with higher frequency selectivity and isotropic orthogonal transform algorithm (IOTA) as well as Hermite design perform well in channels with time variations. Based on signal-to-interference ratio (SIR) plots, ACFB deduced that their technique outperforms OFDM and traditional FMT-FBMC in systems especially those with mobility.

4.2.2.2. FMT Modulation for UWA communication

Gomes and Stojanovic (G&S) [8] evaluated FMT modulation technique for a shallow underwater channel. Unlike the overlapping subcarriers in an OFDM system, the total bandwidth is split into several separate sub-bands, which are used to modulate SC signals creating an MC system. Thus, there are a smaller number of subcarriers in a fixed bandwidth as compared to OFDM. Resultantly, a short symbol duration and non-overlapping subcarriers, reduces the ICI and ISI respectively to a larger extent. G&S propose a decision-feedback-equalization (DFE) technique built upon channel estimation. The channel estimator works separately for each sub band and the estimated results are then combined through a fusion technique. Simulations and real experiments were conducted for bandwidths of 1.5 kHz and 4.5 kHz, a 5.5 kHz carrier frequency and a TX-RX separation of 800 meters. Simulation results shows FMT as a better OFDM alternative over fast varying channels and experimental results have suggested using a smaller number of 8 sub-bands for a small bandwidth like the ones mentioned above.

4.2.2.3. MMSE equalization for FMT-FBMC

Sun-Wang-Zhang-Li-Huang (SWZLH) have proposed an MMSE based equalization strategy [119] combined with channel estimation (CE) for a UWA FBMC system based on FMT. An MMSE based turbo equalizer is preferred choice due to its simplicity and performance gains but a CE based MMSE equalizer is computationally complex compared to a non-CE equalizer. Adaptive MMSE equalizers are used to suppress ISI but due to large delay spread of the channel their performance for UWA FBMC

systems are not within acceptable limits. To deal with this issue, SWZLH have proposed a simplified CE-MMSE adaptive equalizer with turbo coding and tested it using simulations.

The input data is encoded using error control codes and an RRC filter with a roll-off factor of 0.5 has been used at the transmitter. ICI was supposed to be negligible due to FMT carrier isolation and turbo equalization is used to suppress the ISI. By using a linear equalizer instead of a DFE, the computation simplicity is achieved. A discrete time channel response is used for simulations with TX-RX separation of 350 meters.

SER and BER performance of the system suggest that the channel estimation based MMSE equalization technique is superior to a traditional non-estimating MMSE equalizer. Experimental results were collected for TX-RX separation of 6.5 m in a pool and the frequency band was 8-16 kHz. The proposed technique performs well in both the cases, but the data rate is halved if compared against a traditional MMSE equalizer. However, system's performance gains improve at higher bit rates.

4.2.2.4. OQAM-FBMC based acoustic transceiver design

Lin et al. have developed an underwater acoustic transceiver [120] for image and video communication in the UWA channel. It was argued that due to high spectral efficiency of FBMC systems, they are more suited to scenario like image and video transmission which require low latency communication. Low-density parity-check (LDPC) error correcting codes have been employed to ensure reliable transmission while reducing SER. Adaptive modulation was incorporated and the allowed SER threshold for voice transmission was kept at 10^{-3} and for video transmission it was fixed at 10^{-4} . A window detecting function is used to measure SNR and power adjustments. For simulations, the transmission distance was 1 km, the center frequency was 11.5 kHz and a bandwidth of 3.9 kHz. A successful image and audio transmission were achieved with acceptable quality of service.

A relatively similar technique was implemented in [123] where a direct mapping (DM) based MIMO-FBMC schemes was evaluated for audio and visual data transmission. After the LDPC coding block, the encoded data is transmitted through a 2x2 DM-MIMO scheme. The SER for BPSK-FBMC were better than OQAM-FBMC for the transmitted data over a 1 km transmitter between the transmitter and receiver.

4.2.2.5. FBMC performance in UWA channel

Bocus et. al [114] have evaluated OQAM-FBMC and FMT-FBMC techniques for UWA channel and compared them against a UWA OFDM system. The OQAM-FBMC has been developed using polyphase networks technique to reduce the complexity of the system. FMT uses pulse shaping filters to reduce spectral leakages. Reed-Solomon and Turbo codes have been used to improve the bit error rates. A Rayleigh multipath channel model has been used with time variations and underwater absorption pathloss. Two different channel designs have been discussed including a vertical configuration and a horizontal configuration-based transmitter-receiver placements. It was observed that Turbo codes performed well as compared to RS codes in a UWA channel. FBMC offers a higher spectral efficiency and improved rates since it does not use a CP but all this is achieved at the cost of added complexity.

Pranitha and Anjaneyulu (P&A) [124] have assessed the efficacy of an OQAM based FBMC system for the underwater channel and compared it against OFDM. An OQAM-FBMC system was simulated in MATLAB for only the pathloss and ambient noise effects of the UWA channel. At the transmitter side, the modulated input symbols pass through synthesis filter bank (SFB) which performs

the frequency division multiplexing of the input. While an analysis filter bank (AFB) separated this multiplexed data into multiple subcarriers. Ambient noise and frequency dependent pathloss have been modelled for an underwater channel. The paper lacks some details as channel and transceiver parameters including the carrier frequency, bandwidth, modulation, distance etc. have not been mentioned. The SER results for an unknown channel show that FBMC outperforms OFDM for an ambient noise channel without multipath.

4.2.2.6. OQAM-FBMC based video transmission in UWA channel

Bocus, Agrafiotis and Doufexi (BA&D) have proposed a transceiver design [91] for video transmission in the underwater channel. They have employed a preamble-based channel estimation technique in their system based on interference approximation method together with a forward error correction scheme. SER performance is evaluated while simulating a multipath underwater channel with transmitter-receiver distance of 1 km, bandwidth of 25 kHz and the carrier frequency is 32.5 kHz. The UWA channels delay spread is 2.6 ms, maximum doppler shift is 2 Hz and colored noise has been used instead of AWGN for modelling accuracy. A single-tap equalizer has been incorporated in the receiver for OFDM while as a 3-tap equalizer is being used in case of FBMC. The SER results for MIMO OFDM and MIMO OQAM-FBMC have been presented. For a compressed video signal, BA&D have observed that turbo-coded FBMC and turbo-coded MIMO FBMC both show significant performance gains over a turbo-coded MIMO OFDM system. A gain of more than 17% is achieved in terms of bit rate compared to a MIMO OFDM.

4.2.3. Filtered Orthogonal Frequency Division Multiplexing

Conventional OFDM waveforms exhibit a frequency spectrum that is not localized. In addition, OFDM suffers from inter-symbol and inter-carrier interferences. F-OFDM was proposed in 2015 [125] to address such issues of OFDM. F-OFDM employs a specially designed filter such that the filter length exceeds the cyclic prefix of OFDM. As a result, desired frequency localization is achieved along with ISI and ICI being within acceptable limits. A typical F-OFDM is similar to a conventional OFDM system except that after CP insertion, the signal to be transmitted is convolved with a spectrum shaping filter. A complex conjugate version of the transmit filter that is matched to the transmit filter is applied to the received signal which is then passed through the usual OFDM blocks for recovery of transmitted data.

Table 4.4: Summary of Work Done in F-OFDM for UWA Channels

Performance Metric	Contribution	Related Work	UWA Channel Modeling
SER, OOB emissions	Performance evaluation of coded F-OFDM system for a modelled channel based on t-distribution.	[126]	Time-variant multipath propagation channel

4.2.3.1. Performance analysis of filtered-OFDM for statistically characterized UWA channel

Ahmed et. al [126] have evaluated the performance of an F-OFDM system with turbo and convolutional coding for a UWA channel that was statistically characterized using T-distribution. F-OFDM is a promising technique for future 5G networks due to its ability to reduce OOB emissions, decreasing

PAPR of the system and implementation simplicity. An F-OFDM system is spectrally more efficient since filtering is performed after the IFFT block that reduces OOB emission and enables the subcarriers to be more tightly placed by reducing ICI.

Noise samples for UW channel were taken at various depths and through curve fitting it was observed that the noise distribution of the observed channel followed a t-distribution. Error probabilities for BPSK and QPSK were evaluated for the said distribution. A stationary channel was assumed, that is time-invariant and without multipath components. Two type of coding schemes were evaluated for data-rate improvements: turbo and convolutional codes. For filtering, an RRC pulse shape was found to be more effective due to its ability to balance time and frequency localization. Through Matlab simulations, SER results were obtained for a UWA channel based on T-distribution.

The BPSK and QPSK error-rate results largely matched the theoretical estimates for a t-distribution based UWA noise channel, where BPSK slightly outperformed QPSK modulation. The results demonstrated that coded OFDM and F-OFDM have the same SER performance with turbo-coded OFDM and F-OFDM besting their convolutional-coded variants. A PSD analysis is performed with F-OFDM having very low OOB emissions as compared to OFDM and the performance improves with increasing roll-off factor (α) values.

4.2.4. Concluding Remarks

Previous three sections have presented an overview of the latest developments in the domain of GFDM, FBMC and F-OFDM for UWA channels. While FBMC and GFDM have a slightly higher computational complexity when compared with OFDM [127], research in the domain of complexity reduction techniques will soon fill the gap. Other candidate waveforms suffer from a higher complexity. When it comes to OOB leakage, both GFDM and FBMC are considered to be the most efficient. Hence, it is natural to evaluate their performance in UWA channels as the bandwidth of such channels is limited. Substantial work can be found where the performance of FBMC for UWA channels has been evaluated but there is a lot of room to do such kind of work in the GFDM and F-OFDM.

4.3. System Architecture of the Proposed GFDM Transceiver

To the best of our knowledge, there is no comprehensive work that reports the performance of GFDM in UWA channels by evaluating the metrics such as error performance, peak to average power ratio and spectrum efficiency in a single paper. Work done in this area lacks the performance evaluation of these important metrics as a function of the pulse shapes and their roll off factors, TX-RX distances and UWA multipath channel profiles. We have tried to fill this gap. The subsections that follow give the details of the proposed GFDM modem architecture for a UWA channel. The details include the transceiver structure, a summary of pulse shapes used and a brief description of the two equalization techniques that have been used in this work.

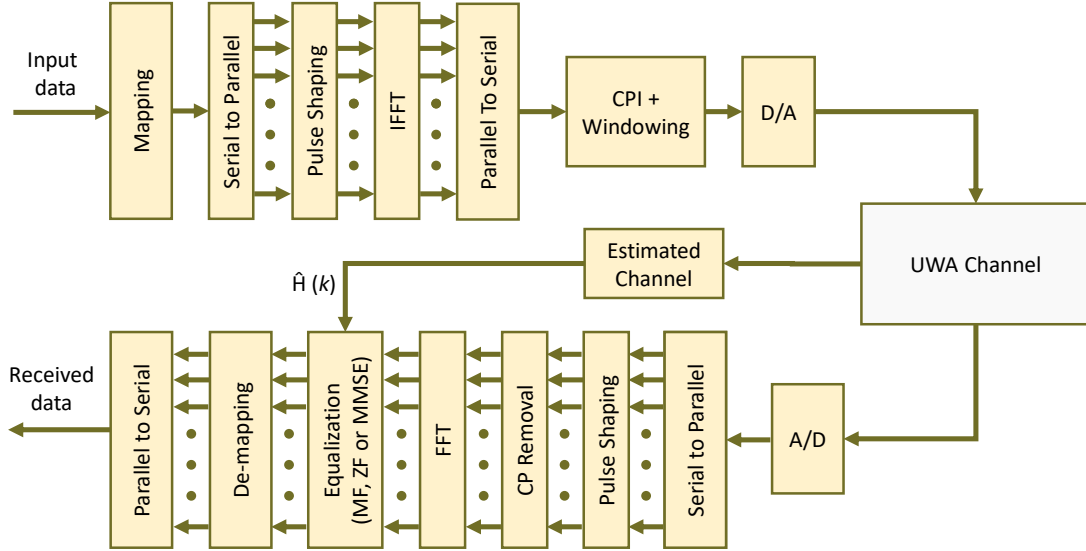


Figure 4.1. GFDM transceiver architecture

4.3.1. Transmitter Architecture

GFDM was first proposed in the year 2009 by Gerhard Fettweis. Since then several publications have appeared that evaluate the performance of a typical GFDM system in different scenarios – see for example, [128-133]. A typical GFDM transceiver for UWA channel is shown in Fig. 4.1. Let the input data be in the form of binary bits that passes through a mapper such as QAM to form symbols that belong to a 2^μ -QAM constellation where μ is the modulation order. Let the output of the mapper, i.e., the mapped symbols, be denoted by a vector \vec{c} .

If K represents the number of subcarriers, M represents the number of subsymbols and $N = KM$, then a serial to parallel converter takes the serial stream of \vec{c} symbols and converts them into a parallel stream of N elements represented as $\mathbf{C} = (\vec{c}_0^T, \dots, \vec{c}_{M-1}^T)^T$ where $\vec{c}_m = (c_{0,m}, \dots, c_{K-1,m})^T$. Hence, \mathbf{C} is a $K \times M$ matrix where each element $c_{k,m}$ represents the data transmitted on the k th subcarrier in the m th subsymbol. The resulting block of data passes through a pulse shaping filter and then an IFFT block represented mathematically as:

$$g_{k,m}[n] = g[(n - mK) \bmod N]e^{j2\pi\frac{k}{K}n}, \quad (4.3)$$

It can be observed that the pulse shaping filter $g_{k,m}[n]$ is circularly shifted in time using the modulo operation. Moreover, it is also shifted in frequency by taking the IFFT. The transmitted signal $x[n]$ is then obtained as follows:

$$x[n] = \sum_{k=0}^{K-1} \sum_{m=0}^{M-1} g_{k,m}[n]c_{k,m}. \quad (4.4)$$

$$n = 0, 1, \dots, N - 1$$

The above expression can also be written in a matrix form as follows:

$$\vec{x} = A\vec{c}, \quad (4.5)$$

where A is a matrix having $KM \times KM$ dimensions [134] whose each column is a vector $\vec{g}_{k,m}$ given by $(g_{k,m}[n])^T$ and \vec{c} is a vector having $KM \times 1$ dimensions. Then the matrix A can be represented as:

$$A = (\vec{g}_{0,0} \dots \vec{g}_{K-1,0} \quad \vec{g}_{0,1} \quad \dots \quad \vec{g}_{K-1,M-1}). \quad (4.6)$$

Finally, a cyclic prefix – denoted as N_{CP} – is added to \vec{x} and the digital signal is converted into analog before transmission.

4.3.2. Pulse Shaping Filters

Choice of transmitter pulse shaping filter is an important factor in the performance of a GFDM system. In this work, we explore five different pulse shaping filters namely raised cosine (RC), root raised cosine (RRC), 1st Xia, 4th Xia (introduced in [135]) and Dirichlet [136]. These filters influence the out-of-band (OOB) radiation as well as the error performance of a GFDM system. Fig. 4.2 shows a plot of the pulse shape filters while their frequency response expressions are shown in Table 4.5. Further details of the pulse shaping filters with reference to GFDM can be found in [137].

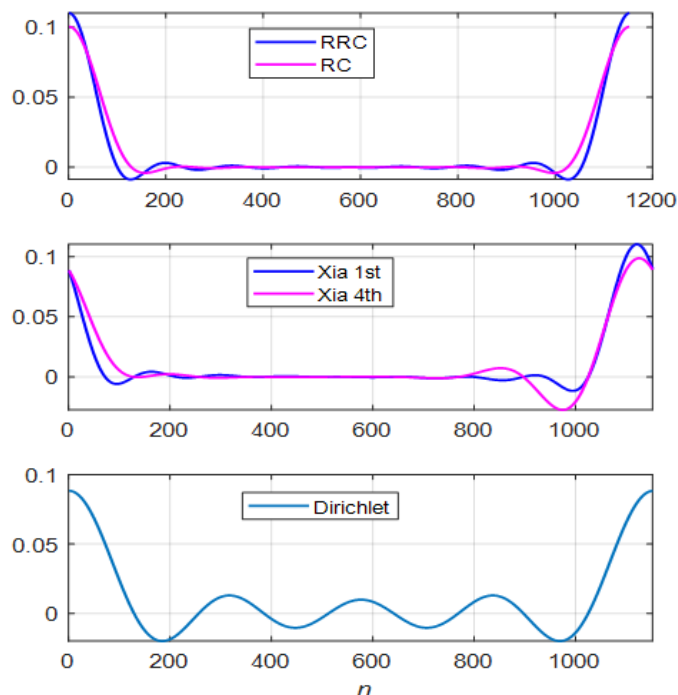


Figure 4.2. Pulse shapes for the five pulses used in this work

Table 4.5: Pulse Shaping Filters [138]

Pulse Shape	Frequency Response
RC	$G_{RC}[f] = \frac{1}{2} \left[1 - \cos \left(\pi \text{lin}_\alpha \left(\frac{f}{M} \right) \right) \right]$,
RRC	$G_{RRC}[f] = \sqrt{G_{RC}[f]}$
1st Xia	$G_{Xia1st}[f] = \frac{1}{2} \left[1 - e^{-j\pi \text{lin}_\alpha \left(\frac{f}{M} \right) \text{sign}(f)} \right]$
4th Xia	$G_{Xia4th}[f] = \frac{1}{2} \left[1 - e^{-j\pi p_4 \text{lin}_\alpha \left(\frac{f}{M} \right) \text{sign}(f)} \right]$

4.3.3. Receiver Architecture

The received analog signal – denoted by $\hat{x}(t)$ and also shown in Fig. 4.3 – is converted into a digital signal, then it passes through the pulse shaping filter followed by CP removal and then the FFT is performed to obtain the signal \vec{y} that is given by:

$$\vec{y} = H\vec{x} + \vec{n} \quad (4.7)$$

where H is the channel matrix, \vec{n} is the AWGN vector with $\vec{n} \sim \mathcal{N}(0, \sigma^2)$ and σ^2 being the noise variance. Using equation 4.5 and 4.7, \vec{y} can be written as:

$$\vec{y} = HA\vec{c} + \vec{n} \quad (4.8)$$

Assuming that the channel is known, both sides of equation 4.8 are pre-multiplied by H^{-1} to get the following expression:

$$H^{-1}\vec{y} = H^{-1}HA\vec{c} + H^{-1}\vec{n} \quad (4.9)$$

$$\tilde{\vec{y}} = A\vec{c} + \tilde{\vec{n}} \quad (4.10)$$

where $\tilde{\vec{y}} = H^{-1}\vec{y}$ and $\tilde{\vec{n}} = H^{-1}\vec{n}$. To extract \vec{c} , equation 4.10 can be re-written as:

$$\hat{\vec{c}} = Z\tilde{\vec{y}} \quad (4.11)$$

where $\hat{\vec{c}}$ are an estimation of the transmitted symbols and Z is a matrix having $KM \times KM$ dimensions. The method of computing Z determines the type of receiver being employed to estimate the transmitted symbols.

In this work, we evaluate the performance of a GFDM system over UWA channels using two types of receivers – zero forcing and matched filter. In the following, we briefly describe each one of them.

4.3.3.1. Zero Forcing receiver

In this type of receiver, $Z = A^{-1}$. However, since A may not be square, its inverse cannot be computed, rather, its pseudo-inverse – denoted as A^+ , is determined using the following relationship:

$$A^+ = (A^H A)^{-1} A^H \quad (4.12)$$

where A^H is the Hermitian of A . Hence, in equation 4.11, $Z = A^+$ for a zero-forcing receiver. Such a receiver alleviates the self-interference but enhances the noise.

4.3.3.2. Matched Filter receiver

If Z is set to be A^H in equation 4.11, the resulting receiver is called matched filter receiver. This type of receiver would maximize the SNR for each subcarrier at the cost of causing self-interference in case a non-orthogonal pulse is used in the transmitter.

4.4. Shallow Underwater Acoustic Channel

The UWA channel is doubly selective in nature and undergoes both frequency and time selectivity [2]. Acoustic signals undergo absorption loss in a UWA channel and this together with the ambient noise and multipath components limits the bandwidth over 1 km ranges to a few kilo Hertz [91]. Thus, for an MC communication system, the carrier spacing will be reduced to a greater extent owing to limited bandwidth availability [17]. ICI will arise due to the presence of even a smaller value of Doppler shifts in such systems. Another issue is that of the severity of motion based attenuation as the speed of sound in an underwater medium is much less as compared to RF signals on ground [15]. An underwater channel having L time shifted multipath components will have a response expressed mathematically as [2]

$$H(t, \tau) = \sum_{p=1}^L A_p(t) \delta(\tau - \tau_p(t)) \quad (4.13)$$

where $\tau_p(t)$ and $A_p(t)$ are the delay coefficients and amplitude of p th multipath component respectively, and $\delta(t)$ is the Dirac delta function. We have split the shallow underwater channel envelop response into two major factors:

- deterministic channel response.
- random multipath fading.

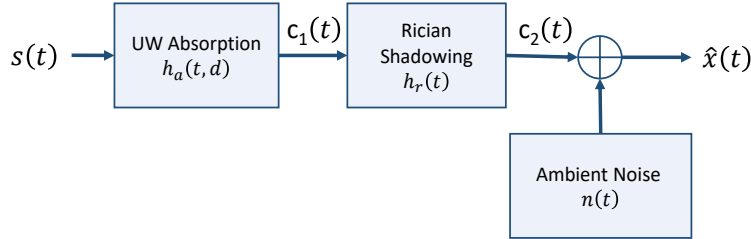


Figure 4.3. Proposed UWA channel model.

With reference to Fig. 4.3, let $s(t)$ be the transmitted signal that passes through an underwater channel. This channel model is close to a real underwater channel as it contains absorption and angular pathloss, multipath fading as well as noise of a realistic underwater channel. The model allows for adjusting and controlling the SNR of the system, and the ability to select number of channel taps to introduce multipath fading based upon Rician shadowing. In this model, using Thorp's formula [61], we can also select and adjust the parameters for pathloss that happens due to absorption of an acoustic signal in a shallow UWA channel. These settings of parameter variations include selecting ocean depth profile, channel geometry, delay spread, maximum Doppler frequency, average multipath gains, various parameters affecting the speed of sound in underwater, the TX-RX distance, and the relative depth of transmitter and receiver. For a typical UWA channel, the delay spread is approximately 10 to 20 ms which at times may go up to as large as 100 ms [92].

4.4.1. Deterministic channel response

A signal's energy in a medium usually gets attenuated as a function of both frequency and distance. In case of UWA transmission, the pathloss of an acoustic signal in an underwater medium is a combination of both absorption and geometric spreading. In the frequency domain, the mathematical transmission loss expression of a scalar wave propagating in the positive z direction, when time variation is $e^{j\omega t}$ is

$$E(z) = E_0 e^{-\gamma z} = E_0 e^{-\alpha z} e^{-j\beta z}, \quad (4.14)$$

where E_0 is the scaling constant. In such a scenario, the deterministic channel transfer function $H_a(f, d)$ [62, 63] can be written as:

$$H_a(f, d) = A_d e^{-\gamma(f)d}, \quad (4.15)$$

where A_d is a scaling constant, d is channel's physical length or the distance between transmitter and receiver in meters and γ is the complex propagation constant, expressed in m^{-1} and given by:

$$\gamma(f) = \alpha(f) + j\beta(f), \quad (4.16)$$

where $\alpha(f)$ is the absorption coefficient and $\beta(f)$ is the phase constant. In a UWA channel, the absorption is dependent on frequency of the carrier because significant energy is lost to heat, thus decreasing the acoustic pressure. The absorption coefficient $\alpha_{dB}(f)$ is calculated in dB/km using Thorp's formula [61] given as:

$$\alpha_{dB}(f) = 1.094 \left(0.003 + \frac{0.1f^2}{1+f^2} + \frac{40f^2}{4100+f^2} + 0.000275f^2 \right), \quad (4.17)$$

and converted to Np/m using the expression:

$$\alpha(f) = \frac{\alpha_{dB}(f)}{8686}, \quad (4.18)$$

Fig. 4.4 shows the absorption pathloss transfer function for various TX-RX distances and a fixed depth. The phase constant $\beta(f)$ in $\frac{rad}{m}$ is computed as:

$$\beta(f) = \frac{2\pi f}{c_s}, \quad (4.19)$$

where c_s is the sound speed [64] in ms^{-1} , computed as:

$$c_s = 1449.2 + 4.6T - 0.055T^2 + 0.00029T^3 + ((1.34 - 0.01)T)(S - 35) + 0.016 Z_M, \quad (4.20)$$

where T is temperature (in degrees Celsius), S is the value of salinity (in parts per thousand), and Z_M is depth in meters. This equation is also called Medwin's equation [64] and it considers values approximately that of a realistic underwater channel; temperature is taken in the range of 0° to $35^\circ C$, salinity between 0 to 45 PPT and depth of up to 1000 m. The signal $c_1(t)$ in Fig. 4.3, is then computed as:

$$c_1(t) = h_a(t, d) \otimes s(t), \quad (4.21)$$

here, $h_a(t, d)$ is obtained by taking the inverse fast Fourier transform of channel transfer function $H_a(f, d)$ and the symbol \otimes stands for time convolution.

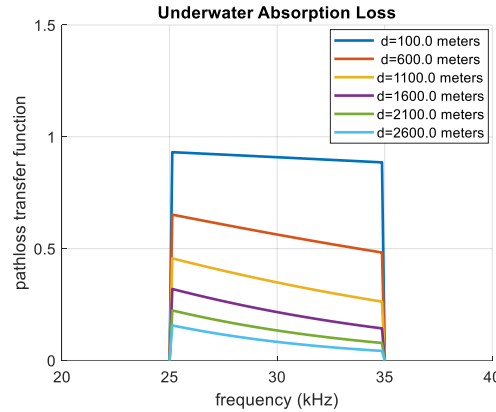


Figure 4.4. Frequency dependent absorption.

4.4.2. Random channel

As discussed in earlier chapters, researchers and scientists historically agree over several fading models that dominate the RF channel propagation modeling domain, but there lacks a consensus over the fading models used in UWA communication. However, some of the experimental observations suggest that the fading observed by an acoustic signal in a UW channel is closer to Rician fading [93]. For our proposed channel model, we have statistically modeled multipath fading using a Rician shadowed distribution. In [59] and [60], experimental data from sea trials was used to fit Rician, K and Rayleigh distributions and the goodness of the fits was compared. The Rician shadowed distribution parameters used in this work are: $k = 2.0$ and $m = 0.4$ [65]. The spreading factor $k = 1.5$ can also be considered [67]. By adding the multipath fading response, the signal $c_2(t)$ becomes,

$$c_2(t) = h_r(t) \otimes c_1(t) + n(t) \quad (4.22)$$

where $n(t)$ is the noise (additive) and $h_r(t)$ – the impulse response of the Rician channel [68] – is the IFFT of $H_r(f)$ – the Rician channel transfer function. We modelled Rician channel using Matlab's Rician channel object and the average path gains and the delay profile sample used in this work for simulations is depicted in Fig. 4.5.

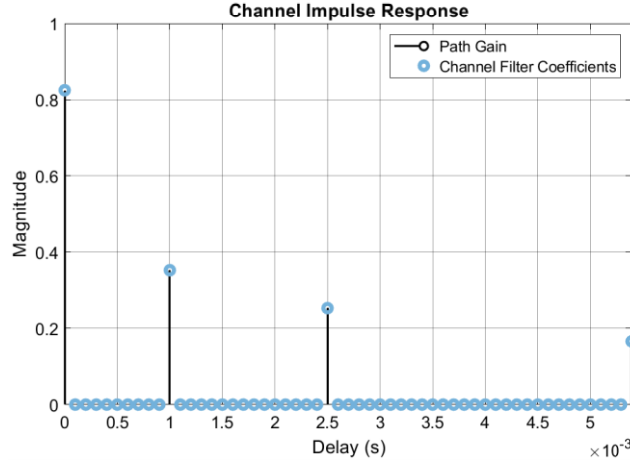


Figure 4.5. Channel impulse response.

4.4.3. Noise power

In a realistic UWA channel, the noise is not white and depends upon various acoustic frequencies. For our simulations, we use additive white Gaussian noise (AWGN), which although not frequency dependent, is still the worst-case additive noise and simplifies the implementation process. Thus, SNR in decibels (dB) for a given transmitted signal is given by

$$SNR = 10 \log_{10} \frac{c_2(t)^2}{n(t)^2} \quad (4.23)$$

Hence, the noise power $\overline{n^2(t)}$ added to the signal is

$$\overline{n^2(t)} = \overline{c_2(t)^2} \times 10^{-SNR/10} \quad (4.24)$$

where $c_2(t)$ is the signal at the output of the multipath fading block. We also add an ambient noise block, if a more realistic realization of the ambient noise in an underwater channel is required. The model is based on the sum of all frequency dependent noises, particularly from four sources; thermal, shipping, turbulence and wave noise [69]. The power spectral densities (PSD) in *dB re μPa/Hz* are given as:

$$10 \log N_{shipping}(f) = 40 + 20(s - 0.5) + 26 \log f - 60 \log(f + 0.03), \quad (4.25)$$

$$10 \log N_{turbulence}(f) = 17 - 30 \log f, \quad (4.26)$$

$$10 \log N_{wave}(f) = 50 + 7.5\sqrt{w} + 20 \log f - 40 \log(f + 0.4), \quad (4.27)$$

$$10 \log N_{thermal}(f) = -15 + 20 \log f, \quad (4.28)$$

where s is the shipping activity factor having a value of 0 for light shipping, 0.5 for moderate and 1 for high shipping. w represents the wind speed in ms^{-1} and f is frequency in *KHz*. The total noise PSD comes out to be

$$N(f) = 10 \log \left(10^{\frac{N_{shipping}(f)}{10}} + 10^{\frac{N_{turbulence}(f)}{10}} + 10^{\frac{N_{wave}(f)}{10}} + 10^{\frac{N_{thermal}(f)}{10}} \right). \quad (4.29)$$

It can be modelled as colored Gaussian noise and added to the transmitted signal. As evident, the noise is location specific and it is observed that the noise amplitude is high at both lower and higher frequencies whereas it is at its minimum around 60 kHz [96].

4.5. Simulation Setup

We have implemented a GFDM transceiver model in MATLAB based on [102], together with our proposed UW channel realization. Table 4.6 shows three configurations of transmitter and receiver parameters while Table 4.7 shows the channel parameters used in our simulations. A $K \times M$ random binary stream is generated followed by M -ary mapping according to the value of modulation index μ and the chosen mapper (which is QAM in this work). These mapped symbols are then modulated according to the pulse shape and its roll-off factor α . Then an IFFT operation is applied to the stream. Finally, a CP is added to the modulated waveform every M sub-symbols (we use a CP of length $K/4$ in our simulations). This is the transmitted signal.

Table 4.6: Simulation Parameters

Parameters	GFDM	OFDM
Number of CP symbols (N_{cp})	$K/4$	$K/4$
Configuration 1		
Number of subcarriers (K)	512	512
Number of time slots (M)	25	1
Mapping	4-QAM	4-QAM
Active subcarriers (K_{on})	392	-
Active sub-symbols (M_{on})	11, 17, 21	-
Roll-off factor (α)	0.25	0
Pulse shape	RRC	RECT
Configuration 2		
Number of subcarriers (K)	128	128
Number of time slots (M)	9	1
Mapping	4-QAM	4-QAM
Active subcarriers (K_{on})	96	-
Active sub-symbols (M_{on})	7	-
Roll-off factor (α)	0.1, 0.3, 0.5, 0.7	0
Pulse shape	RRC, RC, 1 st Xia, 4 th Xia	RECT
Configuration 3		
Number of subcarriers (K)	32	256
Number of time slots (M)	8	1
Mapping	4-QAM	4-QAM
Active subcarriers (K_{on})	32	-
Active sub-symbols (M_{on})	8	-
Roll-off factor (α)	0.1 to 0.9	0
Pulse shape	RRC, RC, 1 st Xia, 4 th Xia	RECT
Configuration 4		
Number of subcarriers (K)	128	128, 256, 384, 512
Number of time slots (M)	3 - 25	1
Mapping	4-QAM	4-QAM
Active subcarriers (K_{on})	32	-
Active sub-symbols (M_{on})	5 - 21	-
Roll-off factor (α)	0.1 to 0.9	0
Pulse shape	RRC, RC, 1 st Xia, 4 th Xia	RECT

Table 4.7: Channel Parameters

Symbol	Quantity
TX-RX distance	100, 600, 1100, 1600, 2100 m
Depth	10 m
Max doppler shift	10 Hz
Gain vector	[0; -1.5; -2.5; -7; -2] dB
Tau vector	[0; 1; 2.5; 5; 7] ms

4.6. Results

Simulation results evaluating the spectral efficiency, bit error rates and peak to average power ration for different transceiver and channel parameters.

4.6.1 Power Spectral Density

First, the PSD of the transmitted signal is computed. Fig. 4.6 shows the PSD of a GFDM transmitted signal for three different values of M_{ON} when the signal was generated using Configuration 1. The figure also compares the PSD with that of OFDM. It can be noticed that OOB emissions of a GFDM transmitter are significantly lower as compared to an OFDM signal. It is further observed that the spectral efficiency of GFDM deteriorates as the number of active sub-symbols increase.

Fig. 4.7 compares the PSD of the transmitted and received GFDM signals generated for a channel with max Doppler shift of 10 Hz, a bandwidth of 10 kHz, a distance of 750 m and the number of subcarriers as 512 out of which 392 subcarriers are active. An RC pulse shape is used with a roll-off factor of 0.5. It is noted that the PSD of the GFDM signal deteriorates after passing through the UWA channel. This is to be expected as the UWA channel is a doubly selective dispersive channel that severely affects the transmitted signal.

Figures 4.8-11 show the PSD of a GFDM signal for four different types of pulse shapes (using Configuration 2 from Table 4.6) and with varying values of the roll-off factor α . It is observed that the choice of the pulse shape as well as the value of the roll off factor influence the OOB emissions and the shape of the PSD. It is also observed that the higher the value of the roll off factor, lower the OOB emissions.

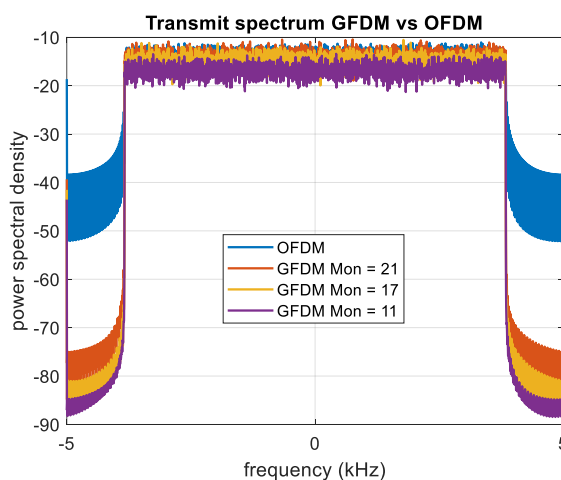


Figure 4.6. PSD comparing OFDM with $K = 512$ and GFDM with $K = 512$, $M = 25$, RRC pulse with roll-off of 0.25 and various M_{ON} (actual time slots utilized) values.

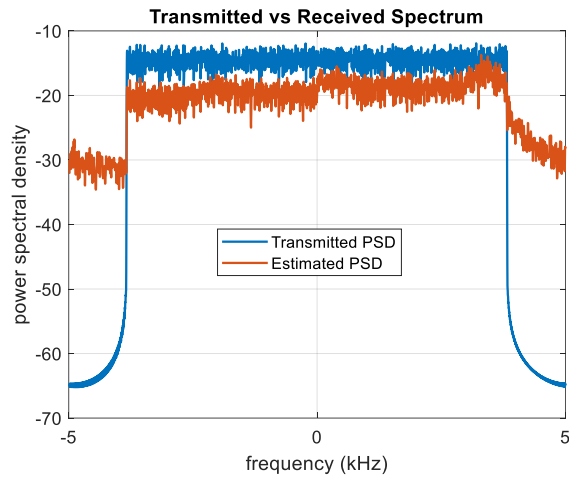


Figure 4.7. PSD of the transmitted and received signals.

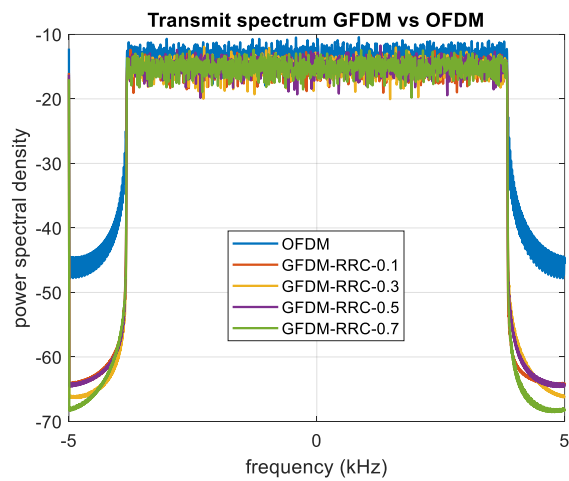


Figure 4.8. PSD OOB emissions comparison for various roll-off factors of RRC pulse.

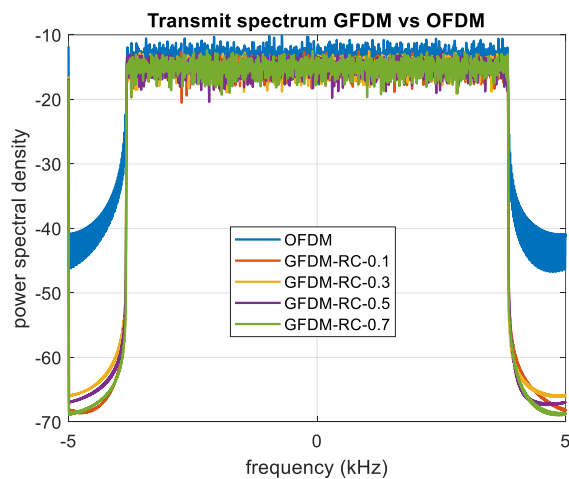


Figure 4.9. PSD OOB emissions comparison for RC pulse with varying values of α .

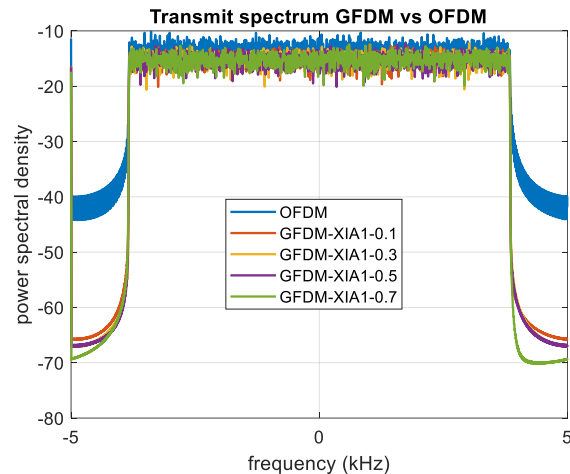


Figure 4.10. PSD OOB emissions comparison for various roll-off factor values of 1st Xia.

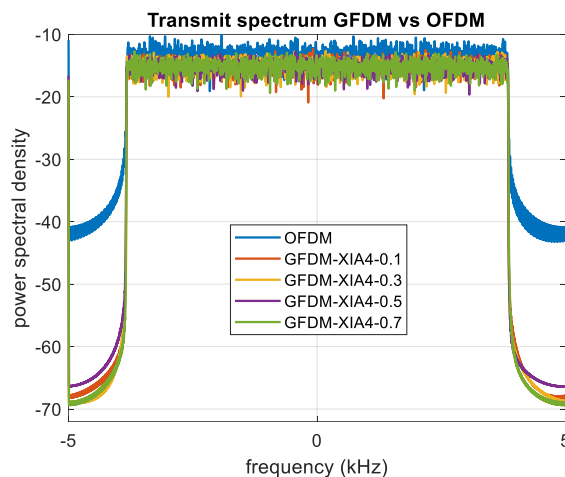


Figure 4.11. PSD OOB emissions comparison for multiple values of roll-off factor of 4th Xia.

4.6.2. Peak to Average Power Ratio

The PAPR performance of GFD was evaluated through simulations using Configuration 3 (Table 4.6). Random blocks of 10,000 symbols were passed through the GFD transmitter with $K = 32$ and $M = 8$ using different pulse shapes with varying values of roll off factor. Then the complementary cumulative distribution function (CCDF) was plotted in all the cases. The results obtained are shown in Figs. 4.12 to 15.

It is noted that the PAPR performance of all the GFD signals are comparable to OFDM with several cases marginally worse than OFDM. It is further noted that pulse shaping filters significantly impact the PAPR of GFD and the best PAPR performance is exhibited when the pulse shape is 4th Xia. Moreover, for all the pulse shapes, the higher the value of the roll off factor, the worse is the PAPR.

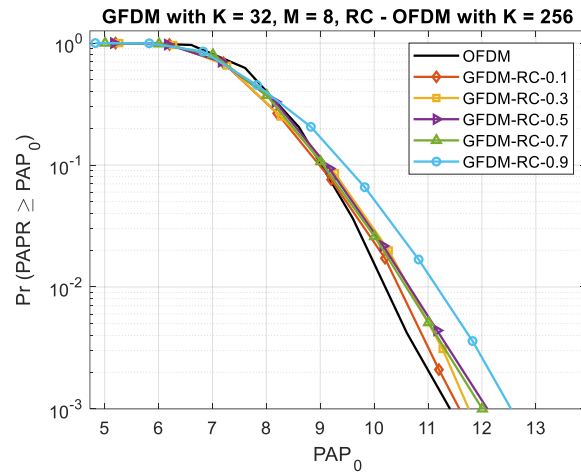


Figure 4.12. PAPR performance for various roll-off factors of RC pulse.

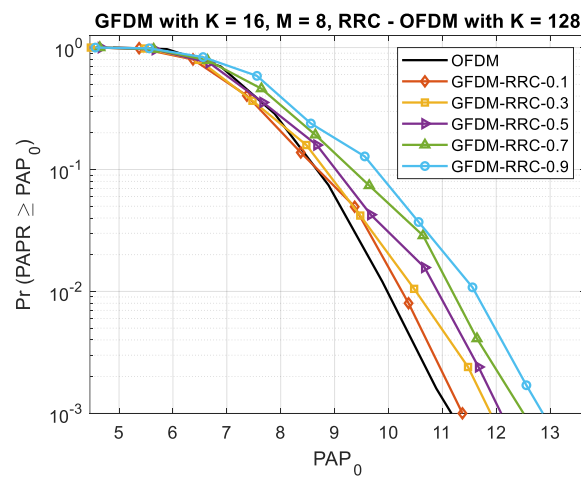


Figure 4.13. PAPR performance for RRC pulse with varying values of α .

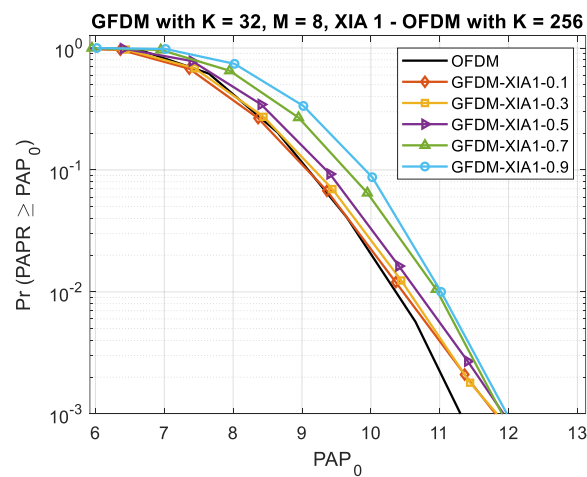


Figure 4.14. PAPR performance for various values of roll-off factor of 1st Xia.

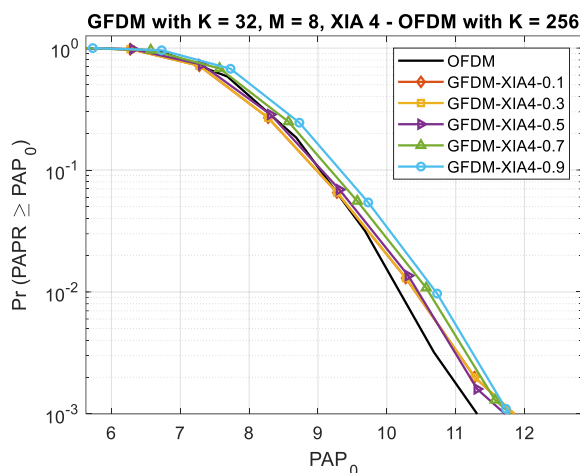


Figure 4.15. PAPR performance for various values of roll-off factor of 4th Xia.

4.6.3. Symbol Error Rate

To compute the symbol error rates (SER), the transmitted signal is passed through the UWA channel. The channel is implemented in MATLAB using the theory presented in Section 4.3. Its pathloss transfer function is obtained via the distance and bandwidth information, and the matrix thus obtained is passed to the IFFT block to obtain its time domain version.

Now the transmitted signal is convolved with the time domain version of the channel matrix. To add frequency selective fading to this signal, we use MATLAB's Rician Channel function. Finally, ambient noise $N(f)$ is computed using equation 29, its IFFT is taken and added to the transmitted signal.

To recover the transmitted symbols, the received signal passes through the pulse shaping filter followed by CP removal and then the FFT. Since the channel is assumed to be known, the received signal is pre-multiplied by the inverse of the channel matrix as has been explained in sub section 4.3.2. Next, the resulting symbols are pre-multiplied by A^+ to implement a zero-forcing receiver and with A^H to implement a matched filter receiver. The sequence thus obtained is compared with the transmitted symbols and the SER is computed.

The error performance of proposed GFDM system was evaluated over UWA channels for the two receivers introduced in sub section 4.3.2, namely, zero forcing and matched filter. Configuration 4 was used to obtain the results shown in Figs. 4.16 to 19. These results are generated as a function of: (a) TX-RX distance, (b) channel bandwidth, and (c) Mon while Fig. 4.19 compares a typical GFDM system with OFDM. As shown in Fig. 4.16, SER deteriorates as the TX-RX distance increases. The reason behind this degradation is that underwater acoustic signals undergo absorption. This absorption increases as the distance increases thus worsening the SER.

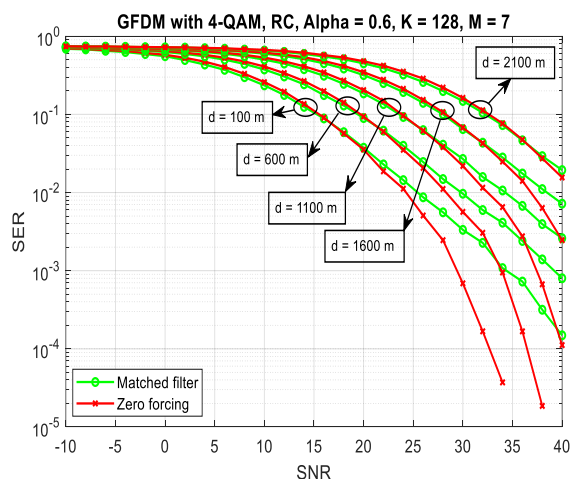


Figure 4.16. SER performance for both MF and ZF equalizers at various TX-RX distances with $K = 128$, $M = 7$, RC pulse with roll-off value of 0.6, 10 kHz bandwidth and $\mu = 2$.

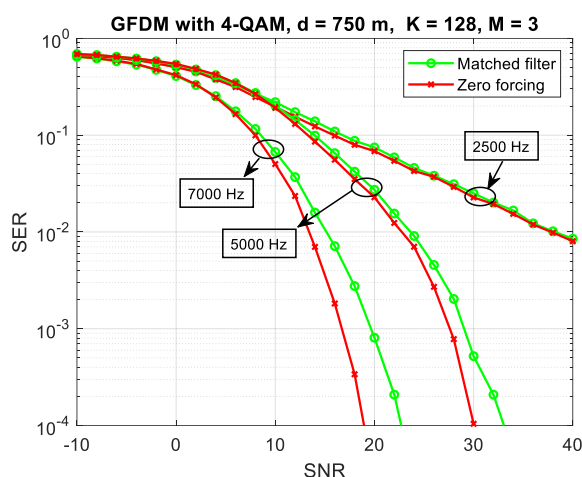


Figure 4.17. SER performance for both MF and ZF equalizers at various bandwidths with $K = 128$, $M = 3$, RC pulse with roll-off value of 0.6 and $\mu = 2$.

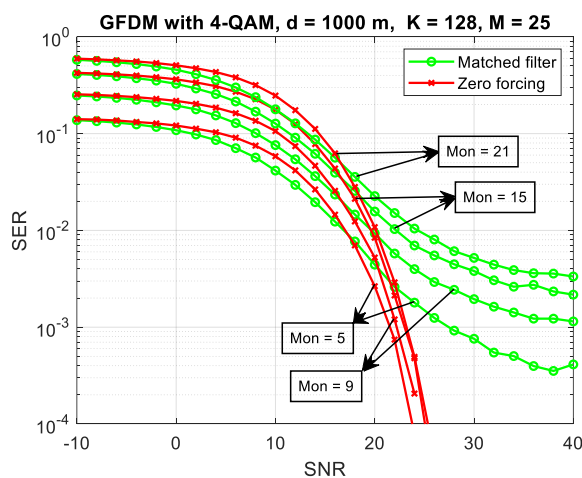


Figure 4.18. SER performance for both MF and ZF equalizers for various M_{ON} values with $K = 128$, $M = 25$, RRC pulse with roll-off value of 0.6 and $\mu = 2$.

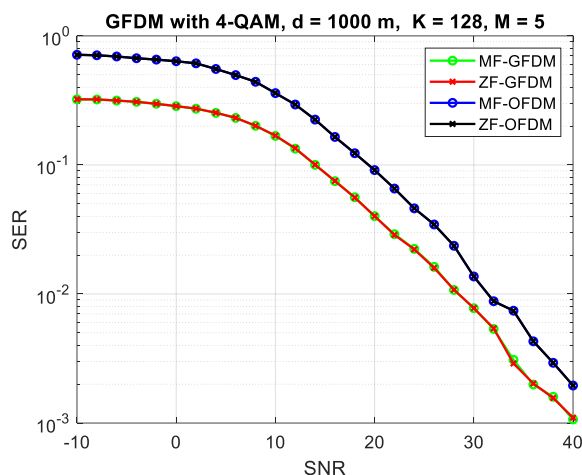


Figure 4.19. SER comparison of GFDM and OFDM for $d = 1$ km, $K = 128$, $\mu = 2$ and a similar bandwidth of 5 kHz.

Fig. 4.17 shows the SER of GFDM when the bandwidth is varied. It is noted that the SER deteriorates as the bandwidth decreases. This is due to the fact that the frequency band allocated to each subcarrier decreases with decreasing bandwidth. As a result, ICI increases that degrades the SER. It is also evident that the performance of both the receivers is almost identical. SER performance when Mon is varied is shown in Fig. 4.18. It is observed that the SER improves as Mon decreases when M is fixed at 25. That is, SER improvement is achieved at the cost of sending lesser number of data carrying sub-symbols.

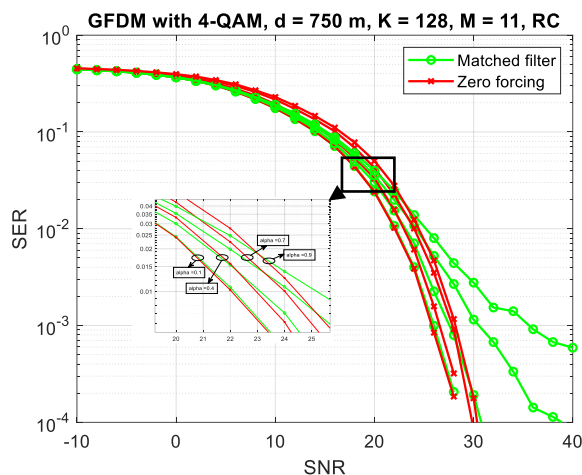


Figure 4.20. SER performance for different roll-off factors for RC pulse shape.

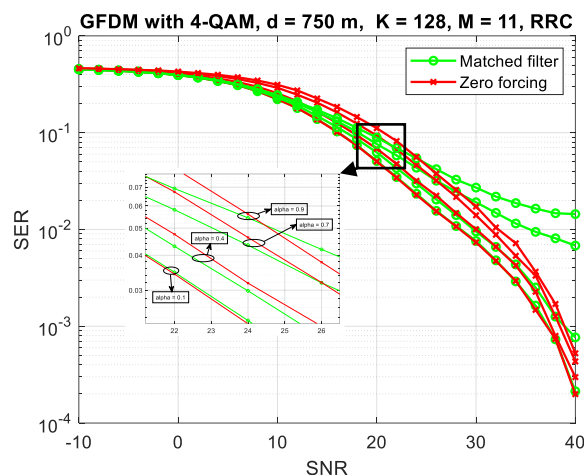


Figure 4.21. SER performance for RRC pulse with varying values of α .

The SER performance of a typical GFDM system is compared with that of an OFDM system in Fig. 4.19. It is observed that the SER performance of GFDM is better than OFDM for a 1 km distance between the transmitter and receiver, $K = 128$, $M = 5$, and an RC pulse shape with roll off equal to 0.1. There is a gain of almost 4 dB in the case of GFDM for an SER of 10^{-2} . Furthermore, the performance of zero forcing and matched filter receivers is identical for the chosen parameters for both OFDM and GFDM.

The SER performance of proposed GFDM system is also evaluated as a function of pulse shapes and the value of the roll off factor. Figures 4.20 to 23 show the simulation results. Fig. 4.20 shows the SER performance for four different pulse shapes and four different values of the roll off factor. The choice of the pulse shape and the value of the roll off factor play a significant role in determining the SER performance of the GFDM system. Best SER performance is achieved with 1st Xia pulse and the roll off factor equal to 0.1 – as shown in Fig. 4.22. At the same time, it is seen that the GFDM system using 1st Xia pulse is the most sensitive among the four cases to the choice of the roll off factor. On the other hand, a GFDM system using RC and RRC pulse shapes is the least sensitive among the four cases to the value of the roll off factor – evident from Figs. 4.20 and 4.21. It is observed that for all the four cases, the SER degrades as the value of the roll off factor increases.

Another interesting observation is that for several values of the roll off factor, the performance of the zero-forcing receiver is better than that of the matched filter receiver when the pulse shape employed is RC or RRC. On the other hand, the performance of the matched filter receiver is better than that of the zero-forcing receiver when the pulse shape employed is 1st or 4th Xia. In conclusion, if SER performance is the sole design criterion, a pulse shape of 1st Xia with a roll off factor of 0.1 seems to be the most appropriate choice.

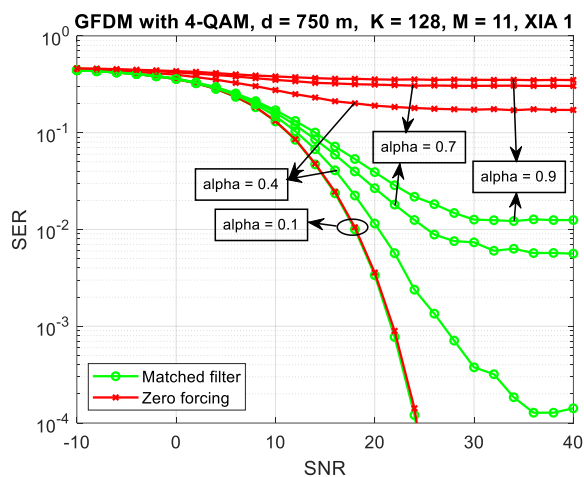


Figure 4.22. SER performance for various values of roll-off factor α with Xia 1st pulse shape.

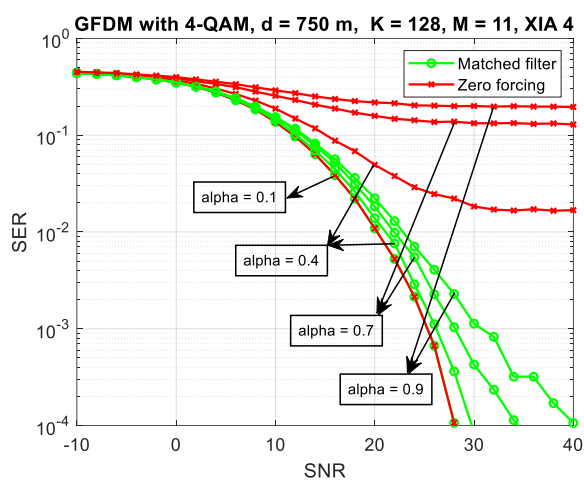


Figure 4.23. SER performance for various roll-off factor α values of Xia 4th pulse shape.

An overall comparison of proposed GFDM and OFDM based upon our findings and the simulation study is shown in Fig. 4.24 that shows the superiority of GFDM. A better performance is ranked higher e.g. in case of complexity, low value of complexity ranks higher than a higher value of complexity. Similarly, for BER, low BER ranks higher in the spider web and a high BER ranks lower.

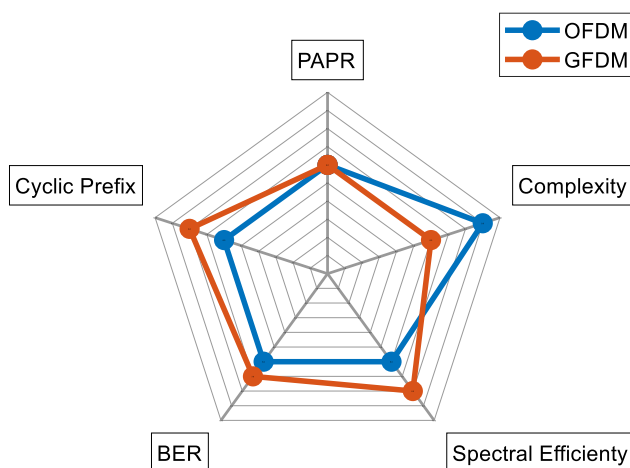


Figure 4.24. GFDM and OFDM comparison (higher is better).

4.7. Conclusion

We presented a survey of post-OFDM multicarrier waveforms for UWA channels. We have reported our findings and conclude that for future multicarrier systems, GFDM and FBMC have proven to be ideal candidates for underwater communication due to their improved spectral efficiency and immunity against ICI and ISI. GFDM offers a more robust and flexible solution at the cost of slight increase in computational complexity for transmission in the underwater medium. Our simulation results have shown that GFDM exhibits a better SER performance compared to an OFDM system for a UWA channel. Moreover, the spectral efficiency gains for a GFDM system are quite high as compared with other MC candidates. We have also shown that the choice of pulse shapes and the associated roll off factor play a significant role in determining the spectral efficiency and the SER of a GFDM system. A higher value of the roll off factor decreases the OOB emissions but at the cost of SER and a slight increase in PAPR.

The ability to utilize fragmented spectrum and varying spectral efficiency through various pulse shapes and their roll-off factors makes GFDM an ideal choice for spectrum limited UWA networks. Given its flexibility and lack of GFDM research in UWA domain, it is critical to study the performance of various low-complexity PAPR reduction, channel estimation and equalization techniques for UWA GFDM systems that will make it an ideal waveform for high data-rate acoustic communication.

Chapter 5: PAPR Reduction using Ciphered-BCH Codes

Like channel estimation and spectral efficiency, PAPR reduction of a UWA OFDM transmitter is a challenging task due to low bandwidth availability along with computational and power limitations [139]. In this chapter, we propose an effective, low complexity and multifaceted scheme for peak-to-average power ratio reduction of orthogonal frequency division multiplexing system for underwater acoustic channels. The proposed scheme takes advantage of XOR-ciphering and generates ciphered BCH codes that have low PAPR. This scheme is based upon an algorithm that computes several keys offline such that when the BCH codes are XOR-ciphered with these keys, it lowers the PAPR of BCH encoded signals. Subsequent low PAPR modified BCH codes produced using the chosen keys are used in transmission. This technique is ideal for UWA systems as it does not require additional computational power at the transceiver during live transmission. The advantage of proposed scheme is threefold. First, it reduces the PAPR, second, since it uses BCH codes, the BER of the system improves, and third, a level of encryption is introduced via XOR-ciphering, enabling secure communication. Simulations are performed in a realistic UWA channel and results demonstrate that the proposed scheme indeed achieves all the three objectives with minimum computational power.

The rest of the chapter is structured as follows: Section 5.2 details the recent advances in the domain of PAPR reduction for underwater acoustic channels, coding techniques proposed for UWA OFDM and using coding for PAPR reduction in OFDM systems. Section 5.3 briefly describes the OFDM transceiver architecture, the UWA channel model and the coding technique utilized. Section 5.4 gives a detailed overview of the proposed PAPR reduction technique followed by section 5.5 which is devoted to results and discussions. In the end, a short conclusion is provided in section 5.6.

5.1. Introduction

Despite its advantages, one of the foremost issues associated with OFDM is the high peak to average power ratio at the transmitter. It is a widely studied topic in the field of RF OFDM [140-144], whereas computational and bandwidth limitation renders it a unique problem in the acoustic domain [145]. A large PAPR value usually results from constructive overlapping of random symbol phases to create peaks in time domain. The presence of non-linear power amplifiers at the transmitter side makes it mandatory to reduce the average power of the system which causes a loss in performance. In-band distortions and spectral spreading are observed when such a signal passes through non-linear devices such as high-power amplifiers. Thus, a high peak to average power ratio causes in-band distortions in an OFDM system and further increases the complexity of implementation of other blocks such as analog-to-digital and digital-to-analog convertors [146]. Various techniques have been suggested to reduce PAPR of OFDM systems including: 1) signal distortion techniques e.g. clipping and filtering, windowing, companding and peak cancellation 2) probabilistic techniques including partial transmit sequences, selective mapping, tone injection and tone reservation 3) schemes based upon coding such as linear block coding, Golay sequences and turbo coding [144].

BCH codes have been used in communication systems for error correction to reduce bit error rates [147]. BCH codes are cyclic codes operating on a group of data bits or blocks rather than individual bits [148]. Due to their ability to fix multiple errors and simplicity in coding and decoding implementations, they find their uses in various applications. The decoding energy consumption of BCH codes is observed to be a linear function of the number of corrected errors t and the length of code words [149]. Some of the common codes used in this work and their generator polynomials generated using MATLAB's `bchgenpoly()` function are mentioned in Table 5.1.

Table 5.1: BCH Coding Parameters

Codes	n	k	t	Generator Polynomials
BCH (31,6)	31	6	7	11001011011110101000100111
BCH (31,11)	31	11	5	101100010011011010101
BCH (31,16)	31	16	3	1000111110101111
BCH (63,7)	63	7	15	10101001100100010010110110 00111010000110101110011110 11111
BCH (63,10)	63	10	13	10011101011001001001100010 1101010111010101010000011011 01
BCH (63,16)	63	16	11	11001101100100110000101111 0111010011101100101011
BCH (63,24)	63	24	7	11110110100110101100001000 00100100100001
BCH (127,8)	127	8	31	11100010011101011010000010 10101111010010000110001101 01001100111110010010100010 111001101110111111101101100 1011000010001111
BCH (127,22)	127	22	23	10100110111111100001110001 00000100111010010101010010 10001110110010010111001011 01100111111101001110001000 11
BCH (127,36)	127	36	15	11001100110000111100110110 11010101001000011110100010 01001111101001011111001110 10001111011101
BCH (127,50)	127	50	13	10110010010011010100101010 10100110110011000000010101 00010001101000001100010001

Vernam cipher was first used by Gilbert Vernam in 1917 for encrypting telegraph messaging [150]. Also called XOR cipher, its biggest advantage is that the encryption and decryption are both achieved using the same operation. At the transmitter, the input data is converted into binary and divided

into blocks. An XOR operation is performed for the input message data with a predefined key of the same block length. The obtained ciphertext is then transmitted whereby the receiver performs an XOR operation for the received data with the same key to get the original message.

In this work, we use XOR-ciphering on BCH codes to propose a low-complexity PAPR reduction scheme for an underwater acoustic OFDM. The proposed XOR-ciphered BCH codes not only have low PAPR, but they also provide a medium level of encryption of the transmitted data while improving the BER as well at the same time. The main contributions are:

- A low-complexity scheme based on XOR-ciphered BCH encoded symbols for PAPR reduction in UWA OFDM systems.
- An offline vector identification technique to shortlist random key vectors that will result in lowest possible PAPR of XOR-ciphered BCH codes.
- Evaluation of proposed technique using a shallow underwater channel model showing PAPR as well as BER reduction.

5.2. Related Work

In this section, we detail some of the recent advances in the domain of PAPR reduction and error correcting codes for UWA OFDM systems. Various schemes, to reduce PAPR on an OFDM system, have been proposed for underwater channels [9, 54, 145, 151-155] including partial transmit sequences (PTS), low-density parity-check (LDPC) coding, DFT precoding, and companding transforms, to name a few.

To deal with high peaks of the OFDM modulated systems, Rojo and Stojanovic (R&S) [145] have proposed a tone injection technique to reduce the peak to average power of an underwater acoustic OFDM system. The set of tones are injected out of the normal transducer bandwidth to minimize the peaks and are added to the system just before D/A conversion. These tones are subsequently filtered out after the signal has passed through the power amplifier but before transmitting the final signal. This filtering is the additional process that is required for tone suppression. Multiple techniques have been proposed by R&S for optimal placement of the chosen tones including a random search technique based on limited selection from a set of sequences, as an exhaustive search will not be feasible. A PAPR reduction of approximately 0.5 dB to a maximum of 2.5 dB takes place based upon whether the tones have been injected above or below the useful bandwidth and how far are the tones from the useful bandwidth. The data-rate is unaffected in this scheme as there are no overheads. Authors in [156] propose orthogonal signal division multiplexing (OSDM) for underwater acoustic communication due to its enhanced PAPR reduction performance. However, complexity of the direct channel equalizer is quite high. An indexed modulated OFDM scheme is proposed in [157] with a PAPR improvement of up to 7dB over traditional systems.

Historically, various implementations such as [158-161] have explored block coding techniques to reduce PAPR of OFDM systems for radio channels. Jones, Wilkinson, and Barton (JW&B) explored block coding for PAPR reduction of OFDM systems [162]. Input data is organized into blocks and for each block a code with least PAPR value of all is chosen from a list of selected code words. But they require exhaustive search and lookup tables incurring heavy processing costs. Tasadduq and Rao (T&R) [163] analyzed the performance of a PAPR reduction technique based on linear block codes and weighting functions for an OFDM system. The codes are chosen according to the number of subcarriers used e.g., Hamming (7,4) for an 8-subcarrier system. While the resulting coded words are not in powers

of 2, a redundant bit is added for easy IFFT implementation. If the number of sub-carriers used in an OFDM system are N , we use the fundamental principles of [162] and [163] while employing $BCH(n, k)$ codes to perform offline exhaustive search for lower orders of k and random selection sets in case of higher order of k , to come up with a single key vector of $(N - 1)$ bits that results in lowest PAPR values for most of the combinations.

Carrascosa and Stojanovic (C&S) employed quadrature phase shift keying (QPSK) signals encoded using BCH (64,10) for a low-complexity channel estimation technique for underwater acoustic MIMO OFDM systems [164]. Kim *et al.* evaluated various error correcting coding schemes for an underwater OFDM system [165]. The short-length codes evaluated were convolutional, turbo and BCH codes. Simulations using Bellhop [166] and real sea test results demonstrated that BCH codes had the best overall error correction performance for acoustic OFDM in underwater channels.

Additive ciphers [167] work by adding a sequence of k bits to the input sequence m to obtain ciphered sequence c . Huo and Gong (H&G) [168] have compared the performance of XOR cipher and phase cipher for an OFDM system. The encryption was performed both before channel coding and after channel coding. The XOR ciphering technique is computationally less intensive while having almost similar symbol error rate compared to phase cipher. Instead of a traditional first encrypt then encode technique, Gligoroski *et al.* evaluated the concept of cryptcoding schemes [169] whereby encryption and channel coding are integrated into a single block. The evaluated combined systems are more efficient and less complex.

In an underwater acoustic channel, frequency dependent pathloss, doppler spreading and multipath fading makes it very difficult to achieve a good bit rate. Similarly, securing the transmitted data while maintaining computational simplicity is a challenge. Thus, the idea of a reliable channel coding technique, combined with a moderate level of security, that can depress the high PAPR of a UWA OFDM system is intriguing.

5.3. System Architecture

In this section, we briefly explain the various components of our proposed system including the OFDM transmitter and receiver, the underwater channel model and the cipher and coding technique used.

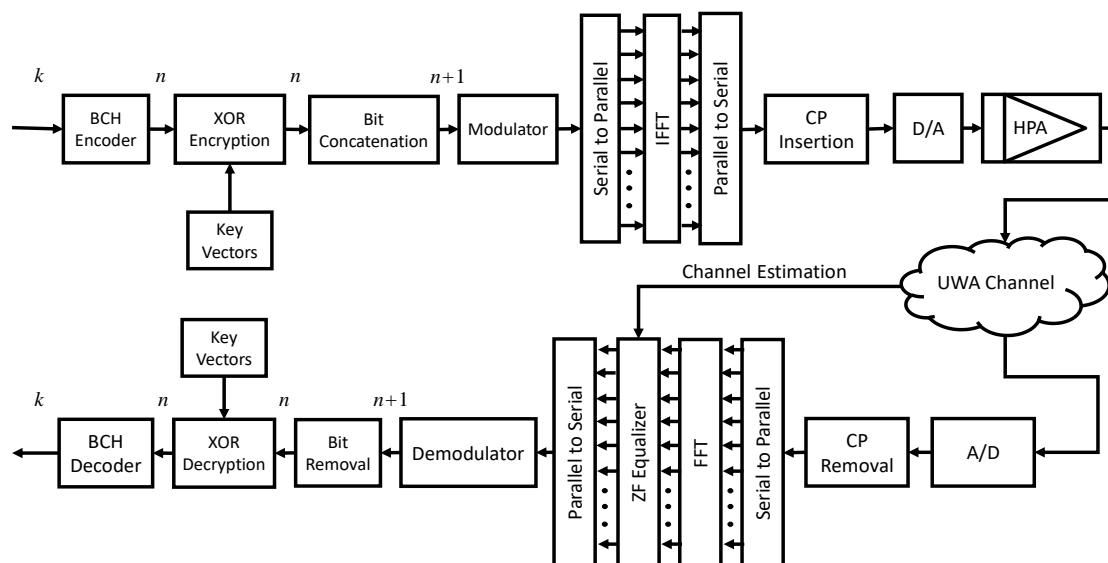


Figure 5.1. Proposed Ciphered-BCH OFDM Architecture

5.3.1. OFDM Transceiver

An OFDM based transceiver model is demonstrated in Fig. 5.1. The input binary stream b_i is randomly generated having a value of 0 or 1 where $i = 0, 1, 2, \dots$. The serial stream is then block encoded using a BCH(n, k) encoder. The output from the BCH encoder then undergoes XOR encryption. In a typical BCH(n, k) code, the value of n is a prime number while the number of sub-carriers N in an OFDM system are in powers of 2. Therefore, a single bit is appended to each of the encoded sequence. Then the bits pass through the modulator block where MPSK, QAM or DPSK mapping takes place. Typically, the output of the modulator is a complex number. Next, the serial stream of complex numbers is converted into a parallel stream that can be represented in vector form as:

$$C_p = [c_{p,0}, c_{p,1}, c_{p,2}, \dots, c_{p,N-1}]^T \quad (3.1)$$

where C_p is a vector of complex numbers for p th OFDM symbol and $c_{p,q}$ is the complex number for p th OFDM symbol and q th subcarrier. These signals are then converted to their discrete time-domain complex equivalents using an IFFT block of size N and are represented as:

$$X_p = [x_{p,0}, x_{p,1}, \dots, x_{p,N-1}]^T \quad (3.2)$$

where X_p is a vector representing the p th OFDM symbol and $x_{p,q}$ is the q th sample of p th OFDM symbol. A parallel to serial operation is performed and a CP is attached at the start of the OFDM symbol by copying tail samples of the symbol.

The discrete-time OFDM symbols are then converted into continuous-time signals using the digital to analog conversion block followed by a high-power amplifier block. The final output of the transmitter is then given by:

$$x_p(t) = \frac{1}{\sqrt{T}} \sum_{q=0}^{N-1} c_{p,q} e^{j2\pi f_q t} \quad (3.3)$$

where $x_p(t)$ is the continuous-time equivalent signal of p th OFDM symbol and the duration of an OFDM symbol is T . The symbol $x(t)$ will be used for the OFDM signal that has been transmitted for all the symbols. The transmitted signal then passes through the underwater acoustic channel. On the receiver, all the steps that were performed at the transmitter are performed in the reverse order. The received signal $\hat{x}(t)$, which is the degraded form of the transmitted signal, is converted back to discrete-time symbols using analog to digital convertor. The CP is discarded and serial to parallel operation is performed. The FFT block then produces the discrete frequency domain symbol vector given as:

$$\hat{C}_p = [\hat{c}_{p,0}, \hat{c}_{p,1}, \hat{c}_{p,2}, \dots, \hat{c}_{p,N-1}]^T \quad (3.4)$$

A zero-forcing equalizer has been employed assuming the channel state information (CSI) is known. The symbols are de-mapped after parallel to serial conversion. This is followed by an XOR decryption block and finally BCH decoding takes place giving estimated binary sequence \hat{b}_l .

5.3.2. XOR Encryption

Figure 5.2 depicts basic operation of an XOR encryption system [168]. The input message blocks m are bitwise XORed with the same size key k to generate encrypted data blocks c . In the proposed OFDM system, each binary plaintext/ciphertext block and key has the same size as the number of OFDM sub-carriers. However, the keys here are unique, and are determined based on the maximum PAPR reduction they can achieve when XORed with a BCH code.

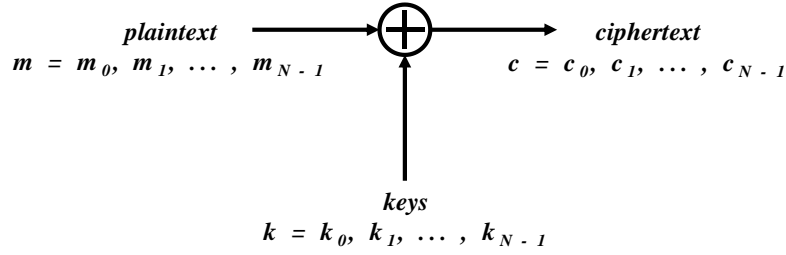


Figure 5.2. XOR encryption [168].

5.3.3. Shallow Underwater Channel Model

The system is tested using a shallow water underwater channel model [170] based on Rician fading along with absorption path loss and UWA noise. Due to the doubly selective behavior of the underwater channel, acoustic signals experience both time and frequency selectivity [2]. The carrier spacing is greatly reduced [17] since the available bandwidth is of the order of several kHz over longer distances due to the presence of ambient noise as well as losses incurred because of absorption of acoustic waves underwater [91]. Also, the propagation velocity of sound waves in water is quite less compared to terrestrial radio signals [15]. Thus, chances of an OFDM system experiencing ICI are greatly enhanced deteriorating the communication. Equation (5) expresses an underwater acoustic channel response [2] having L multipaths as:

$$H(t, \tau) = \sum_{x=1}^L A_x(t) \delta(\tau - \tau_x(t)), \quad (3.5)$$

$\tau_x(t)$ represents the delay coefficients, $A_p(t)$ is the amplitude of x th multipath, whereas $\delta(t)$ is Dirac delta function. The delay spread for underwater acoustic channels is anything between approximately 10 ms to 100 ms [92]. The Doppler shifts affect different subcarriers differently since the channel is wideband in nature.

Fig. 5.3 details the channel model [170] used in this work. The transmitted signal represented by $s(t)$ passes through the absorption loss block followed by Rician distribution-based fading and then the frequency dependent ambient noise is added.

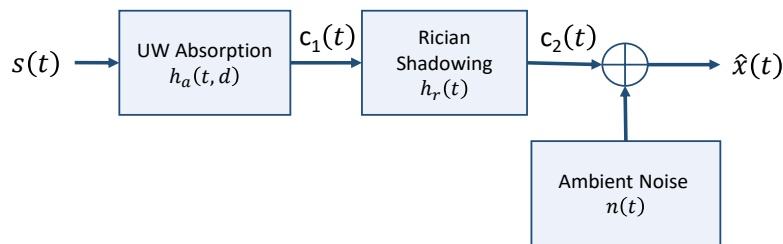


Figure 5.3. UWA Channel Model [170, 171]

The acoustic pathloss in an underwater channel is a result of absorption as well as geometric spreading of the acoustic signals. Thus, the obtained channel transfer function $H_a(f, d)$ [62, 63] can be written as:

$$H_a(f, d) = A_d e^{-\gamma(f)d}, \quad (3.6)$$

A_d is scaling constant and d represents transmitter-receiver separation in meters and $\gamma(f)$ is the propagation constant which is complex. The signal $c_1(t)$ in Fig. 5.3, is then computed as the convolution of inverse Fourier transform of the transfer function and the transmitted signal $s(t)$.

$$c_1(t) = h_a(t, d) \otimes s(t) \quad (3.7)$$

It is evident from experimental data fitting models that the fading observed by a sound signal in an underwater channel can be modelled using Rician distribution [65, 66, 93]. The parameters used in this work are $k = 2.0$; $m = 0.4$ [65]. The signal $c_2(t)$ becomes,

$$c_2(t) = h_r(t) \otimes c_1(t) + n(t) \quad (3.8)$$

where $n(t)$ represents the additive channel noise and $h_r(t)$ represents the inverse Fourier transform of transfer function [68]. Figure 5.4 shows an instance of the delay profile used in this work and the average path gains.

For an underwater channel, the ambient noise is a combination of various frequency dependent noises, major noise sources include: thermal noise, shipping activity, noise from turbulence and wave noise [69]. From the noise equation, it is evident that the noise is location dependent. Furthermore, the amplitude is higher at the low and high ends of the spectrum and at its minimum at the frequency of 60 kHz [96].

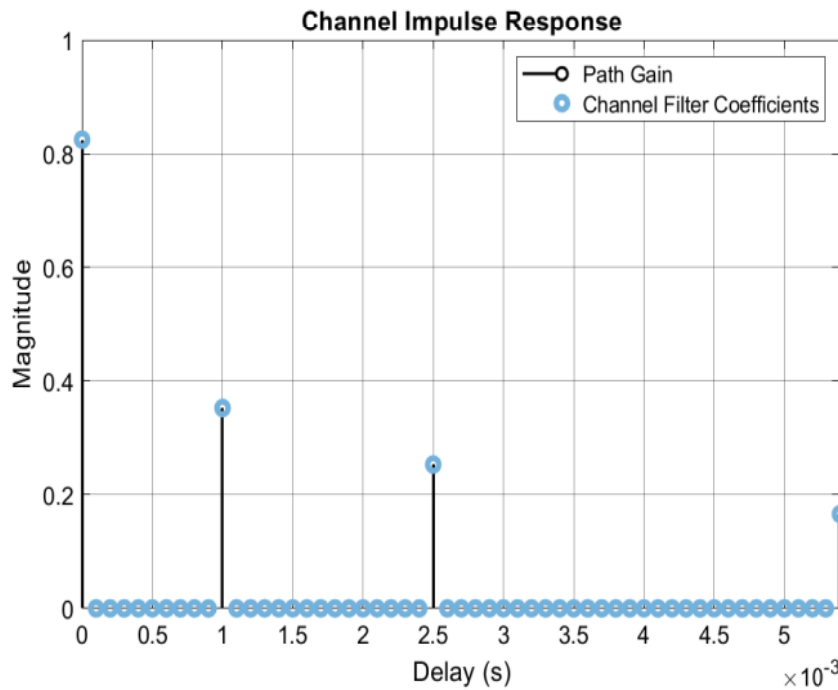


Figure 5.4. Channel impulse response

5.3.4. Peak to Average Power Ratio

PAPR refers to the ratio between peak power and average power of the system. OFDM adds a PAPR of $10 \log K$ dB to the original PAPR if the system, where K is the number of used subcarriers. The PAPR of an OFDM system is calculated as:

$$\text{PAPR (dB)} = 10 \log_{10} \frac{\max[|x_n|^2]}{E[|x_n|^2]} \quad (3.9)$$

where x_n is the discrete time domain OFDM signal, $\max[|x_n|^2]$ is the peak signal power and $E[|x_n|^2]$ is the average signal power. The PAPR performance is usually evaluated using complementary cumulative distribution function (CCDF). CCDF is a plot that shows the probability of exceeding a certain value of PAPR. Additionally, in this work, we use ‘‘PAPR gain’’ to evaluate the effectiveness of a certain ciphered BCH code. We define ‘‘PAPR gain’’ as the amount of reduction in PAPR when compared with the maximum possible PAPR of an OFDM signal. The maximum possible PAPR, of an OFDM signal with N subcarriers, is given by $10 \log_{10} N$.

5.4. Proposed Technique

We propose a ciphered BCH (C-BCH) encoded OFDM scheme that uses predetermined keys to obtain the lowest possible PAPR for an N sub-carrier system. It may be noted that the proposed key selection algorithm is offline and several keys that would produce low PAPR are determined for each code. These key vectors are then used in the live system to produce ciphered codes for reducing the PAPR as depicted in Figure 5.5, improving the error performance and to provide secure communication. Since the key vectors are obtained in advance using a computer, real time calculations for determining low PAPR combinations are not needed at the transmitter. The only overhead is an XOR operation, but this operation also adds a level of encryption to the system.

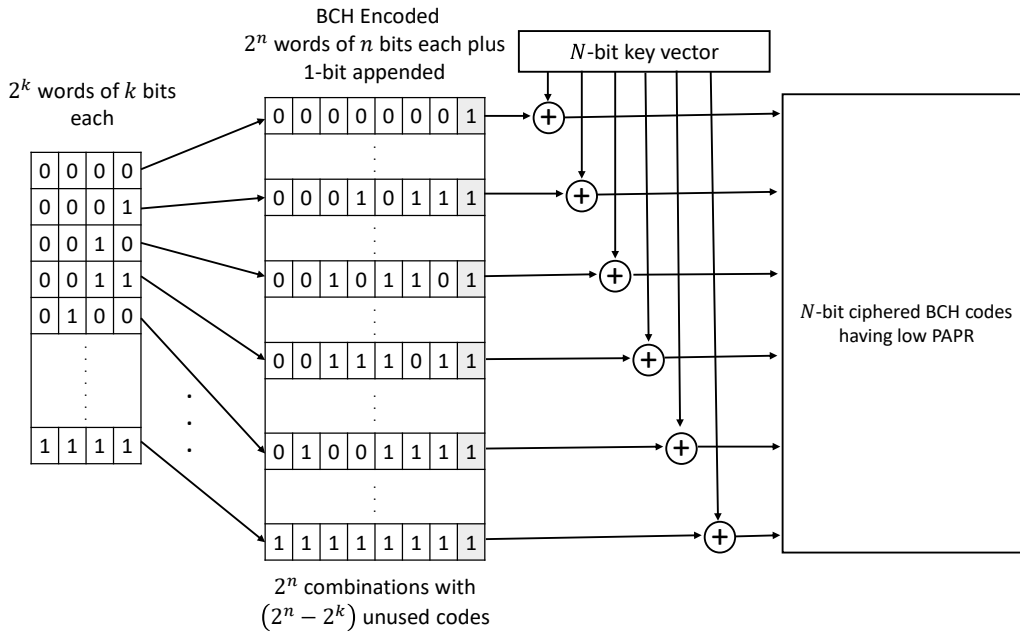


Figure 5.5. An example of generation of ciphered BCH(n,k) codes for an 8-subcarrier OFDM system with $k = 4$, $n = 7$.

The n value of the BCH(n, k) encoder is selected based on the number of bits required in one OFDM symbol. For example, for an OFDM system with 64 subcarriers and BPSK modulation, BCH(63, k) would be selected. BCH(63, k) will also be used for an OFDM system that has 32 subcarriers and QPSK modulation since in this case also, one OFDM symbol will have 64 bits. The value of k is based on the desired error and PAPR performances. It is known that the lower the code rate (k/n), better is the error performance. Additionally, such lower code rates can also translate to higher PAPR gains using the proposed algorithm – as will be shown in Section V. Hence, a BCH(63,10) code will give a better error performance as well as better PAPR gain than a BCH(63,45) code.

Algorithm 1 summarizes the steps for determining the best key vectors for an N sub-carrier BPSK-OFDM scheme and works as follows. A BCH(n, k) encoder is chosen based upon the value of N such that $n = N - 1$. Since the value of k is a design parameter, it is chosen based on the desired error performance and required PAPR gain. If the value of k is reasonably small such that all possible k -bit words can be generated, then N_R , i.e., the number of k -bit words to be generated are given by 2^k . If the value of k is large enough such that it is computationally impractical to generate all possible k -

bit words, then N_R is chosen to be an arbitrarily large number. After generating N_R number of k -bit words, the words are encoded using the chosen $\text{BCH}(n, k)$ encoder. Next, N_w number of n -bit key vectors are randomly generated. The value of N_w is chosen based upon trial and error and will be described in detail in Section 5.5.

Algorithm 1: Key Vector Selection

1. Initialize $N_w, N_R, j = 0$
 2. **Repeat N_R times**
 - a. Generate a k -bit binary sequence R_j
 - b. Encode R_j using $\text{BCH}(n, k)$ and generate encoded sequence E_j
 - c. $j = j + 1$
 3. $i = 0$
 4. **Repeat N_w times**
 - a. Randomly generate an n -bit key vector k_i
 - b. $j = 0$
 - c. **Repeat N_R times**
 - i. $C_j = k_i \oplus E_j$
 - ii. $\text{PAPR}_j = \text{PAPR}\{C_j\}$
 - iii. $j = j + 1$
 - d. $\text{PAPR}_{max}^i = \max_{\forall j} \text{PAPR}_j$
 - e. $i = i + 1$
 5. $\text{PAPR}_{min} = \min_{\forall i} \text{PAPR}_{max}^i$
 6. $l = \arg \left\{ \min_{\forall i} \text{PAPR}_{max}^i \right\}$
 7. $\text{Key}_{best} = k_l$
-

One key vector is chosen from the set of N_w key vectors and all the BCH encoded words that were generated in the previous step are XORed with this key vector resulting in a new set of BCH codes called ‘‘ciphered BCH codes’’. The PAPR of each of these ciphered codes is computed and the maximum value is stored. Then the next key vector is chosen from the set of N_w key vectors and the process of producing ciphered codes, determining their PAPRs and storing the maximum PAPR is repeated until all N_w key vectors are exhausted. This results in N_w values of maximum PAPRs along with their corresponding key vectors. Finally, the minimum value from the stored maximum PAPRs is selected along with its corresponding key vector. Since there will be multiple instances of minimum PAPRs and their corresponding key vectors, several key vectors are selected for later use in the live system. The number of key vectors to be selected is a design parameter and depends upon the desired level of security. The higher the level of desired security, the more the number of key vectors selected. Selected key vectors are then used in the live system in a round robin fashion to do the XOR operation as has been shown in Fig. 5.2. The set of selected key vectors are shared with the receiver before putting the system to live operation. However, in the proposed system, side information is not required to be transmitted to the receiver.

A single bit (either 0 or 1) is appended to each of the encoded symbols to make them N -bit long. This step is necessary for two reasons. First, higher PAPR gains are possible only when the number of bits in the encoded sequence are equal to the number of bits in one OFDM symbol.

Second, to facilitate efficient computation of FFT algorithm, the number of sub-carriers in an OFDM system are kept in powers of 2. There are three options of appending the extra bit to the ciphered

BCH code. One option is to add this bit arbitrarily. This will make the total encoded bits equal to N and will save computational power. However, the added bit shall not be used and will be wasted. Second option is to utilize this bit for channel estimation. This may marginally increase the computational complexity of the system but can improve the error performance of the system. Third option is to use this bit to get further gains in PAPR. However, to determine whether appending a bit 0 or a bit 1 gives more gains in PAPR, the PAPR will have to be computed twice for each OFDM symbol: one when appending a binary 1 and another when appending a binary 0. Our observation is that the computational power required in the third option far outweighs the gain obtained in PAPR.

Hence, out of the three options, second option is the most feasible. Table 5.2 lists some of the key vectors computed for several BCH codes using the proposed algorithm. For each BCH code, we use four key vectors and use them in rotation after every subcarrier block. The vectors and their rotation orders are known at the receiver side thus the data is encrypted and only a receiver with the knowledge of the key vectors used will be able to decipher the received information.

Table 5.2: Selected Keys and Gains Achieved

Code	No. of Symbols	No. of Vectors	Key Vectors (Hex)	Gain over BCH (dB)
BCH (31,6)	All 2^k	900 x 10^3	0DA1BDB0	7.6588
		10 x 10^3	5813A4C0	7.4783
		50 x 10^3	7C2157D4	7.4397
		100 x 10^3	243ADB40	7.6109
BCH (31,11)	All 2^k	30 x 10^3	0C912BDC	4.9975
		30 x 10^3	31CF7963	4.9975
		30 x 10^3	45EE06B4	4.9975
		30 x 10^3	03BC0550	4.9975
BCH (31,16)	All 2^k	10 x 10^3	778D14A4	3.2545
		10 x 10^3	6E9E5E56	3.2545
		2500	37D46C5D	3.2545
		2500	4599D87C	3.2545
BCH (63,7)	All 2^k	20 x 10^3	31DC0A4E92769604	9.8923
		50 x 10^3	64F1EA51AFD4CF7E	9.7317
		50 x 10^3	344DDD2044A4BEAC	9.8782
		50 x 10^3	2924410DE70648C3	9.8218
BCH (63,10)	All 2^k	10 x 10^3	3AB7480E3466653B	8.5194
		10 x 10^3	25FD2809A8DA12B5	8.5194
		20 x 10^3	571232A7E4372046	8.5194
		10 x 10^3	17AC03EFE0B5814D	8.5194
BCH (63,16)	All 2^k	1000	4CEF656704A38285	6.0206
		1000	6E892F8204C475FE	6.0206
		1000	4CA8A16F750B7891	6.5812
		1000	47C2E8C0DD58608D	6.0206
BCH (63,24)	Random 2^{18}	6000	1BD6BEB858D9AF8D	1.4927
		500	42B4DF5FA1F308A0	1.5664
		1000	3D4DBDC2F65C0AEC	1.0067
		400	33B03FB68BC55EF3	1.4927
BCH (127,8)	Random 2^{20}	100	3938BBED30C10407F8AB226D735D56AC	11.6499
		100	2E5678670CCF3D50F32840268A11AB4E	11.7250
		500	3D430D3A3A137AA36128FD9AF05C4853	11.5146
		100	195AE63DC2718151B55338F761F95625	11.7058
BCH (127,22)	Random 2^{20}	300	455EA099475B134A14C375EA9CBF8018	7.8241
		1000	1F27F92B1A3EEE260B89073BCDC4854B	8.5194
		1000	6ED23998D6EDA9D4939D85F76738753B	8.5194
		100	7C72213050301219B2ECEC77FF2C0EC3	8.1648
BCH (127,36)	Random 2^{20}	100	51874DF0E5A3550DEFA7C12EADDE812E	1.8035
		100	372AC8B3BD34F81FCE3A58193396A821	1.7430
		100	0B9D9E7FC5D042409B3A77AA4A0E8370	1.5278
		100	1D23FAA5C239438B4E9D917118A172E2	1.8035
BCH (127,50)	Random 2^{20}	100	6B9372C81B6A95C4BE47BC9F543F5ADB	0.9485
		100	0E6950513B228A58D4809AC1AF7CA5A0	0.6437
		100	77E4C718EA54FC99141B0983B1055CE6	0.9485
		100	3C13DC982F9922E6EC58AEF7AB35CB0D	0.8899

5.5. Simulation Setup and Results

We have implemented an OFDM transceiver model in MATLAB together with a UW channel realization. Table 5.3 shows the configurations for transceiver used in our simulations. Whereas Table 5.4 shows the UW channel parameters used. We present the PAPR performance as well as the BER performance of the proposed algorithm in the following two subsections.

Table 5.3: Transceiver Parameters

Symbol	Quantity
No. of subcarriers	32, 64, 128
Mapping	BPSK
FFT size	32, 64, 128
CP length	$N/4$
Equalizer	Zero Forcing
Bandwidth	10 kHz

Table 5.4: Channel Parameters

Symbol	Quantity
TX-RX distance	500, 1500 m
Depth	10 m
Max doppler shift	10 Hz
Gain vector	[0; -1.5; -2.5; -2] dB
Tau vector	[0; 1; 2.5; 7] ms
Atmospheric pressure	1.01325×10^5 Pa
Salinity	35 parts/1000
Density	10^3 Kg/m ³
Water temperature	25° C

5.5.1. PAPR Performance

In this work, “gain in PAPR” refers to reduction in maximum possible PAPR and the maximum possible PAPR for an OFDM system with N number of subcarriers is given by $10 \log_{10} N$. Figure 5.8(a) illustrates the gain achieved in PAPR as an example for a 32-subcarrier system. We simulated three OFDM systems having 32, 64 and 128 subcarriers. Ciphered BCH(31, k) codes and the associated keys are used for a 32-subcarrier system, ciphered BCH(63, k) and the associated keys for a 64-subcarrier system and ciphered BCH(127, k) and the associated keys for a 128-subcarrier system. Although, for large values of k , a huge number of possible keys are randomly generated, it has been observed that using a very large pool of randomly generated keys does not produce a key that would give any appreciable gain in PAPR. In other words, a small subset of randomly generated keys is enough to provide the most appropriate keys that give substantial gain in PAPR. One such example is shown in Fig. 5.6, where increasing the pool of random keys, only gives marginal improvement in PAPR and 6 dB gain is possible using the key obtained from a set of 50 randomly generated keys.

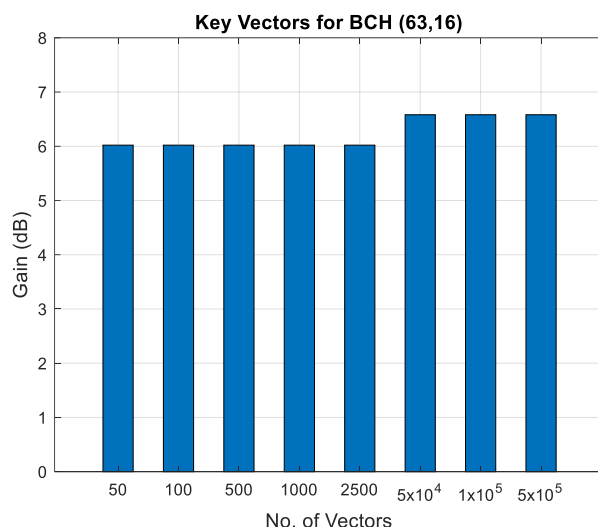


Figure 5.6. Possible PAPR gain from a set of multiple random keys.

Fig. 5.7 shows the gain in maximum PAPR for the three types of ciphered BCH codes used in this work. It is noted that the smaller the value of k , the more the gain in PAPR. For a 32-subcarrier OFDM system, the maximum gain obtained is approximately 8 dB for a ciphered BCH(31,6) OFDM system. Since the maximum possible PAPR for an uncoded 32-subcarrier OFDM system is 15.05 dB, this means that the maximum PAPR of proposed system never exceeds 7.05 dB. For a 64-subcarrier OFDM system, the maximum gain obtained is approximately 10 dB for a ciphered BCH(63,7) OFDM system which means that the maximum PAPR of the proposed system never exceeds 8.06 dB. Similarly, for a 128-subcarrier OFDM system, the maximum gain obtained is approximately 12 dB for a ciphered BCH(127,8) OFDM system.

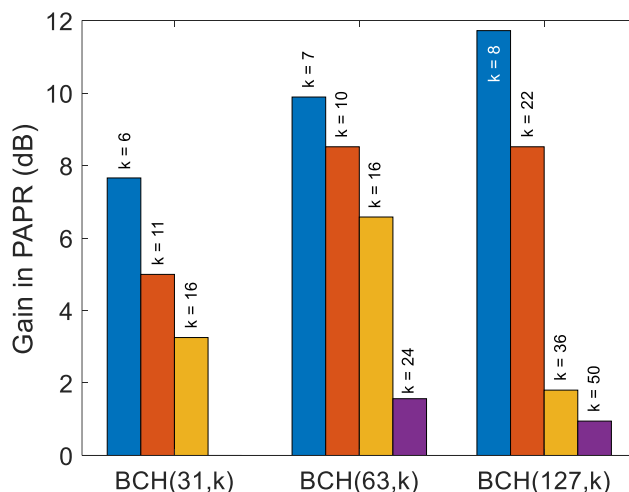


Figure 5.7. Gain in maximum PAPR as a function of various ciphered BCH codes

Fig. 5.8 compares the PAPR performances of proposed 32-subcarrier OFDM systems with uncoded and with BCH encoded OFDM systems using CCDF plots. Figs. 5.8(a), (c) and (e) compare the PAPR performances of ciphered BCH(31, k) with those of uncoded systems while Figs. 5.8(b), (d) and (f) compare the PAPR performances of ciphered BCH(31, k) with those of BCH(31, k) encoded systems. As shown in Fig. 5.8(a), the PAPR performance of ciphered BCH(31,6) is much superior to that of an uncoded OFDM system. In Fig. 5.8(b), when comparing the PAPR performance of ciphered BCH(31,6) with that of conventional BCH(31,6), it is observed that the PAPR of a conventional

BCH(31,6) encoded system remains high with a high probability unlike uncoded OFDM system. Similar phenomenon is observed in Fig. 5.8(d). As would be expected, the PAPR performance of ciphered BCH codes for higher values of k is not at par with the systems where the value of k is small, as shown in Figs. 5.8(e) and 5.8(f). This is due to the fact that when the code rate k/n becomes large, there are fewer number of possible key vectors that will produce low PAPR sequences. Hence, there does not exist a key vector that would give the same gain in PAPR as given by the key vector when the code rate is low.

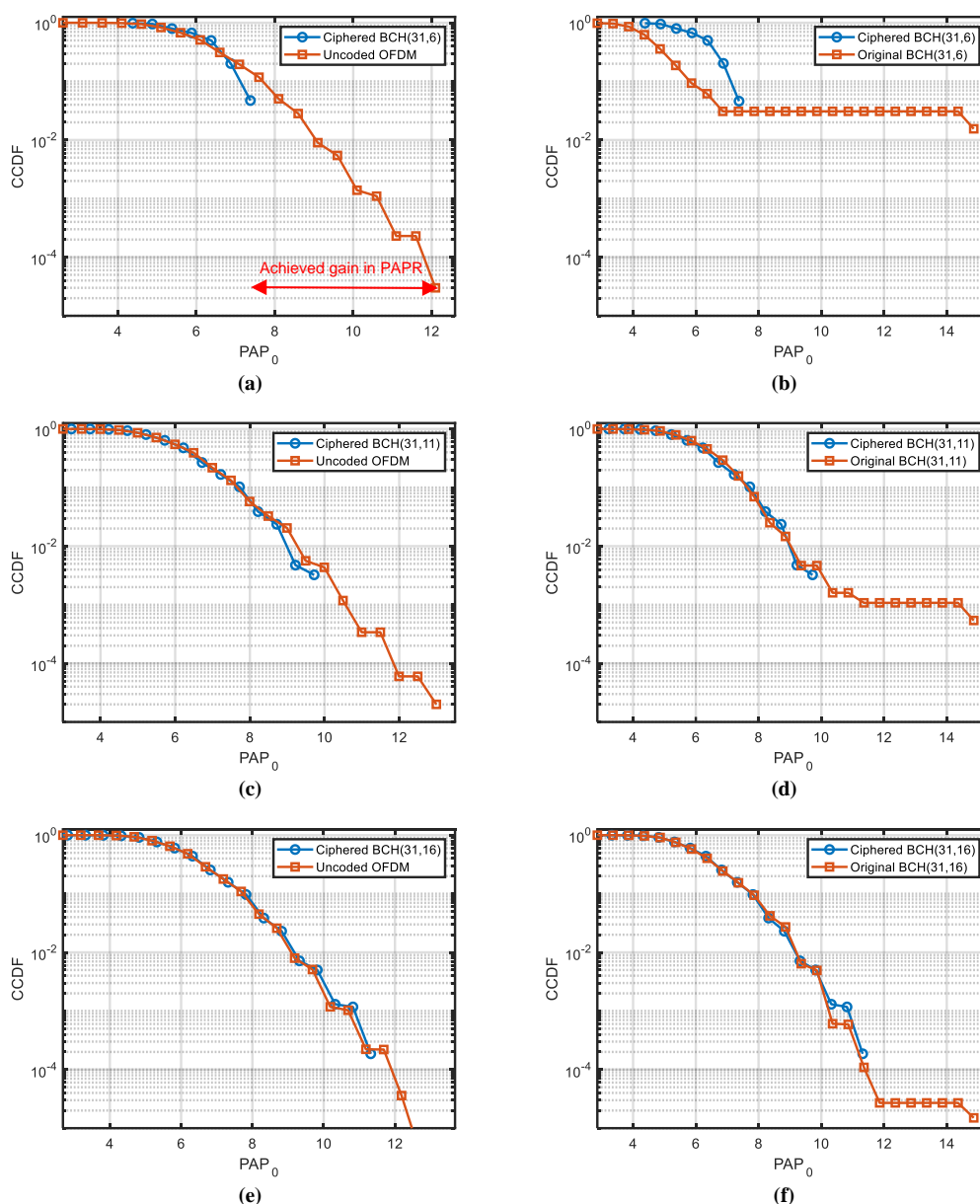


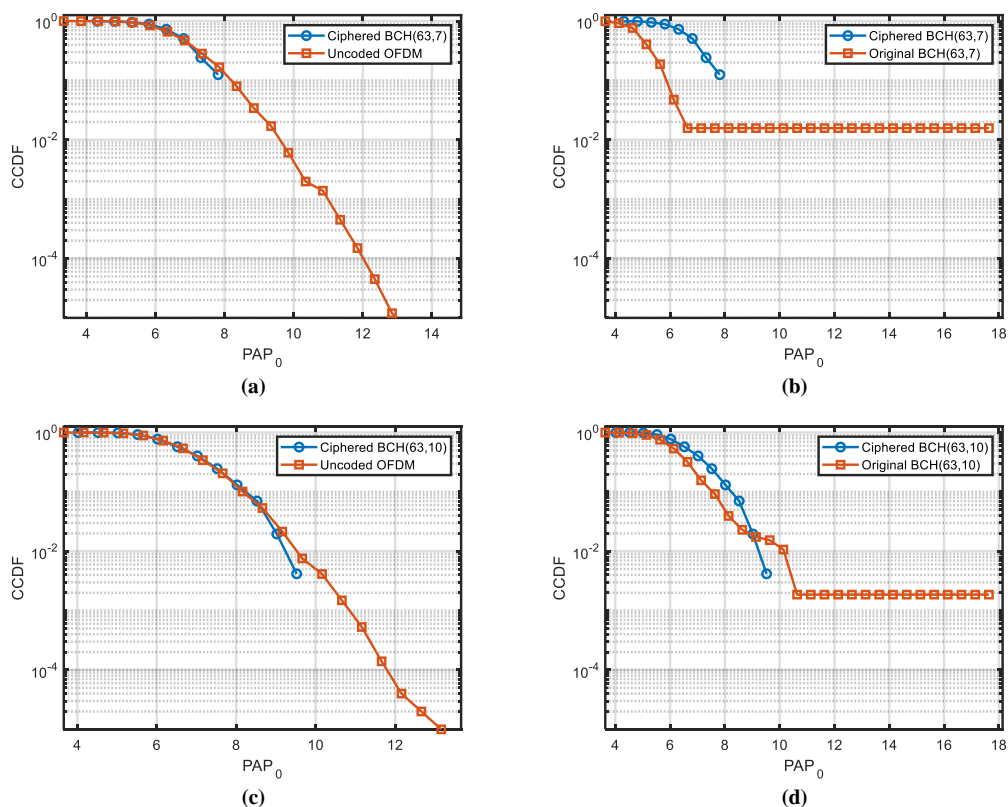
Figure 5.8. PAPR performance of the proposed technique for Ciphered-BCH(31, k).

However, it must be noted that although, there is not an appreciable gain in PAPR for higher rate ciphered BCH codes but their PAPR performance is still much better than the conventional BCH codes. As a result, the bit error rate performance is significantly improved without any deterioration in PAPR performance.

Fig. 5.9 compares the PAPR performances of proposed 64-subcarrier OFDM systems with uncoded and with BCH encoded OFDM systems using CCDF plots. Figs. 5.9(a), (c) and (e) compare

the PAPR performances of ciphered BCH(63, k) with those of uncoded systems while Figs. 5.9(b), (d) and (f) compare the PAPR performances of ciphered BCH(63, k) with those of BCH(63, k) encoded systems. As shown in Fig. 5.9(a), the PAPR performance of ciphered BCH(31, 6) is much superior to that of an uncoded OFDM system. In Fig. 5.9(b), when comparing the PAPR performance of ciphered BCH(63, 10) with that of conventional BCH(63, 10), it is observed that the PAPR of a conventional BCH(63, 10) encoded system remains high with a high probability unlike uncoded OFDM system – a phenomenon that was also observed in the case of 32-subcarrier system. Similar phenomenon is observed in Fig. 5.9(d). In this case also, the PAPR performance of ciphered BCH codes for higher values of k is not at par with the systems where the value of k is small, as shown in Figs. 5.9(e) to 5.9(h).

The PAPR performances of 128-subcarrier OFDM systems are shown in Fig. 5.10. It is observed that the PAPR performance of proposed system is significantly better than uncoded and BCH encoded OFDM systems for ciphered BCH(127, 8) codes – as is shown in Fig. 5.10(a) and 5.10(b). However, for other codes, we do not observe appreciable reduction in PAPR. The reason is the relatively large value of k . When the value of k is 22, 36 and 50, the space of possible key vectors becomes very large as the number of possible key vectors are 2^{22} , 2^{36} and 2^{50} respectively. Hence, the problem of finding the best key vector becomes intractable.



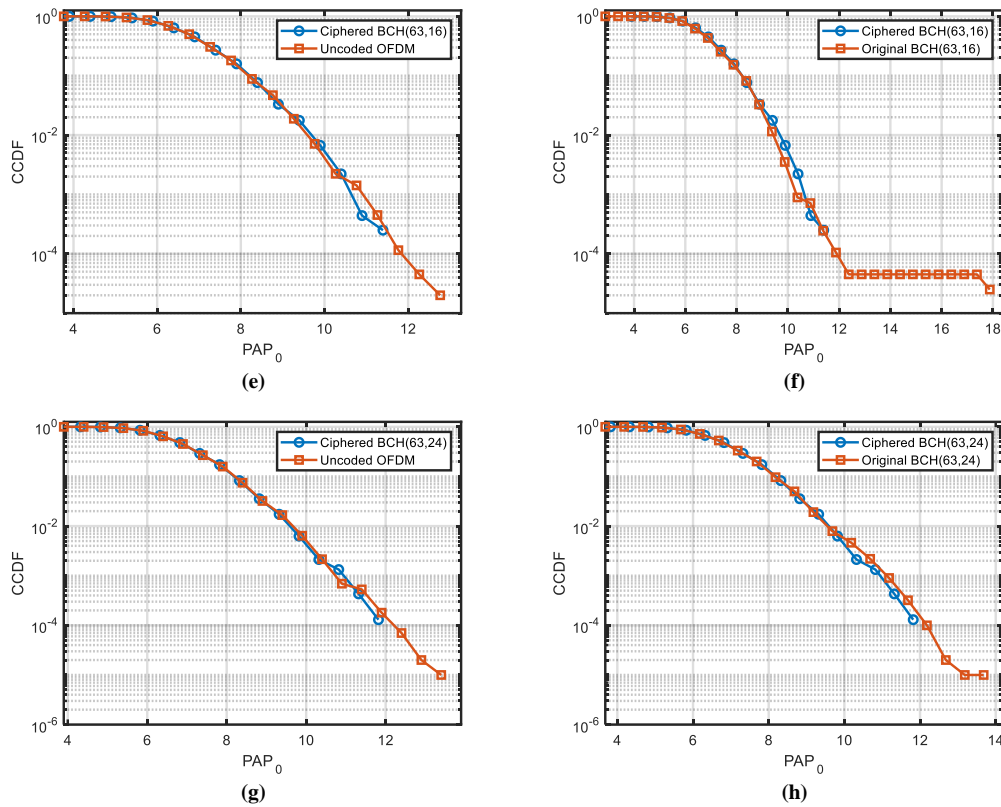
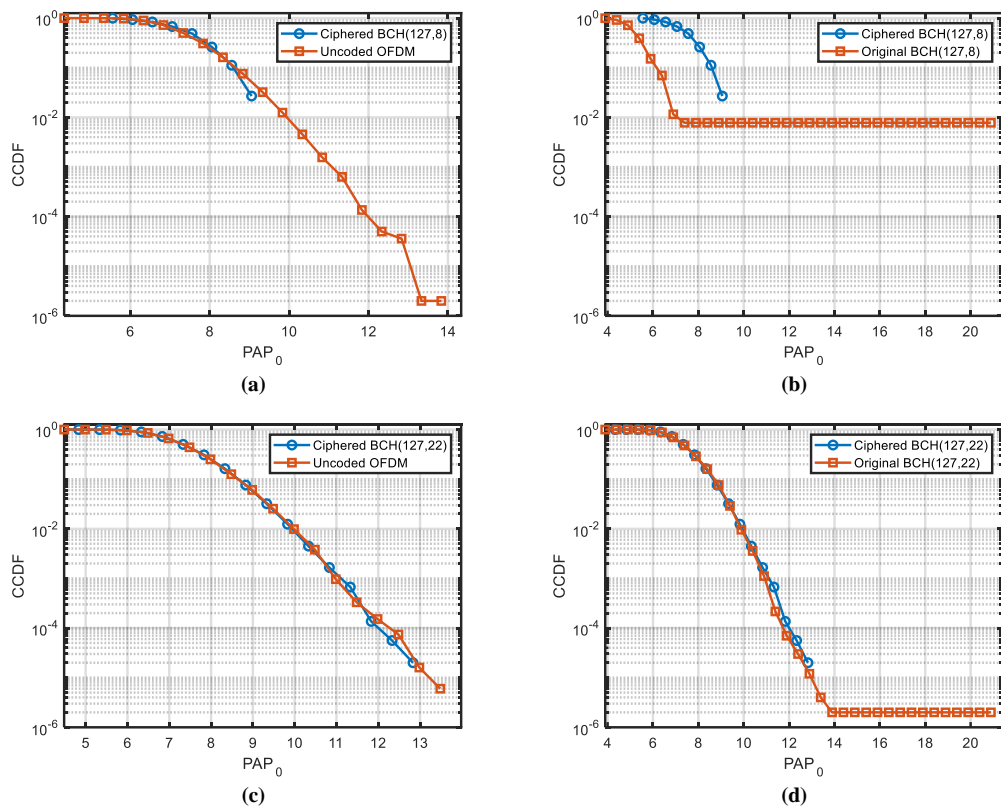


Figure 5.9. PAPR performance of the proposed technique for Ciphered-BCH(63, k).



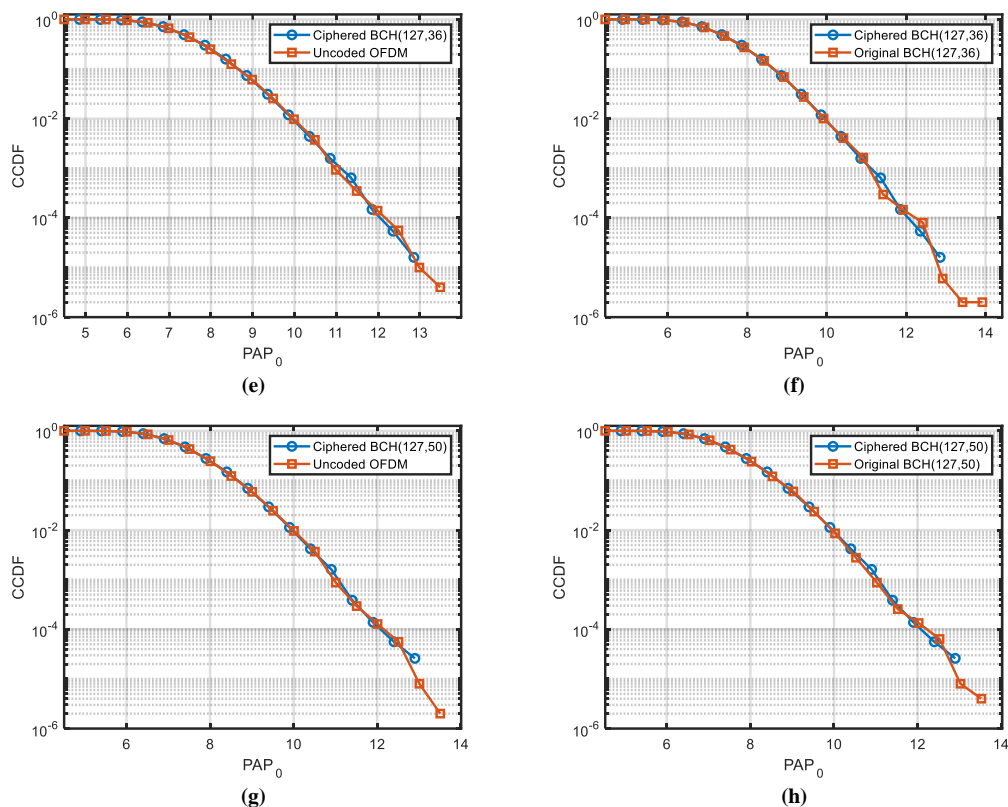


Figure 5.10. PAPR performance of the proposed technique for Ciphered-BCH(127, k).

5.5.2. BER Performance

In this section, we demonstrate the BER performance of proposed ciphered BCH codes and show that the error correcting capability of original BCH codes remains preserved for the proposed system. Fig. 5.11 compares the BER performance of the proposed system against the ordinary uncoded OFDM for a transmitter-receiver distance of 1500 m . It is observed that all the ciphered BCH codes improve the BER performance of the OFDM system as would be expected. It is pertinent to mention that the BER results for ciphered BCH codes having lowest k values show significant improvement, but the overhead is too high and are ideal for scenarios where very reliable transmission of low data-rate information is required. The channel state information was assumed to be known and used in the zero-forcing equalizer. For BCH(31, k), the lowest BER values are associated with $k = 6$. For the same codes, we did not report k values higher than 16 as there was very insignificant improvement in BER performance and PAPR reduction due to lack of unused combinations at higher k values. This holds true for BCH(63, k) and BCH(127, k) as well.

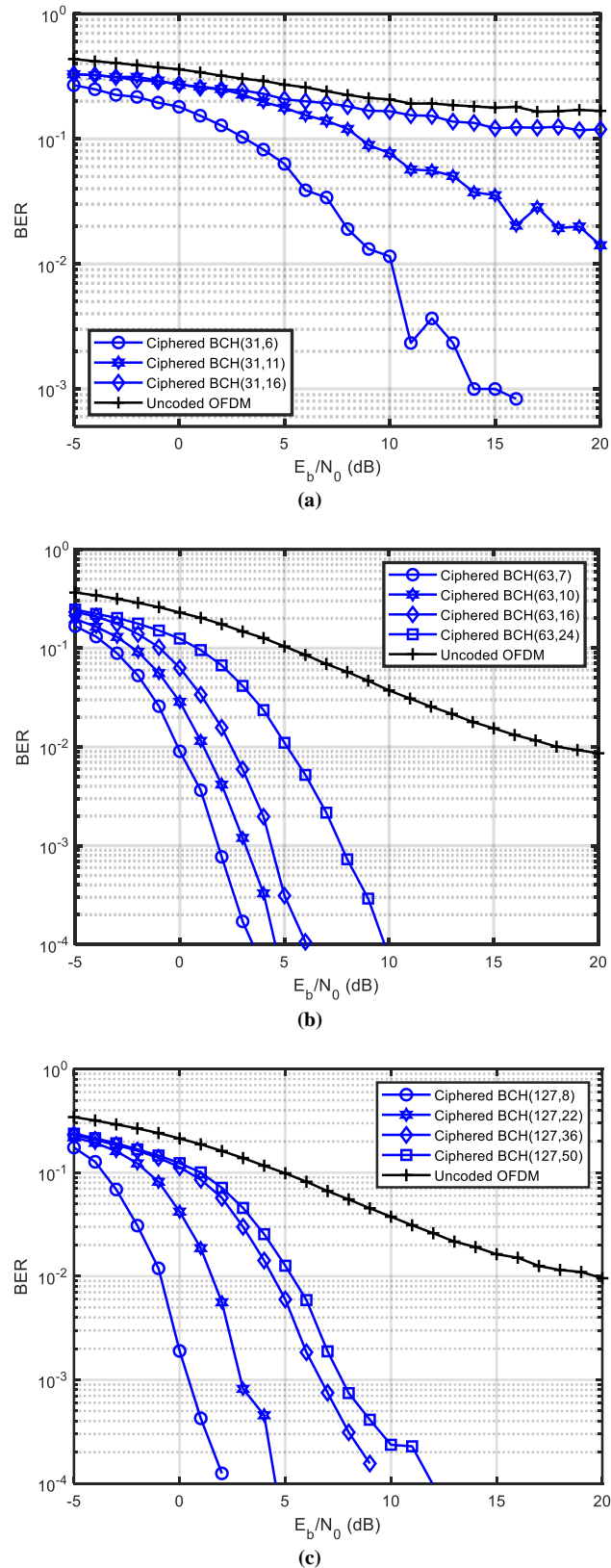


Figure 5.11. BER performance of C-BCH(31, k), C-BCH(63, k) and C-BCH(127, k).

5.6. Conclusion

A low complexity PAPR reduction technique for underwater acoustic OFDM transceiver is proposed and demonstrated. It consists of multiple pre-determined cipher keys, generated once using a high-end PC and saved in the transceiver system, that are used for XOR ciphering of the BCH encoded and decoded data at the OFDM transmitter and receiver respectively. Our findings suggest that while reducing PAPR, the ciphered-BCH technique improves BER performance of the system using channel coding. It is observed that a higher PAPR reduction and a lower BER is achieved when lower code rate BCH codes are used. Using multiple keys, known to both the transmitter and receiver, a level of encryption is achieved as an added advantage. Given power and processing limitations of the underwater acoustic nodes, the proposed technique is easy to implement and reduces computational complexity of the transceiver as most of the processing for key vector search is done offline. The most appropriate keys generated are stored in both the transmitter and receiver and are used for ciphering purposes and to reduce PAPR of the OFDM signal.

Chapter 6: Continuous Phase Modulation OFDM

We propose and evaluate the performance of a continuous phase modulation based orthogonal frequency division multiplexing (CPM-OFDM) transceiver for underwater acoustic communication. In the proposed technique, the mapper in traditional OFDM is replaced by CPM while a realistic model of underwater channel is employed. Bit error rate as well as peak to average power ratio performance of the proposed scheme is evaluated using Monte-Carlo simulations. The error performance observed clearly establishes the superiority of CPM-OFDM over traditional OFDM schemes. Specifically, a value of 7/16 or 9/16 for the modulation index gives the best error performance. Furthermore, the error performance of the proposed scheme is within acceptable values up to a transmitter–receiver distance of 1.5 *km*. Additionally, the PAPR performance of the proposed scheme suggests that like other OFDM schemes, a PAPR reduction scheme is mandatory for acceptable PAPR performance of CPM-OFDM. Besides, another advantage CPM-OFDM signals can bring along is the reduction in PAPR when multi-amplitude CPM is utilized in conjunction with partial transmit sequences.

The remaining chapter is organized in the following manner. Section 6.2 contains a survey of the work done in the domain of CPM-OFDM and related technologies. Section 6.3 present the details of a typical CPM-OFDM transceiver that includes CPM modulator and demodulator. We also detailed the shallow underwater acoustic channel model that was used for the simulations. Simulation setup and results are presented in section 6.4 along with discussions on the outcome of our simulation studies. Finally, the chapter is concluded in section 6.5.

6.1. Introduction

Continuous phase modulation (CPM) employing correlated phase states and continuous phase frequency shift keying (CPFSK) have been used in communication systems for more than four decades. However, very limited work has been done incorporating CPM in the mapper of an OFDM system particularly in the domain of underwater acoustic channels. Key advantages of employing these schemes in OFDM are that the signal is power and spectrum efficient, has a constant envelope, has less out of band radiation, and possesses phase continuity. Traditional OFDM systems use memoryless modulation schemes such as PSK and QAM in the mapper. The introduction of correlation among neighboring symbols through proper selection of mapping parameters is a key advantage of CPM based OFDM systems. This allows for multi-symbol detection techniques as memory can be introduced through appropriate selection of a single parameter h while allowing exceptional flexibility for the communication system designer to control memory introduced at the transmitter. One of the concerns, in CPM-OFDM systems, is the complexity of receivers. Consequently, detection of CPM signals is a complex process. Nevertheless, it becomes less complex and economical if a maximum likelihood Viterbi decoder is employed. Restricting the modulation index h to be rational, the number of states in CPM trellis can be kept to a manageable number that also facilitates the use of Viterbi algorithm (VA). The distance between received signal and all the trellis paths entering each state at an instant i is calculated by VA. This is followed by the removal of those paths that are probably not the candidates for maximum likelihood. For two paths entering the same state, the one having the best metric is selected and it is named the “surviving path”. For all the states, similar surviving paths are selected. By continuing in a similar manner, VA advances deeper into the trellis and the decisions are made by removing the paths that are least likely. Although such decisions are not maximum likelihood in the true sense, but if decision depth is long enough, these decisions can be almost as good as in the case of true maximum likelihood. Literature suggests that Viterbi decoders—though suboptimum—when used to detect CPM signals, offers performance that is comparable to optimum CPM receivers at a much-reduced complexity. Besides, another advantage CPM-OFDM signals can bring along is the reduction in PAPR when multi-amplitude CPM is utilized in conjunction with partial transmit sequences.

Continuous phase modulation (CPM) and continuous phase frequency shift keying (CPFSK) have been employed in communication systems for more than four decades [172]. The main advantages of these schemes are that the signal is power and spectrum efficient, has a constant envelope, has less out of band radiation, and possesses phase continuity [173-175]. Traditional OFDM systems use memoryless modulation schemes such as PSK and QAM in the mapper. Very limited work has been done incorporating CPM in the mapper of an OFDM system. In this work, we evaluate the performance of a typical CPM-OFDM system over doubly-selective underwater acoustic (UWA) channels [19, 176]. The main contributions of this work are as follows:

- An overview of the work done on CPM-OFDM and similar schemes (presented in this section).
- Design of a CPM-OFDM transceiver for low bandwidth and doubly-selective UWA channel.
- Performance evaluation of the proposed transceiver over the UWA channel using computer simulations. Specifically, we present:
 - Bit error rate vs. SNR plots for various rational values of the modulation indices and identification and analysis of good performing indices.

- Bit error rate vs. SNR plots for varying transmitter-receiver distances and a discussion of the results.
- Bit error rate vs. SNR plots for various values of channel bandwidths and a discussion of the results.
- Peak to average power ratio plots as a function of modulation indices.

6.2. Related Work

In CPM, the continuity of the phase from symbol to symbol introduces memory and correlation among symbols [177]. Since the inception of this class of signals, several interesting and useful works have been published and are still being published [178-180]. Utilizing the favorable properties of CPM, the pioneering work to combine CPM and OFDM was first reported in 2002 [181]. In this type of scheme, the traditional mappers such as PSK, QAM, etc., are replaced by CPM. The proposed scheme was named OFDM-CPM. (In this work, we call it CPM-OFDM owing to the norm currently being followed in literature.) It was shown that these signals offered much superior performance over traditional OFDM signals in multipath fading channels. After introducing CPM-OFDM signals in [181], the performance of different types of optimum and suboptimum receivers for CPM was evaluated over multipath-fading channels and reported in [182-184]. Viterbi decoder—though suboptimum—when used to detect CPM signals, offers performance that is comparable to optimum CPM receivers at a much-reduced complexity. As a natural consequence, the performance of Viterbi decoder to detect CPM-OFDM signals was presented in [185]. The performance of these signals over indoor wireless channels has also been assessed and reported in [186]. In [187], authors have evaluated the performance of convolutionally encoded CPM based OFDM systems for aeronautical telemetry. MIMO CPM-OFDM was studied in [188]. Authors have employed L2-orthogonal space-time codes and a zero-forcing equalizer at the receiver. They have shown that by using their proposed scheme, the complexity of CPM decoding can be significantly reduced. In [189], authors have implemented a typical CPM-OFDM system using software defined radio and have evaluated its performance over AWGN channels. Authors have shown that a value of 0.75 for the modulation index gives the best performance among the three modulation indices evaluated. However, they have not evaluated the performance of their proposed system over frequency-selective fading channels, which is the main ground of implementation for such systems. Moreover, they only evaluated their system only for three values of the modulation index.

High PAPR is one of the disadvantages of a typical OFDM system. By using multi-amplitude CPM, it was shown that the PAPR of CPM-OFDM can significantly be reduced [190]. Another way to reduce the PAPR of CPM-OFDM is to use constant envelope OFDM [191, 192]. It should be noted that constant envelope OFDM is a different type of CPM-OFDM than the one proposed in [193] and other subsequent works discussed in the previous paragraph. In constant envelope OFDM, phase modulation is done after taking the IFFT of the signal, which is contrary to what was proposed in [193] where the continuous phase modulation was done before taking the IFFT. Constant envelope OFDM becomes CPM-OFDM if the phase continuity is maintained. Otherwise, it is a memoryless phase modulation. The scheme was named constant envelope-OFDM (CE-OFDM) or OFDM-phase modulation (OFDM-PM), and it was shown that CE-OFDM yield 0 dB PAPR constant envelope signals. In another work, authors have evaluated CE-OFDM for various multipath fading channels [194]. Two types of equalizers have been employed in the receiver: minimum mean square error (MMSE) and zero forcing (ZF) equalizers. Results presented show significant BER performance improvements over a traditional

OFDM system. Moreover, authors show that through the optimum variation of the modulation index, improved bandwidth efficiency and BER performance can be achieved. The same authors have employed chaotic interleaving to CE-OFDM after doing continuous phase modulation [195]. Although authors claim that their system offers improvements in BER as compared to the one reported in [191, 192], the reported results show only marginal improvements. In [196], the authors have studied a CE-OFDM system and evaluated its performance for a 1 Gbps wireless link at 60 GHz frequency. Authors have used a maximum ratio combining (MRC) receiver and the results show that the proposed scheme is 3 dB superior to CPM-OFDM. BER performance of constant envelope multicarrier modulation was evaluated in [197]. In this work, instead of using IFFT, authors have employed discrete cosine transform (DCT). The justifications given by the authors for using DCT were, the capability of DCT to process time and frequency domain data using real numbers, and bandwidth efficiency of DCT over DFT as the former requires half the bandwidth when compared with the latter. A thorough literature survey suggests that no work has been done to date that evaluates the performance of CPM-OFDM over underwater acoustic channels. Hence, the proposed work is the first of its kind and significantly contributes to the body of knowledge.

6.3. System Architecture

In this section, we briefly explain the various components of the CPM-OFDM transceiver and the continuous phase modulation.

6.3.1. CPM-OFDM Transmitter

The proposed OFDM transceiver is shown in Figure 1. The OFDM transmitter is implemented as an N -point inverse discrete Fourier transform (IDFT) on a block of N information symbols. Practically, the IDFT operation is implemented using an inverse fast Fourier transform (IFFT) because it is computationally efficient.

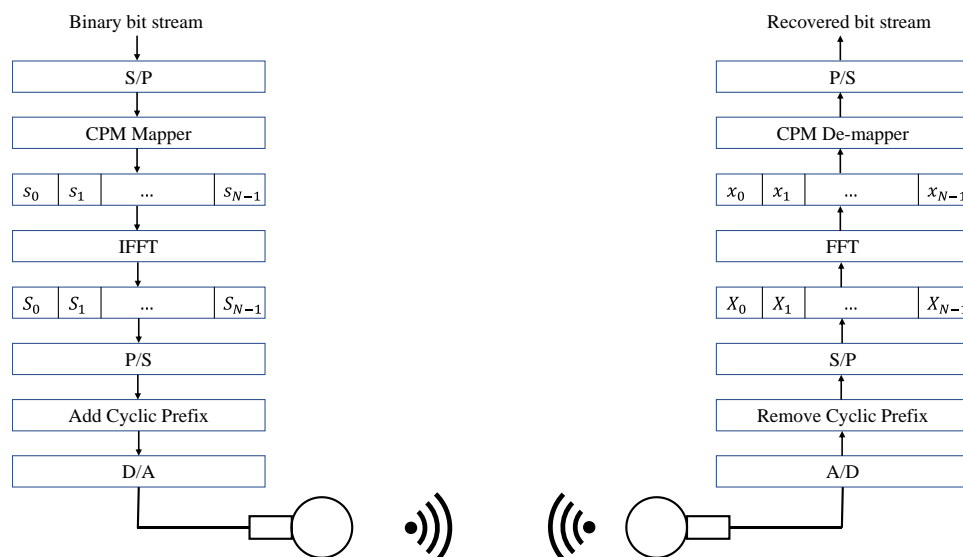


Figure 6.1. Proposed CPM-OFDM transceiver for underwater acoustic channel.

Let $\{s_k, k = 0, 1, \dots, N - 1\}$ represent a block of N complex data symbols which is the output of the CPM mapper—explained in the next subsection. The IDFT of the data block is

$$S_n = \sum_{k=0}^{N-1} s_k \exp\left\{\frac{j2\pi nk}{N}\right\}, n = 0, 1, \dots, N - 1 \quad (6.1)$$

outputting the time-domain sequence S_n . Each OFDM symbol of N IFFT coefficients is preceded by N_g samples—called cyclic prefix (CP) or a guard interval. The number of N_g samples is either equal to or greater than the channel length N_h in samples, where $N_h = \frac{T_h}{T_s}N$, T_h is the length of the channel in seconds, and T_s is the duration of an OFDM symbol in seconds. The CP samples are a repetition of the last N_g samples of the OFDM symbol. Hence, $N + N_g$ becomes the total number of samples of each OFDM symbol.

6.3.2. Continuous Phase Modulation (CPM)

The complex data symbols s_k for the k th subcarrier at the output of the CPM mapper follow the rules of continuous phase modulation. These complex symbols can be represented as

$$s_k = \cos \theta_k + j \sin \theta_k \quad (6.2)$$

where

$$\theta_k = \pi \sum_{i=-\infty}^{n-1} h_i I_i + \pi h_n I_n q(t - nT_s) \quad (6.3)$$

$\{I_i\}$ represents the sequence of M -ary symbols of information that are typically selected from the set $\pm 1, \pm 3, \dots, \pm(M - 1)$, $\{h_i\}$ are called modulation indices, and $q(t)$ represents the pulse shape. If $h_i = h$ for all i , the modulation index is fixed for all symbols and such a scheme is called “single h ” CPM. A scheme in which $\{h_i\}$ is different from symbol to symbol is called “multi- h ” CPM. In multi- h CPM, the $\{h_i\}$ varies in a cyclic manner through all the h values. The most useful feature of a CPM scheme is that it contains memory—represented by the first term in Equation (3). It can be seen that this term is the accumulation of all symbols up to time $(n - 1)T_s$ where n represents the present symbol index [177, 181]. Figure 6.2 shows the values of θ_k as a function of symbol times when $h = 1/2$ for a binary CPM. Solid lines indicate transition due to $I = +1$ (when the information bit is a 1), whereas broken lines indicate transition when $I = -1$ (when the information bit is a 0). The latest value of θ_k is computed by adding πh (if $I = +1$) or subtracting πh (if $I = -1$) to the previous value of θ_k . It is noted that the transition of θ_k from previous to the current value is discrete in nature, although transitions in Figure 6.2 are shown using continuous lines. Regardless of the value of θ_k , the complex numbers shall always lie on a circle.

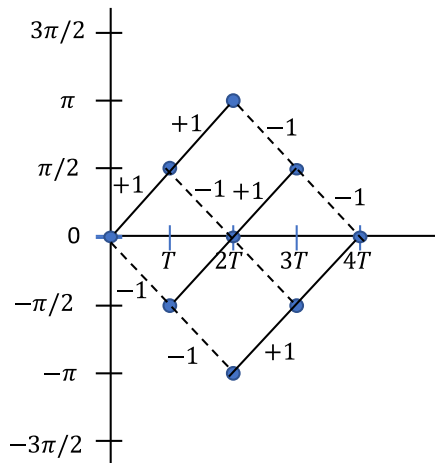


Figure 6.2. Trellis diagram for $h = 1/2$.

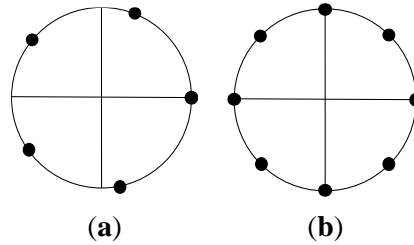
The modulation index h is selected to be $0 < h < 1$ and rational, i.e., ratio of two relatively prime integers p and q , the total number of points in the CPM constellation are kept to a reasonable number and catastrophic phase states are avoided [198]. When p is even, the phase states θ_k are given as,

$$\theta = \left\{ 0, \pi \frac{p}{q}, 2\pi \frac{p}{q}, \dots, (q-1)\pi \frac{p}{q} \right\} \quad (6.4)$$

In contrast, if p is odd, the phase states θ_k are given as,

$$\theta = \left\{ 0, \pi \frac{p}{q}, 2\pi \frac{p}{q}, \dots, (2q-1)\pi \frac{p}{q} \right\} \quad (6.5)$$

It follows from Equation (4) and Equation (5) that there are q points in the signal constellation when p is even and $2q$ when p is odd. For instance, there are five points in the signal constellation if $h = 2/5$, and 8 points if $h = 1/4$. Figure 6.3 shows the two scenarios.


 Figure 6.3. Constellation diagram for (a) $h = 2/5$ (b) $h = 1/4$.

6.3.3. CPM-OFDM Receiver

Using a sampling interval of $\Delta T = T_s/N$, the received complex signal is sampled with an analog-to-digital converter (A/D). After A/D, the N_g samples, i.e., the CP of each OFDM symbol, is discarded. This operation removes the effects of ISI provided $N_g \geq N_h$. After the removal of CP, each block of N received samples $\{X_k, k = 0, 1, \dots, N-1\}$ is transformed back to the frequency domain using an FFT that is the OFDM demodulation, as shown in Figure 1. The recovered complex data symbols x_k then pass through the CPM de-mapper to recover the data sequence that was transmitted.

6.3.3.1. Viterbi Decoder

Detection of CPM signals is a complex process. However, it becomes less complex and economical if a Viterbi decoder—also called Viterbi algorithm (VA)—is used [185]. This decoding technique was proposed in 1967 by A.J. Viterbi to decode convolutional codes [199]. As was demonstrated by Omura [200], VA is a maximum likelihood decoder. Furthermore, VA has also been used in the detection of signals that have been transmitted over linear models of voiceband channels [201, 202]. Other applications of VA include digital estimation problems. Some examples include voice recognition, recording systems with partial response channels, and optical character recognition [203, 204], etc. As was noted earlier, restricting the modulation index h to be rational, the number of states in CPM trellis can be kept to a manageable number that also facilitates the use of VA. Figure 4 shows the angle θ , the respective complex numbers and paths through the trellis for a typical data sequence and an arbitrary subcarrier when $h = 1/2$. Starting from state $\theta = 0$ ($s_k = 1 + j0$), a specific path can be traced based on the data sequence. For illustration purposes, a data sequence 1011 has been shown using slightly thick lines.

The distance between received signal and all the trellis paths entering each state at an instant i is calculated by VA. This is followed by the removal of those paths that are probably not the candidates for maximum likelihood. For two paths entering the same state, the one having the best metric is selected and it is named the “surviving path”. For all the states, similar surviving paths are selected. By continuing in a similar manner, VA advances deeper into the trellis and the decisions are made by removing the paths that are least likely [205]. Although such decisions are not maximum likelihood in the true sense, if the decision depth is long enough, these decisions can be almost as good as in the case of true maximum likelihood [206].

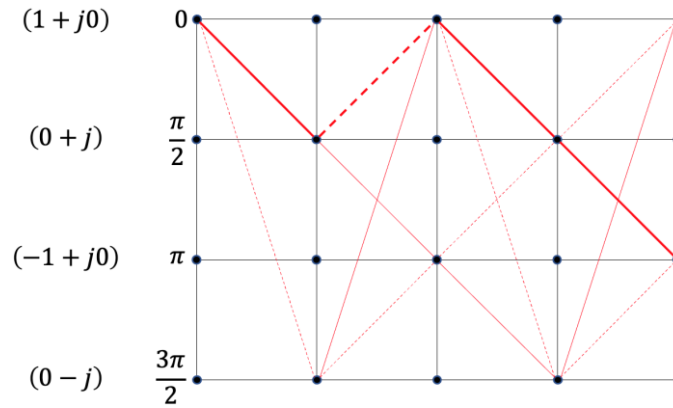


Figure 6.4. All the possible paths through the trellis for $h = 1/2$. Solid lines indicate bit 1, broken lines indicate bit 0, and bold lines indicate a typical bit sequence of 1011. The complex numbers beside the figure are the possible CPM mapper output.

The technique for computing the distances between the received and likelihood sequences is as follows. Recall that the received sequence of complex numbers for the k th subcarrier at the output of FFT is x_k and the transmitted sequence of complex numbers for the k th subcarrier is s_k . It follows that,

$$\begin{aligned} s_k &= u_k + jv_k \\ x_k &= \hat{u}_k + j\hat{v}_k \end{aligned} \quad (6.6)$$

Here, u_k and \hat{u}_k are the real parts of the transmitted and received complex numbers, respectively, while v_k and \hat{v}_k are the imaginary parts of the transmitted and received complex numbers, respectively. If d_k denotes the squared distance between two complex number sequences, then,

$$d_k = (u_k - \hat{u}_k)^2 + (v_k - \hat{v}_k)^2 \quad (6.7)$$

At each symbol interval, these distances are successively updated. Moreover, all possible state transitions are extended. The path having highest likelihood is retained at next symbol interval, while all others are deleted. After tracing the complete signal sequence, all contenders terminate in a common node at the extreme end of the trellis. Hence, the required sequence is the one that is the most likely of them. Since the modulation index h is the ratio of two relatively prime integers p and q , VA only keeps track of q or $2q$ states at each time interval. If m represents the decision depth in number of symbols, then VA produces a decision on the entire sequence of m symbols at the end of m symbol intervals reducing the complexity of the CPM de-mapper.

6.3.4. Shallow Underwater Channel Model

For a channel with L multipath components that are time shifted, the response [2] can be expressed mathematically as:

$$H(t, \tau) = \sum_{p=1}^L A_p(t) \delta(\tau - \tau_p(t)) \quad (6.8)$$

where A_p denotes the amplitude of the p th component, τ_p represents its delay coefficient, and δ is the Dirac delta function. The envelope response of the shallow underwater channel was divided into two parts: the deterministic response and the random multipath fading.

Considering $s(t)$ to be the CPM modulated time domain digital signal from equation 6.1, Figure 6.5 shows it passing through the channel blocks. This allows for controlling the SNR, modifying channel taps and the acoustic absorption pathloss parameters from Thorp's formula [61]. The typical delay spread for a shallow underwater acoustic channel is between 10 to 20 ms and can be as long as 100 ms [92].

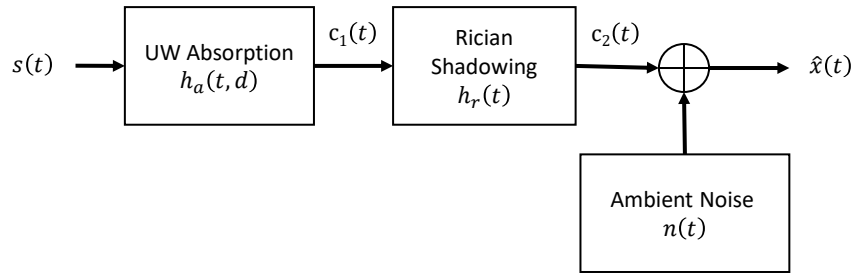


Figure 6.5. Shallow underwater acoustic channel model.

6.3.4.1. Deterministic Response

In an underwater medium the energy of an acoustic signal gets attenuated both as a function of distance as well as frequency, and the pathloss is a combination of geometric spreading as well as absorption. Mathematically, if the variation in time is $e^{j\omega t}$ the path frequency domain transmission loss expression in the positive z direction will be:

$$E(z) = E_0 e^{-\gamma z} = E_0 e^{-\alpha z} e^{-j\beta z} \quad (6.9)$$

where a scaling constant is denoted by E_0 . The channel's deterministic transfer function $H_a(f, d)$ [62, 63] is:

$$H_a(f, d) = A_d e^{-\gamma(f)d} \quad (6.10)$$

where A_d and d are a scaling constant and transmitter-receiver distance, respectively, while γ denotes a complex propagation constant, in m^{-1} :

$$\gamma(f) = \alpha(f) + j\beta(f) \quad (6.11)$$

where $\alpha(f)$ and $\beta(f)$ are absorption and phase constants, respectively. In UWA channels the absorption is a function of frequency as acoustic pressure is reduced due to energy losses in heat. According to the Thorp formula [61], the absorption coefficient is computed in dB/km as:

$$\alpha_{dB}(f) = 1.094 \left(0.003 + \frac{0.1f^2}{1+f^2} + \frac{40f^2}{4100+f^2} + 0.000275f^2 \right) \quad (6.12)$$

Figure 6.6a shows, for multiple distances, the absorption pathloss transfer function. Similarly, phase constant in rad/m is:

$$\beta(f) = \frac{2\pi f}{c_s} \quad (6.13)$$

where c_s represents sound velocity [64] in ms^{-1} , calculated as:

$$c_s = 1449.2 + 4.6T - 0.055T^2 + 0.00029T^3 + ((1.34 - 0.01)T)(S - 35) \quad (6.14)$$

where T, S , and Z_M are temperature, salinity, and depth, respectively. Equation 6.14 is called Medwin's equation [64]. The realistic channel values are considered with temperature between 0° to 35° C while salinity is from 0 to 45 PPT. The signal $c_1(t)$ in Figure 6.5 can be expressed as:

$$c_1(t) = h_a(t, d) \otimes s(t) \quad (6.15)$$

where $h_a(t, d)$ represents the IFFT of the channel transfer function convolved with the transmitted signal $s(t)$.

6.3.4.2. Random Channel

Various fading models exist for RF channels and there is a general agreement between scientists and researchers over their usage. However, the domain of fading models for UWA channels is still open and lacks consensus. Experimental studies conducted suggest that a Rician fading model accurately represents the fading observed by acoustic signals in a UWA channel [93]. Researchers studied sea trial data, with Rician shadowed distribution having the closet fit [66, 94]. The parameters selected in this work are $m = 0.4$ and $k = 2.0$ [94]. The value of spreading factor $k = 1.5$ can also be assumed [67]. The signal $c_2(t)$ from Figure 6.5 can be represented as:

$$c_2(t) = h_r(t) \otimes c_1(t) + n(t) \quad (6.16)$$

where $n(t)$ and $h_r(t)$ are noise and Rician fading [68] impulse response modelled using Rician channel object in MATLAB R2019b by MathWorks, respectively. Figure 6.6b shows the sample of channel path gains and delay profile.

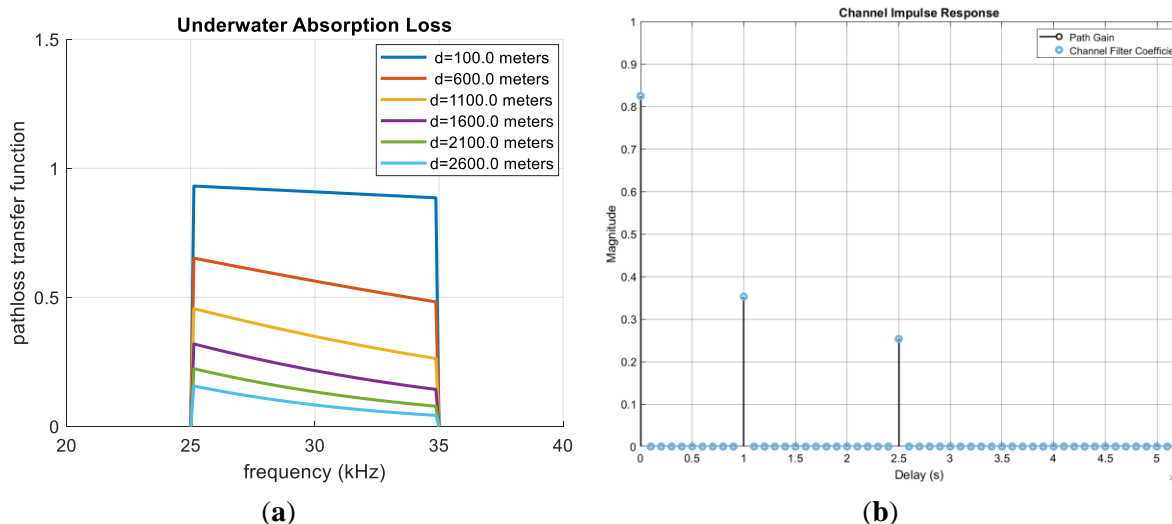


Figure 6.6. Shallow acoustic channel characteristics: (a) frequency dependent absorption; (b) channel impulse response.

6.3.4.3. Ambient Noise

In a realistic UWA channel, the noise is not white and depends upon various acoustic frequencies. For our simulations, we use an ambient noise model that is a combination of thermal, shipping, wave, and turbulence noise [69]. The power spectral density (PSD) of the total noise is:

$$N(f) = 10 \log \left(10^{\frac{N_{shipping}(f)}{10}} + 10^{\frac{N_{turbulence}(f)}{10}} + 10^{\frac{N_{wave}(f)}{10}} + 10^{\frac{N_{thermal}(f)}{10}} \right) \quad (6.17)$$

The noise is location specific and can be modeled as color noise, and its amplitude is high at both the lower and upper end of the spectrum while minimum around 60 kHz [96].

6.4. Simulation Setup and Results

The performance of the proposed system was evaluated using simulations where a CPM-OFDM transceiver is communicating over a UWA channel. The simulation parameters used are shown in Table 6.1.

We selected the values of the modulation index h by varying the numerator p from 1 to 15. We chose the values of the denominator q by varying it from 2 to 16 such that p/q remains rational. This gave us a total of 23 values of h . Any other values outside this set do not give any better performance, and we found this set to be sufficient to assess the performance of the intended system. Moreover, selecting higher values of p and q would result in higher number of points in the constellation, increasing the decoder complexity. The error performance of a typical CPM-OFDM system for these 23 values of h is shown in Figure 6.7.

Based upon the BER values, the curves have been divided into two categories: A and B. As is evident from Figure 6.7, Category A represents those curves that show good BER performance, whereas Category B represents those curves that show poor BER performance. The best BER is achieved when the value of h is either $7/16$ or $9/16$. The BER performance for these two values of h is not identical but because they are very close, they appear to be overlapping each other.

In addition to these two values, there are more curves in Figure 6.7 that appear to be overlapping each other. Therefore, we have also shown the BER performance using two tables—Tables 6.2 and 6.3. The difference between these two tables is the way they have been sorted. Table 6.2 is sorted on p and q , and Table 6.3 has been sorted on the BER values when SNR is 20 dB.

Table 6.1. Simulation parameters.

Parameters	Values
Number of Subcarriers	512
CP Length	128 (typically, 1/4th the no. of subcarriers)
Modulation Index	23 rational values
Bandwidth	10 kHz
Average Path Gains	[0; -1.5; -2.5; -7.0] dB
Path Delays	[0; 1; 2.5; 5.4] ms
Sampling Frequency	10,000 samples per second
OFDM Symbol Duration	51.2 ms
No. of OFDM Symbols Transmitted	160,000
No. of Simulation Runs	20
Tx-Rx Distance	500 m
Transmitter Depth	50 m
Receiver Depth	50 m
Doppler Frequency	10 Hz
Atmospheric pressure	1.01325×10^5 Pa
Salinity	35 parts/1000
Density	10^3 kg/m ³
Water temperature	25°C

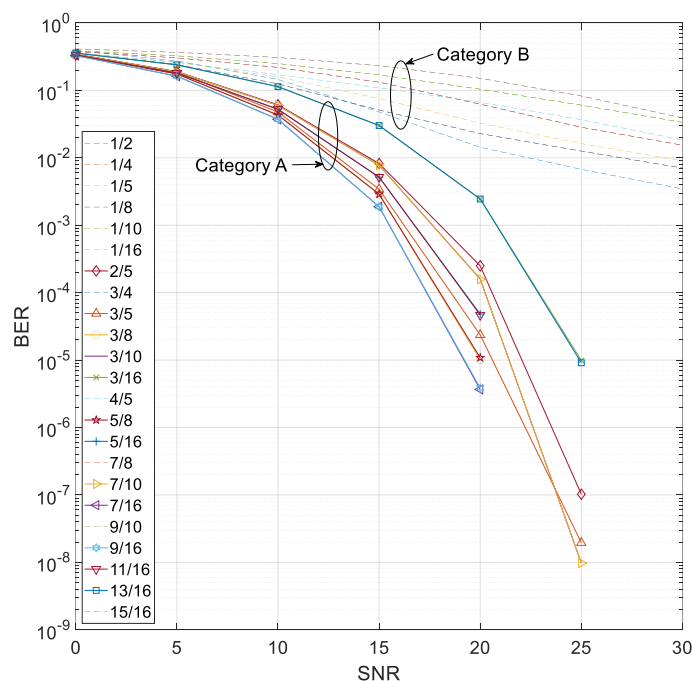


Figure 6.7. Error performance of CPM-OFDM for 23 rational values of modulation index h with $N = 512$ and transmitter-receiver distance 500 meters.

It is evident that the best BER is achieved when h is $7/16$, which has been highlighted with a yellow color. The performance of $h = 9/16$ is very similar to the case when $h = 7/16$ and is highlighted with an orange color. In both these cases, the number of points in the constellation will be $2q$, i.e., 32. If a smaller number of points are desired in the constellation to decrease the decoder complexity, then h values with a smaller q could be selected, such as $h = 3/8$ that gives 16 points in the signal constellation at a slightly inferior BER. Another choice could be $h = 3/5$ that would give only 10 points in the signal constellation at the cost of BER. From the two tables, it is observed that in Category A, there is only one value of h that has an even value of p and it is $h = 2/5$. Although it gives the minimum number of points in the signal constellation, its BER is much inferior when compared to the best case of $h = 7/16$ or $h = 9/16$.

The BER performance of the proposed scheme with varying transmitter-receiver distances is shown in Figure 6.8. Although performance degradation as the distance increases is obvious, CPM-OFDM still gives acceptable BER up to 1.5 km. Figure 6.9 illustrates the BER performance as a function of channel bandwidth. The lowest BER is noted for a channel bandwidth of 10 kHz. It is also noted that, as would be expected, the BER degrades as the channel bandwidth decreases. However, the BER performance for channel bandwidths of 5 kHz and 2.5 kHz are very similar with the BER offered by 2.5 kHz being slightly better than that offered by a bandwidth of 5 kHz.

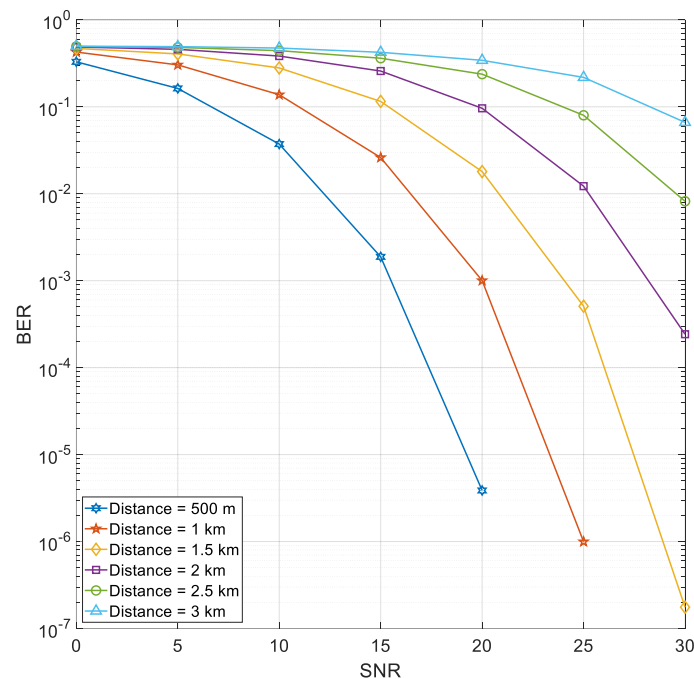


Figure 6.8. BER performance of CPM-OFDM as a function of transmitter-receiver distances with $N = 512$, $h = 7/16$.

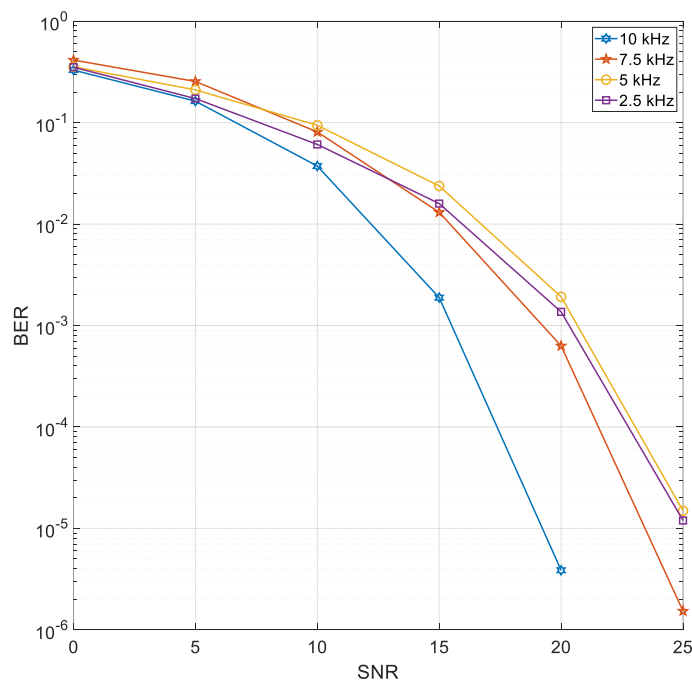


Figure 6.9. BER performance of CPM-OFDM as a function of channel bandwidth with $N = 512$, $h = 7/16$.

Table 6.2. BER values for various modulation indices and SNRs (sorted on values of p and q).

$h = p/q$		SNR (dB)						
p	q	0	5	10	15	20	25	30
1	2	0.389864	0.274086	0.145444	0.04784	0.01437	0.006743	0.003461
1	4	0.358647	0.241738	0.124955	0.051068	0.022901	0.012591	0.007052
1	5	0.360902	0.261278	0.158968	0.075665	0.032758	0.016251	0.009047
1	8	0.377929	0.303389	0.219292	0.132342	0.06248	0.028433	0.015397
1	10	0.388773	0.325632	0.250118	0.169976	0.10423	0.060461	0.033599
1	16	0.412185	0.367027	0.307857	0.232441	0.151332	0.082683	0.039188
2	5	0.343899	0.189986	0.06111	0.008237	0.00025	1.03×10^{-7}	0
3	4	0.358597	0.241657	0.124931	0.051127	0.022885	0.012581	0.007057
3	5	0.343854	0.186318	0.047827	0.003423	2.36×10^{-5}	1.95×10^{-8}	0
3	8	0.337594	0.175321	0.043152	0.002893	1.01×10^{-5}	0	0
3	10	0.341311	0.188547	0.059988	0.007768	0.00016	9.77×10^{-9}	0
3	16	0.357686	0.239549	0.113669	0.030198	0.002457	9.90×10^{-6}	0
4	5	0.360941	0.261225	0.170811	0.109233	0.06671	0.0368	0.018393
5	8	0.337572	0.175237	0.043122	0.002893	1.09×10^{-5}	0	0
5	16	0.337189	0.180792	0.052542	0.005163	4.81×10^{-5}	0	0
7	8	0.37788	0.303382	0.219266	0.132345	0.06243	0.028404	0.015389
7	10	0.341236	0.188574	0.059911	0.00778	0.000159	9.77×10^{-9}	0
7	16	0.329276	0.162725	0.037263	0.001883	3.67×10^{-6}	0	0
9	10	0.388748	0.325557	0.250039	0.169949	0.104257	0.060448	0.033613
9	16	0.329302	0.16274	0.037281	0.001882	3.87×10^{-6}	0	0
11	16	0.337094	0.180739	0.052517	0.005183	4.67×10^{-5}	0	0
13	16	0.357658	0.239519	0.113663	0.030164	0.002452	9.13×10^{-6}	0
15	16	0.412149	0.367034	0.30793	0.232537	0.151276	0.082633	0.039155

Table 6.3. BER values for various modulation indices and SNRs (sorted on values of BER at SNR = 20 dB).

		$h = p/q$		SNR (dB)						
		p	q	0	5	10	15	20	25	30
Category A		7	16	0.329276	0.162725	0.037263	0.001883	3.67×10^{-6}	0	0
		9	16	0.329302	0.16274	0.037281	0.001882	3.87×10^{-6}	0	0
		3	8	0.337594	0.175321	0.043152	0.002893	1.01×10^{-5}	0	0
		5	8	0.337572	0.175237	0.043122	0.002893	1.09×10^{-5}	0	0
		3	5	0.343854	0.186318	0.047827	0.003423	2.36×10^{-5}	1.95×10^{-8}	0
		11	16	0.337094	0.180739	0.052517	0.005183	4.67×10^{-5}	0	0
		5	16	0.337189	0.180792	0.052542	0.005163	4.81×10^{-5}	0	0
		7	10	0.341236	0.188574	0.059911	0.00778	0.000159	9.77×10^{-9}	0
		3	10	0.341311	0.188547	0.059988	0.007768	0.00016	9.77×10^{-9}	0
		2	5	0.343899	0.189986	0.06111	0.008237	0.00025	1.03×10^{-7}	0
		13	16	0.357658	0.239519	0.113663	0.030164	0.002452	9.13×10^{-6}	0
		3	16	0.357686	0.239549	0.113669	0.030198	0.002457	9.90×10^{-6}	0
	Category B		1	2	0.389864	0.274086	0.145444	0.04784	0.01437	0.006743
		3	4	0.358597	0.241657	0.124931	0.051127	0.022885	0.012581	0.007057
		1	4	0.358647	0.241738	0.124955	0.051068	0.022901	0.012591	0.007052
		1	5	0.360902	0.261278	0.158968	0.075665	0.032758	0.016251	0.009047
		7	8	0.37788	0.303382	0.219266	0.132345	0.06243	0.028404	0.015389
		1	8	0.377929	0.303389	0.219292	0.132342	0.06248	0.028433	0.015397
		4	5	0.360941	0.261225	0.170811	0.109233	0.06671	0.0368	0.018393
		1	10	0.388773	0.325632	0.250118	0.169976	0.10423	0.060461	0.033599
		9	10	0.388748	0.325557	0.250039	0.169949	0.104257	0.060448	0.033613
		15	16	0.412149	0.367034	0.30793	0.232537	0.151276	0.082633	0.039155
		1	16	0.412185	0.367027	0.307857	0.232441	0.151332	0.082683	0.039188

We also evaluated the PAPR performance of CPM-OFDM for all the 23 values of h . The complementary cumulative distribution function (CCDF) for each value of h is plotted in Figure 6.10. For comparison, the CCDF of a typical PSK-OFDM scheme is also plotted. The best PAPR is observed when $h = 1/2$, which is almost identical to that of PSK-OFDM. The PAPR of other values of h is marginally inferior to PSK-OFDM and $h = 1/2$.

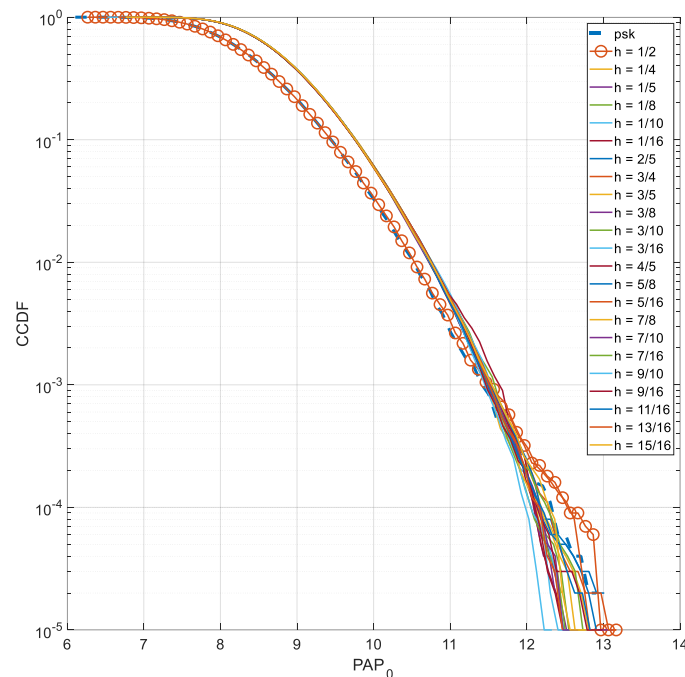


Figure 6.10. PAPR performance of CPM-OFDM as a function of 23 values of h with $N = 512$ and transmitter-receiver distance 500 m.

6.5. Conclusion

Through computer simulations, it has been shown that CPM-OFDM is an attractive candidate for underwater acoustic communication. This scheme offers an excellent error performance without employing any equalization technique. The best error performance is achieved when the CPM modulation index h is chosen as either $7/16$ or $9/16$. Moreover, acceptable error performance is observed up to a transmitter-receiver distance of 500 meters. The PAPR performance of CPM-OFDM has also been evaluated and shown to be similar to those offered by other traditional OFDM schemes. Hence, a PAPR reduction technique is mandatory when employing CPM-OFDM for underwater acoustic communication. In this work, we evaluated the performance of binary CPM-OFDM and without any PAPR reduction technique. The performance of M-ary CPM-OFDM with PAPR reduction technique remains to be studied.

This page intentionally left blank

Chapter 7: Conclusions and Future Work

This chapter summarizes the proposed techniques and work done in this dissertation. It also details a few directions in which this work can be extended.

7.1. Conclusions

The primary objective of this work was to explore the domain of multicarrier underwater acoustic communication systems and develop a working simulation model for testing multiple performance improvements.

First, a reconfigurable OFDM soft modem architecture for underwater communication has been presented along with a capability to modify and tune various parameters. An underwater channel model that incorporates ambient noise and AWGN, acoustic absorption in water and multipath has been developed in MATLAB. Rician shadowing model has been assumed for the multipath channel. Simulations have been carried out using Monte-Carlo simulations and BER plots have been presented. Results have been shown with and without equalization. Zero-forcing equalization has been used assuming perfect channel information. The model has been used to simulate MPSK-OFDM but it can be used for other mapping schemes as well such as QAM and DPSK, etc. The ability to add different channel estimation techniques further allows us to try and test various methods used to reduce bit errors. The channel model allows for evaluating the transceiver for different UWA environments by simply modifying the channel parameters such as ambient noise and multipath fading along with bathymetry and geometrical profiles.

Further building upon the proposed testbed, we proposed a pilot-based channel estimation technique while comparing two equalizers to improve the error performance of an OFDM-based UWA system. Both equalizers employ pilot subcarriers to estimate the UWA channel. Using computer simulations, it is observed that, for an acceptable error performance, the number of pilots should be one-fourth the number of subcarriers. Moreover, if the energy of the pilots is increased without changing the overall symbol energy, the error performance degrades. It is also noted that both the LS and ZF equalizers give an acceptable error performance with the ZF performing marginally better than the LS. Furthermore, the error performance of the proposed system is evaluated as a function of the transmitter-receiver distance and an acceptable error performance is observed even at 1250 m.

Several 5G contender waveforms were studied and we presented a survey of post-OFDM multicarrier waveforms for UWA channels. We have reported our findings and conclude that for future multicarrier systems, GFDM and FBMC have proven to be ideal candidates for underwater communication due to their improved spectral efficiency and immunity against ICI and ISI. GFDM offers a more robust and flexible solution at the cost of slight increase in computational complexity for transmission in the underwater medium. Our simulation results have shown that GFDM exhibits a better SER performance compared to an OFDM system for a UWA channel. Moreover, the spectral efficiency gains for a GFDM system are quite high as compared with other MC candidates. We have also shown that the choice of pulse shapes and the associated roll off factor play a significant role in determining the spectral efficiency and the SER of a GFDM system. A higher value of the roll off factor decreases the OOB emissions but at the cost of SER and a slight increase in PAPR.

A low complexity PAPR reduction technique for underwater acoustic OFDM transceiver is proposed and demonstrated. It consists of multiple pre-determined cipher keys, generated using a high-end PC, that are used for XOR ciphering of the BCH encoded and decoded data at the OFDM transmitter and receiver respectively. Our findings suggest that while reducing PAPR, the ciphered-BCH technique improves BER performance of the system using channel coding. It is observed that a higher PAPR reduction and a lower BER is achieved when lower code rate BCH codes are used. Using multiple keys,

known to both the transmitter and receiver, a level of encryption is achieved as an added advantage. Given power and processing limitations of the underwater acoustic nodes, the proposed technique is easy to implement and reduces computational complexity of the transceiver as most of the processing for key vector search is done offline. The most appropriate keys generated are stored in both the transmitter and receiver and are used for ciphering purposes and to reduce PAPR of the OFDM signal.

We proposed a memory-based mapper for UWA OFDM and evaluate the performance of CPM-OFDM transceiver for underwater acoustic communication. In the proposed technique, the mapper in traditional OFDM is replaced by CPM while a realistic model of underwater channel is employed. Bit error rate as well as peak to average power ratio performance of the proposed scheme is evaluated using Monte-Carlo simulations. The error performance observed clearly establishes the superiority of CPM-OFDM over traditional OFDM schemes. Specifically, a value of 7/16 or 9/16 for the modulation index gives the best error performance. Furthermore, the error performance of the proposed scheme is within acceptable values up to a transmitter–receiver distance of 1.5 *km*. Additionally, the PAPR performance of the proposed scheme suggests that like other OFDM schemes, a PAPR reduction scheme is mandatory for acceptable PAPR performance of CPM-OFDM.

7.2. Future work

The focus of this dissertation was design and implementation of a soft modem that was developed using Mathworks MATLAB along with a shallow underwater acoustic channel model. Field testing the proposed techniques and conducting sea trials will be of paramount importance to verify the viability of the proposed designs. We intend to implement the proposed OFDM architecture on a Linux based single board computer along with integrating the system with hydrophones and related circuitry.

While the use of pilots subcarriers aids in channel estimation, their location plays an important role. Since several pilot positioning schemes exists in literature, it will be intriguing to explore the performance of a pilot-based estimation by varying the location of pilots in a frame.

GFDM solves the OOB emission issue, but the complexity and PAPR are still high. Various techniques can be explored to reduce the complexity of a GFDM transceiver system along with exploring low complexity PAPR reduction techniques. We intend to implement a coded GFDM transceiver to further improve BER performance of the system and study the use of block codes on PAPR of the system.

Continuous phase modulation based OFDM mapper helps in reducing the complexity of transceiver for UWA communication. However, error performance can be significantly improved by introducing channel coding techniques, specifically block codes. It will also be interesting to introduce a low complexity PAPR reduction technique to make it more viable.

Bibliography

- [1] I. F. Akyildiz, D. Pompili, and T. Melodia, "Challenges for efficient communication in underwater acoustic sensor networks," *ACM Sigbed Review*, vol. 1, no. 2, pp. 3-8, 2004.
- [2] C. Liu, Y. V. Zakharov, and T. Chen, "Doubly Selective Underwater Acoustic Channel Model for a Moving Transmitter/Receiver," *IEEE Transactions on Vehicular Technology*, vol. 61, no. 3, pp. 938-950, 2012.
- [3] M. Chitre, S. Shahabudeen, L. Freitag, and M. Stojanovic, "Recent advances in underwater acoustic communications & networking," in *OCEANS 2008*, 2008, pp. 1-10: IEEE.
- [4] X. Xiaoka, W. Zhaohui, Z. Shengli, and L. Wan, "Parameterizing both path amplitude and delay variations of underwater acoustic channels for block decoding of orthogonal frequency division multiplexing," *J. Acoustical Society of America*, vol. 131, no. 6, pp. 4672-4679, 2012.
- [5] M. Stojanovic and J. Preisig, "Underwater acoustic communication channels: Propagation models and statistical characterization," *IEEE communications magazine*, vol. 47, no. 1, pp. 84-89, 2009.
- [6] B. Li, S. Zhou, M. Stojanovic, and L. Freitag, *Pilot-tone based ZP-OFDM demodulation for an underwater acoustic channel*. IEEE, 2006.
- [7] M. Stojanovic, *Low complexity OFDM detector for underwater acoustic channels*. IEEE, 2006.
- [8] M. Stojanovic, "Performance analysis of filtered multitone modulation systems for underwater communication," in *OCEANS 2009*, 2009, pp. 1-9: IEEE.
- [9] J. Huang, S. Zhou, and P. Willett, "Nonbinary LDPC coding for multicarrier underwater acoustic communication," *IEEE Journal on Selected Areas in Communications*, vol. 26, no. 9, pp. 1684-1696, 2008.
- [10] B. Li, S. Zhou, M. Stojanovic, L. Freitag, and P. Willett, "Multicarrier underwater acoustic communications over fast-varying channels," *IEEE journal of Oceanic Engineering*, vol. 33, no. 2, pp. 198-209, 2008.
- [11] B. Li, S. Zhou, M. Stojanovic, L. Freitag, and P. Willett, "Multicarrier communication over underwater acoustic channels with nonuniform Doppler shifts," *IEEE Journal of Oceanic Engineering*, vol. 33, no. 2, pp. 198-209, 2008.
- [12] S.-J. Hwang and P. Schniter, "Efficient multicarrier communication for highly spread underwater acoustic channels," *IEEE Journal on Selected Areas in Communications*, vol. 26, no. 9, pp. 1674-1683, 2008.
- [13] P. Amini, R.-R. Chen, and B. Farhang-Boroujeny, "Filterbank multicarrier communications for underwater acoustic channels," *IEEE Journal of Oceanic Engineering*, vol. 40, no. 1, pp. 115-130, 2014.
- [14] P. Zhu, X. Xu, X. Tu, Y. Chen, and Y. Tao, "Anti-Multipath Orthogonal Chirp Division Multiplexing for Underwater Acoustic Communication," *IEEE Access*, vol. 8, pp. 13305-13314, 2020.
- [15] M. Stojanovic, "Underwater Acoustic Communications: Design Considerations on the Physical Layer," in *Proc. Wireless on Demand Network Systems and Services*, 2008, pp. 1-10.
- [16] A. Khelifi and R. Bouallegue, "Performance analysis of LS and LMMSE channel estimation techniques for LTE downlink systems," *arXiv preprint arXiv:1111.1666*, 2011.
- [17] X. Wang, J. Wang, L. He, and J. Song, "Doubly selective underwater acoustic channel estimation with basis expansion model," in *2017 IEEE International Conference on Communications (ICC)*, 2017, pp. 1-6.
- [18] P. Schniter, "Low-complexity equalization of OFDM in doubly selective channels," *IEEE Transactions on Signal Processing*, vol. 52, no. 4, pp. 1002-1011, 2004.
- [19] M. Murad, I. A. Tasadduq, P. Otero, and J. Poncela, "Flexible OFDM Transceiver for Underwater Acoustic Channel: Modeling, Implementation and Parameter Tuning," *Wireless Personal Communications*, vol. 116, no. 2, pp. 1423-1441, 2021.
- [20] G. Qiao, Z. Babar, L. Ma, S. Liu, and J. Wu, "MIMO-OFDM underwater acoustic communication systems—A review," *Physical Communication*, vol. 23, pp. 56-64, 2017/06/01/ 2017.

- [21] S. Mason, R. Anstett, N. Anicette, and S. Zhou, "A broadband underwater acoustic modem implementation using coherent OFDM," in *Proc. of National Conference for Undergraduate Research (NCUR)*, 2007.
- [22] M. Stojanovic, "Low Complexity OFDM Detector for Underwater Acoustic Channels," in *OCEANS*, 2006, pp. 1-6.
- [23] X. Wang, X. Wang, R. Jiang, W. Wang, Q. Chen, and X. Wang, "Channel Modelling and Estimation for Shallow Underwater Acoustic OFDM Communication via Simulation Platform," *Applied Sciences*, vol. 9, no. 3, p. 447, 2019.
- [24] W. Yonggang, "Underwater acoustic channel estimation for pilot based OFDM," in *2011 IEEE International Conference on Signal Processing, Communications and Computing (ICSPCC)*, 2011, pp. 1-5: IEEE.
- [25] B. Li *et al.*, "MIMO-OFDM for high-rate underwater acoustic communications," *IEEE Journal of Oceanic Engineering*, vol. 34, no. 4, pp. 634-644, 2009.
- [26] M. Stojanovic, "OFDM for underwater acoustic communications: Adaptive synchronization and sparse channel estimation," in *Acoustics, Speech and Signal Processing, 2008. ICASSP 2008. IEEE International Conference on*, 2008, pp. 5288-5291: IEEE.
- [27] U. M. Qureshi *et al.*, "RF Path and Absorption Loss Estimation for Underwater Wireless Sensor Networks in Different Water Environments," (in eng), *Sensors (Basel, Switzerland)*, vol. 16, no. 6, p. 890, 2016.
- [28] N. Chirdchoo, W. Soh, and K. C. Chua, "Aloha-Based MAC Protocols with Collision Avoidance for Underwater Acoustic Networks," in *IEEE INFOCOM 2007 - 26th IEEE International Conference on Computer Communications*, 2007, pp. 2271-2275.
- [29] B. Cochenour and L. Mullen, "Free-space optical communications underwater," in *Advanced Optical Wireless Communication Systems*, G. Karagiannidis, J. Barry, M. Uysal, R. Schober, and S. Arnon, Eds. Cambridge: Cambridge University Press, 2012, pp. 201-239.
- [30] F. B. Jensen, W. A. Kuperman, M. B. Porter, and H. Schmidt, *Computational ocean acoustics*. Springer Science & Business Media, 2011.
- [31] M. Stojanovic, "Low complexity OFDM detector for underwater acoustic channels," presented at the OCEANS, 2006.
- [32] A. Dayal, "Nonlinear Doppler Warp Correction for Acoustic OFDM," Masters Thesis, Virginia Tech, 2016.
- [33] W. Pan, P. Liu, F. Chen, F. Ji, and J. Feng, "Doppler-shift estimation of flat underwater channel using data-aided least-square approach," *International Journal of Naval Architecture and Ocean Engineering*, vol. 7, no. 2, pp. 426-434, 2015.
- [34] E. Bejjani and J. Belfiore, "Multicarrier coherent communications for the underwater acoustic channel," in *OCEANS 96 MTS/IEEE Conference Proceedings. The Coastal Ocean - Prospects for the 21st Century*, 1996, vol. 3, pp. 1125-1130 vol.3.
- [35] W. K. Lam and R. F. Ormondroyd, "A coherent COFDM modulation system for a time-varying frequency-selective underwater acoustic channel," in *Seventh International Conference on Electronic Engineering in Oceanography, 1997. Technology Transfer from Research to Industry.*, 1997, pp. 198-203.
- [36] E. Sang, X. Xu, G. Qiao, and J. Su, "Study on ZP-OFDM for underwater acoustic communication," in *2008 International Conference on Neural Networks and Signal Processing*, 2008, pp. 299-302.
- [37] X. Wang, X. Shen, and S. Ma, "A Time-reversal based CP-free OFDM system for underwater acoustic communication," in *OCEANS 2019 - Marseille*, 2019, pp. 1-6.
- [38] H. Kulhandjian and T. Melodia, "Modeling Underwater Acoustic Channels in Short-range Shallow Water Environments," presented at the Proceedings of the International Conference on Underwater Networks & Systems, Rome, Italy, 2014.
- [39] A. Song, J. Senne, M. Badiy, and K. B. Smith, "Underwater acoustic communication channel simulation using parabolic equation," presented at the Proceedings of the Sixth ACM International Workshop on Underwater Networks, Seattle, Washington, 2011.
- [40] J. F. Cañete *et al.*, "Measurement and Modeling of Narrowband Channels for Ultrasonic Underwater Communications," *Sensors*, vol. 16, no. 2, 2016.

- [41] M. Y. I. Zia, P. Otero, and J. Poncela, "Design of a Low-Cost Modem for Short-Range Underwater Acoustic Communications," *Wireless Personal Communications*, vol. 101, no. 1, pp. 375-390, 2018.
- [42] X. Cheng and L. Yang, "Study and Implementation of IEEE 802.11 p PHY for OFDM Underwater Acoustic Communications."
- [43] M. Y. I. Zia, A. M. Khan, P. Otero, and J. Poncela, "Investigation of underwater acoustic modems: Architecture, test environment & performance," in *Computing for Sustainable Global Development (INDIACom), 2016 3rd International Conference on*, 2016, pp. 2031-2036: IEEE.
- [44] F. Frassati, C. Lafon, P.-A. Laurent, and J.-M. Passerieux, "Experimental assessment of OFDM and DSSS modulations for use in littoral waters underwater acoustic communications," in *Oceans 2005-Europe*, 2005, vol. 2, pp. 826-831: IEEE.
- [45] H. Yan, S. Zhou, Z. J. Shi, and B. Li, "A DSP implementation of OFDM acoustic modem," in *Proceedings of the second workshop on Underwater networks*, 2007, pp. 89-92: ACM.
- [46] H. Yan *et al.*, "DSP based receiver implementation for OFDM acoustic modems," *Physical Communication*, vol. 5, no. 1, pp. 22-32, 2012.
- [47] Z. Kun, Q. S. Sen, K. T. Aik, and T. B. Aik, "A real-time coded OFDM acoustic modem in very shallow underwater communications," *OCEANS 2006-Asia Pacific*, pp. 1-5, 2007.
- [48] K. Pelekanakis *et al.*, "A modem design for underwater acoustic networking in the high north," in *2018 Fourth Underwater Communications and Networking Conference (UComms)*, 2018, pp. 1-5: IEEE.
- [49] M. Porter. *Bellhop code*. Available: <http://oalib.hlsresearch.com/Rays/index.html>
- [50] L. Wan *et al.*, "Adaptive modulation and coding for underwater acoustic OFDM," *IEEE Journal of Oceanic Engineering*, vol. 40, no. 2, pp. 327-336, 2015.
- [51] Q. Dong, Y. Wang, and X. Guan, "The Design and Implementation of an Underwater Multimode Acoustic Modem for Autonomous Underwater Vehicles," in *2018 37th Chinese Control Conference (CCC)*, 2018, pp. 4201-4205: IEEE.
- [52] T. MinhHai, S. Rie, T. Suzuki, and T. Wada, "An acoustic OFDM System with symbol-by-symbol Doppler compensation for underwater communication," *The Scientific World Journal*, vol. 2016, 2016.
- [53] X. Ma and C. Zheng, "Decision fractional fast Fourier transform Doppler compensation in underwater acoustic orthogonal frequency division multiplexing," *The Journal of the Acoustical Society of America*, vol. 140, no. 5, pp. EL429-EL433, 2016.
- [54] J. Wu, G. Qiao, and X. Qi, "The research on improved companding transformation for reducing PAPR in underwater acoustic OFDM communication system," *Discrete Dynamics in Nature and Society*, vol. 2016, 2016.
- [55] R. Gomathi and J. Martin Leo Manickam, "PAPR reduction technique using combined DCT and LDPC based OFDM system for underwater acoustic communication," *ARPJ Journal of Engineering and Applied Sciences*, vol. 11, no. 7, pp. 4424-4430, 2016.
- [56] W. Shen, H. Sun, E. Cheng, and Y. Zhang, "Performance analysis of DFT-spread based OFDM transmission system over underwater acoustic channels," *Journal of Convergence Information Technology, AICIT*, vol. 6, no. 7, pp. 79-86, 2011.
- [57] A. Radosevic, R. Ahmed, T. M. Duman, J. G. Proakis, and M. Stojanovic, "Adaptive OFDM modulation for underwater acoustic communications: Design considerations and experimental results," *IEEE Journal of Oceanic Engineering*, vol. 39, no. 2, pp. 357-370, 2014.
- [58] X. L. Shi, Y. X. Yang, and L. Yang, "An OFDM System for Long-Range Underwater Acoustic Communications," *Applied Mechanics and Materials*, vol. 321-324, pp. 1274-1277, 2013.
- [59] Y. Zhou and F. Tong, "Research and Development of a Highly Reconfigurable OFDM MODEM for Shallow Water Acoustic Communication," *IEEE Access*, vol. 7, pp. 123569-123582, 2019.
- [60] E. Panayirci, M. T. Altabbaa, M. Uysal, and H. V. Poor, "Sparse Channel Estimation for OFDM-Based Underwater Acoustic Systems in Rician Fading With a New OMP-MAP Algorithm," *IEEE Transactions on Signal Processing*, vol. 67, no. 6, pp. 1550-1565, 2019.
- [61] R. J. Urick, *Sound Propagation in the Sea*. Peninsula Publishing, 1982.
- [62] K. U. I. Philip M. Morse, *Theoretical Acoustics*. Princeton University Press, 1986.

- [63] P. Otero, *Fundamentos de propagación de ondas*. Malaga: Universidad de Malaga, Manual, 2015.
- [64] H. Medwin, "Speed of sound in water: A simple equation for realistic parameters," *The Journal of the Acoustical Society of America*, vol. 58, no. 6, pp. 1318-1319, 1975.
- [65] F. Ruiz-Vega, M. C. Clemente, P. Otero, and J. F. Paris, "Ricean shadowed statistical characterization of shallow water acoustic channels for wireless communications," *arXiv preprint arXiv:1112.4410*, 2011.
- [66] A. Radosevic, J. G. Proakis, and M. Stojanovic, "Statistical characterization and capacity of shallow water acoustic channels," in *OCEANS 2009-EUROPE*, 2009, pp. 1-8.
- [67] T. Melodia, H. Kulhandjian, L. Kuo, and E. Demirors, "Mobile ad hoc networking: cutting edge directions," *Advances in Underwater Acoustic Networking*, 2013.
- [68] M. Jeruchim, P. Balaban, and K. S. Shanmugan, *Simulation of Communication Systems*, Second ed. New York: Kluwer Academic/Plenum, 2000.
- [69] M. Stojanovic, "On the relationship between capacity and distance in an underwater acoustic communication channel," *ACM SIGMOBILE Mobile Computing and Communications Review*, vol. 11, no. 4, pp. 34-43, 2007.
- [70] M. Chitre, "A high-frequency warm shallow water acoustic communications channel model and measurements," *The Journal of the Acoustical Society of America*, vol. 122, no. 5, pp. 2580-2586, 2007.
- [71] M. Murad, I. A. Tasadduq, and P. Otero, "Pilot-Assisted OFDM for Underwater Acoustic Communication," *Journal of Marine Science and Engineering*, vol. 9, no. 12, p. 1382, 2021.
- [72] J.-J. Van De Beek, O. Edfors, M. Sandell, S. K. Wilson, and P. O. Borjesson, "On channel estimation in OFDM systems," in *1995 IEEE 45th Vehicular Technology Conference. Countdown to the Wireless Twenty-First Century*, 1995, vol. 2, pp. 815-819: IEEE.
- [73] G. B. Giannakis and C. Tepedelenlioglu, "Basis expansion models and diversity techniques for blind identification and equalization of time-varying channels," *Proceedings of the IEEE*, vol. 86, no. 10, pp. 1969-1986, 1998.
- [74] L. Yang, R. Tian, M. Jia, and F. Li, "A Modified LS Channel Estimation Algorithm for OFDM System in Mountain Wireless Environment," *Procedia Engineering*, vol. 29, pp. 2732-2736, 2012.
- [75] S. Tiiro, J. Ylioinas, M. Myllyla, and M. Juntti, "Implementation of the least squares channel estimation algorithm for MIMO-OFDM systems," in *Proc. of the International ITG Workshop on Smart Antennas (WSA 2009)*, 2009, pp. 16-18.
- [76] M. Stojanovic, "Adaptive channel estimation for underwater acoustic MIMO OFDM systems," in *2009 IEEE 13th Digital Signal Processing Workshop and 5th IEEE Signal Processing Education Workshop*, 2009, pp. 132-137: IEEE.
- [77] R. Jiang, X. Wang, S. Cao, J. Zhao, and X. Li, "Deep neural networks for channel estimation in underwater acoustic OFDM systems," *IEEE Access*, vol. 7, pp. 23579-23594, 2019.
- [78] B. Kamışlıoğlu and A. Akbal, "LSE Channel Estimation and Performance Analysis of OFDM Systems," *Firat University Turkish Journal of Science & Technology*, vol. 12, no. 2, pp. 53-57, 2017.
- [79] N. U. R. Junejo, H. Esmail, H. Sun, Z. A. Qasem, and J. Wang, "Pilot-Based Adaptive Channel Estimation for Underwater Spatial Modulation Technologies," *Symmetry*, vol. 11, no. 5, p. 711, 2019.
- [80] J. Preisig, B. Blair, and W. Li, "Channel estimation for underwater acoustic communications: sparse channels, soft input data, and Bayesian techniques," *The Journal of the Acoustical Society of America*, vol. 123, no. 5, pp. 3892-3892, 2008.
- [81] J. Gomes and V. Barroso, "Time-reversed OFDM communication in underwater channels," in *IEEE 5th Workshop on Signal Processing Advances in Wireless Communications, 2004.*, 2004, pp. 626-630: IEEE.
- [82] K. Ramadan, M. Dessouky, S. Elagoz, M. Elkordy, and F. A. El-Samie, "Equalization and carrier frequency offset compensation for underwater acoustic OFDM systems," *Annals of Data Science*, vol. 5, no. 2, pp. 259-272, 2018.
- [83] M. T. Altabbaa and E. Panayirci, "Channel estimation and equalization algorithm for OFDM-based underwater acoustic communications systems," *ICWMC 2017*, p. 121, 2017.

- [84] J. Yin, W. Ge, X. Han, and L. Guo, "Frequency-domain equalization with interference rejection combining for single carrier multiple-input multiple-output underwater acoustic communications," *The Journal of the Acoustical Society of America*, vol. 147, no. 2, pp. EL138-EL143, 2020.
- [85] Q. He, S. Wang, and W. Zhang, "Low-complexity MMSE iterative equalization for multiband OFDM systems in underwater acoustic channels," in *2017 IEEE 9th International Conference on Communication Software and Networks (ICCSN)*, 2017, pp. 492-497: IEEE.
- [86] Z. Sui and S. Yan, "Frequency Channel Equalization Based on Variable Step-Size LMS Algorithm for OFDM Underwater Communications," in *2019 IEEE International Conference on Signal Processing, Communications and Computing (ICSPCC)*, 2019, pp. 1-5: IEEE.
- [87] R. Otnes and T. H. Eggen, "Underwater acoustic communications: long-term test of turbo equalization in shallow water," *IEEE Journal of Oceanic engineering*, vol. 33, no. 3, pp. 321-334, 2008.
- [88] X. Cai and G. B. Giannakis, "Error probability minimizing pilots for OFDM with M-PSK modulation over Rayleigh-fading channels," *IEEE transactions on vehicular technology*, vol. 53, no. 1, pp. 146-155, 2004.
- [89] S. M. Kay, *Fundamentals of statistical signal processing*. Prentice Hall PTR, 1993.
- [90] M. Murad, I. A. Tasadduq, and P. J. I. A. Otero, "Towards multicarrier waveforms beyond OFDM: performance analysis of GFDM modulation for underwater acoustic channels," vol. 8, pp. 222782-222799, 2020.
- [91] M. J. Bocus, D. Agrafiotis, and A. Doufexi, "Underwater acoustic video transmission using MIMO-FBMC," in *2018 OCEANS-MTS/IEEE Kobe Techno-Oceans (OTO)*, 2018, pp. 1-6: IEEE.
- [92] L. Wan, "Underwater acoustic OFDM: algorithm design, DSP implementation, and field performance," 2014.
- [93] H. Kulhandjian and T. Melodia, "Modeling underwater acoustic channels in short-range shallow water environments," in *Proceedings of the International Conference on Underwater Networks & Systems*, 2014, pp. 1-5.
- [94] M. C. C. F. Ruiz-Vega, J. F. Paris, P. Otero, "Ricean shadowed statistical characterization of shallow water acoustic channels for wireless communications," presented at the IEEE Conf. Underwater Communications: Channel Modelling & Validation, UComms, Sestri Levante, Italy, September, 2012, 2012.
- [95] I. A. Tasadduq, M. Murad, P. J. J. o. M. S. Otero, and Engineering, "CPM-OFDM Performance over Underwater Acoustic Channels," vol. 9, no. 10, p. 1104, 2021.
- [96] R. P. Hebbar and P. G. Poddar, "Generalized frequency division multiplexing-based acoustic communication for underwater systems," *International Journal of Communication Systems*, p. e4292, 2020.
- [97] P. v. Walree, R. Otnes, and T. Jenserud, "The Watermark manual and user's guide-version 1.0," 2016.
- [98] P. A. van Walree, F.-X. Socheleau, R. Otnes, and T. J. I. J. o. O. E. Jenserud, "The watermark benchmark for underwater acoustic modulation schemes," vol. 42, no. 4, pp. 1007-1018, 2017.
- [99] M. Stojanovic, "Underwater acoustic communication," *Wiley Encyclopedia of Electrical and Electronics Engineering*, pp. 1-12, 1999.
- [100] H. Esmail and D. Jiang, "Multicarrier communication for underwater acoustic channel," *Int'l J. of Communications, Network and System Sciences*, vol. 6, no. 08, p. 361, 2013.
- [101] M. Bellanger, D. Mattera, and M. Tanda, "Lapped-OFDM as an alternative to CP-OFDM for 5G asynchronous access and cognitive radio," in *2015 IEEE 81st Vehicular Technology Conference (VTC Spring)*, 2015, pp. 1-5: IEEE.
- [102] G. Fettweis, M. Krondorf, and S. Bittner, "GFDM-generalized frequency division multiplexing," in *VTC Spring 2009-IEEE 69th Vehicular Technology Conference*, 2009, pp. 1-4: IEEE.
- [103] R. Gerzaguat *et al.*, "The 5G candidate waveform race: a comparison of complexity and performance," *EURASIP Journal on Wireless Communications and Networking*, vol. 2017, no. 1, p. 13, 2017.

- [104] F. A. de Figueiredo, N. F. Aniceto, J. Seki, I. Moerman, and G. Fraidenraich, "Comparing f-OFDM and OFDM Performance for MIMO Systems Considering a 5G Scenario," in *2019 IEEE 2nd 5G World Forum (5GWF)*, 2019, pp. 532-535: IEEE.
- [105] Y. Tao, L. Liu, S. Liu, and Z. Zhang, "A survey: Several technologies of non-orthogonal transmission for 5G," *China communications*, vol. 12, no. 10, pp. 1-15, 2015.
- [106] M. Agiwal, A. Roy, and N. Saxena, "Next generation 5G wireless networks: A comprehensive survey," *IEEE Communications Surveys & Tutorials*, vol. 18, no. 3, pp. 1617-1655, 2016.
- [107] A. R. Jafri, J. Majid, L. Zhang, M. A. Imran, and M. Najam-ul-Islam, "FPGA implementation of UFMC based baseband transmitter: Case study for LTE 10MHz channelization," *Wireless Communications and Mobile Computing*, vol. 2018, 2018.
- [108] Z. Guo, Q. Liu, W. Zhang, and S. Wang, "Low Complexity Implementation of Universal Filtered Multi-Carrier Transmitter," *IEEE Access*, vol. 8, pp. 24799-24807, 2020.
- [109] J. Wu, X. Ma, X. Qi, Z. Babar, and W. Zheng, "Influence of pulse shaping filters on PAPR performance of underwater 5G communication system technique: GFDM," *Wireless communications and mobile computing*, vol. 2017, 2017.
- [110] R. P. Hebbar and P. G. Poddar, "Generalized frequency division multiplexing for acoustic communication in underwater systems," in *2017 International Conference on Circuits, Controls, and Communications (CCUBE)*, 2017, pp. 86-90: IEEE.
- [111] W. Jinqiu, Q. Gang, and K. Pengbin, "Emerging 5g multicarrier chaotic sequence spread spectrum technology for underwater acoustic communication," *Complexity*, vol. 2018, 2018.
- [112] J. Wua, L. Maa, G. Qiaoa, X. Maa, and X. Qia, "GFDM-A potential technique for the next generation underwater communication systems with low PAPR," presented at the 4th International Conference and Exhibition on Underwater Acoustics (UACE2017), Skiathos, Greece, September, 2017, 2017.
- [113] A. Hilario-Tacuri, "A Closed-Form Spectral Analysis of GFDM in Underwater Communication Systems," in *2019 IEEE Latin-American Conference on Communications (LATINCOM)*, 2019, pp. 1-6: IEEE.
- [114] M. J. Bocus, A. Doufexi, and D. Agrafiotis, "Performance evaluation of filterbank multicarrier systems in an underwater acoustic channel," in *2016 IEEE 27th Annual International Symposium on Personal, Indoor, and Mobile Radio Communications (PIMRC)*, 2016, pp. 1-6: IEEE.
- [115] K. Chithra *et al.*, "Underwater communication implementation with OFDM," 2015.
- [116] H.-P. Ren, C. Bai, Q. Kong, M. S. Baptista, and C. Grebogi, "A chaotic spread spectrum system for underwater acoustic communication," *Physica A: Statistical Mechanics and its Applications*, vol. 478, pp. 77-92, 2017.
- [117] P. P. Vaidyanathan, "Multirate digital filters, filter banks, polyphase networks, and applications: a tutorial," *Proceedings of the IEEE*, vol. 78, no. 1, pp. 56-93, 1990.
- [118] T. Jiang, D. Chen, C. Ni, and D. Qu, *OQAM/FBMC for Future Wireless Communications: Principles, Technologies and Applications*. Academic Press, 2017.
- [119] L. Sun, M. Wang, G. Zhang, H. Li, and L. Huang, "Filtered multitone modulation underwater acoustic communications using low-complexity channel-estimation-based MMSE turbo equalization," *Sensors*, vol. 19, no. 12, p. 2714, 2019.
- [120] C.-F. Lin, Y.-T. Hung, H.-W. Lu, S.-H. Chang, I. Parinov, and S. Shevtsov, "FBMC/LDPC-based underwater transceiver architecture for voice and image transmission," *J. Mar. Sci. Technol*, vol. 26, pp. 327-334, 2018.
- [121] J. Zhang and Y. R. Zheng, "Bandwidth-efficient frequency-domain equalization for single carrier multiple-input multiple-output underwater acoustic communications," *The Journal of the Acoustical Society of America*, vol. 128, no. 5, pp. 2910-2919, 2010.
- [122] Y. R. Z. a. C. X. Jian Zhang, "Frequency-domain equalization for single carrier MIMO underwater acoustic communications," in *OCEANS 2008*, Quebec City, QC, 2008.
- [123] C.-F. Lin *et al.*, "Direct-Mapping-Based MIMO-FBMC Underwater Acoustic Communication Architecture for Multimedia Signals," *Applied Sciences*, vol. 10, no. 1, p. 233, 2020.
- [124] B. Pranitha and L. Anjaneyulu, "Assessment of UWAC System Performance Using FBMC Technique," in *Recent Trends in Signal and Image Processing*: Springer, 2019, pp. 53-62.

- [125] J. Abdoli, M. Jia, and J. Ma, "Filtered OFDM: A new waveform for future wireless systems," in *2015 IEEE 16th International Workshop on Signal Processing Advances in Wireless Communications (SPAWC)*, 2015, pp. 66-70: IEEE.
- [126] M. S. Ahmed, N. S. M. Shah, F. Ghawbar, Y. A. Jawhar, and A. A. Almohammed, "Filtered-OFDM with channel coding based on T-distribution noise for underwater acoustic communication," *Journal of Ambient Intelligence and Humanized Computing*, pp. 1-14, 2020.
- [127] M. Van Eeckhaute, A. Bourdoux, P. De Doncker, and F. Horlin, "Performance of emerging multi-carrier waveforms for 5G asynchronous communications," *EURASIP Journal on wireless communications and networking*, vol. 2017, no. 1, p. 29, 2017.
- [128] R. Datta, N. Michailow, S. Krone, M. Lentmaier, and G. Fettweis, "Generalized Frequency Division Multiplexing in cognitive radio," in *Signal Processing Conference (EUSIPCO), 2012 Proceedings of the 20th European*, 2012, pp. 2679-2683.
- [129] I. Gaspar, M. Matthe, N. Michailow, L. Mendes, D. Zhang, and G. Fettweis, "Frequency-shift Offset-QAM for GFDM," *Communications Letters, IEEE*, vol. PP, no. 99, pp. 1-1, 2015.
- [130] Matthe, x, M., N. Michailow, I. Gaspar, and G. Fettweis, "Influence of pulse shaping on bit error rate performance and out of band radiation of Generalized Frequency Division Multiplexing," in *Communications Workshops (ICC), 2014 IEEE International Conference on*, 2014, pp. 43-48.
- [131] N. Michailow, R. Datta, S. Krone, M. Lentmaier, and G. Fettweis, "Generalized frequency division multiplexing: a flexible multi-carrier modulation scheme for 5th generation cellular networks," in *German Microwave Conference (GeMiC)*, 2012.
- [132] N. Michailow, I. Gaspar, S. Krone, M. Lentmaier, and G. Fettweis, "Generalized frequency division multiplexing: Analysis of an alternative multi-carrier technique for next generation cellular systems," in *Wireless Communication Systems (ISWCS), 2012 International Symposium on*, 2012, pp. 171-175: IEEE.
- [133] N. Michailow, S. Krone, M. Lentmaier, and G. Fettweis, "Bit error rate performance of generalized frequency division multiplexing," in *2012 IEEE Vehicular Technology Conference (VTC Fall)*, 2012, pp. 1-5: IEEE.
- [134] N. Michailow, S. Krone, M. Lentmaier, and G. Fettweis, "Bit Error Rate Performance of Generalized Frequency Division Multiplexing," in *Vehicular Technology Conference (VTC Fall), 2012 IEEE*, 2012, pp. 1-5.
- [135] X.-G. Xia, "A family of pulse-shaping filters with ISI-free matched and unmatched filter properties," *IEEE Transactions on Communications*, vol. 45, no. 10, pp. 1157-1158, 1997.
- [136] B. S. Thomson, A. M. Bruckner, and J. B. Bruckner, *Real Analysis*. ClassicalRealAnalysis.com, 2008.
- [137] M. Matthé, N. Michailow, I. Gaspar, and G. P. Fettweis, "Influence of pulse shaping on bit error rate performance and out of band radiation of Generalized Frequency Division Multiplexing," in *ICC Workshops*, 2014, pp. 43-48.
- [138] N. Michailow *et al.*, "Generalized Frequency Division Multiplexing for 5th Generation Cellular Networks," *Communications, IEEE Transactions on*, vol. 62, no. 9, pp. 3045-3061, 2014.
- [139] M. Murad, I. A. Tasadduq, and P. Otero, "Ciphred BCH Codes for PAPR Reduction in the OFDM in Underwater Acoustic Channels," *Journal of Marine Science and Engineering*, vol. 10, no. 1, p. 91, 2022.
- [140] S. H. Han and J. H. Lee, "PAPR reduction of OFDM signals using a reduced complexity PTS technique," *IEEE Signal Processing Letters*, vol. 11, no. 11, pp. 887-890, 2004.
- [141] T. Jiang, Y. Yang, and Y.-H. Song, "Exponential companding technique for PAPR reduction in OFDM systems," *IEEE Transactions on broadcasting*, vol. 51, no. 2, pp. 244-248, 2005.
- [142] Y. Jiang, "New companding transform for PAPR reduction in OFDM," *IEEE Communications Letters*, vol. 14, no. 4, pp. 282-284, 2010.
- [143] K. T. Wong, B. Wang, and J.-C. Chen, "OFDM PAPR reduction by switching null subcarriers and data-subcarriers," *Electronics letters*, vol. 47, no. 1, pp. 62-63, 2011.
- [144] Y. Rahmatallah and S. Mohan, "Peak-to-average power ratio reduction in OFDM systems: A survey and taxonomy," *IEEE communications surveys & tutorials*, vol. 15, no. 4, pp. 1567-1592, 2013.

- [145] G. Rojo and M. Stojanovic, "Peak-to-average power ratio (PAR) reduction for acoustic OFDM systems," in *OCEANS 2009*, 2009, pp. 1-7: IEEE.
- [146] Y. A. Jawhar *et al.*, "A review of partial transmit sequence for PAPR reduction in the OFDM systems," *IEEE Access*, vol. 7, pp. 18021-18041, 2019.
- [147] L. Hanzo, R. Steele, and P.-M. Fortune, "A subband coding, BCH coding, and 16-QAM system for mobile radio speech communications," *IEEE Transactions on vehicular technology*, vol. 39, no. 4, pp. 327-339, 1990.
- [148] I. Krasikov and S. Litsyn, "On spectra of BCH codes," *IEEE Transactions on Information Theory*, vol. 41, no. 3, pp. 786-788, 1995.
- [149] Z. H. Kashani and M. Shiva, "BCH coding and multi-hop communication in wireless sensor networks," in *2006 IFIP International Conference on Wireless and Optical Communications Networks*, 2006, pp. 5 pp.-5: IEEE.
- [150] N. Nagaraj, V. Vaidya, and P. G. Vaidya, "Re-visiting the One-Time Pad," *arXiv preprint cs/0508079*, 2005.
- [151] P. Kumar and P. Kumar, "Performance evaluation of DFT-spread OFDM and DCT-spread OFDM for underwater acoustic communication," in *2012 IEEE Vehicular Technology Conference (VTC Fall)*, 2012, pp. 1-5: IEEE.
- [152] J. Tao, "DFT-precoded MIMO OFDM underwater acoustic communications," *IEEE Journal of Oceanic Engineering*, vol. 43, no. 3, pp. 805-819, 2017.
- [153] R. Gomathi and J. M. L. Manickam, "PAPR reduction technique using combined DCT and LDPC based OFDM system for underwater acoustic communication," *ARPJ Journal of Engineering and Applied Sciences*, vol. 11, no. 7, pp. 4424-4430, 2016.
- [154] M. S. Abd El-Galil, N. F. Soliman, M. Abdalla, M. A. Elaskily, and F. E. Abd El-Samie, "TanhR Nonlinear Companding Scheme for UWA System," *International Journal of Electronics Letters*, 2020.
- [155] S. Xing, G. Qiao, and L. Ma, "A blind side information detection method for partial transmitted sequence peak-to-average power reduction scheme in OFDM underwater acoustic communication system," *IEEE Access*, vol. 6, pp. 24128-24136, 2018.
- [156] J. Han, S. Ma, Y. Wang, and G. Leus, "Low-complexity equalization of MIMO-OSDM," *IEEE Transactions on Vehicular Technology*, vol. 69, no. 2, pp. 2301-2305, 2019.
- [157] Z. A. Qasem, H. A. Leftah, H. Sun, J. Qi, and H. J. I. S. J. Esmail, "X-Transform Time-Domain Synchronous IM-OFDM-SS for Underwater Acoustic Communication," 2021.
- [158] T. Jiang, G. Zhu, and J. Zheng, "Block coding scheme for reducing PAPR in OFDM systems with large number of subcarriers," *Journal of Electronics*, vol. 21, no. 6, pp. 482-489, 2004.
- [159] T. Jiang and G. Zhu, "Complement block coding for reduction in peak-to-average power ratio of OFDM signals," *IEEE Communications Magazine*, vol. 43, no. 9, pp. S17-S22, 2005.
- [160] A. Ghassemi and T. A. Gulliver, "PAPR reduction of OFDM using PTS and error-correcting code subblocking-Transactions Papers," *IEEE Transactions on wireless communications*, vol. 9, no. 3, pp. 980-989, 2010.
- [161] K. Yang and S.-I. Chang, "Peak-to-average power control in OFDM using standard arrays of linear block codes," *IEEE Communications letters*, vol. 7, no. 4, pp. 174-176, 2003.
- [162] A. E. Jones, T. A. Wilkinson, and S. Barton, "Block coding scheme for reduction of peak to mean envelope power ratio of multicarrier transmission schemes," *Electronics letters*, vol. 30, no. 25, pp. 2098-2099, 1994.
- [163] I. A. Tasadduq and R. K. Rao, "Weighted OFDM with block codes for wireless communication," in *2001 IEEE Pacific Rim Conference on Communications, Computers and Signal Processing (IEEE Cat. No. 01CH37233)*, 2001, vol. 2, pp. 441-444: IEEE.
- [164] P. C. Carrascosa and M. Stojanovic, "Adaptive channel estimation and data detection for underwater acoustic MIMO-OFDM systems," *IEEE Journal of Oceanic Engineering*, vol. 35, no. 3, pp. 635-646, 2010.
- [165] J. Kim, Y.-H. Cho, H. Ko, and T. Im, "Performance Comparison of Short-Length Error-Correcting Codes in an underwater OFDM systems," in *2019 International Conference on Information and Communication Technology Convergence (ICTC)*, 2019, pp. 121-123: IEEE.
- [166] M. Porter, "BELLHOP code.[Online] Available: <http://oalib.hlsresearch.com>," *Rays/index.html*.

- [167] W. Tutte, "Fish and I, Coding Theory and Cryptography (Annapolis, MD, 1998)," ed: Springer, Berlin, 2000.
- [168] F. Huo and G. Gong, "XOR encryption versus phase encryption, an in-depth analysis," *IEEE Transactions on Electromagnetic Compatibility*, vol. 57, no. 4, pp. 903-911, 2015.
- [169] D. Gligoroski, S. J. Knapskog, and S. Andova, "Cryptocoding-Encryption and Error-Correction Coding in a Single Step," in *Security and Management*, 2006, pp. 145-151: Citeseer.
- [170] M. Murad, I. A. Tasadduq, P. Otero, and J. Poncela, "Flexible OFDM Transceiver for Underwater Acoustic Channel: Modeling, Implementation and Parameter Tuning," *Wireless Personal Communications*, 2020/11/04 2020.
- [171] M. Murad, I. A. Tasadduq, and P. J. I. A. Otero, "Towards multicarrier waveforms beyond OFDM: Performance analysis of GFDM modulation for underwater acoustic channels," 2020.
- [172] T. Aulin and C.-E. Sundberg, "Bounds on the performance of binary CPFSK type of signaling with input data symbol pulse shaping," in *NTC'78; National Telecommunications Conference, Volume 1*, 1978, vol. 1, pp. 6.5. 1-6.5. 5.
- [173] T. Aulin and C.-E. Sundberg, "Continuous phase modulation-Part I: Full Response Signaling," *IEEE Transactions on Communications*, vol. COM-29, no. 3, pp. 196-209, 1981.
- [174] T. Aulin, N. Rydbeck, and C.-E. Sundberg, "Continuous phase modulation-Part II: Partial response signaling," *IEEE Transactions on Communications*, vol. 29, no. 3, pp. 210-225, 1981.
- [175] Y. Sun, "Optimal Parameter Design of Continuous Phase Modulation for Future GNSS Signals," *IEEE Access*, vol. 9, pp. 58487-58502, 2021.
- [176] B. Peng, P. S. Rossi, H. Dong, and K. Kansanen, "Time-domain oversampled OFDM communication in doubly-selective underwater acoustic channels," *IEEE Communications Letters*, vol. 19, no. 6, pp. 1081-1084, 2015.
- [177] J. G. Proakis and M. Salehi, *Digital communications*. McGraw-Hill., 2008.
- [178] K. Kassan, H. Farès, D. C. Glattli, and Y. Louët, "Performance vs. Spectral Properties For Single-Sideband Continuous Phase Modulation," *IEEE Transactions on Communications*, vol. 69, no. 7, pp. 4402-4416, July 2021.
- [179] U. Güntürkün and L. Vandendorpe, "Low-Complexity LMMSE-SIC Turbo Receiver for Continuous Phase Modulation, Based on a Multiaccess-Multipath Analogy," *IEEE Transactions on Communications*, vol. 68, no. 12, pp. 7672-7686, 2020.
- [180] Z. Xu and Q. Wang, "Autocorrelation Function of Full-Response CPM Signals and Its Application to Synchronization," *IEEE Access*, vol. 7, pp. 133781-133786, 2019.
- [181] I. A. Tasadduq and R. K. Rao, "OFDM-CPM signals," *Electronics Letters*, vol. 38, no. 2, pp. 80-81, 2002.
- [182] I. A. Tasadduq and R. K. Rao, "Detection of OFDM-CPM signals over multipath channels," in *2002 IEEE International Conference on Communications. Conference Proceedings. ICC 2002 (Cat. No. 02CH37333)*, 2002, vol. 3, pp. 1651-1655: IEEE.
- [183] I. A. Tasadduq and R. K. Rao, "OFDM-CPM signals for wireless communications," *Canadian Journal of Electrical and Computer Engineering*, vol. 28, no. 1, pp. 19-25, 2003.
- [184] I. A. Tasadduq and R. K. Rao, "Performance of optimum and suboptimum OFDM-CPM receivers over multipath fading channels," *Wireless Communications and Mobile Computing*, vol. 5, no. 3, pp. 365-374, 2005.
- [185] I. A. Tasadduq and R. K. Rao, "Viterbi decoding of OFDM-CPM signals," *Arabian Journal for Science and Engineering*, vol. 28, pp. 71-80, 2003.
- [186] I. A. Tasadduq and R. K. Rao, "OFDM-CPM signals for indoor wireless communications," in *Proc. 14th International Conference on Wireless Communications, Wireless*, 2002, pp. 8-10.
- [187] M. Wylie and G. Green, "On the Performance of Serially Concatenated CPM-OFDMA Schemes for Aeronautical Telemetry," Air Force Flight Test Center Edwards AFB CA2011.
- [188] M. A. Hisojo, J. Lebrun, and L. Deneire, "Zero-Forcing approach for L2-Orthogonal ST-Codes with CPM-OFDM schemes and frequency selective Rayleigh fading channels," in *2014 IEEE Military Communications Conference*, 2014, pp. 563-568: IEEE.
- [189] K. Morioka *et al.*, "An implementation of CPFSK-OFDM systems by using software defined radio," in *WAMICON 2014*, 2014, pp. 1-3: IEEE.
- [190] I. Tasadduq and R. Rao, "PAPR reduction of OFDM signals using multi-amplitude CPM," *Electronics letters*, vol. 38, no. 16, pp. 915-917, 2002.

- [191] S. C. Thompson, A. U. Ahmed, J. G. Proakis, J. R. Zeidler, and M. J. Geile, "Constant envelope OFDM," *IEEE transactions on communications*, vol. 56, no. 8, pp. 1300-1312, 2008.
- [192] S. C. Thompson, A. U. Ahmed, J. G. Proakis, and J. R. Zeidler, "Constant envelope OFDM phase modulation: spectral containment, signal space properties and performance," in *IEEE MILCOM 2004. Military Communications Conference, 2004.*, vol. 2, pp. 1129-1135.
- [193] I. A. Tasadduq, "Novel OFDM-CPM Signals for Wireless Communications: Properties, Receivers and Performance," Ph.D., Electrical and Computer Engineering, University of Western Ontario, London, ON, 2002.
- [194] E. S. Hassan, X. Zhu, S. E. El-Khamy, M. I. Dessouky, S. A. El-Dolil, and F. E. A. El-Samie, "Performance evaluation of OFDM and single-carrier systems using frequency domain equalization and phase modulation," *International Journal of Communication Systems*, vol. 24, no. 1, pp. 1-13, 2011.
- [195] E. S. Hassan, X. Zhu, S. E. El-Khamy, M. I. Dessouky, S. A. El-Dolil, and F. E. Abd El-Samie, "Chaotic interleaving scheme for single-and multi-carrier modulation techniques implementing continuous phase modulation," *Journal of the Franklin Institute*, vol. 350, no. 4, pp. 770-789, 2013.
- [196] M. Kiviranta, A. Mammela, D. Cabric, D. A. Sobel, and R. W. Brodersen, "Constant envelope multicarrier modulation: performance evaluation AWGN and fading channels," in *MILCOM 2005-2005 IEEE Military Communications Conference, 2005*, pp. 807-813: IEEE.
- [197] J. Tan and G. L. Stuber, "Constant envelope multi-carrier modulation," in *MILCOM 2002. Proceedings, 2002*, vol. 1, pp. 607-611: IEEE.
- [198] J. B. Anderson and T. Aulin, *Digital Phase Modulation*. New York: Plenum, 1986.
- [199] A. Viterbi, "Error bounds for convolutional codes and an asymptotically optimum decoding algorithm," *IEEE transactions on Information Theory*, vol. 13, no. 2, pp. 260-269, 1967.
- [200] J. Omura, "On the Viterbi decoding algorithm," *IEEE transactions on Information Theory*, vol. 15, no. 1, pp. 177-179, 1969.
- [201] H. Kobayashi, "Correlative level coding and maximum-likelihood decoding," *IEEE Transactions on Information Theory*, vol. 17, no. 5, pp. 586-594, 1971.
- [202] G. D. Forney, "The viterbi algorithm," *Proceedings of the IEEE*, vol. 61, no. 3, pp. 268-278, 1973.
- [203] J. F. Hayes, "The Viterbi algorithm applied to digital data transmission," *IEEE Communications Magazine*, vol. 40, no. 5, pp. 26-32, 2002.
- [204] J. Hayes, "The Viterbi algorithm applied to digital data transmission," *Communications Society*, vol. 13, no. 2, pp. 15-20, 1975.
- [205] B. Sklar, *Digital communications: fundamentals and applications*, Second ed. Prentice-hall Englewood Cliffs, NJ, 2001.
- [206] S. Haykin, *Communication systems*. John Wiley & Sons, 2008.

Appendix A

Curriculum Vitae

Mohsin Murad

Experience

Lecturer, Department of Computer Engineering (2012–date)
Umm Al Qura University, Makkah, Saudi Arabia

Lecturer, Department of Computer Systems Engineering (2009–2011)
University of Engineering and Technology, Peshawar, Pakistan

Education

PhD Telecommunication Engineering (Dissertation submitted) (2016–2022)
University of Malaga, Málaga, Spain

MSc Computer Systems Engineering (2009–2011)
University of Engineering & Technology, Peshawar, Pakistan

BSc Computer Systems Engineering (2005–2009)
University of Engineering & Technology, Peshawar, Pakistan

Training / certifications

NI Software Radio Peripherals (USRP) Software Defined Radio, Saudi Arabia 2019
NI LabVIEW based 4G Communications, Saudi Arabia 2019

Publications

- Mohsin Murad, Imran A. Tasadduq, Pablo Otero, and Javier Poncela. "Flexible OFDM Transceiver for Underwater Acoustic Channel: Modeling, Implementation and Parameter Tuning." *Wireless Personal Communications* (2020): 1423-1441. DOI: 10.1007/s11277-020-07850-w.
- Mohsin Murad, Imran A. Tasadduq, and Pablo Otero. "Towards multicarrier waveforms beyond OFDM: Performance analysis of GFDM modulation for underwater acoustic channels." *IEEE Access* (2020). DOI: 10.1109/ACCESS.2020.3043718.
- Mohsin Murad, Imran A. Tasadduq, and Pablo Otero. "Pilot-Assisted OFDM for Underwater Acoustic Communication." *Journal of Marine Science and Engineering* (2021). DOI: 10.3390/jmse9121382.

- M. Murad, Imran A. Tasadduq, and Pablo Otero. "Ciphered BCH codes for PAPR reduction in the OFDM in underwater acoustic channels." *Journal of Marine Science and Engineering* (2022). DOI: 10.3390/jmse10010091.
- Imran A. Tasadduq, Mohsin Murad, and Pablo Otero. "CPM-OFDM Performance over Underwater Acoustic Channels." *Journal of Marine Science and Engineering* (2021). DOI: 10.3390/jmse9101104.
- M. Murad, M. Y. I. Zia and I. A. Tasadduq, "Monitoring Pollution and Air Quality of Pedestrian and Automotive Tunnels in the City of Makkah," 2020 Industrial & Systems Engineering Conference (ISEC), 2020, pp. 1-5, doi: 10.1109/ISEC49495.2020.9229955.
- Mohsin Murad, Pablo Otero and Javier Poncela. "An OFDM Transceiver Model for Experimental Investigations in Underwater Acoustic Channel." 3rd Global Conference on Wireless and Optical Communications (GCWOC'18) (2018), Malaga, Spain.
- Mohsin Murad, Imran A. Tasadduq, and Pablo Otero. "Pilots based LSE Channel Estimation for Underwater Acoustic OFDM Communication." *Global Conference on Wireless and Optical Technologies (GCWOT)* (2020), Malaga, Spain.
- Mohsin Murad, Imran A. Tasadduq, and Pablo Otero. "Linear Equalization Techniques for Underwater Acoustic OFDM Communication." *Global Conference on Wireless and Optical Technologies (GCWOT)* (2020), Malaga, Spain.

Patents

- EA Felemban, AAA Sheikh, M Murad, MA Manzoor, "A method, apparatus and system for enabling communication using multi-protocol gateway and virtual resource manager" US Patent US 2017 / 0244635 A1.
- EA Felemban, AAA Sheikh, M Murad, MA Manzoor, "A Method, Apparatus and System for Enabling Communication using Multi-Protocol Gateway and Virtual Resource Manager" WO Patent WO/2015/198,087.